Alternative splice codes for neuronal diversification and synapse specification

Inauguraldissertation
zur
Erlangung der Würde eines Doktors der Philosophie
vorgelegt der
Philosophisch-Naturwissenschaftlichen Fakultät
der Universität Basel

von

Lisa Traunmüller
aus Österreich

Basel, 2020

Genehmigt von der Philosophisch-Naturwissenschaftlichen Fakultät

auf Auftrag von:

Prof. Dr. Peter Scheiffele

Prof. Dr. Fiona Doetsch

Basel den, 25. Juni 2019

Prof. Dr. Martin Spiess
Dekan der Philosophisch-
Naturwissenschaftlichen Fakultät

Table of contents

Summary 6

1. Introduction 8

1.1 General Introduction 9

1.2 Neuronal diversity 12

1.2.1 Distinct neuronal cell types and their functions 13
1.2.2 The developmental origin of cortical neurons 18
1.2.3 Molecular profiling to characterize cell types 19
1.2.4 Dynamics of transcriptomic diversity 20
1.2.5 How many cell types are there? 21

1.3 Transcriptomic diversity and synaptic specificity 22

1.3.1 Generation of transcriptomic diversity 22
1.3.2 Neuronal wiring through self-avoidance 26
1.3.3 Trans-synaptic molecular recognition codes 29
1.3.4 Target-specific patterns for synaptic connectivity 34

1.4 RNA binding proteins – keys for identifying a molecular code? 36

1.4.1 Cell-class specific action of RBPs 37
1.4.2 Investigation of STAR-family RBPs for cell type-specific splicing programs 38

1.5 The dissertation project 41

2. Results 42

2.1 Preface 43

2.2 Control of Neuronal Synapse Specification by a Highly Dedicated Alternative Splicing Program 45

2.3 Landscape of ribosome-engaged alternative transcript isoforms across neuronal cell classes 63

2.4 Cell class-specific actions of SLM2 in specifying synaptic properties 105

3. Discussion and further directions 129

3.1 A molecular code for neuronal specificity? 130

3.1.1 Contributions of selective expression of RNA binding proteins to neuronal specificity 131

3.1.2 The power of RNA binding motifs 134

3.1.3 Additional mechanisms contributing to the molecular code for neuronal specification 135

3.2 Functional implications of alternative splicing programs 136

3.2.1 RBPs as master regulators of synaptic specificity 136

3.2.2 Why would the brain require dedicated RBPs to control synapse specification? 138

3.2.2 One RNA-binding protein - two sides of one coin? 139

3.3 Conclusions 141

4. Materials and Methods 143

5. Appendix 165

5.1 Index of figures covered in the introduction 166

5.2 Index of abbreviations 167

6. References 170

Acknowledgements 191

Curriculum Vitae ..... **Error! Bookmark not defined.**

Summary

Mammalian nervous systems exhibit an immense structural and functional complexity ranging from billions of neurons to their precise synaptic communication. Neuronal circuits consist of hierarchical assemblies of highly specialized neuronal cell types. Their intrinsic properties and the functional specification of their synapses are fundamental for how circuits process information. However, how diverse classes of neurons establish their cellular and synaptic specificity remains largely unclear. In this thesis, I explored whether cell type-specific alternative splicing programs contribute to the regulation of neuronal and synaptic properties, thereby shaping neuronal connectivity and circuit function.

To investigate whether alternative splicing programs play cell type-specific roles in the mouse brain, I performed global assessments of alternative splicing regulation across neuronal cell classes as well as targeted loss of function studies for one specific alternative splicing regulator. I focused on the RNA binding protein SLM2 which exhibits a remarkable neuronal cell class-specific expression in the mouse brain and had been previously implicated in the regulation of alternative splicing of the synaptic adhesion molecules Neurexin1,2, and 3 (Ehrmann et al., 2013; Iijima et al., 2011). Surprisingly, we found that SLM2 regulates only a handful of transcripts and that loss of SLM2 results in highly selective alterations at glutamatergic synapses in the mouse hippocampus. Genetic correction of the SLM2-dependent target exon of Neurexin 1 was sufficient to rescue synaptic deficits and alterations in the behavior of the Slm2 knock-out animals. Thus, the SLM2 alternative splicing program is highly dedicated to control synapse specification and function in the hippocampus.

In a complementary effort, I investigated how alternative splicing programs are arrayed across different neuronal populations of the forebrain. Systematic mapping of ribosome-associated transcript isoforms in genetically defined cell populations of wild-type animals uncovered extensive transcript isoform diversity across neuronal classes. This revealed that the important drivers for diversification in glutamatergic and GABAergic cells are alternative splicing and transcription start sites. Importantly, we uncovered that such cell class-specific alternative splicing programs mainly target genes implicated in regulating synaptic functions and the intrinsic properties of neurons.

Finally, I explored whether a single RNA binding protein controls common or divergent splicing events and cellular functions in different neuronal populations. We analyzed SLM2-dependent alternative splicing programs in two hippocampal glutamatergic cell classes and somatostatin positive GABAergic neurons. Our findings indicate that there are unique sets of SLM2-dependent transcript isoforms and divergent synaptic phenotypes in different cell populations.

In sum, this work uncovers major roles for cell class-specific alternative splicing programs in the genetic determination of neuronal function and synapse specification

1. Introduction

1.1 General Introduction

The human brain is one of the most complex organs in our body required for fundamental body functions like breathing as well as more complex tasks like navigating in our environment or learning and memory. The execution of all of these functions requires the precise temporal activation of hundreds of different neuronal cell types organized into different brain areas. Neurons need to communicate with each other via synapses both within and between brain areas, which is dependent on the correct assembly of functional neuronal circuits. The precise organization and properties of synaptic connections are crucial for correct neuronal activity and normal brain function. However, how diverse classes of neurons orchestrate their synaptic and functional properties is still largely unclear. Over the past decade, genome-wide studies have identified hundreds of risk genes involved in neurological conditions such as autism or alzheimers. These studies have linked mutations in synaptic genes to the pathogenesis of these conditions (Autism Genome Project et al., 2007; Geschwind and State, 2015). Therefore, it has been hypothesized that incorrect synaptic connectivity and function might contribute to disease etiology. Deciphering the molecular code that instructs neuronal and synaptic specificity will be not only crucial to understand complex behaviors but will also contribute to our understanding of the pathophysiology underlying neurological conditions.

In order to mediate diverse set of functions, different brain areas are required to communicate within and between each other. Thus, individual neurons need to form highly specific connections to be capable of integrating information and performing complicated tasks. The requirement for precise synaptic connectivity and function can be illustrated by the macroscopic view of sensory perception in mice. In rodents, sensory information from the whiskers is transmitted through multiple brain areas that function as relay stations, such as the brain stem and hypothalamus, before reaching higher order brain regions such as the somatosensory cortex. Within the somatosensory cortex, whisker sensory information is transmitted to the barrel cortex, which is organized as a precise neuronal map of the whiskers on the snout of the animal (Aronoff et al., 2010). Only after the sensory information has been processed in the barrel cortex, output neurons are activated to elicit a response. Each of these brain regions contains different classes of interconnected neurons important for integrating and transmitting the information. Thus, reacting to an environmental cue requires transmission of information across multiple brain areas, cell types and synaptic connections.

One of the best studied examples for information processing within a given brain structure is the hippocampus, contributing to learning and memory formation. Its laminar structure, precise

positioning of neuronal cells and their interconnection, and well-characterized synapses make it one of the best brain structures to investigate synaptic communication between different types of neurons (Figure 1, see figure legend for description of information flow). Neurons can, in part, be classified based on the type of neurotransmitters they use. The two major neurotransmitter systems are glutamate to excite and gamma-aminobutyric acid (GABA) to inhibit neurons (neuronal diversity will be discussed in detail in chapter 1.2). As a general principle, information is transmitted via glutamatergic synapses, and is temporally and locally controlled by the GABAergic inhibition of excitatory neurons.

The hippocampus is one of the brain areas central for my PhD thesis. Some of its specific features are recurrent throughout this dissertation and will be discussed during the results sections. Thus, I will be giving a brief overview on hippocampal synaptic transmission below.

Hippocampal pathways have been intensively studied with respect to synaptic terminal specification. It is becoming increasingly clear that precise formation of specific synapses and their unique functional properties have major implications for the processing of information. An additional layer of complexity arises from the fact that synapses are not static but undergo plastic changes in their receptor composition over time in response to activation or inhibition. There are multiple types of plasticity-dependent synaptic changes, however I will briefly illustrate two that are classically used in the hippocampus. The first one is long-term potentiation (LTP). LTP is a form of plasticity that requires the activation of post-synaptic glutamatergic N-methyl-D-aspartate (NMDA) receptors and insertion of glutamatergic α-amino-3-hydroxy-5-methyl-4-isoxazolepropionic acid (AMPA) receptors due to calcium influx and Ca^{2+}/calmodulin-dependent protein kinase 2 (CamK2) activation (Abraham, 2003; Bliss and Lomo, 1973). Moreover, LTP requires prolonged stimulation, which long-lastingly alters synaptic strength from minutes to hours. Even though LTP can occur at any excitatory synapse in the brain, intra-hippocampal information processing from *cornu ammonis* layer 3 (CA3) to CA1 through the Schaffer collaterals (SC) has been most intensively studied due to robust post-synaptic responses (Herring and Nicoll, 2016). Another source of hippocampal LTP emerges from excitatory inputs directly from the entorhinal cortex onto CA1 which are carrying sensory information (Cutsuridis et al., 2010).

As a second example, the brain also relies on plasticity forms that are used for rapid information processing and temporal filtering. So called Short-term facilitation (STF) which happens between milliseconds and seconds. STF depends on residual elevation of presynaptic Ca^{2+} which leads to vesicle fusion and release of a given neurotransmitter into the synaptic cleft. Thus, short-term facilitation is commonly thought to be correlated with the release properties of a given synapse. In the hippocampus, STF has been intensely investigated between CA1 pyramidal neurons and their post-synaptic partners like

somatostatin (SST) and parvalbumin (PV) positive interneurons (Jackman and Regehr, 2017; Pouille and Scanziani, 2004).

Importantly and as a take home message, both of these plasticity paradigms, LTP and STF, require the involvement of different neuronal cell types with specialized synaptic connections, not only between excitatory neurons, but also between inhibitory neurons.

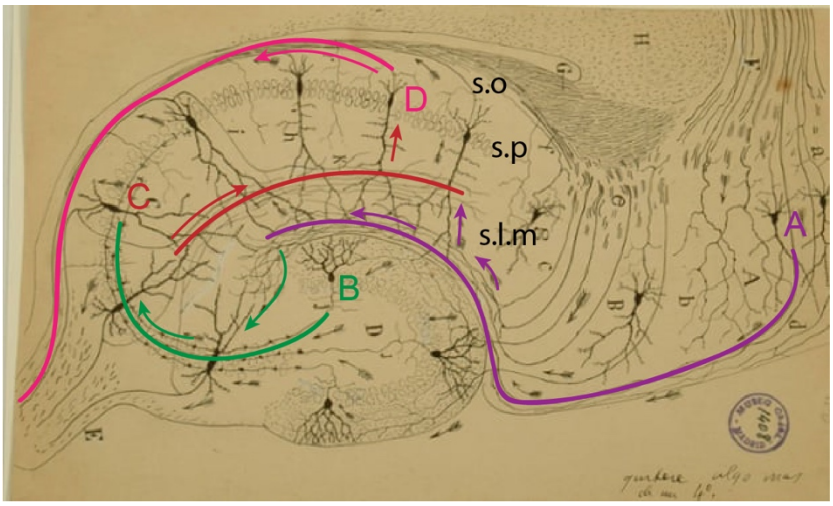

Figure 1: Drawing neuronal cell types and information flow in the rat hippocampus by Ramón y Cajal

Illustration of the hippocampal circuitry with additional modifications. In a simplified view excitatory input from pyramidal neurons in the entorhinal cortex (A) is transmitted to excitatory dentate gyrus granule cells (B) – performant path - or CA1 pyramidal neurons (D) via synapses in s.l.m – temporo-ammonic pathway (TA). In the intrahippocampal pathway, granule cells form mossy fibers contacting CA3 pyramidal neurons (C), which in turn form the Schaffer collateral pathway to CA1 pyramidal neurons (D) which sit in s.p. Axon collaterals of CA1 neurons form the alveus which leave the hippocampus via s.o and transmit information into the subiculum and cortex. s.l.m = stratum laconusum moleculare, s.p = stratum pyramidale, s.o = stratum oriens

These examples illustrate some of the specific requirements for brain function and also highlight open questions in neurobiology: How can billions of neurons, with divergent anatomical and functional properties, form synapses at the right location, at the right time, to generate neuronal circuits which perform according functions? Furthermore, synapses formed by divergent neuronal cell populations can exhibit differential transmission properties. The diversity of synaptic properties can be appreciated even on the single cell and synapse level. There is a growing body of literature supporting that features of neuronal diversity and synaptic specificity can be shaped by activity, but that the majority of neuronal features are molecularly encoded. This view is supported by the fact that neuronal circuits can be formed and maintained with only minimal neuronal activity (Sando et al., 2017; Sigler et al., 2017), and that neurons display reliable intrinsic firing properties and molecular markers *in vivo* and *in vitro*, despite constant integration of excitatory and inhibitory inputs. Thus, the majority of the identity

and synaptic specificity of individual neurons is hardwired. However, where cellular neuronal diversity and the high degree of synaptic specificity are intertwined and how this is regulated still remains to be further elucidated.

The following introduction chapter will discuss aspects of neuronal diversity with respect to individual classes of neurons with unique functions and synaptic properties. Furthermore, I will discuss how we can integrate functional information with newly emerging knowledge on the molecularly defined identity of neurons and their synaptic specificity.

1.2 Neuronal diversity

In the 1880s Ramón y Cajal described the immense anatomical diversity of neurons and the highly structured connectivity patterns of neuronal cells. He pioneered the characterization and classification of individual neurons into neuron types based on their morphology. In recent years, a lot of effort has been made to further identify what parameters, apart from morphology, can be used to characterize neuronal cell identity. Neurons can be grouped into different classes based on converging criteria: Their morphology, their transcriptomics, as determined by their genetic makeup; their intrinsic properties, measured by action potential firing patterns; and their structural specificity, determined by their synaptic connections (Figure 2). These different characteristics build the essential frameworks for how neurons integrate into circuits and relay information. Disruption of any of these properties can alter the function of neuronal networks and ultimately the behavior of an animal.

Thus, the appropriate categorization and identification of cell types is extremely relevant to further understand mechanisms underlying brain function. One additional global category for grouping cells into different classes is based on their neurotransmitter phenotype. The two major neurotransmitter classes in the brain are glutamatergic and GABAergic cells, which will be described in more detail in the following section. Moreover, I will focus on different cell classes, with emphasis on their origin and functional implications. Early classifications have allowed us to group cells into different classes. However, with technological advances such as single cell sequencing, it is becoming increasingly clear that neuronal cell types within one class are not as homogeneous as previously thought. Thus, I will also discuss recent efforts to further dissect the heterogeneity within neuron types.

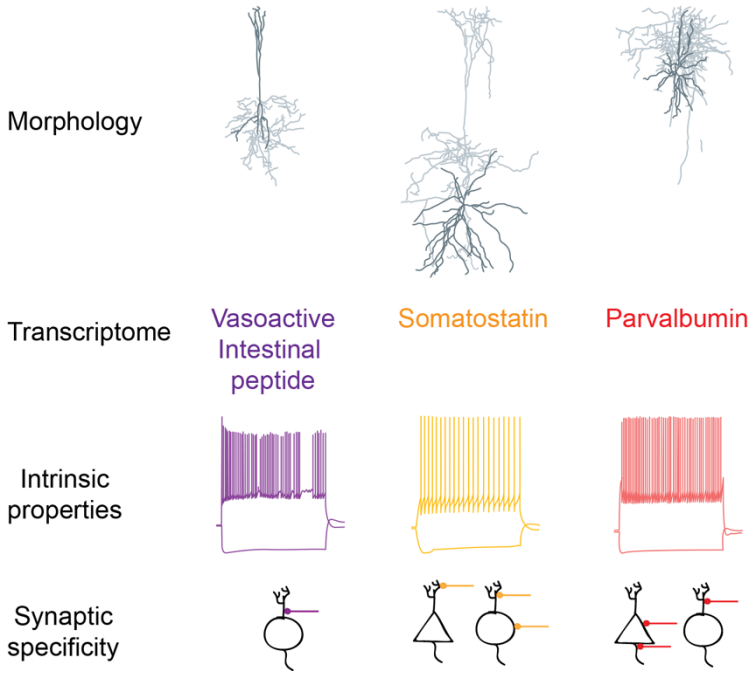

Figure 2: Parameters for classification of neuronal cell types

Neurons can be grouped into different classes based on multiple criteria: Morphology, neurochemistry and the genes expressed, intrinsic properties and input-output connectivity. Round cells represent inhibitory neurons, triangle cells principle neurons. Adapted from (Kepecs and Fishell, 2014; Zeng and Sanes, 2017)

1.2.1 Distinct neuronal cell types and their functions

Neuronal cells require genetic programs to reproducibly follow a given fate and establish their unique cellular properties and synaptic specificity. In the following chapter I will summarize the properties, functional importance and synaptic target specificity of two major interneuron classes in the brain.

In the central nervous system signal propagation is mediated, in part, by neurotransmitters released at the chemical synapse of a neuron. The most abundant neurotransmitters in the brain are glutamate, γ-aminobutric acid (GABA) and coincide with excitatory or inhibitory functions of neurons, respectively. This is because they exert opposing effects at the corresponding receptors residing in the postsynaptic membrane. Release of glutamate into the synaptic cleft induces depolarization of the membrane through influx of sodium and calcium, and thus leads to the generation of action potentials and the activation of cells. GABAergic synapses generate hyperpolarization due to the efflux of potassium or the influx of chloride. During the hyperpolarized state the postsynaptic neuron is not able to generate action potentials and is therefore, inhibited.

Glutamatergic neurons, also called principle neurons, predominantly form long-range projections to transmit information within and between different brain areas, and make up approximately 80% of the total neuron population. Inhibitory neurons on the other hand only represent a minority with 10-15% of the total neuronal population being inhibitory (Meyer et al., 2011). However, due to their vast variability in subcellular targeting domains, synaptic kinetics and connectivity patterns, they can act as precise regulators by gating principal neuron activity (Kepecs and Fishell, 2014). Therefore, interneurons are essential for proper network function by sculpturing local network dynamics.

Interneurons in neocortical areas or the hippocampus, are highly diverse and have initially been grouped into different classes based on their morphology, molecular composition and electrophysiological properties: Parvalbumin (PV), Somatostatin (SST), Vasoactive intestinal peptide (VIP), cholecystokin (CCK), calretinin (CR) and Reelin (Kepecs and Fishell, 2014). Within those, PV and SST positive interneurons account for ~70% of all interneurons (Tremblay et al., 2016). Therefore, I will discuss these two neuron classes in more detail to illustrate their functional differences, differential synaptic targeting specificity and the heterogeneity within interneuron classes.

Parvalbumin interneurons

Parvalbumin positive interneurons have obtained their name due to the expression of the Ca^{2+} binding protein parvalbumin (Celio, 1986). PV neurons can be sub-divided into fast-spiking basket cells and chandelier neurons (Figure 3, red boxes). They greatly differ in their target specificity, as basket neurons preferentially provide strong inhibition onto the soma and proximal dendrites, whereas chandelier cells preferentially target the axon initial segment (Figure 2) (Fishell and Rudy, 2011; Howard et al., 2005). Both PV interneuron types can provide either feedforward (direct) or feedback (indirect) inhibition. However, there is still an ongoing debate of whether both PV types only exert inhibitory functions, as chandelier neurons have also been demonstrated to depolarize postsynaptic neurons due to higher Cl^- concentrations at the axon initial segment (Jiang et al., 2015; Szabadics et al., 2006). Moreover, their axonal arborization greatly differs in such that basket cells are thought to provide both long-range and local inhibition, whereas chandelier axons are mainly local. Fast spiking parvalbumin positive interneurons in the neocortex also display a great heterogeneity with respect to their firing patterns, including delayed vs. non-delayed initial action potential firing (Petilla Interneuron Nomenclature et al., 2008). A recent study identified that this feature is, in part, genetically encoded and dependent on the expression of the transcription factor Er81 which can be activity-dependently regulated (Dehorter et al., 2015). Taken together the distinct features of PV neurons are critical for controlling the activity of local microcircuits and

targets in other brain areas, and thereby synchronize different brain areas through the generation of network oscillations, such as theta or gamma oscillations which are crucial for correct neuronal network function (Hu et al., 2014).

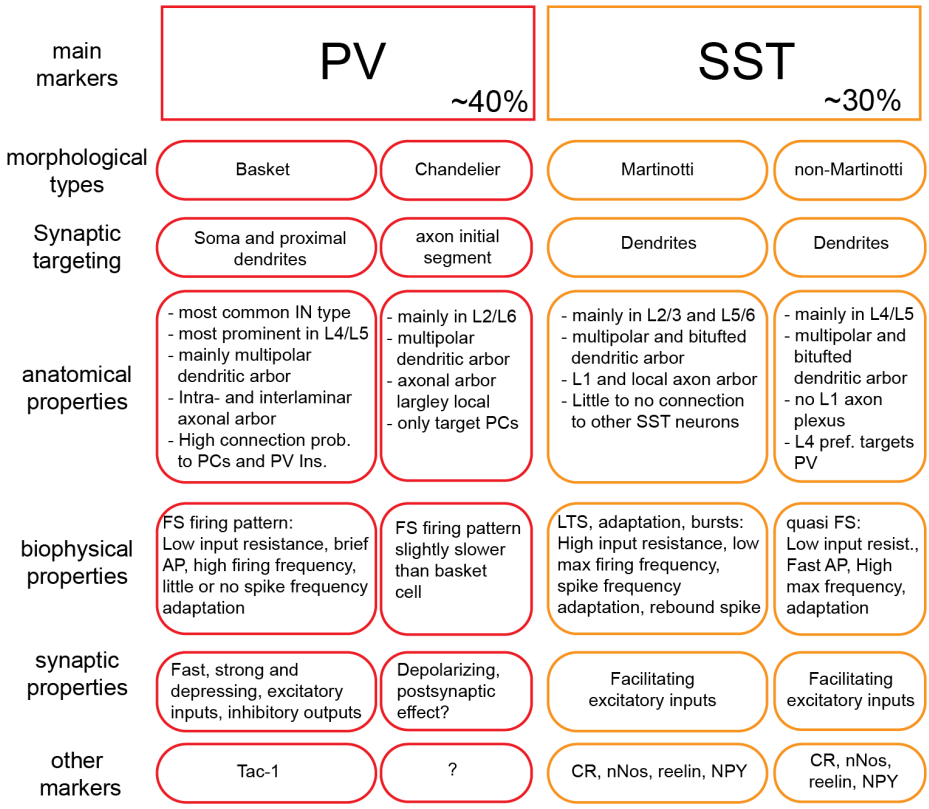

Figure 3: Structural and functional characteristics of PV and SST neurons

Illustration of structural and functional diversity of two main inhibitory neuron classes: parvalbumin (PV) and somatostatin (SST). Percentages within inhibitory neurons only (10-15% of total population). PV and SST neuron classes can be further subdivided into two main cell types: Basket vs. Chandelier for PV; Martinotti vs. non-Martinotti for SST. All of these show distinct properties and can be morphologically and electrophysiologically distinguished.
AP = action potential, FS = Fast spiking, L2/3 = Layer2/3, LTS = Low threshold spiking, PC = principle neuron, prob = probability, resist. = resistance
Adapted from (Tremblay et al., 2016)

Somatostatin interneurons

Somatostatin positive interneurons can be assigned to two major cell populations: Martinotti, which represent the majority of SST neurons, and non-Martinotti cells. These two SST classes can be morphologically and electrophysiologically distinguished (Tremblay et al., 2016) (Figure 3). In contrast to parvalbumin positive interneurons, SST neurons are targeting dendrites of pyramidal neurons. Martinotti cells preferentially inhibit the distal dendrites of pyramidal cells, whereas non-Martinotti cells do not possess an elongated axon and have been shown to predominantly target local PV neurons (Figure 2) (Xu et al., 2013). SST neurons also differ

from other interneurons with respect to their excitatory inputs. Generally, interneuron populations display moderately to strongly depressing excitatory synapses. In contrast, in both SST classes, input synapses are strongly facilitating (Pouille and Scanziani, 2004). A feature that is commonly correlated with a low release probability of neurotransmitters at the presynaptic terminal. The facilitating dynamics of excitatory inputs allow the summation of excitatory postsynaptic potentials and the production of supralinear responses. This means that even one single high-frequency burst from the presynaptic neuron is sufficient to induce SST-dependent feedback inhibition (Kapfer et al., 2007).

Hippocampal SST interneurons

In one chapter of this thesis (Results 2.4), we will investigate hippocampal SST interneurons in the context of synaptic specificity and its functional importance in more detail. Thus, I am providing more detailed information on these neurons here.

In the hippocampus, oriens lacunosum moleculare (OLM) neurons display Martinotti cell-like features. They are SST neurons residing in the stratum oriens (s.o) with horizontally extending dendrites and a long axon innervating the distal dendrites of CA1 pyramidal neurons in stratum lacunosum moleculare (s.l.m) (Maccaferri and McBain, 1996; Sik et al., 1995). This is the same area in which direct excitatory input from the entorhinal cortex is transmitted to the hippocampus, forming the temporoammonic (TA) pathway (Maccaferri and McBain, 1995). Estimations indicate that a single CA1 pyramidal neuron is innervated by ~10 synapses of one OLM interneuron which provide strong, dendritic feedback inhibition (Bezaire and Soltesz, 2013). In turn, OLM cells receive their main excitatory input from CA1 pyramidal neurons (Sun et al., 2014) which display strongly facilitating properties. CA1 pyramidal neurons fire in distinct temporal patterns – theta and ripple oscillations (Klausberger et al., 2003). During theta oscillations, OLM neurons initially exhibit weak inhibition onto distal CA1 dendrites. However, their mediated inhibition gains strength over time and in response to repeated activation or ripples. Thus, hippocampal network activity can be modulated in a state-dependent manner by OLM interneurons (Klausberger et al., 2003; Müller and Remy, 2014). GABAergic synapses are distributed along the dendrites of CA1 pyramidal neurons. Importantly, SST neurons of the s.o, preferentially activate nonlinear outward-rectifying α5-subunit-containing $GABA_A$ receptors at the distal dendrites of CA1 pyramidal neurons (Schulz et al., 2018). Thus, investigation of inward and outward currents evoked by SST-dependent inhibition in CA1, provides a strategy to investigate alterations in non-linear mediated inhibition dependent on the $GABA_A$-receptor composition. This represents a powerful tool to control action potential output of pyramidal neurons at times of high activity.

OLM interneurons can be identified due to the expression of the neuropeptide SST and extracellular leucine-rich fibronectin containing 1 protein (ELFN1) in the soma and metabotropic glutamate receptor 1α (mGluR1α) and the nicotinic acetylcholine receptor α2 subunit (nACHRα2) in dendrites (Ishii et al., 2005; Klausberger et al., 2003; Sylwestrak and Ghosh, 2012) Furthermore, glutamatergic input can be identified based on the high levels of mGluR7 (Shigemoto et al., 1996; Somogyi et al., 2003). Importantly, these genes not only allow us to molecularly identify these neurons, but they are also highly involved in specifying synaptic and functional properties of OLM interneurons. An example describing the importance of the Elfn1 for target-selective synapse specification is given in more detail in section 1.3.4.

Another example of how molecular identification of genes can be used to functionally investigate aspects of OLM interneurons, is a novel mouse model generated by the Kullander laboratory using cre driven expression under the Chrna2 promoter (Chrna2-cre mice) (Leao et al., 2012). Hippocampal CA1 pyramidal neurons receive two major excitatory inputs: Intrahippocampal information is processed from CA3-CA1 via the Schaffer collateral (SC) pathway at proximal dendrites of CA1 pyramidal neurons, in *stratum radiatum* (s.r). Whereas information from layer III of the entorhinal cortex is transmitted via distal CA1 dendrites in s.l.m forming the temporoammonic pathway. Previous studies suggested that Schaffer-collateral CA1 long-term potentiation (LTP) is enhanced and TA-dependent LTP is suppressed by nicotine, respectively (Nakauchi et al., 2007). Given that OLM interneurons express high levels of the nicotinic acetylcholine receptor α2 subunit (nACHRα2) in dendrites, Leao and colleagues investigated whether this phenomenon was mediated by OLM interneurons (Leao et al., 2012). Using the novel Chrna2-cre mouse line, combined with electrophysiological recordings and voltage dye imaging, they demonstrated that, similarly to what has been observed with application of nicotine, OLM interneurons modulate LTP from the entorhinal cortex onto CA1 pyramidal neurons due to inhibition of the temporoammonic pathway. However, they facilitated SC LTP by inhibiting interneurons which synapse onto the proximal dendrites of CA1, where CA3 excitatory input is mediated. Thus, OLM interneurons contribute to gating the hippocampal-mediated information flow.

In sum, within brain areas such as the hippocampus, excitatory pyramidal neurons and PV and SST interneurons from highly functional neuronal clusters of microcircuits. Each of the neuronal subtypes contributes to brain function by precise, but distinct, synaptic targeting of their post-synaptic neurons, and their synaptic properties which can be molecularly defined.

1.2.2 The developmental origin of cortical neurons

The molecular diversity and function of a given interneuron class appears to be specified early during development (Kepecs and Fishell, 2014). Almost all cortical GABAergic interneurons arise from one of the two embryonic progenitor zones, the medial ganglionic eminence (MGE) or caudal ganglionic eminence (CGE) (Anderson et al., 1997). Specifically, progenitors of the MGE give rise to PV and SST positive interneurons, whereas VIP neurons are derived from CGE progenitors (Kepecs and Fishell, 2014; Marin and Müller, 2014). At the initiation of migration, these interneurons are post-mitotic and first migrate along well-defined tangential routes into the developing neocortex. Only after reaching the cortex, they start migrating radially to reach their target layer (Marin, 2013). Importantly, transcription factors that are unique for a given interneuron population are already present in the progenitor neurons and are still expressed in neurons once they have reached their target region. However, there is an ongoing debate of whether interneurons acquire their distinct identity already shortly after birth when becoming post-mitotic, or whether their identity is mainly established when they have reached their target region and started to interact with the cortical environment (Wamsley and Fishell, 2017). Recent studies supported the hypothesis that MGE- and CGE-derived interneuron subgroups already acquire a molecularly distinct transcriptome shortly after exiting the cell cycle (Mayer et al., 2018; Mi et al., 2018b). This indicates that the fate of a neuron is already established early in life, is intrinsically determined and provides the foundation for functional interneuron diversity. Thus, activity-dependent mechanisms might not modulate interneuron diversity, but rather play more important roles for development and refinement of cortical circuits later in life (De Marco Garcia et al., 2011).

Opposing to what is observed in interneurons which undergo intensive migration before integrating into their target area, cortical glutamatergic excitatory neurons are derived from progenitor cells residing in the ventricular or subventricular zones. These are multipotent and give rise to any class of pyramidal neuron by changing their fate in a defined temporal order. The daughter cells then migrate radially in an inside-out fashion – early born neurons form deep, late born neurons form superficial cortical layers as they migrate along already integrated pyramidal neurons and form the emerging neocortical wall (Franco and Muller, 2013). Interestingly, already in the 1980s transplantation experiments in young ferrets demonstrated that the fate of cortical excitatory neurons was genetically defined (McConnell, 1988). Further transplantation experiments of embryonic (E18.5) neurons into the cortex of adult mice showed that, after injury, these neurons mature into functional pyramidal neurons which appropriately integrate into the existing, mature cortical circuits (Falkner et al., 2016). Thus, this suggests that, neuronal migration and diversity for both glutamatergic and GABAergic cells is molecularly encoded and is later fine-tuned by neuronal activity and

interactions of cells with their environment. Therefore, there must be molecular markers to assign neurons to a certain cell class.

1.2.3 Molecular profiling to characterize cell types

Starting from pioneer work from Ramón y Cajal until today, scientists are intrigued by the challenge to classify morphologically distinct neurons into certain classes and to understand the underlying molecular mechanisms of neuronal diversification. Thus, the systematic categorization of cell types is one prerequisite to further understand individual functions of neuronal cells. Until recently, neuron cell class categorization was proven to be a highly laborious task due to limitations in methods and were mainly obtained from separate efforts describing either morphological, physiological, molecular or connectivity categories. However, recent advances in genome-wide methods improved the ability to assess transcriptomes of single cells in an unbiased manner. This unraveled that all of the previously individually assigned properties of neurons including morphology or synaptic connectivity, actually match with neuron classes identified purely based on their transcriptome. Thus, these joint efforts revealed a stunning, highly complex, picture, that suggests a much larger neuronal diversity than previously thought.

Single cell deep-RNA sequencing allows us to gain access to the transcriptome of thousands of individual cells and has advanced our understanding of how neurons are defined into the different major interneuron classes or pyramidal cells. Tasic and colleagues isolated excitatory and inhibitory neurons of the visual cortex or anterior lateral motor cortex using available cre driver lines combined with FACS (Fluorescence activated cell sorting) followed by single-cell deep sequencing (Tasic et al., 2016; Tasic et al., 2018). Using this strategy, they identified 19 glutamatergic and 23 GABAergic transcriptomically distinct cell types in visual cortex (Tasic et al., 2016). Thus, major interneuron classes like SST neurons cannot only be separated into martinotti vs. non-martinotti cells, but are comprised of at least six transcriptomic subtypes. Importantly, there was also a certain correlation between transcriptomically identified cell types and previously known morphological and electrical properties for interneurons or long-range projection specificity (Tasic et al., 2016; Tasic et al., 2018). Thus, the function and target specificity of neuronal cells is molecularly defined.

One additional major goal of cell type classification is to identify new markers and candidate determinants that can be used to obtain more insight on cell-type specific function. Recently, it has been investigated whether there are gene families whose differential expression could give information about the underlying core identities of GABAergic neurons

in the cortex (Paul et al., 2017). Interestingly, this single cell transcriptomic analysis of six genetically labelled interneuron populations revealed that gene families implicated in regulating synaptic communication (e.g neurotransmitters, ion channels, cell-adhesion molecules) best distinguished different neuronal cell populations. Thus, the authors proposed that the architecture of synaptic molecules represents key determinants in giving a neuron its identity.

1.2.4 Dynamics of transcriptomic diversity

The function of neuronal circuits relies on genetically determined programs. However, activity-dependent transcriptional responses represent an additional layer of complexity since they lead to the fine-tuning of cellular adaptions for appropriate brain function. Sensory experience can be used as one means to identify changes in activity-dependent transcription by exposing dark-reared mice to light for a certain amount of time (Spiegel et al., 2014). Studies implementing RiboTRAP, a method that allows isolation of cell type-specific RNA associated with the ribosome by the use of cre-driver lines (Sanz et al., 2009), have begun to dissect activity-dependent gene expression programs in glutamatergic vs. GABAergic neurons and their functional implications for synaptic function in response to light stimulation (Spiegel et al., 2014). Furthermore, the authors identified the transcription factor Npas4 to be expressed in both excitatory and inhibitory neurons and to regulate divergent down-stream transcription programs for synaptic function (Spiegel et al., 2014). However, despite this progress, a comprehensive, unbiased understanding of which cell types respond to a specific sensory stimulus was still lacking. Thus, Hrvatin and colleagues performed unbiased single cell RNA sequencing of RNA obtained from the visual cortex after periods of visual stimulations. They could classify cells into 30 different cell types (including excitatory, inhibitory, non-neuronal cells) and identified more than 600 stimulus-responsive genes, some of which exhibited highly selective cell type or layer specific regulation (Hrvatin et al., 2018).

Taken together, these studies provide additional information on transcriptional changes induced by acute sensory experience and neuronal activity. These large-scale analyses of alterations in cellular states will be crucial for intersecting our knowledge on cell type-specific gene expression programs and their potential to regulate neuronal network function in response to neuronal activity.

1.2.5 How many cell types are there?

There is a growing body of literature illustrating cell type diversity in the mouse neocortex. Similar analyses of static or dynamic gene expression programs in other brain areas will be essential for obtaining a more complete understanding of neuronal function in the central nervous system. In the hippocampus, anatomical, morphological and synaptic innervation properties lead to the classification of 21 different GABAergic and at least three CA1 pyramidal neuron types within CA1 (Klausberger and Somogyi, 2008). A deep sequencing study from the Linnarsson lab reinforced the view that CA1 pyramidal neurons only exhibited minimal differences in gene expression since they could only identify two CA1 neuron types (Zeisel et al., 2015). This was surprising given that there had been several lines of evidence that suggested that the CA1 region displayed differences in anatomical and physiological properties along the dorsal-ventral or superficial-deep axis (Dougherty et al., 2012; Malik et al., 2016; Mizuseki et al., 2011). Thus, CA1 pyramidal neuron diversity was systematically assessed with second generation RNA sequencing of pools of cells (Cembrowski et al., 2016). This study compared CA1 gene expression profiles along the dorsal-ventral and proximal-distal axis; and superficial-deep layers. With this approach, they identified highly divergent transcriptomic gradients along these axes. Furthermore, the differences in CA1 dorsal-ventral pyramidal neuron types was as pronounced as compared to distinct pyramidal cell types, such as CA1 vs. CA3 neurons. Importantly, this heterogeneity within a given cell type seems to be a common feature of other hippocampal glutamatergic neurons like CA3 or subiculum pyramidal neurons (Cembrowski and Spruston, 2019). This supports the hypothesis that pyramidal neurons exhibit a similar cell type complexity as GABAergic interneurons.

However, where do we start and where do we end? Single cell transcriptomics have started to broaden our knowledge on the diversity of cell types, but how do we intersect this with the activity-dependent regulation of transcripts? Is it really true that deep and superficial layers of the CA1 region display so many different cell types? Or could this be reflecting differential states of neurons due to their divergent activity patterns and inputs? Therefore, pure transcriptomics will also reach their limits and it will be important to further link the types of neurons with their activity states, intrinsic properties and synaptic connections.

As a concluding statement of this chapter, I would like to point out that the advances characterizing neuronal cell classes has tremendously expanded our knowledge on neuronal sub type-specific gene expression programs. Furthermore, I would like to emphasize that we are only starting to appreciate the complexity of neuronal cells. Research aimed to further link

the genetic determinants of neuronal diversity with functional and target specificity will be essential to further understand neuronal network function.

1.3 Transcriptomic diversity and synaptic specificity

The central nervous system consists of billions of neurons which are morphologically and functionally distinct from each other and which need to form functional connections to ensure brain function. How does a single neuron recognize its correct wiring partner among the billions of potential partners? This task is even more daunting as it has been estimated that the interactions between neurons can comprise ~10^{15} synapses. The chemoaffinity hypothesis established by Sperry in 1963 poses that neurons recognize their synaptic partners due to molecular identification signals present on each neuron that exhibit chemical affinities (Sperry, 1963). Since then, a lot of effort has been made to understand the underlying molecular mechanisms of synaptic target specificity and the role this plays in the functional diversity of neuronal synapses.

The immense complexity of neuronal networks nicely illustrates that the genetic repertoire of genes (~20.000) alone cannot be solely accountable for the protein diversity needed to assign specific recognition codes to individual synapses of neurons. In the following chapter, I will discuss the complexity of neuronal wiring and its dependence on a large diversity of cell surface recognition modules that contributes to synapse specification. Furthermore, I will describe how the immense transcriptomic diversity can be generated by post-transcriptional mechanisms including alternative splicing and alternative transcription start sites. This will be exemplified on cell adhesion molecules and will highlight the functional importance of trans-synaptic complexes for appropriate neuronal communication based on single gene studies. In the course of this PhD thesis, I will be investigating the hypothesis that post-transcriptional mechanisms contribute to synaptic specificity. Therefore, I am providing more information on diversification by these mechanisms in the following section

1.3.1 Generation of transcriptomic diversity

The limited genetic possibilities raise the question whether the specific features of recognition molecules are instructed by molecular programs - and if, how this is encoded by a limited number of genes. Alternative splicing and alternative transcription start sites have come forward as key post-transcriptional mechanisms to expand the coding power of the genome.

This has been reinforced by estimations that 95-100% of human gene products are diversified by alternative splicing (Pan et al., 2008; Wang et al., 2008) and that >50% of all genes exhibit alternative transcription start sites (Carninci et al., 2006). More recently, a genome-wide survey of alternative splicing regulation across species (humans, mouse, chicken) and a multitude of organs (including brain, muscle, heart, liver), revealed that the brain exhibits the highest degree of diversification by alternative splicing (Tapial et al., 2017). However, the brain is not one massive structure comprised of one type of cells. It consists of neuronal cells and neuronal precursors, but also non-neuronal including glia and epithelial cells, to name a few. Surprisingly, deep bulk RNA-sequencing experiments showed that neuronal cells and precursors differ from other cell types in the brain by exhibiting the highest degree of diversification by differential exon usage (Gokce et al., 2016; Zhang et al., 2014). Therefore, it is becoming increasingly clear that neuronal cells undergo a striking degree of post-transcriptional diversification. Yet, there is still an ongoing debate about the respective contributions of alternative splicing and alternative transcription start sites to the transcriptional diversity of neuronal cells (Pal et al., 2011; Reyes and Huber, 2018).

Alternative pre-mRNA splicing requires the differential usage of splice sites (the different types of alternative splicing regulation are summarized in Figure 4A). The most commonly used alternative splicing event is the “cassette exon”, meaning that one single exon can either be included or skipped leading to two different protein isoforms. One example illustrating the power of this event is a motor-neuron derived isoform of *agrin*, containing additional exons (Z+ *agrin*). Only neurons incorporate the exons necessary to synthesize the Z+ agrin transcript. The resulting protein increases the clustering of acetylcholine-receptors on the muscle surface directly beneath the nerve terminal by ~1000 fold in comparison to Z- agrin proteins, thereby greatly modulating synaptic transmission at the neuromuscular junction (Ruggiu et al., 2009). Another example for the modulation of receptor function by alternative splicing at glutamatergic synapses are the flip-flop variants of the GluA1 subunit of α-amino-3-hydroxy-5-methyl-4-isoxazolepropionic acid receptors (AMPAR). Mutually exclusive inclusion of either of two adjacent exons leads to the generation of two different AMPAR with different pharmacological and kinetic properties in response to glutamate (Sommer et al., 1990). Alternative splicing is not only required for diversification, but is also a key process for transcript localization and stability by modifying the 3’ ends of transcripts (alternative last exon), including coding and non-coding parts of the transcript (Taliaferro et al., 2016; Tushev et al., 2018). Furthermore, alternative splicing can control gene expression through transcript abundance and mRNA stability by targeting transcripts to nonsense-mediated mRNA decay (NMD) (Black, 2003; Lejeune and Maquat, 2005).

Furthermore, a recent study provided a novel, activity-dependent mechanism that uses intron retention to rapidly modify the transcriptome of cortical neurons upon neuronal activity (Mauger et al., 2016). Synthesis of new transcripts is dependent on the elongation rate during transcription which can be between 1-4kb/min and can thus take up to several hours for longer genes (Singh and Padgett, 2009; Veloso et al., 2014). Splicing, on the other hand, only takes seconds to minutes (Martin et al., 2013). Interestingly, intron excision was already induced 15 min after neuronal stimulation and was robustly observed for transcripts of different lengths, but was enriched for long genes (Mauger et al., 2016). Thus, the mechanism described by Mauger and colleagues provides a rapid transcription independent way for intron-retaining transcripts to become functional mRNAs, which are then exported into the cytoplasm to fulfill their specific function in an activity-dependent manner. Importantly, the activity-dependent intron excision is dependent on N-methyl-D-aspartate (NMDA) receptors and calmodulin-dependent kinase (CamK)-activating pathways (Mauger et al., 2016) and could thus, play a critical role in rapidly transcribing genes necessary for synaptic plasticity and learning. This hypothesis could be further supported by an *in-vivo* study in *Drosophila*. Long-lasting memory consolidation in *Drosophila* is, in part, mediated by the Orb2 protein (Keleman et al., 2007; Krüttner et al., 2015). In a recent study, Gill and colleagues demonstrated that *Orb2A* exists in a non-protein coding form due to a retained intron in the mRNA. During behavioral experience and intrinsic motivation, the intron gets excised by the RNA-binding protein (RBP) passilla (a homolgue of the mammalian Nova protein) which leads to the production of the Orb2a protein. This step was crucial for the formation of long-term memory consolidation and demonstrated the importance of activity-dependent splicing for an animals' behavior (Gill et al., 2017).

Additionally, the usage of alternative transcription start sites can also greatly expands the diversity of individual genes (Figure 4B). These alternative first exons can contain alternative promoters that are required for accurate transcription and control of gene expression. A well-known, example is the brain-derived neurotrophic factor (Bdnf), whose transcription can be regulated by nine alternative promoters, which are believed to give rise to the same protein (Barde et al., 1982; Timmusk et al., 1995). However, recent evidence suggested that there could be tissue specific expression of different Bdnf transcripts with selective molecular and behavioral functions (Maynard et al., 2016).

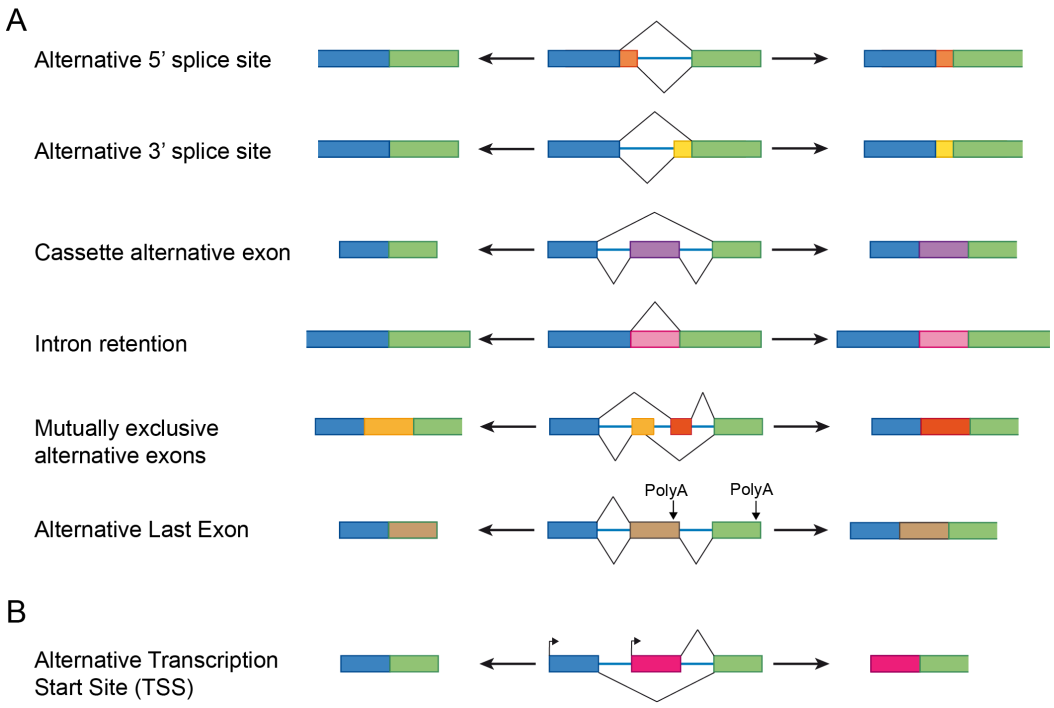

Figure 4: Schematic for diversification by alternative splicing or alternative promoter usage

Illustration of diversification by A) alternative splicing or B) differential promoter usage (Alternative Transcription Start Sites (TSS). Different patterns of alternative splicing regulation include Alternative 5' donor splice site, Alternative 3' Acceptor splice site, Alternative Cassette exons, Intron retention, mutually exclusive exons and Alternative Last Exon (ALE). Constitutive exons are marked in blue and green. Two possible outcomes are depicted on the left or right of the splicing event depicted in the middle. Adapted from (Black, 2003; Nilsen and Graveley, 2010).

The varied patterns of alternative splicing regulation raise the question of how the alternative splicing regulation is controlled. A central challenge for constitutive or alternative pre-mRNA splicing is the selection of correct pairs of donor and acceptor sites which have to be joint after intron or exon removal. In general, pre-mRNA splicing enables intron excision and exon incorporation and is catalyzed by the spliceosome machinery. The spliceosome consists of five small nuclear ribonucleoproteins (snRNPs) – U1, U2, U4, U5 and U6 with more than a hundred auxiliary proteins (Chen and Manley, 2009; Grabowski and Black, 2001). It recognizes sequence elements on the target mRNA which include 5' and 3' splice sites, branching points and the polypyrimidine tract, elements which define exons. Further splicing decisions are mainly achieved through *cis*-acting sequences to enhance or silence the splicing of exons or introns. In a second step, *trans*-acting factors, like splicing factors are recruited to modulate the access of the spliceosome. For example, positive regulators recruited to enhancer splice sites will facilitate its recognition and the recruitment of U1 snRNP to the 5' splice site and U2A to the 3' splice site of the intron; whereas binding of negative regulators to the polypyrimidine

tract will prevent the binding of snRNP subunits like U2A to the 3' splice site. Successful mRNA processing is completed after ligation of consecutive pairs of donor and acceptor splice sites, leading to the incorporation or exclusion of exons and introns, respectively (Black, 2003; Breitbart et al., 1987; Chen and Manley, 2009; Grabowski and Black, 2001)

Taken together, alternative splicing and alternative transcription start sites can be viewed as means to generate transcriptomic diversity and thereby modulate protein function. Genome-wide studies identified that alternative splicing was highest in neuronal tissue. Given the immense complexity of the mammalian brain and its synaptic connectivity, it is conceivable that transcript diversification is used by neuronal cells to specify their identities and synaptic wiring properties. Large-scale transcriptomic studies have been conducted to assess the power of alternative splicing in distinct organs and between cardinal classes of cells. However, given the diversity of neuronal cell types, it will be crucial to further determine alternative splicing choices in neuronal subclasses to obtain a more complete picture of how the striking precision of neuronal communication can be achieved.

1.3.2 Neuronal wiring through self-avoidance

It has been speculated for decades that complex neuronal wiring could be achieved by the extensive usage of divergent transmembrane isoforms present at individual synapses. Indeed, there are some families of neuronal recognition molecules exhibiting large-scale isoform diversity, like the fly Down Syndrom cell adhesion molecule 1 (*Dscam1)* and the family of Protocadherins (*Pcdh*) or Neurexins (*Nrxns)* in vertebrates. The immense diversity of these, and other surface molecule families, is achieved by alternative splicing and the use of alternative promoters, generating thousands of transcript isoforms from single genes. Thus, they provide intriguing candidates to find a molecular code for directing specific synaptic connectivity.

To date, *Drosophila Dscam1* represents one of the most impressive examples for illustrating the diversity of cell surface receptors and their ability to control neuronal connectivity. DSCAM is a single pass transmembrane protein belonging to the immunoglobulin (Ig) superfamily member containing nine Ig domains in the extracellular part of the protein (Schmucker et al., 2000). The *Drosophila Dscam1* gene undergoes extensive alternative splicing and contains three arrays of alternative exons 4, 6 and 9, which contain 12, 48 and 33 mutually exclusive exons, respectively (Sun et al., 2013) (Figure 5A). These exons are complemented with 20 constitutive exons which encode two alternative transmembrane domains. The alternative

exons are spliced in a mutually exclusive manner to ensure that always only one single alternative exon is included into the final transcript. This combinatorial approach leads to the generation of 19,008 different extracellular domains which are linked to one of the two transmembrane segments, resulting in 38,016 different *Dscam1* isoforms (Schmucker et al., 2000; Wojtowicz et al., 2004). Remarkably, 18,496 of the potential 19,008, could be detected by sequencing (Sun et al., 2013). Analysis of splicing reporters revealed that alternative splicing choices in the *Dscam1* gene are probabilistic in individual neurons and change over time (Miura et al., 2013). Thus, each neuron can be composed of a unique set of *Dscam* receptors which provide cell recognition diversity.

Probably the most important function of DSCAM1 is to regulate cell-surface recognition between pre- and postsynaptic neurites in the developing *Drosophila* nervous system. In 2004, Wojtowicz and colleagues demonstrated that every *Dscam1* isoform tested had different recognition specificities in *in vitro* binding assays. Each isoform showed splice isoform-specific homophilic but little to no heterophilic binding (Wojtowicz et al., 2004). During the outgrowth of axons or dendrites, branches from the same neuron need to avoid each other to provide appropriate spreading of synaptic terminals onto postsynaptic neurons. Thus, it is an attractive hypothesis that homophilic interactions between the thousands of cell-specific *Dscam1* isoforms provide the molecular basis for self-recognition, interaction and consequently sister-branch repulsion. Interestingly, knock out of the Dscam1 gene lead to gross deficits in self-avoidance, and re-expression of any single isoform in neurons is sufficient to restore appropriate axon guidance and dendrite branching (Hattori et al., 2007; Matthews et al., 2007; Soba et al., 2007; Zhan et al., 2004). Therefore, the diversity of the Dscam1 gene instructed by alternative splicing provides an elegant way to mediate neuronal wiring specificity in the *Drosophila* nervous system.

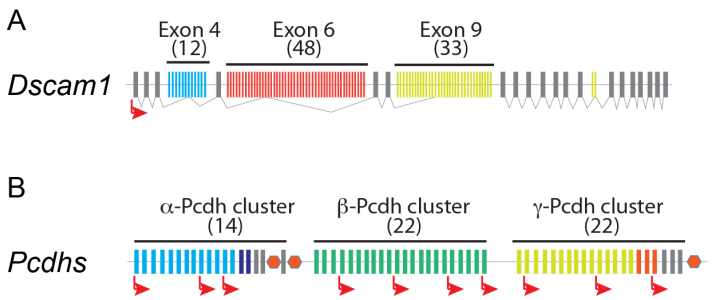

Figure 5: Genomic organization of *Dscam1* and protocadherins (*pcdhs*)

A) The *Dscam1* gene is transcribed from one promoter, but exhibits three alternative splicing clusters 4 (blue), 6 (red) and 9 (yellow) with 12, 48 and 33 alternative exons, respectively. Only one alternative exon is incorporated into the mature transcript. Through this combinatorial approach 38,016 isoforms can be theoretically generated.

B) Simplified illustration of the protocadherin (pcdh) locus with three clusters: α-Pcdh, β-Pchd, γ-Pcdh transcripts can lead to 58 different isoforms which are expressed from individual promoters preceding the alternative exons (exons in blue, green and yellow, some selected promoters are indicated with red arrows. Adapted from (Schreiner et al., 2014b).

In the late 1990s the discovery of clustered protocadherins (Pcdhs) in vertebrates lead to the hypothesis that these cell surface receptors could play analogous roles to the *Drosophila Dscam1*. Thus, providing unique cell surface identities for self-avoidance and appropriate synapse formation in the mammalian central nervous system (Zipursky and Grueber, 2013). Clustered Pcdhs are organized in three clusters, alpha (α)-Pcdh, beta (β)-Pchd and (γ)-Pcdh transcripts with 14, 22 and 22 alterative exons, respectively (Wu and Maniatis, 1999) (Figure 5B). In Pcdhα and Pcdhγ clusters, these variable exons encode the extracellular domain comprising ectodomain (EC) 1-6 that are spliced into a common cytoplasmic tail. The transmembrane domain and short cytoplasmic tail are encoded by constitutive exons. Moreover, each variable exon possesses its own promoter. Single cell PCRs of cerebellar Purkinje neurons linked alternative promoter usage to a stochastic expression of multiple, divergent receptor variants in each neuron. Each Pchdβ cluster on the other hand is encoded by a single, variable exon (Esumi et al., 2005; Kaneko et al., 2006; Tasic et al., 2002; Wang et al., 2002).

The hypothesis that *pcdhs* are the counterparts of *Drosophila Dscam1* in vertebrates with respect to self-avoidance, is supported by several lines of evidence. It has been demonstrated that Pcdhs promote isoform-specific homophilic recognition. Moreover, Pcdhγ clusters form homo-tetramers and hetero-tetramers. Preferential recognition and trans-cellular interactions were highest when all variants of the four variants in the interacting tetramer were perfectly matched (Rubinstein et al., 2015; Schreiner and Weiner, 2010). Thus, even if the theoretical number of Pchd isoforms is much smaller than for *Dscam1*, the combinatorial use of alternative promoters and tetramer formation provides a powerful tool to expand the diversity of Pcdh surface receptors. Second, a study in mouse retinal cells and cerebellar Purkinje neurons revealed that Pcdhγ receptors are important for self-avoidance (Lefebvre et al., 2012). Genetic removal of all 22 exons of the pcdhγ locus lead to disrupted self-avoidance of dendrites in retinal starburst amacrine cells (SACs) and cerebellar Purkinje neurons. Under normal conditions SAC dendrites make contacts with other SAC cells. However, removal of Pcdhγ-cell surface receptor isoforms lead to extensive crossing of sister dendrites and dendrite bundling both in the retina and in the cerebellum. Importantly, these phenotypes could be rescued by the re-expression of an arbitrarily chosen isoform, especially when the same isoforms were present in neighboring cells (Lefebvre et al., 2012). Further studies on the *pcdh*

family indicate their diverse roles in the nervous system including neuronal survival, synapse formation and dendritic arborization (Chen and Maniatis, 2013)

Taken together, the diversity of cell adhesion molecules, either established by classical alternative splicing or by alternative promoter usage provide a powerful tool for accurate neuronal wiring and function of neuronal circuits.

1.3.3 Trans-synaptic molecular recognition codes

Surface receptors like Dscam1 or Pchd contribute to neurite guidance by self-avoidance. Self-recognition is necessary to distinguish the identity of a given neuron from others. However, it does not induce the formation of synapses. Thus, a remaining question in neurobiology is how specific synaptic connections can be generated. Synapses represent highly asymmetric structures and require bidirectional signaling to coordinate the adequate matching of pre- and postsynaptic membranes to ensure efficient neurotransmission. Trans-synaptic adhesion complexes with synaptogenic properties have been identified to be involved in this process. These include the cell adhesion molecules Neurexins (NRXN) and Neuroligins (NL), which form trans-synaptic connections (Dean et al., 2003; Nguyen and Sudhof, 1997; Scheiffele et al., 2000). Trans-synaptic interactions between these proteins will further be discussed in the results section 2.1 of my PhD thesis. Therefore, more information on them is given below.

Co-culture assays between non-neuronal HEK293 (Human embryonic kidney) cells and neurons from pontine extracts, which normally do not form synapses between each other, have demonstrated that ectopic expression of post-synaptic NLs in HEK293T cells promoted the formation of *de-novo* presynaptic structures containing vesicle clusters (Scheiffele et al., 2000). However, not only NLs exhibit synaptogenic functions. NRXNs have also been demonstrated to induce presynaptic structures and trigger the formation of GABAergic and glutamatergic terminals via interactions with NL (Dean et al., 2003; Graf et al., 2004). Importantly, the respective trans-synaptic interactions for the formation of glutamatergic or GABAergic synapses were dependent on alternative splicing of both *Nrxn* and *Nlgn* (Chih et al., 2006). Thus, NRXN-NL complexes represent candidates to explore how trans-synaptic signaling contributes to the regulation of synaptic specificity in the brain.

The Diversity of Neurexins

Neurexins are transmembrane proteins that were first identified as receptors for the black widow spider toxin α-latrotoxin, which induces massive neurotransmitter release (Ushkaryov

et al., 1992). The mammalian nervous system contains three *Nrxn* genes, each of which can be transcribed from two alternative promoters leading to the generation of six transcripts encoded by α-Nrxns and β-Nrxns genes (Tabuchi and Sudhof, 2002). These genes encode identical carboxy-terminal transmembrane regions and cytoplasmic tails but differ in their extracellular sequences. α-*Nrxns* contain six LNS (laminin, Nrxn, sex-hormone-binding globuline) domains interposed with three epidermal growth factor (EGF)- like domains. β-*Nrxns* on the other hand, only contain one LNS domain which corresponds to the α-Nrxns LNS6 domain, with the exception of one amino acid (Ushkaryov et al., 1992). Both Nrxn proteins undergo post-translational modifications in the form of N- and O-glycosylation (Ushkaryov et al., 1994; Ushkaryov et al., 1992).

Recently, a novel, still hardly characterized γ-Nrxn trancripts have been identified. It originates from an internal promoter in the Nrxn gene, thereby generating a short γ-Nrxn transcript that exhibits a specific N-terminal sequence that lacks nearly all extracellular domains (Sterky et al., 2017; Yan et al., 2015). Interestingly, this short isoform can induce presynaptic active zone assembly, vesicle accumulation and clustering of Ca^{2+} channels in *C.elegans* motor neurons (Kurshan et al., 2018). However, further studies will be required to understand the function of γ-Nrxns for synaptic function in the mammalian brain.

Importantly, α-*Nrxns* and β-*Nrxns* undergo extensive alternative splicing at six canonical alternative splice segments (AS1-6) which are encoding the extracellular domain (Figure 6A) (Schreiner et al., 2014a; Tabuchi and Sudhof, 2002; Treutlein et al., 2014). Combining all theoretical possibilities including alternative promoters and alternative splicing could give rise to more than 12.000 different isoforms. Of these, more than 1300 different *Nrxn* isoforms could be significantly detected in the mouse brain using PacBio (Pacific Biosciences) – sequencing (Schreiner et al., 2014a). Furthermore, Schreiner and colleagues demonstrated that the transcript diversity increased with the complexity of the neuronal tissue. This mapping of *Nrxn* isoforms further illustrates the extensive diversification through alternative splicing programs which might specify molecular codes for interactions at synapses. Yet, the biological function of individual *Nrxn* splice isoforms still remains to be determined. Moreover, there is an ongoing debate about how many theoretically possible transcripts actually get translated into protein (Tress et al., 2017; Weatheritt et al., 2016). Even if we don't have the full answer for this yet, initial mass-spectrometry analysis for AS3, AS4 and AS6 demonstrated that some of the possible NRXN variants could indeed be detected in the mouse brain (Schreiner et al., 2015).

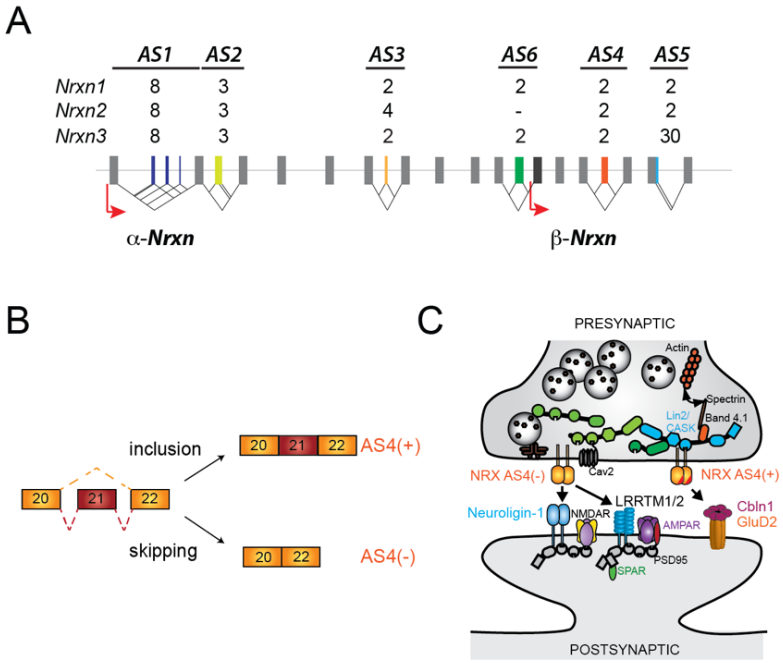

Figure 6: Neurexin diversification by alternative splicing

A) Neurexin genes can be transcribed from two alternative promoters, leading to the generation of alpha and beta Neurexins (*Nrxn*). Moreover, alternative splicing at 6 different alternatively spliced segments (AS) leads to the generation of ~12.000 different isoforms. Adapted from (Schreiner et al., 2014b).
B) Alternative splicing at AS4. Inclusion or exclusion of the alternative exon 21 leads to the generation of AS4(+) or AS4(-) isoforms, respectively.
C) Schematic illustration of trans-synaptic NRXN isoform specificity. AS4(+) and AS4(-) isoforms exhibit different specificities for their postsynaptic partners. NRXN AS4(+) variants preferentially form synapses with e.g Cbln1, whereas NRXN AS4(-) can interact with Neuroligins or Leucine rich repeat transmembrane proteins (LRRTM) 1,2 which in turn recruit and stabilize NMDA or AMPAR.
Selected references (Boucard et al., 2005; Budreck et al., 2013; Chih et al., 2006; de Wit et al., 2009; Matsuda and Yuzaki, 2011; Siddiqui et al., 2010; Uemura et al., 2010)

Functional implications of alternative splicing of Nrxns at AS4

If *Nrxns* are part of a molecular code to instruct synapse specification, it is conceivable that divergent isoforms might be expressed in a cell type-specific manner. On a global level, α and β Nrxn1-3 transcripts are significantly expressed in all brain tissues, with some region-specific enrichments and, in part in an overlapping manner. Their expression patterns suggest that they might be expressed by distinct neuronal populations (Nguyen et al., 2016; Uchigashima et al., 2019; Ullrich et al., 1995). Yet, precise information on which alternative *Nrxn* isoforms are expressed in different neuronal populations has only started to be investigated. Single-cell RT-PCRs (Reverse-transcription polymerase chain reaction) of pairwise cell type comparisons and relative abundance values suggested that *Nrxn* splice isoforms of neurons from the same population were more similar to each other than to other cells (Fuccillo et al., 2015). The

question of cell-class specific expression of *Nrxn* isoforms had also been addressed using Ribotag, a method that allows the isolation of RNA associated with the ribosome in a cre-dependent manner (Nguyen et al., 2016; Sanz et al., 2009) combined with radioactive PCR amplification. This technique allowed more quantitative assessment of absolute isoform transcript amounts. Nguyen and colleagues demonstrated that in the mouse hippocampus, excitatory CA1 neurons and PV+ interneurons contain different pools of Nrxn1 AS6 and Nrxn2 AS2 transcripts. However, the most differential transcript incorporation rates between glutamatergic CA1 and GABAergic PV neurons were the observed at the AS4 splice site for all three Nrxn genes (Nguyen et al., 2016).

The alternative splice site 4 of *Nrxns* represents one of the most studies alternative splice sites. Moreover, this is the *Nrxn* splice site that I have further studied during my PhD. Thus, I will describe its functional implications in more detail here. NRXN AS4 is encoded by a single 90bp long exon 21 (30 amino acids) which can either be included, generating AS4(+) isoforms, or skipped leading to AS4(-) (Figure 6B). These alternative isoforms exhibit different binding affinities for their postsynaptic partners and thereby drastically modify properties of trans-synaptic interactions and the receptor organization of the postsynaptic cell (Figure 6C). The different properties of AS4(+) and AS4(-) are due to conformational changes of the LNS6 module (Koehnke et al., 2010; Shen et al., 2008). The alternative exon encoding AS4 is localized in a loop between two β-sheets. This allows NRXN AS4(-) isoforms to efficiently bind to Neuroligins and LRRTMs, given their overlapping binding epitopes (Chih et al., 2006; de Wit et al., 2009; Ko et al., 2009; Reissner et al., 2013), NLs and LRRTMs in turn recruit and stabiles AMPAR and NMDAR (Budreck et al., 2013; Chih et al., 2005; Shipman et al., 2011). Insertion of the 30 amino acids, causes a re-arrangement of the loop to an α -helix with a prolonged conformation thereby blocking the binding sites for NLs or LRRTMs but instead allows binding to other cell surface receptors like Cerebellin 1 (Cbln) (Reissner et al., 2013; Uemura et al., 2010). Thus, the insertion of a single exon can drastically alter trans-synaptic receptor compositions and might lead to alterations in synaptic signaling.

In-vitro studies convincingly demonstrated that the alternative isoform choice of *Nrxns* at AS4 guides the formation of synapses with specific properties. Intriguingly, alternative splicing at *Nrxn3* AS4 modulates synaptic transmission and plasticity (Aoto et al., 2013). Mice in which the NRXN3 AS4(+) variant was constitutively expressed, exhibited enhanced endocytosis of postsynaptic AMPAR and thus, reduced AMPAR mediated excitatory postsynaptic currents in cultured neurons. To assess alterations in hippocampal LTP, the authors forced the expression of NRXN3 AS4(+) only in CA1 pyramidal neurons, stimulated their axon collaterals and recorded potentiation responses in the postsynaptic neurons residing in the subiculum.

NMDAR-dependent LTP was completely blocked in CA1 output neurons, but could be restored by introducing any of the *Nrxn* AS4(-) isoforms. This suggests that alternative splicing at AS4 of *Nrxn3* trans-synaptically modulates synaptic strength, most likely due to enhanced retention of AMPAR (Aoto et al., 2013). These phenotypes were recapitulated in the hippocampus by global deletion of α/β *Nrxn3* and could be rescued by the sole re-expression of the extracellular domains of NRXN3 AS(-) (Aoto et al., 2015). Interestingly, this was a brain region-specific phenotype. In contrast to the hippocampus, analysis of synaptic transmission in the olfactory bulb showed decreased GABAR-mediated inhibitory responses and alterations in vesicle release probabilities after deletion of α/β *Nrxn3*. Moreover, re-expression of extracellular NRXN3 AS4(-) was not sufficient to rescue the phenotypes in the olfactory bulb. This required the full length α *Nrxn3*, suggesting that the intracellular domain of NRXN3 is required for synaptic transmission in the olfactory bulb (Aoto et al., 2015). Thus, the studies by Aoto and colleagues illustrate context-dependent functions of Nrxn3 splice isoforms.

Recent work by Dai *et al.,* investigated the individual contributions of alternative splicing at AS4 of *Nrxn* 1,2 and 3 to synaptic transmission of CA1 neurons to their output target cells in the hippocampus. They demonstrated that alterations in splicing of either Nrxn1 or 3 genes differentially modulated aspects of postsynaptic NMDAR and AMPAR responses. Thus, constitutive expression of NRXN1 AS4(+) drastically enhanced NMDAR-mediated responses whereas NRXN3 AS(+) suppressed AMPAR-mediated responses, (Dai et al., 2019) as shown previously by Aoto et al. Modulation of alternative splicing of Nrxn2 on the other hand did not affect either. Taken together, work from the Südhof laboratory indicates that divergent isoforms of *Nrxns* exhibit some nonoverlapping functions in the mouse hippocampus. Yet, it would be interesting to know whether these nonoverlapping functions are mainly specific for glutamatergic transmission in the hippocampus or whether they would exhibit other functions in different brain areas or cell types.

Context-dependent functions for alternative splicing at AS4 for *Nrxn1* and *Nrxn3* could also be observed in PV neurons of the hippocampus. Nguyen and colleagues identified that CA1 pyramidal neurons and PV+ interneurons in the hippocampus display divergent AS4(+) and AS4(-) ratios: Glutamatergic neurons preferentially produce the AS4(-) isoform, whereas PV+ interneurons make AS4(+) which also interacted with known AS4(+) binding partners like Cblns (Nguyen et al., 2016). Genetic shift of the splicing pattern in PV neurons from AS4(+) to AS4(-) for *Nrxn1* and *Nrxn3* (*Nrxn1/3*$^{ex21\Delta PV}$ mice) selectively impaired the behavioral performance of these mice in the novel object recognition task. Moreover, it led to an increase in the baseline expression of the neuronal activity marker cFos in CA1 and CA3 (Nguyen et al., 2016). These results indicate that NRXN AS4(+) isoforms might adjust PV neuron mediated inhibition onto target neurons and can modulate recognition memory (Nguyen et al., 2016).

Additionally, a recent study suggested trans-synaptic regulation of post-synaptic kainate receptor function through C1ql2 and C1ql3 and their preferential binding to NRXN Ex25b+, often referred to as AS5(+), at hippocampal mossy fiber to CA3 synapses (Matsuda et al., 2016). Nevertheless, further studies will be needed to characterize the molecular pathways underlying alternative splicing of Nrxns and C1q-like molecules.

The work described in this section illustrates the crucial role of alternative splicing of *Nrxns* for specifying the identity of Neurexin ligands for synaptic specification and function. However, the nervous system relies on precise connectivity between multiple different cell types and thus, requires additional strategies for the instruction of synapse formation.

1.3.4 Target-specific patterns for synaptic connectivity

The specificity of synaptic connections within a neuronal circuit likely involves the integration of multiple different mechanisms that ensure specific patterns of connectivity. Transmembrane proteins are not only important for self-determination and modification of synaptic function, but are also crucial for establishing synaptic connections.

In the cerebellum, for example, NRXN AS4(+) isoforms form tripartite complexes with Cbln1 and GluD2 (glutamate dehydrogenase 2), which are homologous to glutamate receptors but function as cell adhesion molecules (Matsuda et al., 2010; Wei et al., 2012). These complexes regulate the formation of parallel synapses between granule cells and Purkinje neurons. Importantly, synapse formation specifically depends on NRXN AS4(+) since ectopic expression of Nrxn AS4(-) did not induce synapse formation (Uemura et al., 2010).

Despite the power of alternative splicing of *Nrxns* in regulating synapse formation and synaptic properties, there are also other trans-synaptic proteins that coordinate target-specific properties. In the hippocampus, the same CA1 axons can form synapses onto PV neurons which are depressing excitatory synapses, or onto SST interneurons which are strongly facilitating. The formation of different types of synapses is mediated by the expression of the extracellular leucine-rich repeat fibronectin containing 1 (Elfn1) protein expressed in the post-synaptic cell. ELFN1 is highly expressed in SST and absent from PV neurons. Recent studies have demonstrated that it trans-synaptically engages with the pre-synaptic metabotropic glutamate receptor 7 (mGluR7) and GluR6-containing Kainate receptors on the CA1 axons to mediate pre-synaptic release probabilities (Stachniak et al., 2019; Sylwestrak and Ghosh, 2012; Tomioka et al., 2014). Importantly, ectopic expression of ELFN1 in PV neurons,

functionally altered the facilitation properties of pre-synaptic CA1 neurons from normally being depressing to moderately facilitating (Sylwestrak and Ghosh, 2012). These results indicate that postsynaptic molecules can instruct the output properties of their presynaptic interaction partner at CA1-SST synapses in the hippocampus.

In the hippocampus, loss of ELFN1 leads to a drastic reduction of mGluR7 proteins in CA1 axon terminals, suggesting that ELFN1 recruits pre-synaptic mGluR7. However, this does not abolish synapse formation or general synaptic transmission. In the retina, ELFN1 is expressed in presynaptic photoreceptors, rods, and is required for the physical assembly of synapses between rods and their post-synaptic partner, ON-bipolar cells, by recruitment of mGluR6. These connections are crucial for setting the visual threshold (Cao et al., 2015). Thus, in the retina, ELFN1 functions as a pre-synaptic guidance receptor whereas in the hippocampus its predominant role is post-synaptic instruction of presynaptic release. Yet, in both systems interactions mediated by ELFN1 are trans-synaptic and involve metabotropic glutamate receptors to dictate specific circuit properties.

The specificity of synaptic connections also depends on a compartmentalized organization of synaptic connections. Diverse interneuron cell types form synapse onto distinct sites at the postsynaptic neuron. This distribution can be achieved by transcriptional programs already active early during development (Favuzzi et al., 2019). For example, Cbln4 was found to be expressed in SST+ interneurons and chandelier cells and influences the number of pre-synapses formed onto distal dendrites of cortical pyramidal neurons. Miss-expression of Cbln4 in PV neurons led to a significant increase of presynaptic terminals onto the dendritic compartment of pyramidal cells, without modifying synapses normally formed by PV onto the soma or axon-initial segment. Thus, a single, genetically determined factor can greatly contribute to the specific wiring of inhibitory circuits (Favuzzi et al., 2019).

The examples discussed in this entire section serve as illustrations for the immense coding power alternative diversification adds to our genome. However, they also illustrate that within all of this wealth, the same molecular mechanisms also achieve a high degree of specificity. Moreover, I provided examples to illustrate that target specific synapse formation is in part genetically encoded. Thus, fields of neuroscience research have started to dig deeper into a combinatorial code for neuronal wiring specificity.

1.4 RNA binding proteins – keys for identifying a molecular code?

In the previous section, I discussed how alternative splicing is a major driver for diversification of cell adhesion molecules and how it contributes to correct neuronal wiring and synaptic specificity. Thus, spatio-temporal control of alternative splicing regulation is of critical importance for neural development. Splicing regulation is highly dynamic and requires core elements such as donor and acceptor splice sites, the branchpoint and the polypyrimidine tract for spliceosome assembly. The appropriate outcome of alternative splicing is further determined by the activity of *trans-acting* splicing factors, like RNA binding proteins (RBPs). Understanding the key elements underlying alternative splicing regulation in the central nervous system will be of central importance to further dissect molecular codes for neuronal diversity and wiring specificity. Thus, this part of the thesis introduction will cover how alternative splicing choices can be generated and how this impacts neuronal function. This will be illustrated with specific case examples.

RBPs bind exonic or intronic enhancers or silencers of the pre-mRNA and thus, can determine the retention or inclusion of particular exons or introns. Some of the most studied neuronal RBPs include Nova 1/2 (neuro-oncological ventral antigen), the family of Rbfox (RNA-binding-fox), the PTBP (Polypyrimidine tract binding protein) family and members of the STAR (Signal transduction and activator of RNA metabolism) family (Boutz et al., 2007; Galarneau and Richard, 2009; Ule et al., 2005; Vernet and Artzt, 1997; Weyn-Vanhentenryck et al., 2014). The logic of alternative splicing choices by these proteins has not been fully understood. However, recent studies have provided novel insights for emerging principles of alternative splicing in the brain:

First, large-scale transcriptomic mapping of RBP binding sites (motifs) through cross-linking immunoprecipitation (CLIP) studies and mRNA transcript sequencing revealed that alternative splicing choices strongly depend on the motif position relative to the regulated exon. For example, binding of Nova1/2 or Rbfox1/2/3 in the intronic sequence upstream of an exon will frequently lead to exclusion, whereas downstream binding results in exon inclusion (Ule et al., 2006; Weyn-Vanhentenryck et al., 2014). Therefore, the same RBP can have two opposing effects, enhancing and silencing, respectively, and thus, diversifies the alternative splicing choice.

Second, from comparisons across datasets obtained from several different RBPs, the hypothesis emerged that multiple RBPs in a given cell can antagonize or synergize with respect to a single alternatively spliced segment. Antagonistic effects have been demonstrated

for Ptbp1 and nSR100 (neuronal Serine/Arginine-100) during neuronal development in which nSR100 can overcome Ptbp1-mediated repression (Raj et al., 2014), or for Nova and Ptbp1 (Cereda et al., 2014). However, RBPs can also act synergistically, like in the case of some exons commonly regulated by Nova and Rbfox1 (Li et al., 2015). These studies indicate that neuronal alternative splicing programs result from a complex code of co-expression of multiple trans-acting factors (RBPs) with their regulatory functions depending on the cellular context. This further raises the questions of whether and how cell type-specific RBP expression contributes to neuronal specificity.

1.4.1 Cell-class specific action of RBPs

The tissue specific splicing factor Nova2 selectively regulates 591 alternative exons in the mouse brain compared to immune tissues (Ule et al., 2005). This already suggested that Nova2 can exert tissue specific functions in the mammalian body. However, in a recent study by Saito and colleagues Nova2-dependent alternative splicing specificity was observed across excitatory and inhibitory neuron classes within and between different brain areas (Saito et al., 2019). In order to analyze cell type-specific targets of Nova2 in excitatory and inhibitory neurons, the Darnell lab recently applied a novel CLIP method to allow crosslinking of RBPs and their target mRNA in selected cells marked by the cre-lox system (Hwang et al., 2017). Employing this method, Saito *et al.,* now show differential, cell class-specific action of Nova2-dependent alternative splicing regulation on the same transcripts. For example, Nova2 is expressed in both excitatory cerebellar granule cells and inhibitory Purkinje neurons. However, it regulates distinct alternative splicing programs in each of these cell classes leading to transcript diversification. Moreover, Nova2-dependent splicing leads to divergent splicing choices of exons of the same transcripts, thereby altering the function of a single gene in a context dependent manner. Thus, Nova2 function instructed the appropriate development of the laminar structures of cortical excitatory neurons, but not inhibitory neurons, and specifically regulated synapse formation in cerebellar Purkinje cells (Saito et al., 2019).

A second example of cell-class specific alternative splicing regulation by one RBP is a recent study conducted in the Fishell lab (Wamsley et al., 2018). Rbfox1 is a neuron-enriched splicing factor expressed and broadly expressed across many neuronal cell classes (Kiehl et al., 2001). Global knock-out of Rbfox1 leads to alterations in inhibitory transmission onto pyramidal neurons, which could be restored by selective re-expression of the Rbfox1 target vesicle-associated membrane protein 1 (vamp1) in all inhibitory neurons (Vuong et al., 2018).

These two examples indicate that two broadly expressed neuronal RBPs, Nova2 and Rbfox1, regulate transcripts that have important neuronal functions, and that a single RBP can control different splicing events in two populations of neuronal cells. However, it remains a

major question whether there are RBPs that are selectively expressed in neuronal subsets to instruct their properties. Additionally, it is still an open question whether RBPs exert specific actions within cardinal classes of interneurons, like Somatostatin or Parvalbumin positive interneurons or even cell types. For Rbfox1, Wamsley and colleagues reported that it mediated largely non-overlapping splicing programs in SST and PV neurons during neuronal development at P8 (Wamsley et al., 2018). Thus, Rbfox1 may steer cell class-specific alternative splicing programs in inhibitory neurons to further guide appropriate maturation and integration of neurons into functional neuronal circuits.

1.4.2 Investigation of STAR-family RBPs for cell type-specific splicing programs

In the previous sections I described how RBPs regulate alternative splicing. The evidences of cell type-specific action of select RBPs onto target mRNAs lead to the intriguing hypothesis that alternative splicing can shape neuronal connectivity in a cell type-specific manner. However, neuronal RBPs like Nova, Ptbps or Rbfox1 are broadly expressed in the nervous system. During my master and doctoral thesis, I focused on a different class of RBPs: the STAR family which has been implicated in the regulation of gene expression and alternative pre-mRNA splicing (Galarneau and Richard, 2009; Zheng and Black, 2013) Importantly, these proteins are expressed in highly selective neuronal populations and thus, represent good candidates for steering cell type-specific splicing programs for neuronal and synapse specification. Pervious work on these proteins is discussed below.

Members of the STAR family contain K homology (KH)-domain containing RNA binding domains and are highly conserved across species. The STAR family can be divided into three subfamilies: Sam68 (Src-associated substrate in mitosis of 68kDa), QK (quaking) and SF1 (Splicing Factor 1). The Sam68 family consists of the ubiquitously expressed protein Sam68 and its paralogues SLM1 and SLM2 (Sam68-like mammalian proteins 1 and 2) (Di Fruscio et al., 1999; Venables et al., 2004). They share their basic domain organization, ~70% of homology in their amino acid sequence, and are predominantly expressed in the nucleus (Di Fruscio et al., 1999). Sam68, SLM1 and SLM2 contain a single maxi KH-RNA binding domain and achieve specificity of RNA regulation due to homo- and heterodimerization. This has been particularly demonstrated for hetero-dimerization between Sam68 and SLM2 to improve their binding specificity to target mRNAs (Feracci et al., 2016). Moreover, SELEX (Systematic Evolution of Ligands by Exponential enrichment) experiments identified a common RNA binding motif, defined by bipartite U(A/U)AA rich-repeats (Galarneau and Richard, 2009). In

neuronal cells, all three proteins have been shown to regulate alternative splicing of *Nrxns* at AS4 (Ehrmann et al., 2013; Iijima et al., 2014; Iijima et al., 2011). Splice-reporter assays determined that Sam68-, SLM1- and SLM2-mediated splicing of the alternative *Nrxn1* exon was dependent on intronic UA-rich sequences up- and downstream of the target exon (Iijima et al., 2011). Thus, multiple intronic motifs act jointly in regulating alternative splicing of Nrxn1 at AS4.

Interestingly, even though Sam68 and SLM2 have the same consensus motif, only SLM2 and not Sam68 seems to regulate alternative splicing of *Nrxn2* at AS4 (Ehrmann et al., 2013). This selective activity was proposed to be due to the abundance of binding sites around the target exon (Danilenko et al., 2017). Normally, SLM2 regulates the exclusion of *Nrxn2* AS4 due to binding of a 51 nucleotide UA-rich cluster downstream of the target exon (Ehrmann et al., 2013). Duplication of binding sites either upstream and down-stream, or down-stream only of the target exon enabled both Sam68- and SLM2-dependent repression at *Nrxn2* AS4 (Danilenko et al., 2017). This model suggests that the binding motif density within target pre-mRNAs greatly influences the splicing regulation and adds an additional layer for target specificity.

Importantly, while Sam68 is ubiquitously expressed, SLM1 and SLM2 exhibit a highly restricted, non-overlapping expression pattern in the mouse brain (Iijima et al., 2014). In excitatory cells of the hippocampus, SLM1 is expressed in dentate gyrus granule cells, whereas SLM2 exhibits high levels in CA1-3 pyramidal neurons. Furthermore, SLM2 is expressed in subsets of SST and VIP interneurons, all of which exhibit low levels of SLM1 (Iijima et al., 2014; Nguyen et al., 2016). These mutually exclusive expression pattern is achieved by cross-repression between SLM1 and SLM2. Alternative exon inclusions in the *Slm1* mRNA regulated by SLM2, lead to nonsense-mediated mRNA decay and differential protein expression (Traunmüller et al., 2014). Thus, these RBPs provide excellent candidates to investigate cell type-specific alternative splicing programs not only between two major neuron classes, like glutamatergic vs. GABAergic cells, but also within subsets of GABAergic neurons.

The possibility to predict which transcript isoform will be expressed in a particular cell class enabling neurons to exert their specific functions, excites multiple fields of research. However, there is still a long way until we have deciphered how a molecular code for neuronal function comes about. As illustrated in this introduction chapter, neuronal function depends on multiple variables, ranging from individual cell types to highly complex cell adhesion codes for neuronal wiring specificity between individual neurons. Alternative splicing, in part regulated by selectively expressed splicing factors, has emerged as one attractive means to provide a

certain molecular code and thus, further complements the stunning puzzle of cell type diversity and synaptic specificity.

1.5 The dissertation project

The brain exhibits a stunning cellular and anatomical complexity. This includes the variety of different neuronal and non-neuronal cell classes which exhibit a striking precision of synaptic connectivity, ultimately resulting in neuronal circuits that control behavioral output. Much of this neuronal wiring during development is hardwired, for example driven by reproducible temporal routines for cellular growth and molecular cues for synapse formation and specification. Recent deep-sequencing studies have given insight into the transcriptomic diversity within defined neuronal cell types (Tasic et al., 2016). Furthermore, we are starting to better understand the correlation of gene expression to the individual function of neurons or their respective synaptic connectivity (Favuzzi et al., 2019; Paul et al., 2017). However, the contributions of alternative splicing to neuronal wiring, in particular, cell and synapse-specific elements, have been largely overlooked. This is in part because methods for accurate mapping of cell type-specific splice isoforms have been limiting. Interestingly, diversification of alternative splicing is highest in neuronal tissue (Gokce et al., 2016; Tapial et al., 2017). Neuronal phenotypes resulting from disruption of splicing regulators have been very broad, resulting in de-regulation of hundreds of transcripts and severe cellular impairments, often resulting in degeneration. Thus, it remains a major question whether alternative splicing programs encode specific aspects of neuronal or synaptic function, or rather broad aspects of the neuronal transcriptome. Deciphering the logic of alternative splicing regulation in individual cell types will be crucial to further understand neuronal circuit function.

The aim of this thesis project is to unravel the logic of alternative splicing regulation in neuronal cell types and to understand their contribution to neuronal circuit function. In particular, I explored whether there are targeted alternative splicing programs controlling the specification of neuronal and synaptic properties. In order to investigate this, I took different approaches and investigated cell class-specific splicing programs and the functional consequences resulting from the disruption of a specific splicing regulator. Thus, the results chapters of this thesis describe the following sub-projects:

1) Examination of the functional impact of disrupting the neuronal splicing regulator SLM2
2) Performing of deep mapping of cell class-specific alternative splicing programs in the mouse cortex
3) Identify whether the splicing factor SLM2 exhibits unique functions in different cell populations of the mouse hippocampus

2. Results

2.1 Preface

The work presented in the results section of my PhD thesis have been joint efforts with multiple people. Therefore, I am herewith describing individual contributions.
All projects were supervised by Peter, submitted manuscripts have been written amongst co-authors of the studies, the unpublished manuscript was written by me in the context of this thesis.

1) **Control of neuronal synapse specification by a highly dedicated alternative splicing analysis**
   Lisa Traunmüller*, Andrea Gomez*, Thi-Minh Nguyen and Peter Scheiffele published in Science in 2016 (PMID: 27174676)

The work presented in this chapter has been designed and conducted in close collaboration with Andrea M. Gomez, a postdoc in the laboratory and Thi-Minh Nguyen, a previous PhD student.

Specifically, I performed measurements of spine densities, biochemical experiments related to synaptosomal fractionations, surface biotinylation and immuno-precipitations, generation and validation of sequencing and mass-spectrometry data, and behavioral testing of animals. Moreover, I was highly involved in the post-hoc processing of RNA-sequencing and Mass-spectrometry results.

The electrophysiological recordings were performed by Andrea. Thi-Minh generated the Nrxn1 ex21 floxed mice. RNA-sequencing analysis of gene expression and alternative splicing analysis was performed by Frederic Lemoine and Pierre de la Grange (GenoSplice, France) while Mass-spectrometry analysis was carried out by Alexander Schmidt from the Proteomics Core Facility, Biozentrum Basel.

2) **Landscape of of ribosome-engaged alternative transcript isoforms across neuronal cell classes**
   Elisabetta Furlanis*, Lisa Traunmüller*, Geoffrey Fucile and Peter Scheiffele resource manuscript, currently in revision at Nature Neuroscience

The work covered in this part of my PhD thesis was jointly designed and carried out with Elisabetta Furlanis, a fellow PhD student in the lab. Both of us generated and validated the input material for further deep-sequencing analysis and were critically involved in the discussion and processing of the data. Strategies for displaying the data, Gene Ontology analysis and preparation of figures were performed together. Validation of the sequencing

analysis algorithm were joints efforts, in which I performed semi-quantitative PCR reactions and FISH experiments and analysis.

Elisabetta processed the analyzed deep sequencing data with R for Principle Component Analysis (PCA), hierarchical clustering, coverage plots, boxplots and correlation plots. Furthermore, she designed and carried out the experiments for the splicing reporters. Geoffrey, was critically involved in the bioinformatic analysis of gene expression, provided the Sashimi plots and designed and generated the online data website. The gene expression and alternative splicing analysis of the deep sequencing data was performed by Ariane Jolly, Noèmie Robil and Pierre de la Grange from Genosplice. Caroline Bornmann helped with FISH experiments.

3) Cell type-specific actions of SLM2 in specifying synaptic properties

Unpublished data

In the third part of the results section I will present additional data on the function of the RNA binding protein SLM2 in different excitatory or inhibitory neurons of the mouse hippocampus. This part is unpublished and includes data from deep RNA sequencing, electrophysiological recordings and behavioral testing of mice.

Specifically, I generated the input material for the deep-sequencing analysis and was critically involved in post-hoc processing of analyzed data, conducted experiments for histology and quantification, validation experiments, electrophysiological recordings in SST interneurons and behavioral testing of mice.

The deep-sequencing data has been analyzed by Ariane Jolly, Noèmie Robil and Pierre de la Grange (Genosplice, France). Elisabetta was crucially involved in the post-hoc analysis of the deep-sequencing data, generated the PCA, venn diagrams and volcano plots of the sequencing data with R-scripts. Jan Michael Schulz performed electrophysiological recordings using optogenetic stimulation of SST-mediated inhibition onto CA1 pyramidal neurons.

2. Results

2.2 Control of Neuronal Synapse Specification by a Highly Dedicated Alternative Splicing Program

Control of Neuronal Synapse Specification by a Highly Dedicated Alternative Splicing Program

Lisa Traunmüller*, Andrea M. Gomez*, Thi-Minh Nguyen, Peter Scheiffele

Biozentrum, University of Basel
Klingelbergstrasse 50-70, 4056 Basel, Switzerland

Correspondence: Peter Scheiffele, peter.scheiffele@unibas.ch

*** co-first authorship**

One Sentence Summary: The RNA binding protein SLM2 represents a major functional determinant of neuronal function by directing the splice isoform identity of synaptic recognition receptors.

Abstract

Alternative RNA splicing represents a central mechanism for expanding the coding power of genomes. Individual RNA-binding proteins can control alternative splicing choices in hundreds of RNA transcripts, thereby, tuning levels and functions of large numbers of cellular proteins. We found that the RNA-binding protein SLM2 is essential for functional specification of glutamatergic synapses in the mouse hippocampus. Genome-wide mapping revealed a remarkably selective SLM2-dependent splicing program primarily consisting of only a handful of target mRNAs that encode synaptic proteins. Genetic correction of a single SLM2-dependent target exon in the synaptic recognition molecule Neurexin-1 was sufficient to rescue synaptic plasticity and behavioral defects in *Slm2* knock-out mice. These findings uncover a highly selective alternative splicing program that specifies synaptic properties in the central nervous system.

Main Manuscript

Alternative splicing provides a key mechanism for neuron-specific gene expression (Raj and Blencowe, 2015; Schreiner et al., 2014a; Zheng and Black, 2013). An array of RNA-binding proteins broadly expressed in neuronal cells has been implicated in controlling developmentally regulated and neuron-specific alternative splicing programs, with single proteins regulating hundreds of target transcripts (Li et al., 2014; Quesnel-Vallieres et al., 2015; Ule et al., 2005). However, some RNA-binding proteins are selectively expressed in neuronal populations, raising the possibility that they may control cell type- and synapse-specific functions (Norris et al., 2014; Schreiner et al., 2014b).

The KH-domain RNA-binding protein SLM2 is highly expressed in glutamatergic pyramidal cells of the mouse hippocampus and in a specific subset of GABAergic interneurons (Ehrmann et al., 2013; Iijima et al., 2014). In $Slm2^{KO}$ mice, glutamatergic spine synapses formed at normal numbers on the primary apical dendrites of hippocampal CA1 neurons (Fig. 1A,B). Western blot analysis of synaptosome fractions from WT and $Slm2^{KO}$ hippocampi revealed overall normal levels of glutamatergic synapse proteins. However, there was an increase in the AMPA-type glutamate receptor (AMPAR) subunit GluA1, in particular in detergent-soluble fractions from adult $Slm2^{KO}$ mouse synaptosomes (Fig. 1C, 1D). In acute slices from adolescent mice (postnatal day 25) GluA1 levels were elevated in total cell lysates and cell surface fractions whereas NMDA-receptor GluN1 subunit expression was unaltered (Fig. 1E, 1F). Whole-cell voltage clamp recordings from CA1 neurons in $Slm2^{KO}$ hippocampal slices showed no difference in the miniature excitatory postsynaptic current (mEPSC) amplitude and frequency between WT and $Slm2^{KO}$ mice (Fig. 2A,B). However, mEPSC events showed a modest speeding of rise and decay times in $Slm2^{KO}$ CA1 neurons (Fig. 2C,D).

AMPAR/NMDAR ratios were significantly increased in *Slm2*^{KO} mice (Fig. 2E,F). In *Slm2*^{KO} CA1 neurons, stimulation of Schaffer collaterals elicited larger postsynaptic responses as compared to WT (Fig. 2G, and see Fig. S1A for data from field EPSP recordings). Paired-pulse facilitation was normal in *Slm2*^{KO} (Fig. 2H). In sum, these experiments demonstrate an elevation in postsynaptic AMPAR surface expression and function in CA1 neurons of *Slm2*^{KO} mice. Finally, long-term potentiation (LTP) induced by theta-burst stimulation of Schaffer collaterals was significantly reduced in acute slices from *Slm2*^{KO} mice (Fig. 2I).

Candidate gene approaches have identified some transcripts that are altered in *Slm2*^{KO} brains (Ehrmann et al., 2013; Iijima et al., 2014; Iijima et al., 2011; Traunmüller et al., 2014). However, a comprehensive global analysis of SLM2 targets is lacking. Using Illumina paired end sequencing we mapped SLM2-dependent alternative splicing events at a genome-wide level. This analysis revealed highly correlated expression of transcripts between genotypes indicating that SLM2 does not play a major role in tuning overall transcript levels (Fig. 3A). Moreover, transcripts encoding ionotropic and metabotropic glutamate receptors were not significantly changed (Fig. S1B-E). Most significantly altered was the transcript encoding the SLM2 paralogue SLM1*,* which has previously been shown to be up-regulated in *Slm2*^{KO} hippocampus (Traunmüller et al., 2014).

Genome-wide splicing patterns were extracted based on annotations from FAST-DB and splicing indices calculated. The vast majority of exons remained essentially unchanged between WT and *Slm2*^{KO} hippocampi (Fig. 3B, Fig. S2A, analysis includes 4,965 microexons). Notably, alternative exons in four genes showed disproportionally strong de-regulation in the *Slm2*^{KO} hippocampus. There was a > 2 fold increase in the incorporation of exons at the alternatively spliced segment four (AS4) of Neurexins (*Nrxn1, 2* and *3*), three genes that encode synaptic cell surface receptors. Moreover, exon 24 incorporation was 1.58 fold elevated in Tomosyn-2 (*Stxbp5l),* a component of the vesicle fusion machinery. Another seven exons were identified that exhibited significant alterations (p-value < 0.01) although with modest fold-change (Fig. 3C, Table S1). Independent experimental validation confirmed that de-regulation of additional candidate target exons was small or in some cases not detectable (Figure 3D, 3E and S2B). The paralogue SLM1 may compensate for the loss of SLM2 (*11*). However, comparison of candidate exons in *Slm1*^{KO}, *Slm2*^{KO}, and *Slm1:Slm2*^{DKO} (double knock-out) mice revealed that de-regulation was not significantly more severe in the DKO mice (Fig. S2C).

Alternative splicing at *Nrxn* AS4 regulates selective trans-synaptic interactions of Neurexins in the presynaptic terminal with several synaptic receptors (Boucard et al., 2005;

Chih et al., 2006; Matsuda and Yuzaki, 2011; Uemura et al., 2010). For an unbiased identification of interaction partners regulated by this alternative splicing event we performed affinity-purifications on recombinant NRX1β4(+) and NRX1β4(-) isoforms, followed by shot-gun mass-spectrometry (Fig. 4A, Fig. S3A, S3B). We identified 21 candidate binding partners, including known Neurexin binding proteins (Cbln2, LRRTM1,2,4, Neuroligin-1,2, 3 and SORCS) and a number of novel candidate ligands (Complement C3, Chondroadherin-like protein, Neuronal Pentraxin and Neuronal Pentraxin receptor 1, and Astrotactin). For six of these proteins we observed significant differences in the interaction with AS4(+) and AS4(-) NRX1β isoforms, including Neuroligins, Chadl, LRRTMs, and Complement C3 (Fig. 4B, Table S2, p-value < 0.05). Thus, there is an array of synaptic interactions that can be modified by de-regulation of Neurexin alternative splicing in *Slm2*^{KO} mice.

We hypothesized that the modification of endogenous Neurexin alternative splicing in *Slm2*^{KO} hippocampus may disrupt interactions with these splice insertion-sensitive ligands. In co-immunoprecipitation experiments with an anti-Neurexin-1 antibody, we observed that Neuroligin-1 (NL1) and Neuroligin-3 (NL3) are abundant in immunoprecipitates from WT mice. However, both NLs were reduced in precipitates prepared from *Slm2*^{KO} mice (Fig. 4C). Conversely, co-precipitation of C3, a component of the complement system that has been implicated in synapse elimination (Stevens et al., 2007), was slightly elevated in the same precipitates from *Slm2*^{KO} mice (Fig. S3C). Thus, the loss of SLM2 indeed switches synaptic receptor-ligand interactions. NL1 recruits synaptic NMDA-receptors (Budreck et al., 2013; Chih et al., 2005), whereas NL3 and LRRTMs mediate the synaptic recruitment and stabilization of AMPA-receptors (Shipman et al., 2011). Loss of the trans-synaptic interactions with these Neurexin ligands might result in the postsynaptic glutamate receptor deficits in *Slm2*^{KO} mice. To test this hypothesis, we generated *Nrxn1*$^{\Delta ex21}$ mice where *Nrxn1* exon 21 (the alternative cassette exon at AS4) is specifically deleted but total *Nrxn* transcript levels are unchanged (Fig. S4A-C). Heterozygous removal of one *Nrxn1*$^{\Delta ex21}$ allele restored normal *Nrxn1* AS4(-) transcript levels in the *Slm2*^{KO} background (Fig. 4D). Restoration of *Nrxn1* AS4(-) transcripts rescued trans-synaptic cell surface interactions of endogenous Neurexin with NL1 and NL3 in the co-immunoprecipitation assays (Fig. 4E), normalized GluA1 levels in acute hippocampal slices (Fig. 4F), and partially recovered theta burst-induced Schaffer collateral LTP (Fig. 4G). In an object recognition test, a behavioral task that involves the hippocampus (Cohen and Stackman, 2015), *Slm2*^{KO} mice differed significantly from WT mice in that they did not preferentially explore novel objects (Fig. 4H, 4I, Fig. S4D). Also this phenotype and other behavioral alterations were rescued in *Slm2*^{KO}*;Nrxn1*$^{\Delta ex21\ /+}$ mice (Fig. 4H, 4I, Fig. S4E-G). Thus, the control of a single alternative exon by SLM2 has a major contribution to the specification of glutamatergic synapse function, plasticity, and mouse behavior.

Forced expression of *Nrxn3* AS4(+) isoforms was previously shown to reduce postsynaptic AMPAR localization and to impair LTP in the subiculum (Aoto et al., 2013). By contrast, in *Slm2*^{KO} CA1 neurons, total surface AMPAR levels and AMPAR function are elevated. These differences are most likely due to the simultaneous disruption of alternative splicing in all three Neurexin genes in the *Slm2*^{KO} as well as the different cell type-specific context. Compared to other RNA binding proteins SLM2 exhibits highly selective neuronal cell-type-specific expression and only a small set of alternative exons is particularly reliant on SLM2 function. Our genetic rescue experiments demonstrate that restoration of a single alternative exon has a major impact on the *SLM2*^{KO} phenotype. We hypothesize that targeted, cell type–specific splicing regulation of surface receptor recognition systems as reported here for the SLM2/Neurexin system represents a general mechanism for the control of synapse specification in neuronal circuits.

Acknowledgements

We thank Drs. Mauger, Schreiner, and Xiao for insightful comments on the manuscript and Drs. Hayashi and Bischofberger for expert advice. We thank Mrs. Bornmann and Drs. Demougin, Lemoine, de la Grange, Schmidt, and Rüegg for suggestions and experimental support. L.T. was financially supported by the Boehringer Ingelheim PhD Fonds. A.M.G. was supported by an EMBO long-term fellowship. T.M.N. was supported by the International PhD Program University of Basel. This work was supported by funds to P.S. from the Swiss National Science Foundation, EU-AIMS which receives support from the *Innovative Medicines Initiative*, and the Kanton Basel-Stadt. Sequencing data were deposited at the functional genomics data repository GEO (accession number GSE79902).

Figure 1

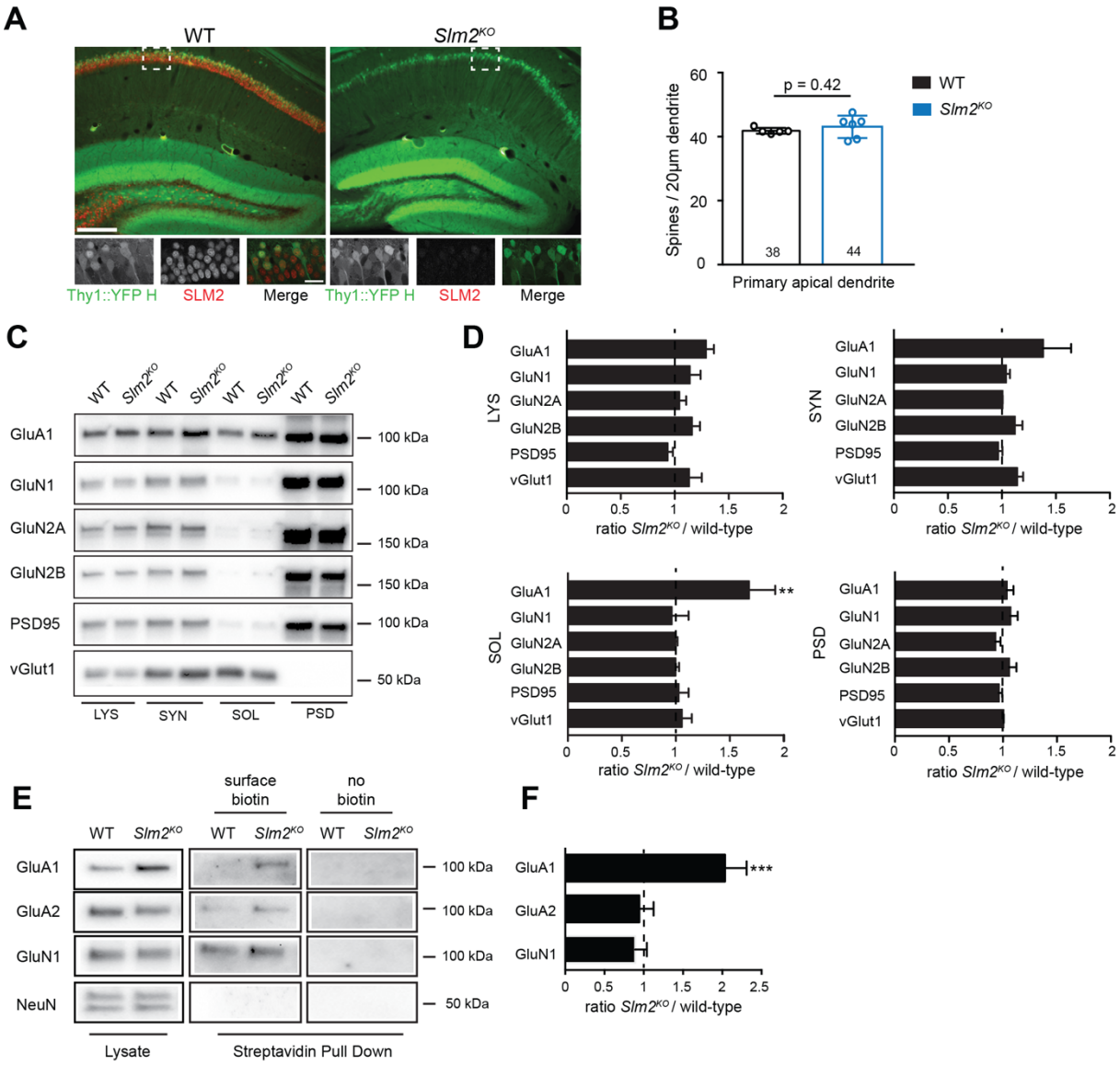

Fig. 1: Synaptic structure and synaptic composition in *Slm2^{KO}* mice

(A) Thy1::YFP-H and Thy1::YFP-H:*Slm2^{KO}* hippocampi (YFP in green, anti-SLM2 in red, scale bar 200µm; 25µm panels below).

(B) Dendritic spine densities along the primary apical dendrite of CA1 cells in the *stratum radiatum* (100µm from pyramidal cell layer). WT n = 5 mice (38 dendrites), *Slm2^{KO}* n = 6 (44 dendrites), unpaired t-test.

(C) Western Blot analysis of glutamatergic proteins in total lysate (LYS), synaptosomes (SYN), Triton X100-soluble fraction at pH = 6 (SOL) and Triton X100-insoluble postsynaptic density (PSD) in hippocampal tissue from adult WT and *Slm2^{KO}* mice.

(D) Mean intensities of expression levels in WT and *Slm2^{KO}* hippocampi (n ≥ 3 mice per genotype, One-Way ANOVA with Dunnett's multiple comparison test, ** $p < 0.01$).

(E) Total and surface glutamate receptor pools were assessed in acute slices from P25 mice by surface biotinylation and streptavidin pull-down; non-biotinylated samples ("no biotin") as negative control.

(F) Quantification for Fig. 1E (One Way ANOVA with Tukey's post-hoc test, *** $p < 0.001$, n ≥ 4 for WT and *Slm2^{KO}*)

Figure 2

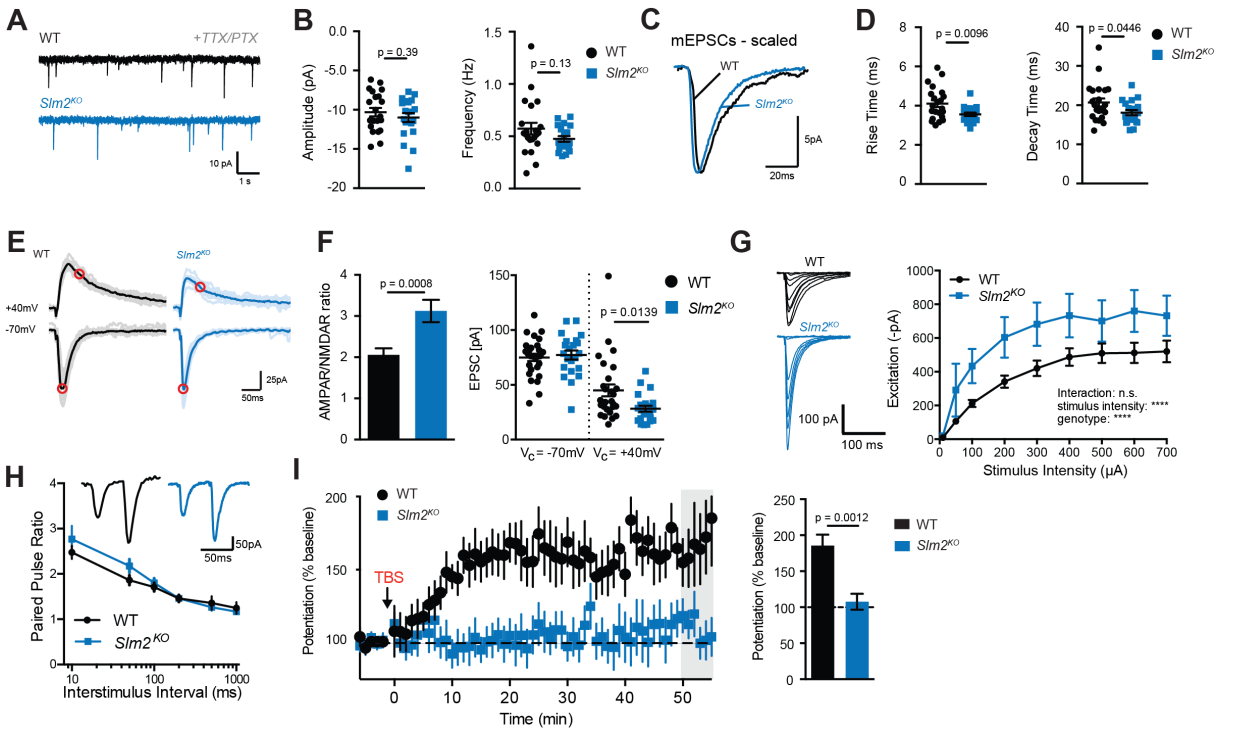

Fig.2. SLM2 is required for normal glutamatergic transmission and plasticity.

(A,B) Amplitude and frequency of spontaneous mEPSCs recorded from CA1 pyramidal neurons in acute hippocampal slices (n ≥ 20 per genotype, N ≥ animals/genotype, mean and SEM, unpaired t-test).

(C,D) Average traces of mEPSCs from A,B scaled to peak amplitude.

(E,F) Average traces and summary data of evoked EPSCs at -70mV (lower trace) and +40mV (upper trace), respectively. Peak EPSC amplitudes were measured at -70mV (peak marked by red circle). NMDAR currents were measured at +40mV (red circle, n ≥ 22 per genotype, N ≥ 4 animals; mean and SEM, unpaired t-test).

(G) Representative traces of EPSCs evoked with varied stimulation intensities in WT or *Slm2*^{KO} CA1 neurons (n ≥ 8 per genotype, N ≥ 3 animals; mean and SEM, two-way ANOVA).

(H) Paired pulse ratio in CA1 neurons from acute hippocampal slices (n ≥ 11 per genotype, N ≥ 4 animals, mean and SEM, two-way ANOVA).

(I) Averaged responses from *Slm2*^{KO} CA1 neurons following a TBS (Theta-Burst stimulus) delivered at V_c= -70mV. The grey bar indicates the interval quantified in the histogram (n ≥ 7 per genotype, N ≥ 6 animals, mean and SEM, unpaired t-test).

Figure 3

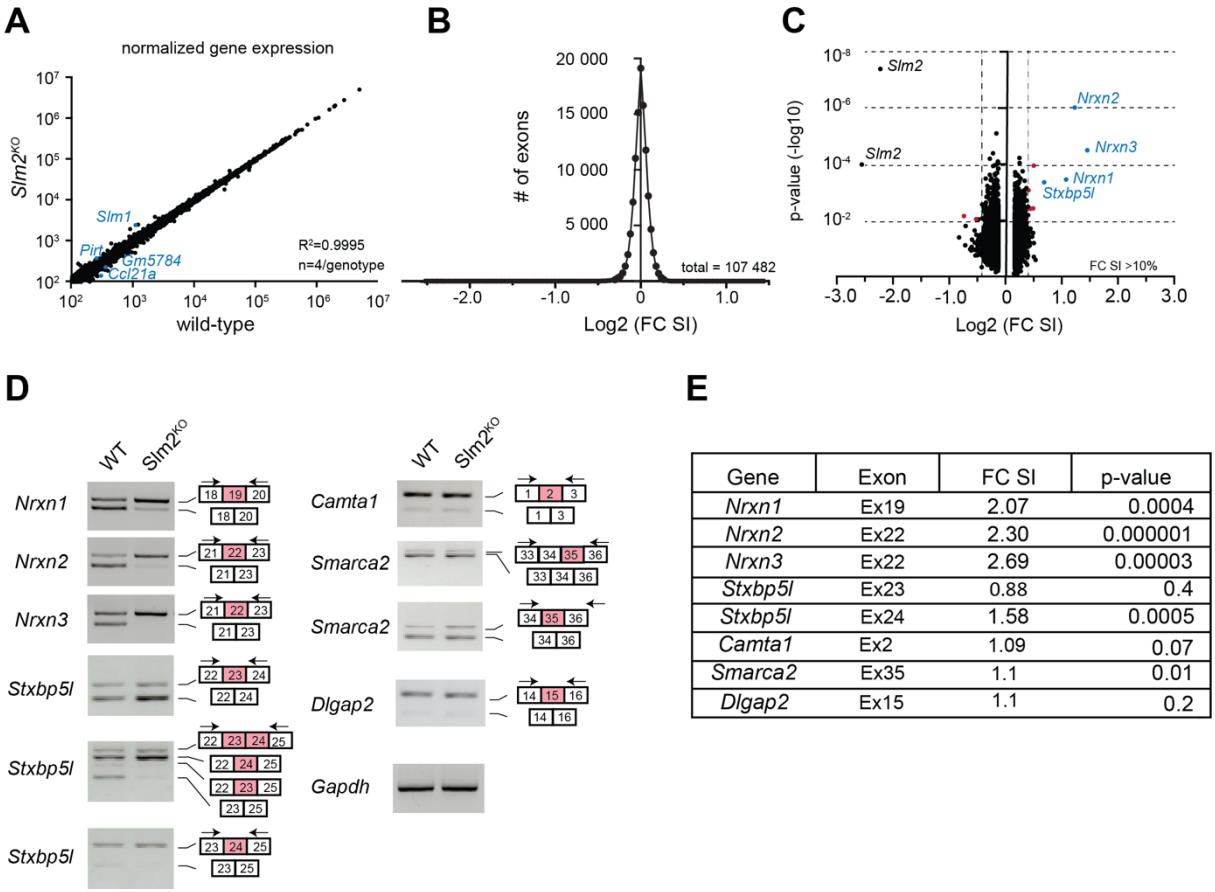

E

Gene	Exon	FC SI	p-value
Nrxn1	Ex19	2.07	0.0004
Nrxn2	Ex22	2.30	0.000001
Nrxn3	Ex22	2.69	0.00003
Stxbp5l	Ex23	0.88	0.4
Stxbp5l	Ex24	1.58	0.0005
Camta1	Ex2	1.09	0.07
Smarca2	Ex35	1.1	0.01
Dlgap2	Ex15	1.1	0.2

Fig.3: Genome-wide mapping of SLM2-dependent alternative splicing program

(A) Correlation analysis of log10 transformed, normalized total transcript counts (for all genes with count ≥ 100 in *Slm2*^{KO}). Transcripts with significant alteration between genotypes ($p < 0.01$, $\Delta FC > 50\%$) are highlighted in blue (n = 4 mice per genotype).

(B) Frequency distribution of exon incorporation rates for 107,482 exons expressed as fold change in splicing index (FC SI) plotted on a log2 scale.

(C) Fold change SI and p-values for all exons with an FC SI > 10% (total of 9110 exons). Exons exhibiting changes of FC SI > 30% and $p < 0.01$ are marked in red (*Pecam1*, *Epha5, Dgkb, Gm1673, Cpne5, Hnrnpul1* and *Cdk16,* threshold indicated by dashed lines*)*. Highly de-regulated exons (FC SI > 50% and $p < 0.01$,) are marked in blue (*Nrxn1, Nrxn2, Nrxn3, Stxbp5l). Slm2* exon 2, deleted in *Slm2*^{KO}, is not displayed.

(D) Experimental assessment of candidate SLM2-dependent exons by RT-PCR in WT and *Slm2*^{KO} hippocampi, alternative exons (red), primer sites (arrows).

(E) Table for fold change SI and p-values for validated exons shown in Figure 3D.

Figure 4

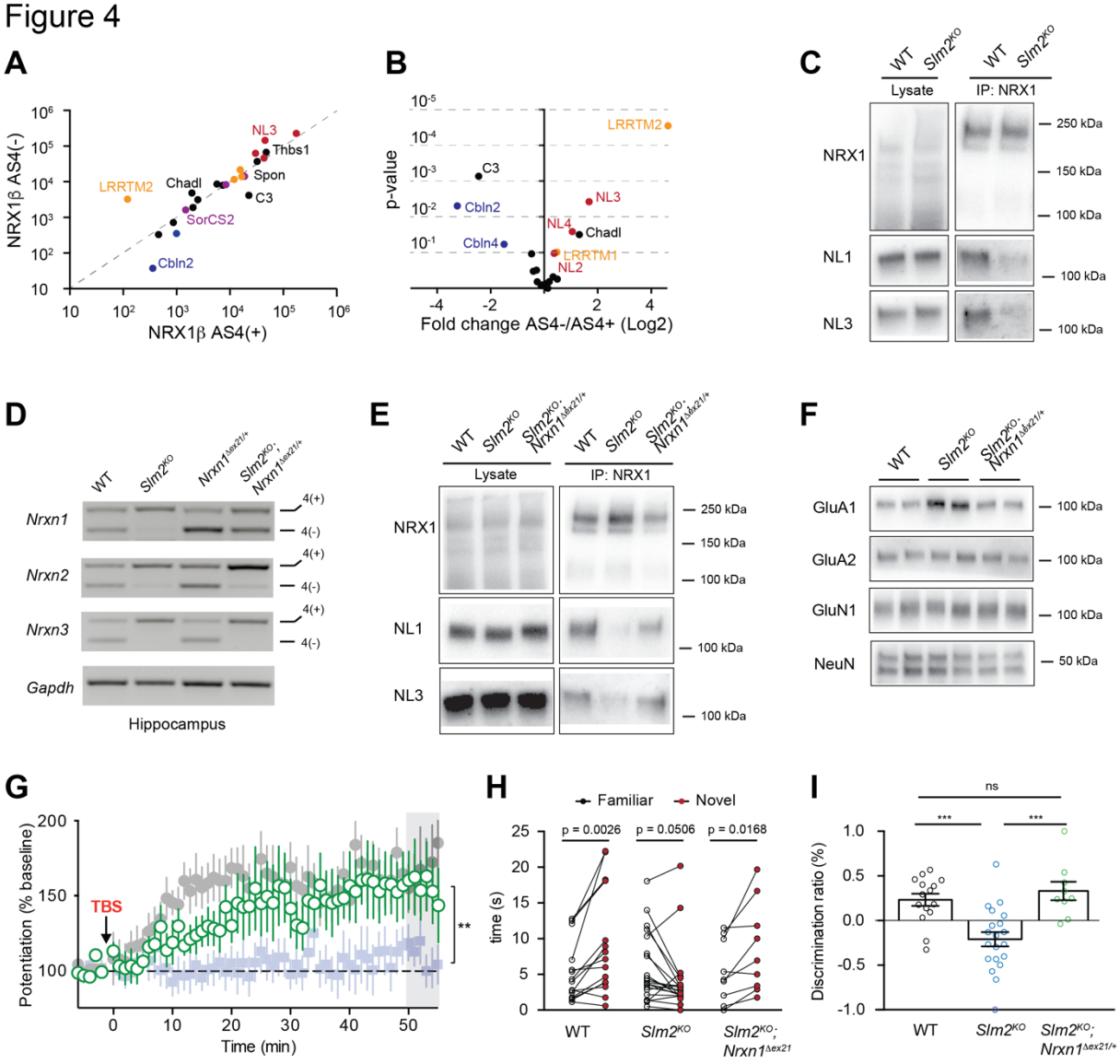

Fig. 4: Heterozygous deletion of *Nrxn1* exon 21 restores synaptic phenotypes in *Slm2*^{KO} hippocampus.

(A) Affinity-purification with recombinant NRX1β AS4(+) and NRX1β AS4(-). Correlation of log10 transformed median spectra counts for all extracellular proteins identified with ≥ 2 peptides recovered on at least one of the two Neurexin isoforms. Paralogues highlighted: NLs (red), Cblns (blue), LRRTMs (orange), SORCs (purple).

(B) Fold change against p-value for all bound extracellular proteins when comparing NRX1 AS4(+) to NRX1 AS4(-).

(C) Anti-NRX1 immunoprecipitation from forebrain lysates of WT and *Slm2*^{KO} animals probed with anti-NRX1, anti-NL1 and anti-NL3 antibodies.

(D) Representative RT-PCR for analysis of *Nrxn1,2,3* AS4 in the hippocampus of WT, *Slm2*^{KO}, *Nrxn*$^{\Delta ex21/+}$ and *Slm2*^{KO};*Nrxn1*$^{\Delta ex21/+}$ animals.

(E) NRX1 immunoprecipitation from forebrain lysates of WT, *Slm2*^{KO} and *Slm2*^{KO};*Nrxn1*$^{\Delta ex21/+}$ animals probed with anti-NRX1, anti-NL1 and anti-NL3 antibodies.

(F) Glutamate receptor expression in acute slices from P25 WT and *Slm2*^{KO} and *Slm2*^{KO};*Nrxn1*$^{\Delta ex21/+}$ hippocampi. Protein levels were probed by western blotting of total lysates (average FC *Slm2*^{KO}/WT 1.94, n=5, Average FC *Slm2*^{KO};*Nrxn1*$^{\Delta ex21/+}$/WT 1.13, n=3).

(G) Averaged responses to a TBS in *Slm2^{KO};Nrxn1$^{\Delta ex21/+}$* CA1 neurons (green) is overlaid on WT (gray) and *Slm2^{KO}* responses (blue) from Fig. 2I (n = 8 cells, N ≥ 5 animals per genotype). Comparison of the responses at 40-60 mins post-induction between *Slm2^{KO}* and *Slm2^{KO};Nrxn1$^{\Delta ex21+/-}$* by ANOVA with Tukey's multiple comparison test (** is $p < 0.01$).

(H,I) Behavioural alterations of WT, *Slm2^{KO}* and *Slm2^{KO};Nrxn1$^{\Delta ex21}$* mice in object recognition task. Time spent investigating a novel and a familiar object during a 5 min trial one hour after acquisition and discrimination ratio are plotted (left panel paired t-test, right panel unpaired t-test, WT n = 15, *Slm2^{KO}* n = 20, *Slm2^{KO};Nrxn1$^{\Delta ex21}$* n = 9).

Figure S1

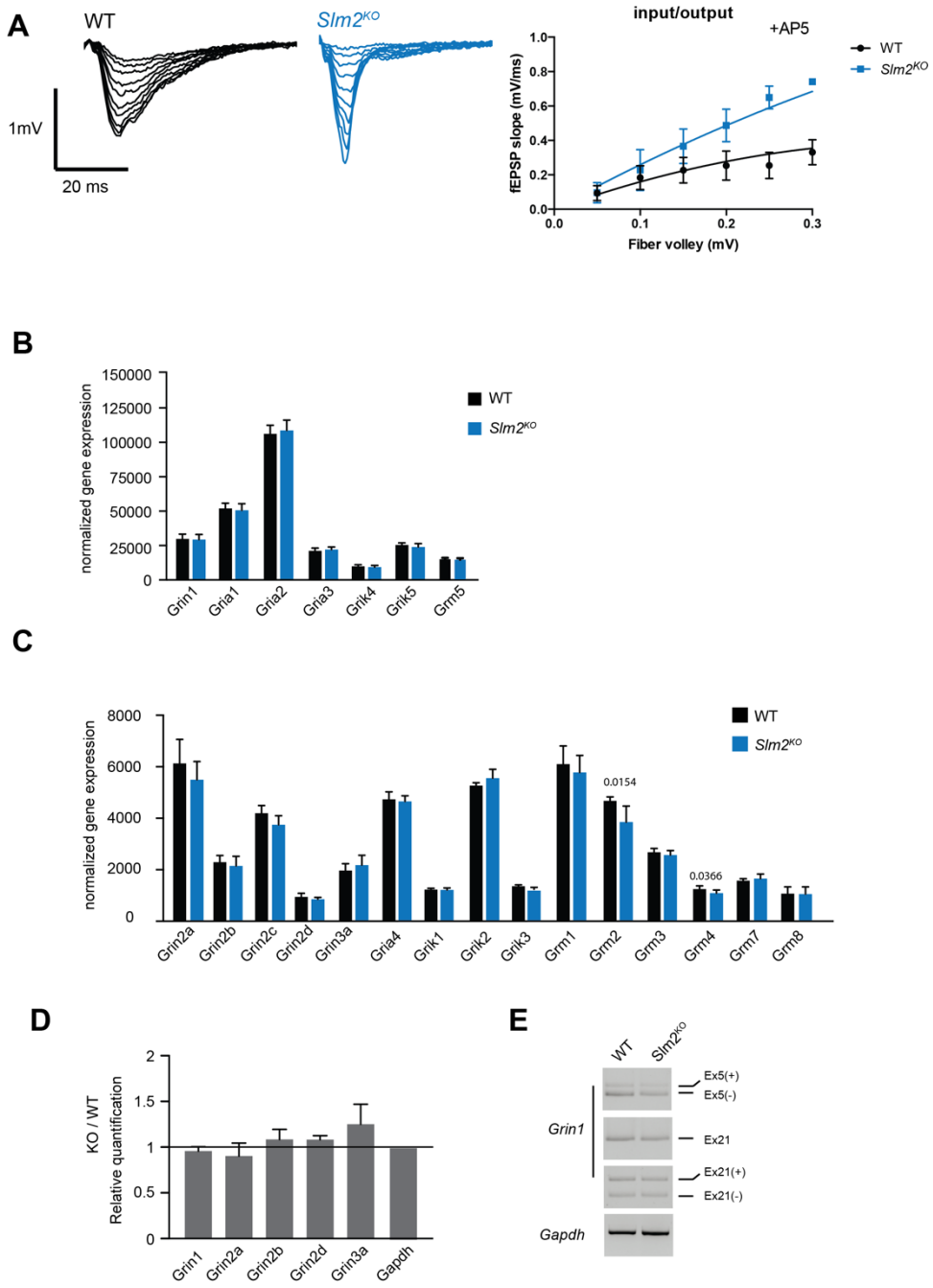

Fig. S1
Function and expression of ionotropic and metabotropic glutamate receptors in *Slm2*^{KO} hippocampus. (A) Representative fEPSPs from input/output curves recorded from WT and *Slm2*^{KO} hippocampal slices at various stimulation intensities. Input/output curves show increased synaptic transmission in *Slm2*^{KO} hippocampal slices (n ≥ 9, N = 3 animals/genotype, two-way ANOVA, mean and s.d.). (B,C) DESeq normalized expression of highly (B) or lower (C) abundant transcripts of AMPAR (*Gria*), NMDAR (*Grin*), Kainate receptors (*Grik*), and metabotropic glutamate receptors (*Grm*). (D) Quantitative real-time PCR for total *Grin1, Grin2a, Grin2b, Grin2d* and *Grin3a* RNA of hippocampal tissue (n = 4 mice/genotype). (E) RT-PCR for detection of differences in splicing events in Exon5, Exon21 and Exon22 of the NMDAR subunit Grin1 between WT and *Slm2*^{KO} mice.

Figure S2

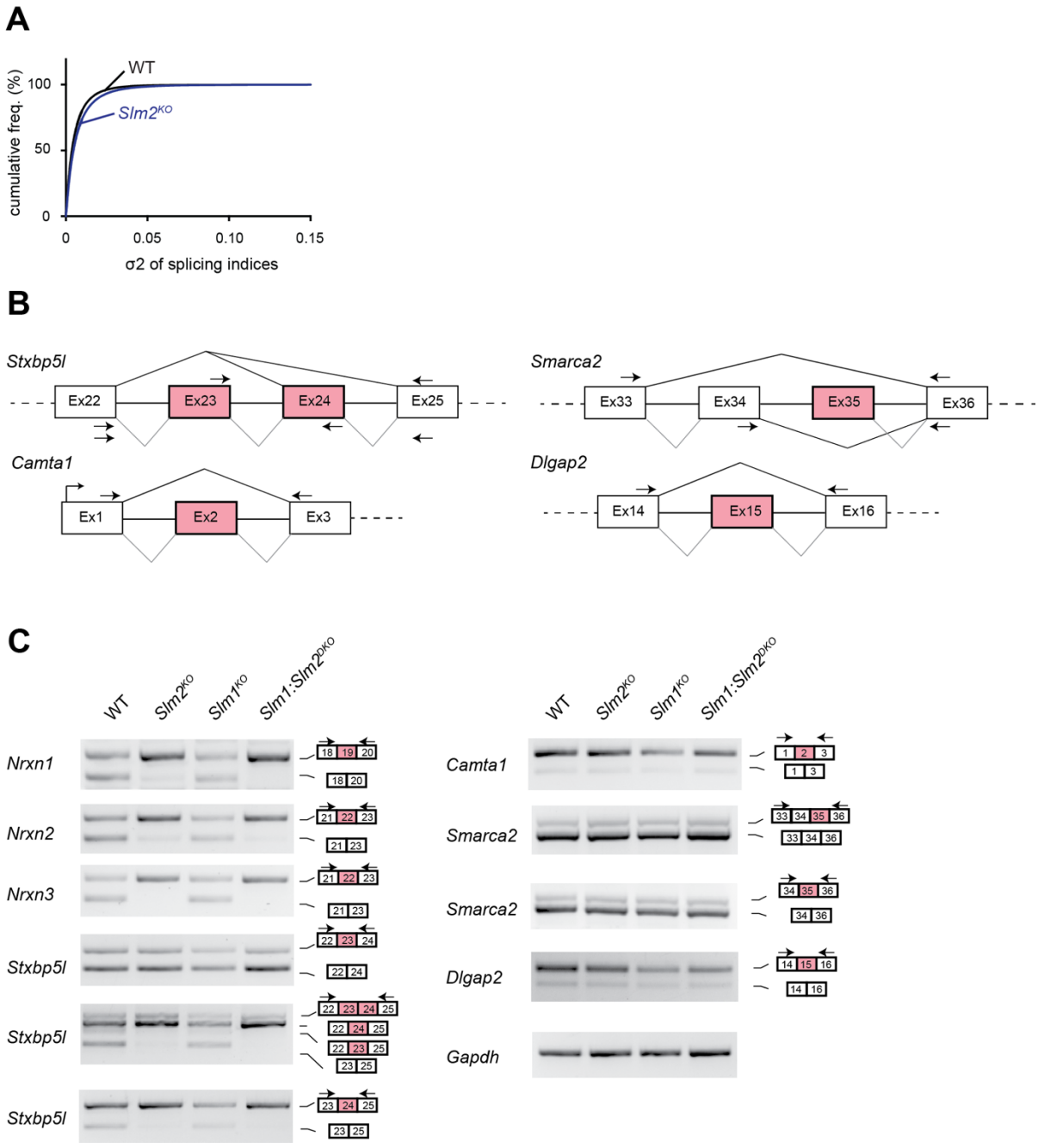

Fig. S2
Alternative splicing changes in *Slm2*^{KO} hippocampus. (A) Cumulative distribution of variances of splicing indices determined for WT and *Slm2*^{KO} sequencing data reveals low variance for the vast majority of splicing indices extracted. (B) Schematic representation of candidate de-regulated exons (alternative exons in red) and primer binding sites for RT-PCR. (C) To assess whether the selectivity of SLM2 for its target exons is partially compensated by SLM1, target exons of Figure 3D were also analyzed with cDNA of WT, *Slm2*^{KO}, *Slm1*^{KO} and *Slm1:Slm2*^{DKO} hippocampi. The investigated targets were not more severely affected in the DKO mice suggesting that the low degree of de-regulation in these exons is not due to compensation by SLM1.

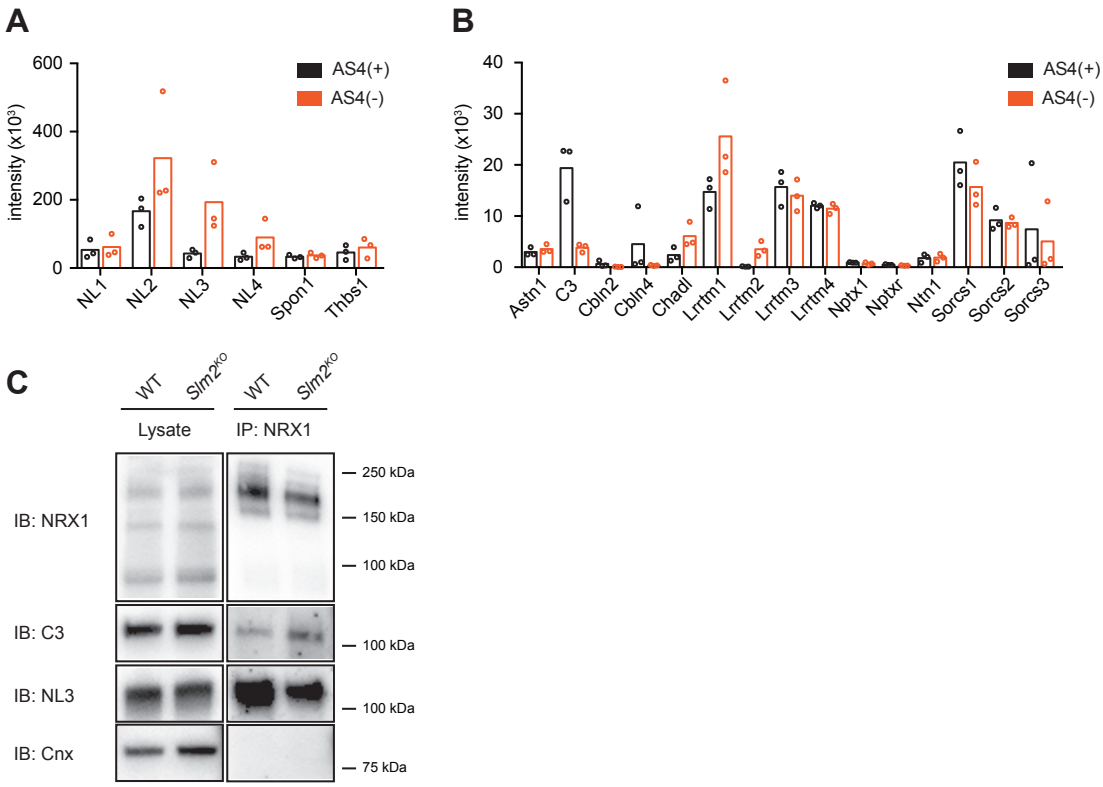

Fig. S3
Visualization of NRX1β binding partners identified by mass-spectrometry.
(A,B) Spectra counts for bound extracellular proteins of three independent trials. Highly abundant proteins including Neuroligin1,2,3, Spondin-1 and Thrombospondin-1 are plotted in A. To visualize less abundant interaction partners, lower abundant proteins are plotted in B. Signals are plotted for recovery on NRX1β AS4(+) (black) and NRX1β AS4(-) (red). (C) Neurexin1 immunoprecipitation from forebrain lysates of WT and *Slm2*^{KO} animals probed with anti-NRX1, anti-C3, anti-NL3 and anti-Calnexin (Cnx) (negative control) antibodies. C3 can be detected in pull downs of both WT and *Slm2*^{KO} mice and exhibits a trend for a higher recovery in the *Slm2*^{KO}, whereas NL3 is reduced. It remains to be investigated whether C3-NRX interactions are direct.

Figure S4

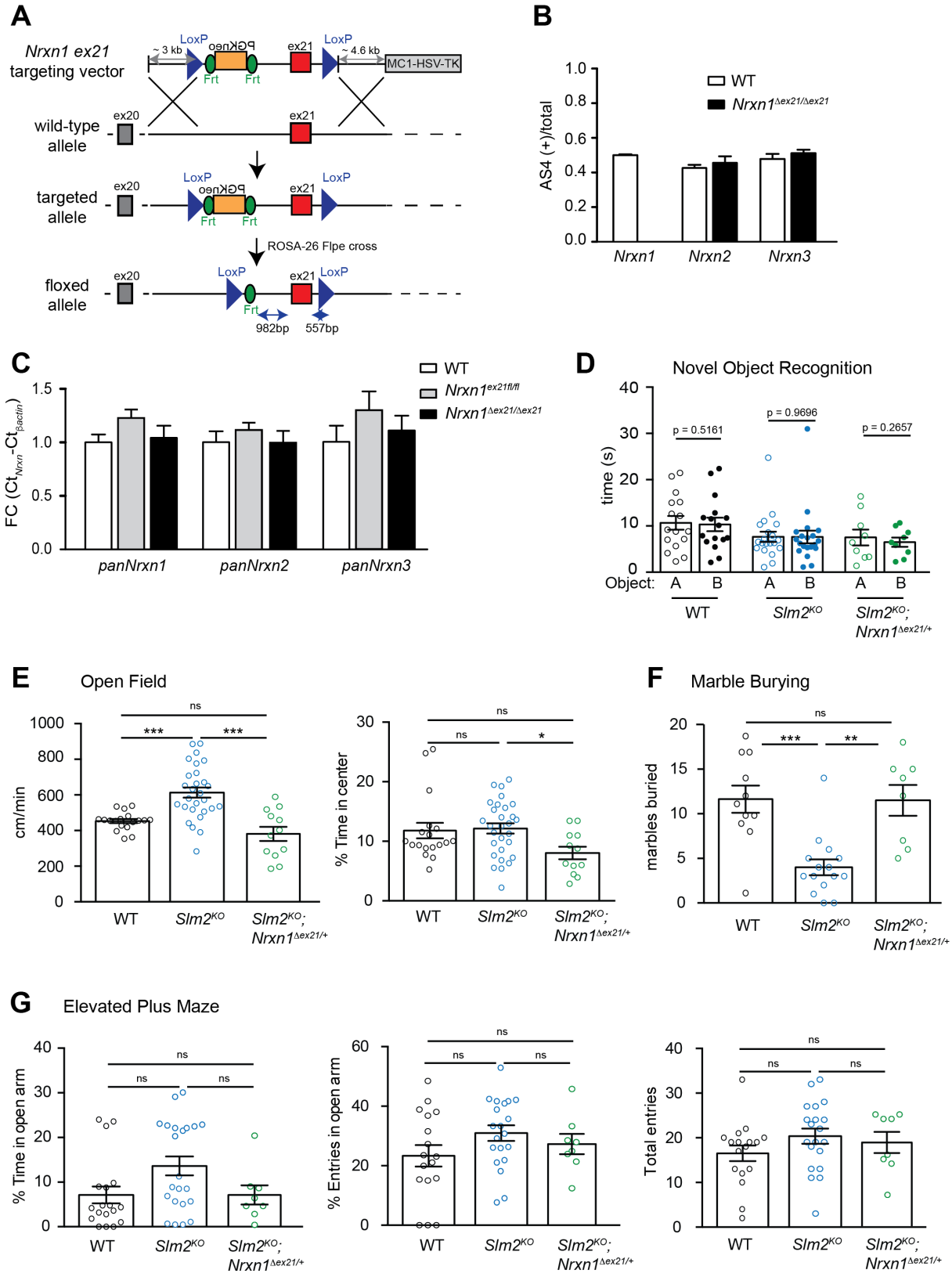
A
Nrxn1 ex21 targeting vector
~ 3 kb
LoxP
PGKneo
Frt
Frt
ex21
LoxP
~ 4.6 kb
MC1-HSV-TK
wild-type allele
ex20
ex21
targeted allele
ROSA-26 Flpe cross
floxed allele
Frt
982bp
557bp
B
AS4 (+)/total
WT
Nrxn1Δex21/Δex21
Nrxn1
Nrxn2
Nrxn3
C
FC (CtNrxn-Ctβactin)
WT
Nrxn1ex21fl/fl
Nrxn1Δex21/Δex21
panNrxn1
panNrxn2
panNrxn3
D
Novel Object Recognition
time (s)
p = 0.5161
p = 0.9696
p = 0.2657
Object: A B A B A B
WT
Slm2KO
Slm2KO; Nrxn1Δex21/+
E
Open Field
cm/min
% Time in center
F
Marble Burying
marbles buried
G
Elevated Plus Maze
% Time in open arm
% Entries in open arm
Total entries
ns
*
**
***

Fig. S4

Analysis of neurexin transcripts in *Nrxn1^{ex21}* mutant mice. (A) Targeting strategy for the generation of *Nrxn1$^{ex21\ fl}$* mice. The alternative exon at AS4 (red) is flanked by loxP sites inserted 982 bp and 557 bp, respectively, up- and downstream of the alternative exon. Constitutive exons in gray. A PGKneo selection marker cassette was removed from the targeted allele by Flp-mediated recombination. (B) Semiquantitative RT-PCR analysis with primers for AS4 transcripts in the hippocampus from WT and *Nrxn1$^{\Delta ex21/\ \Delta ex21}$* mice (P25-40). The fraction of *Nrxn AS4(+)* compared to the total *Nrxn* is plotted (n = 3 mice). (C) Real-time quantitative PCR analysis of transcript levels in the hippocampus for total *Nrxn* transcripts from WT, *Nrxn1$^{ex21\ fl/fl}$* and *Nrxn1$^{\Delta ex21/\ \Delta ex21}$* mice (P25-40). *Nrxn* mRNA/β-actin fold change (FC) values in WT were set to 1.0 and compared to *Nrxn1$^{ex2/\ fl/fl}$* and *Nrxn1$^{\Delta ex21/\ \Delta ex21}$* (n = 3). (D) WT, *Slm2^{KO}* and *Slm2^{KO};Nrxn1$^{\Delta ex21/+}$* were tested in the Novel Object Recognition Task. During the acquisition phase mice were exposed to two identical objects (A and B) for 5min. The time (in seconds) spent investigating the objects is plotted. Neither genotype exhibits a strong preference for either object or their position within the arena (Paired t-test, WT n = 15, *Slm2^{KO}* n = 20, *Slm2^{KO};Nrxn1$^{\Delta ex21/+}$* n = 9). (E) Assessment of locomotion and anxiety by measuring the velocity and the time spent in the center of an Open Field arena during a 10min trial. *Slm2^{KO}* mice exhibit increased velocity, however do not spend more time in the center of the arena compared to WT. *Slm2^{KO};Nrxn1$^{\Delta ex21/+}$* significantly differ from *Slm2^{KO}* mice since their velocity is slightly decreased. The difference in the time in the center may be a consequence of their reduced locomotion (One-way ANOVA with Tukey post-hoc test, *** $p < 0.001$, ** $p < 0.01$, * $p < 0.05$, ns for $p > 0.05$, WT n = 22, *Slm2^{KO}* n = 24, *Slm2^{KO};Nrxn1$^{\Delta ex21/+}$* n = 12). (F) The Marble Burying Test was used as a measurement for stereotypic behavior. *Slm2^{KO}* mice show significant reduction in burying marbles. Restoration of normal *Nrxn1* AS4 expression is sufficient to rescue this phenotype (One-way ANOVA with Tukey post-hoc test, *** $p < 0.001$, ** $p < 0.01$, ns for $p > 0.05$, WT n = 11, *Slm2^{KO}* n = 15, *Slm2^{KO};Nrxn1$^{\Delta ex21/+}$* n = 8). (G) Animals were tested in the Elevated Plus Maze to assess their anxiety behavior. *Slm2^{KO}* mice on average spend slightly more time on the open arm of the maze. In contrast, *Slm2^{KO};Nrxn1$^{\Delta ex21/+}$* exhibit properties resembling WT animals. All animals exhibit similar exploratory behavior as indicated by the number of entries into the arms. (One-way ANOVA with Tukey post-hoc test, ns for $p > 0.05$, WT n = 18, *Slm2^{KO}* n = 22, *Slm2^{KO};Nrxn1$^{\Delta ex21/+}$* n = 8).

Table S1.
Identification of differential exon usage in *Slm2^{KO}* hippocampus. Fold change (log2FC) of exons differentially used in *Slm2^{KO}* hippocampus compared to age-matched WT animals. Genes are sorted by p-value and the differentially used exons are identified by stable IDs of mouse genes present in Fast DB of Genosplice.

Gene	log2FC	log10pval	Label
Nrxn3	1.43	4.49	GSMG0008369:e22
Nrxn2	1.20	6.01	GSMG0019341:e22
Nrxn1	1.05	3.45	GSMG0017970:e19
Stxbp5l	0.66	3.35	GSMG0015722:e24
Trpm3	0.51	0.59	GSMG0019518:e12
Trpm2	0.48	0.70	GSMG0004290:e34
Htt	0.48	1.19	GSMG0029071:e2
Pecam1	0.48	3.94	GSMG0007522:e11
Nipbl	0.47	1.55	GSMG0013751:e34
Dgkb	0.46	2.42	GSMG0007990:e7
Flywch1	0.45	1.42	GSMG0017203:e3
Gm1673	0.42	2.41	GSMG0029053:e4
Hnrnpa1	0.42	1.70	GSMG0013712:e13
Slc15a2	0.42	1.59	GSMG0015717:e14
Nipbl	0.41	1.10	GSMG0013751:e22
Shank2	0.40	1.21	GSMG0035392:e11
Cspp1	0.39	1.68	GSMG0000030:e21
Atp11c	0.39	1.38	GSMG0042554:e15
Slc15a2	0.39	1.24	GSMG0015717:e22
Pclo	0.39	1.27	GSMG0028831:e25
Cpne5	0.39	2.41	GSMG0017325:e2
Epha5	0.38	3.07	GSMG0030673:e5
Shank2	0.38	1.48	GSMG0035392:e11
Isca1	-0.52	1.27	GSMG0010752:e1
Vamp2	-0.52	1.09	GSMG0005394:e1
Cox5a	-0.52	1.12	GSMG0039583:e1
Srrm2	-0.52	0.76	GSMG0016331:e1
Prkar1a	-0.52	1.12	GSMG0006064:e3
Pip5k1c	-0.53	1.20	GSMG0003297:e1
Mapk8	-0.54	0.92	GSMG0012216:e1
Atp5b	-0.54	0.97	GSMG0003678:e1
Nadk	-0.54	1.48	GSMG0027484:e2
Xpo5	-0.56	0.75	GSMG0016720:e6
Hmgn1	-0.57	0.95	GSMG0016117:e3
Bbs9	-0.57	1.64	GSMG0039243:e5
Sbno1	-0.58	1.20	GSMG0031087:e2
Endod1	-0.62	1.31	GSMG0040360:e2
Ndfip1	-0.63	1.05	GSMG0018304:e1

Hmgn1	-0.64	0.92	GSMG0016117:e2
Stk25	-0.65	0.97	GSMG0001919:e1
Clptm1	-0.74	1.80	GSMG0035590:e1
Ypel3	-0.74	1.11	GSMG0035174:e1
Hnrnpul1	-0.76	2.15	GSMG0035655:e1
Usf2	-0.85	1.39	GSMG0035765:e2
Slm2	-2.25	7.38	GSMG0013257:e11
Slm2	-2.58	3.98	GSMG0013257:e10

2. Results

2.3 Landscape of ribosome-engaged alternative transcript isoforms across neuronal cell classes

Landscape of ribosome-engaged alternative transcript isoforms across neuronal cell classes

Elisabetta Furlanis[1,2], Lisa Traunmüller[1,2], Geoffrey Fucile[3], Peter Scheiffele[2,*]

[1]These authors made equal contributions to this work

*Corresponding author: peter.scheiffele@unibas.ch

Affiliations:

[2] Biozentrum, University of Basel, 4056 Basel, Switzerland

[3] Center for Scientific Computing (sciCORE), University of Basel, 4056 Basel, Switzerland

Abstract

Nervous system function relies on complex assemblies of distinct neuronal cell types with unique anatomical and functional properties. These specific cellular features are instructed by molecular programs. Alternative splicing is a key mechanism for the expansion of molecular repertoires and protein splice isoforms shape neuronal cell surface recognition and function. However, the logic of how alternative splicing programs are arrayed across neuronal cells types is poorly understood. We systematically mapped ribosome-associated transcript isoforms in genetically-defined neuron types of the mouse forebrain. Our dataset provides an extensive resource of transcript diversity across major neuron classes. We find that neuronal transcript isoform profiles reliably distinguish even closely-related classes of pyramidal cells and inhibitory interneurons in the mouse hippocampus and neocortex. These highly specific alternative splicing programs selectively control synaptic proteins and intrinsic neuronal properties. Thus, transcript diversification by alternative splicing is a central mechanism for the functional specification of neuronal cell types and circuits.

Introduction

The mammalian brain contains hundreds of cell types with unique anatomical and functional properties. Cell type characteristics are fundamental underpinnings of neuronal circuit function and – ultimately – the control of behaviors. Many of the distinctive neuronal morphologies were recognized one hundred years ago (Ramón y Cajal, 1995). More recent studies uncovered electrophysiological properties and characteristic gene expression profiles that are associated with specific neuron types (Kepecs and Fishell, 2014; Zeng and Sanes, 2017). Yet, we still lack comprehensive knowledge of how the multitude of neuronal properties is encoded by a limited number of genes. Evolutionary comparisons revealed a significant increase in alternative splicing heterogeneity in more complex organisms. Within those, the nervous system exhibits the most extensive usage of alternative transcript isoforms (Barbosa-Morais et al., 2012; Tapial et al., 2017). Single gene studies provided evidence that individual protein variants generated through alternative splicing can exhibit unique isoform-specific functions (Aoto et al., 2013; Beffert et al., 2005; Taliaferro et al., 2016; Traunmüller et al., 2016; Yap et al., 2016). However, in many molecular studies on neuronal connectivity and function the identity of splice isoforms endogenous to the cell type of interest are unknown. This is a significant bottleneck for interpretation of gain and loss-of-function studies. While loss of RNA binding proteins that regulate alternative splicing and cell type-specific knock-outs exhibit severe impacts on neuronal function and synaptic transmission (Calarco et al., 2009; Lee et al., 2016; Quesnel-Vallieres et al., 2016; Vuong et al., 2018; Wang et al., 2012b), most of these proteins are commonly expressed in all neuronal cell types (Darnell, 2013; Furlanis and

Scheiffele, 2018; Li et al., 2014; Saito et al., 2019; Wamsley et al., 2018; Zheng and Black, 2013). Thus, the general logic of how alternative splicing programs relate to brain complexity is poorly understood.

Previous bulk-sequencing analyses contrasted neuronal and non-neuronal splicing regulation (Zhang et al., 2014). Developmental analysis of mouse neocortex uncovered a series of temporally controlled coordinated splicing switches in brain tissues. These developmental switches were pan-neuronal and occurred across all neuronal populations (Weyn-Vanhentenryck et al., 2018; Zhang et al., 2019; Zhang et al., 2016; Zhang et al., 2014). Only very recent studies are beginning to probe whether well-defined neuronal cell types rely on alternative splicing for the regulation of specific biological functions (Saito et al., 2019; Wamsley et al., 2018). However, it remains debated to what extent transcript isoforms detected by RNA-sequencing are indeed recruited for translation to produce protein isoforms (Tress et al., 2017; Weatheritt et al., 2016). To address these questions, we generated genome-wide maps of transcript isoforms that are recruited for translation in genetically-defined neuronal cell populations. Our analysis identified hundreds of differentially regulated splicing events across distinct neuron types. Moreover, we demonstrate that cell type-specific splice isoforms define neuronal cell populations and shape intrinsic properties and synaptic protein complexes. The dataset provides a rich resource for selecting endogenously expressed splice isoforms to be used in functional studies, for interpreting impact of gene mutations in disease states, and for the dissection of enhancers and promoters that drive cell type-specific transcripts from alternative transcription start sites.

Results

Deep mapping of actively translated transcript isoforms in cortical and hippocampal neuron populations

In order to obtain a comprehensive mapping of transcript isoforms in the mouse forebrain we conducted large-scale tagged-ribosomal affinity purification (RiboTRAP) of ribosome-associated mRNAs from genetically-defined neurons (Fig. 1a). The endogenous ribosomal protein Rpl22 was conditionally HA-tagged in glutamatergic neurons (using CamK2-cre for most neocortical pyramidal cells and Scnn1a-cre for spiny stellate and star pyramid layer 4 cells), and GABAergic interneurons [with somatostatin-cre (SST), parvalbumin-cre (PV) and vasointestinal peptide-cre (VIP)]. Within the hippocampus, we further targeted *Cornu ammonis 1 (CA1)* neurons (CamK2-cre), CA3 neurons (Grik4-cre), and SST-positive interneurons (SST-cre) (Fig. 1b, Supplementary Fig. 1). Using an optimized affinity-isolation protocol and strict quality control measures followed by deep RNA-sequencing (paired-end,

read length 100bp, >100 Million reads per biological replicate) we detected > 12'000 genes per sample with full-length coverage across transcripts (Table 1, Supplementary Fig. 2a) and low variance between biological replicates (Fig. 1c). Transcriptome analysis confirmed appropriate enrichment and de-enrichment of known and newly discovered markers (Supplementary Fig. 1b, 2b-d, 3, Supplementary Table 1). Thus, this deep dataset enables reliable dissection of transcript isoforms translated in specific cell types.

Alternative transcript repertoires define neuronal populations

To map transcript repertoires across neuronal cell types we quantified alternative isoforms using two complementary computational methods. First, we analyzed differential exon usage by quantifying reads mapping onto individual exons relative to the number of reads on constitutive exons derived from the same gene (constitutive exons are defined in the annotated transcript database FAST DB(de la Grange et al., 2007), EXON analysis, Supplementary Fig.4, see methods for details). Second, the differential usage of splicing patterns was assessed using exonic and junctional reads mapping to transcript isoforms annotated in FAST DB (PATTERN analysis, Supplementary Fig. 4, see methods for details). This quantitative mapping of alternative transcript isoforms uncovered hundreds of highly differentially regulated transcript isoforms in neocortical and hippocampal cell populations [log2 fold-change (log2FC) in splicing index (SI) ≥ 1 or ≤ -1, p-value ≤ 0.01]. Independent experimental validations with semi-quantitative RT-PCR confirmed the accuracy of the computational pipeline (validation rate > 90%, Supplementary Fig. 5). Therefore, this validated dataset represents a comprehensive resource for alternative transcripts in the major forebrain neuron populations (Supplementary Table 2, 3 and https://scheiffele-splice.scicore.unibas.ch for a web-based look-up tool to query isoforms for individual genes). Divergent transcript isoforms may arise from alternative splicing but also alternative transcription start sites (TSS) (Pal et al., 2011; Reyes and Huber, 2018). The PATTERN analysis enabled us to separate transcript isoforms arising from these mechanistically different forms of transcript diversification. Remarkably, the exons differentially regulated by alternative splicing reliably segregated neuronal cell classes (Fig. 1d). Thus, Scnn1a-defined layer 4 cells are characterized by 310 exons included in 214 different genes. Similarly, the two medial ganglionic eminence (MGE)-derived interneuron classes (PV and SST populations) are distinguished by 628 and 719 exons from 407 and 486 genes, respectively. Moreover, alternative transcript isoforms in the CGE (Caudal Ganglionic Eminence)-derived VIP interneurons were distinct from PV and SST-populations, with 609 exons differentially included in 407 genes. Overall, we did not observe a correlation of changes in splicing indices and gene expression level, indicating that our analysis captures differentially regulated exons across a broad spectrum of transcript expression levels (Supplementary Fig. 6). In previous studies,

microexons (defined as exons 3-27 nucleotides long) were shown to preferentially contribute to transcript diversification in the nervous system(Irimia et al., 2014). Amongst all exons differentially regulated (DR) across neuronal cell classes, we find 3.8-5.3% to be microexons. These percentages are slightly higher compared to the percentage of total microexons detected in the neocortex (2.8%, see methods for details). Thus, differential alternative splicing across cell types is substantial for microexons but also other types of splicing events. In summary, this analysis demonstrates that extensive alternative splicing regulation distinguishes major neuronal cell classes in the mouse neocortex.

Wide use of alternative transcription start sites across cortical neuron sub-classes

We quantified the frequency of distinct patterns underlying the differentially regulated splicing events in neocortical cell populations and found that they distributed over multiple categories (Figure 2a, Supplementary Table 2). Usage of cassette exons was the most frequent differentially regulated alternative splicing event across cell populations (Fig. 2a, 2b for *Dlgap2* as example). Interestingly, alternative last exons (ALE), which result in a modification of the 3'UTR of transcripts, represented about 20% of events (Fig 2a, 2b *Ncam1* as example). This is notable considering that alternative last exons can impose cell type-specific protein expression as well as subcellular localization of mRNAs (Taliaferro et al., 2016; Tushev et al., 2018). In addition to transcript diversification by alternative splicing we found that across all neocortical cell classes, ~30-60% of differentially regulated transcript isoforms arose from alternative TSS (Fig. 2c, Supplementary Table 2). This implies a frequent action of cell type-specific enhancers and promoters. An example for alternative TSS regulation is *Dlgap1,* which encodes a major glutamatergic scaffolding protein. In neocortical PV-positive cells, we identified an alternative TSS in exon3 of *Dlgap1* which switches to exon 5 in the Scnn1a-positive layer 4 cells (Fig. 2d). This differential regulation results in transcripts that differ in the 5'UTR and the N-terminal amino acids (see Fig. 2d *Rapgef5* for an additional example). When comparing the segregation of differential TSSs and ALEs we find that either of these types of events efficiently segregated neocortical excitatory and inhibitory cell classes, including MGE- and CGE-derived interneurons (Supplementary Fig. S7 a and b, respectively. Exon numbers involved are indicated in the figure legend). Thus, our analysis demonstrates that not only alternative splicing but also alternative TSS are major drivers of neuronal cell type-specific transcript isoform expression in the mouse forebrain.

Divergent alternative splicing programs across closely related cells in different anatomical positions

Hippocampal CA1 and CA3 pyramidal neurons exhibit certain unique functional properties and overall similar transcriptomes (Cembrowski et al., 2016). Thus, we explored

whether there are differential splicing programs specific for these closely-related glutamatergic cell classes. We identified hundreds of differentially expressed transcript isoforms arising from different patterns of alternative splicing, as well as alternative TSS between CA1 and CA3 cell preparations (253 DR exons, log2FC ≥ 1 or ≤ -1, p-value ≤ 0.01, Fig. 3a, Supplementary Fig. 8, Supplementary Table 3). These include key isoforms with well-characterized functional properties such as the mutually exclusive exons which regulate flip/flop variants of the *Gria1* AMPAR subunit (Sommer et al., 1990), or alternative last exons in *Brevican*, which control expression of a secreted Brevican isoform implicated in neuronal adhesion (Brakebusch et al., 2002) (Fig. 3b). Similarly, cortical L4 excitatory neurons and hippocampal CA1 pyramidal neurons exhibited 276 differentially regulated exons (Figure 3a) and transcript isoforms derived from multiple patterns of alternative splicing (Figure 3c *Nrxn3* as example, Supplementary Fig. 8, Supplementary Table 4). These comparisons highlight vastly divergent transcript isoform content between different classes of glutamatergic neurons, including closely related pyramidal cells from hippocampal sub-fields. By comparison, splicing programs were much more similar between hippocampal *versus* neocortical SST-positive interneurons (only 151 highly differentially regulated exons Fig. 3a, 3c cassette exon regulation in *Fat1* as example, Supplementary Fig. 8, Supplementary Table 4, Supplementary Table 5 for an overview of differentially expressed genes and alternatively regulated splicing events). In sum, we conclude that alternative splicing plays a major role in diversifying molecular repertoires at the level of neuronal sub-classes and cell types within and across anatomical positions.

Identification of neuronal subclass-specific splicing factors in neocortical and hippocampal cells

Most neuronal RNA binding proteins (RBPs) studied thus far are pan-neuronally expressed. Given the extensive differential alternative transcript regulation in neuronal sub-classes, we sought to identify RBPs that might regulate alternative splicing in a cell type-specific manner. We generated a hand-curated list of 57 *bona fide* splicing regulators based on databases and previous publications and evaluated their expression across neuronal populations (Supplementary Table 6). As expected, several splicing factor transcripts exhibited broad expression with little difference across neocortical and hippocampal cell classes (e.g., *Hnrnpa2b1, Hnrnpl, Srrm1,* Fig. 4a, Supplementary Table 6). By contrast, other splicing factors showed highly selective expression with some segregating between glutamatergic and GABAergic neuron groups and others highly enriched in certain neuron classes (Fig. 4a). For example, the Rbm20 transcript is preferentially expressed in PV-interneurons, *Ptbp1* in VIP-interneurons, and *Rbfox3* – also called NeuN – is preferentially expressed in glutamatergic cells *(*Fig. 4a, Supplementary Table 6). Fluorescent *in situ* hybridizations for select RBPs confirmed the differential expression patterns extracted from RiboTRAP sequencing data

(Supplementary Fig. S9, Supplementary Table 6 for statistical analysis). To investigate whether some of the differentially expressed splicing factors represent candidates that drive cell type-specific alternative splicing choices, we employed splice reporter assays in Neuroblastoma 2A (N2A) cells (see Methods for details). We generated reporter constructs for exons that we found to be differentially regulated across neocortical neurons (alternative cassette exons in neurotransmitter receptors Gabrg2 and Grin1, and the voltage-gated potassium channel Kcnq2, Fig. 4b). Co-expression in N2A cells of several RBPs (e.g., hnRNP A1, hnRNP H1, Ptbp3) did not shift splicing patterns *in vitro*. On the other hand, co-expression of Ptbp1 (which is preferentially expressed in VIP-interneurons Fig. 4a,d) shifted splicing of Gabrg2 and Kcnq2 reporters to the pattern observed for endogenous mRNAs in VIP-interneurons (Fig 4c). Similarly, Rbfox3 shifted the Grin1 reporter splicing to the pattern enriched in Scnn1a cells (which express high levels of Rbfox3) (Fig. 4c,d). Thus, these differentially expressed splicing regulators represent possible candidates for the regulation of the respective splicing events *in vivo*. In summary, this analysis identifies candidate neuronal cell class-specific splicing regulators for the differential regulation of transcripts.

Alternative splicing programs are highly dedicated to controlling synaptic interactions and neuronal architecture

To probe which cellular properties are regulated by alternative splicing, we assessed the enrichment of Gene Ontology (GO) terms for transcripts regulated across all neocortical cell classes, hippocampal comparisons, and across brain regions. Given that alternative first exons result from transcriptional regulation, we excluded them from this analysis. Remarkably, the differential alternative splicing regulation almost exclusively targets transcripts encoding for synaptic proteins and intrinsic neuronal properties. Enrichment of the top GO terms significant for genes differentially regulated by splicing was 2 - 4 fold higher as compared to genes differentially expressed (Fig. 5a, Supplementary Fig. 10a,b for enriched categories of differentially expressed genes, Supplementary Table 7 for all GO terms). Note that the enrichment of genes encoding synaptic proteins was not simply a consequence of such genes containing larger numbers of exons (Supplementary Figure 10c). Specifically, the enriched GO terms map onto five key categories, which fundamentally shape synapse function and intrinsic neuronal properties: Adhesion complexes (e.g. *Cntn4, Cntnap2, Ncam1, Nlgn1, Nrxn3, Nfasc, Ptprs, Robo2*) implicated in formation and specification of neuronal synapses (de Wit and Ghosh, 2016; Shen and Scheiffele, 2010; Takahashi and Craig, 2013), voltage-gated calcium channels (e.g. *Cacnb2, Cacnab4, Cacna1g, Cacna1d*), presynaptic release machinery (e.g. *Rims, Synj1, Stxbp1, Syt17, Unc13b*), postsynaptic neurotransmitter receptor complexes (e.g. *Grm1, Grm5, Gria1, Gria2, Shisa9*) and associated scaffolding proteins (e.g. *Camk2, Dlgap1, Rapgef4, Shank3, Tiam1*) (Fig. 5b). All of these genes encode key regulators of synaptic

function and plasticity. Three further categories highly targeted by cell type-specific alternative splicing are potassium channels, motor proteins, and regulators of cytoskeletal rearrangements – elements central for the control of intrinsic neuronal properties (Fig. 5c). In particular, potassium channels are key determinants of neuronal excitability at the level of after-hyperpolarization upon action potential firing (Kcnn2), at the level of M-currents (Kcnq2), or through calcium-dependent regulation of A-currents (Kcnip1,4) (Coetzee et al., 1999). Thus, neuronal cell type-specific alternative splicing programs specifically encode intrinsic neuronal properties and synapse specification.

Discussion

Previous studies highlighted an expansion of splicing complexity across vertebrate species with a particular increase in alternative exon usage in the brain (Barbosa-Morais et al., 2012). This increase in alternative splicing may relate to neuronal cell types and functions in multiple ways. Single gene studies illustrated stochastic splice isoform choices at the single cell level (Kise and Schmucker, 2013; Miura et al., 2013) but also reproducible splicing patterns linked to cell types (Fuccillo et al., 2015; Iijima et al., 2014; Nguyen et al., 2016; Saito et al., 2019; Schreiner et al., 2014a; Wamsley et al., 2018). Here, we demonstrate that complex alternative splicing programs define sub-classes of cortical and hippocampal neuron types. Thus, the selection of cell type-specific transcript variants is not an exceptional feature for individual protein families but a fundamental program of highly differentiated cell types in a complex organism. During embryonic development, the lineage decisions for interneuron and pyramidal cell differentiation are mainly driven by transcription factor codes (Mayer et al., 2018; Mi et al., 2018a). We propose that cell type-specific expression of RNA-binding proteins imposes splicing-dependent regulation for terminal differentiation of these neuron classes. Consistent with this notion, several of the candidate splicing specificity factors that we mapped here are already detected in interneurons at embryonic stages of development (Lim et al., 2018; Mi et al., 2018a).

An unexpected finding was the highly divergent usage of alternative transcription start sites across neuronal populations. This suggests prominent roles for cell type-specific enhancers and promoters in generating transcript isoforms. We propose that this complex transcript regulation evolved not only to modify protein isoforms but also to afford unique spatio-temporal modulation of neuronal gene expression. Complex alternative splicing programs control diverse biological processes from chromatin and RNA regulators, to ion homeostasis and mitochondrial function. Considering this broad range of splicing-regulated processes, it is remarkable that the neuronal cell type-specific splicing programs are selectively geared to the control of synaptic and intrinsic neuronal properties. Splice isoforms of neuronal

receptors, ion channels, synaptic adhesion and scaffolding proteins exhibit fundamentally divergent functions (Furlanis and Scheiffele, 2018; Vuong et al., 2016) and significant splicing disruptions have been linked to neurodevelopmental disorders (Irimia et al., 2014). In humans, more than 90% of gene products are modified by alternative splicing. A major impediment for exploring the functional relevance of transcript isoforms in neuronal wiring has been the lack of knowledge of how splice isoforms are arrayed over neuronal cell types. Our comprehensive genome-wide analysis uncovers hundreds of cell class-specific transcript isoforms encoding key regulators of synaptic function and intrinsic neuronal properties. To maximize the accessibility of this large dataset and to simplify the identification of differentially expressed transcript isoforms, we established a web-based "splicecode database" where users can retrieve differential isoform expression data for any gene of interest (https://scheiffele-splice.scicore.unibas.ch). In the future, targeted manipulation of cell type-specific splicing events may open the door for a new class of therapeutic interventions in disease states.

Acknowledgements

We are grateful to Fiona Doetsch, Oriane Mauger and Le Xiao for constructive comments on the manuscript and to members of the Scheiffele Lab for discussions, in particular to Thi-Minh Nguyen for setting up the protocol for RiboTRAP purifications and Caroline Bornmann for expert help with fluorescent in situ hybridizations. We are grateful to Sinisa Hrvatin and Michael E. Greenberg for sharing detailed data from single cell sequencing studies for comparison to our dataset and to Beatriz Rico for sharing data at an early stage of this project. We thank Pierre de la Grange, Noémie Robil and Ariane Jolly at Genosplice for help with analysis, Francesco Ambrosetti for occasional support with coding. Part of calculations were performed at sciCORE (http://scicore.unibas.ch/) scientific computing center at the University of Basel, with support by the SIB - Swiss Institute of Bioinformatics. Sequencing and library preparations were performed with support from the Life Science Training Facility and the Quantitative Genomics Facility Basel. L.T. was supported by a Fellowship from the Boehringer Ingelheim PhD Fonds and the Doris Dietschy Stiftung. This work was supported by funds to P.S. from the Swiss National Science Foundation, a European Research Council Advanced Grant (SPLICECODE), and the Kanton Basel-Stadt.

Author contributions

This work was jointly conceived by E.F., L.T. and P.S., all wet lab procedures were performed by E.F. and L.T., data analysis was conducted by E.F., L.T. and G.F., website design was performed by G.F., and the manuscript was jointly written by E.F., L.T. and P.S., with editing provided by G.F.

Competing interests: The authors have no competing interests.

Figure 1

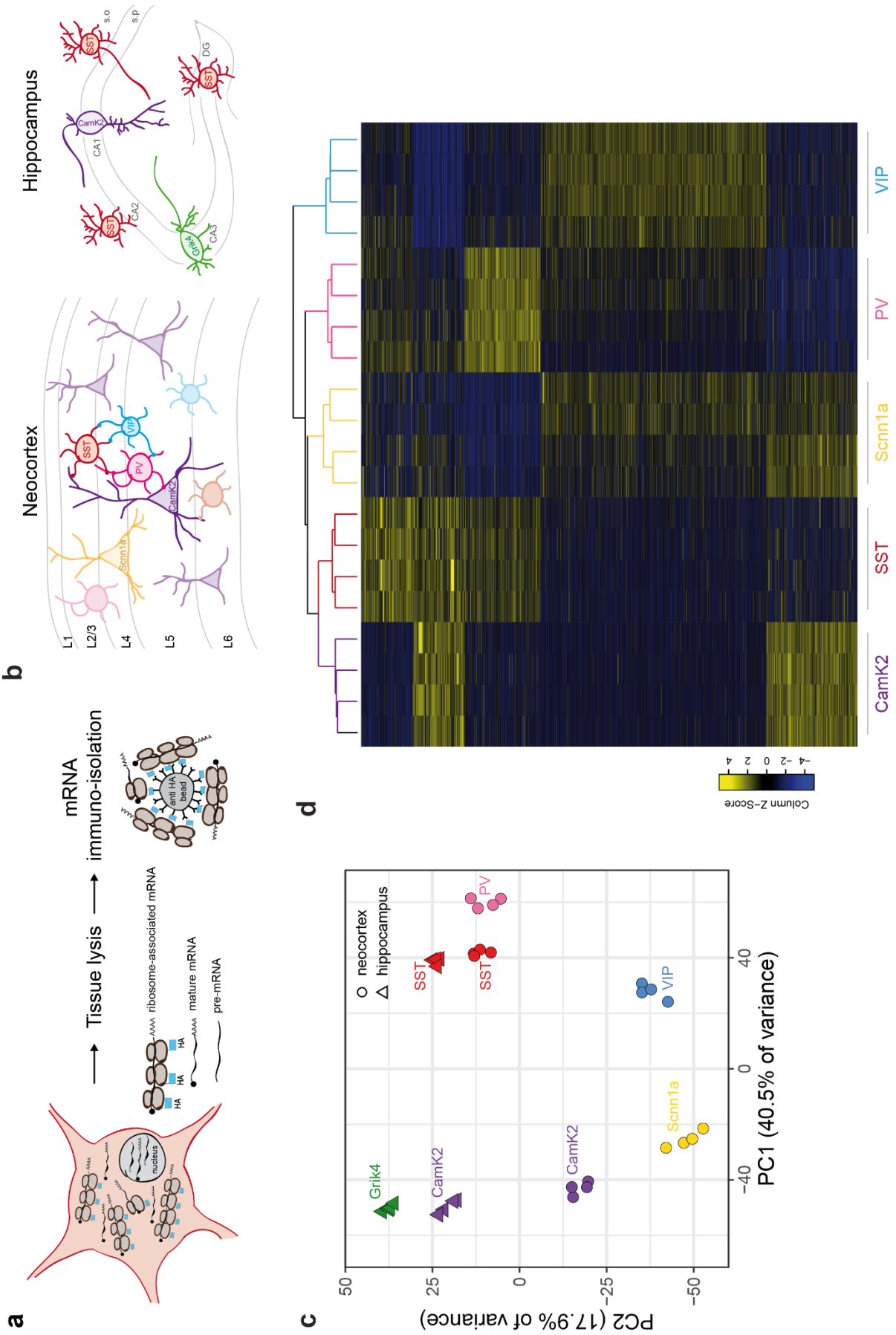
a
Tissue lysis
immuno-isolation
mRNA
ribosome-associated mRNA
mature mRNA
pre-mRNA
anti HA bead
nucleus
b
Neocortex
Hippocampus
L1
L2/3
L4
L5
L6
SST
VIP
PV
CamK2
Scnn1a
Grik4
CA1
CA2
CA3
DG
s.o
s.p
c
neocortex
hippocampus
PC2 (17.9% of variance)
PC1 (40.5% of variance)
d
Column Z-Score
CamK2
SST
Scnn1a
PV
VIP

Fig. 1: Extensive alternative exon usage defines classes of forebrain neurons.
a, Schematic representation of RiboTRAP pulldowns. HA-tagged ribosomes in the cytoplasm of genetically defined cell populations load fully mature mRNAs. Following whole tissue lysis, ribosome-associated mRNAs are immuno-isolated using anti-HA beads and subsequently purified. **b**, Cartoons representing neuronal cell populations isolated from mouse neocortex (*left panel*) and hippocampus (*right panel*). **c**, Principal component analysis of genes expressed in each biological replicate of neocortical and hippocampal samples. Variance explained by the principal components 1 and 2 (PC1 and PC2) is indicated. Gene expression values were normalized by Variance Stabilizing Transformation (VST) **d**, Heatmap of SI values obtained from EXON analysis for each neocortical cell class (see methods for details) of all 2898 differentially regulated exons involved in alternative splicing events (log2(FC) ≥ 1 and ≤ -1, p-value ≤ 0.01. Base mean includes all neocortical samples). Alternative exon inclusion identifies sub-groups of exons that define distinct neocortical populations.

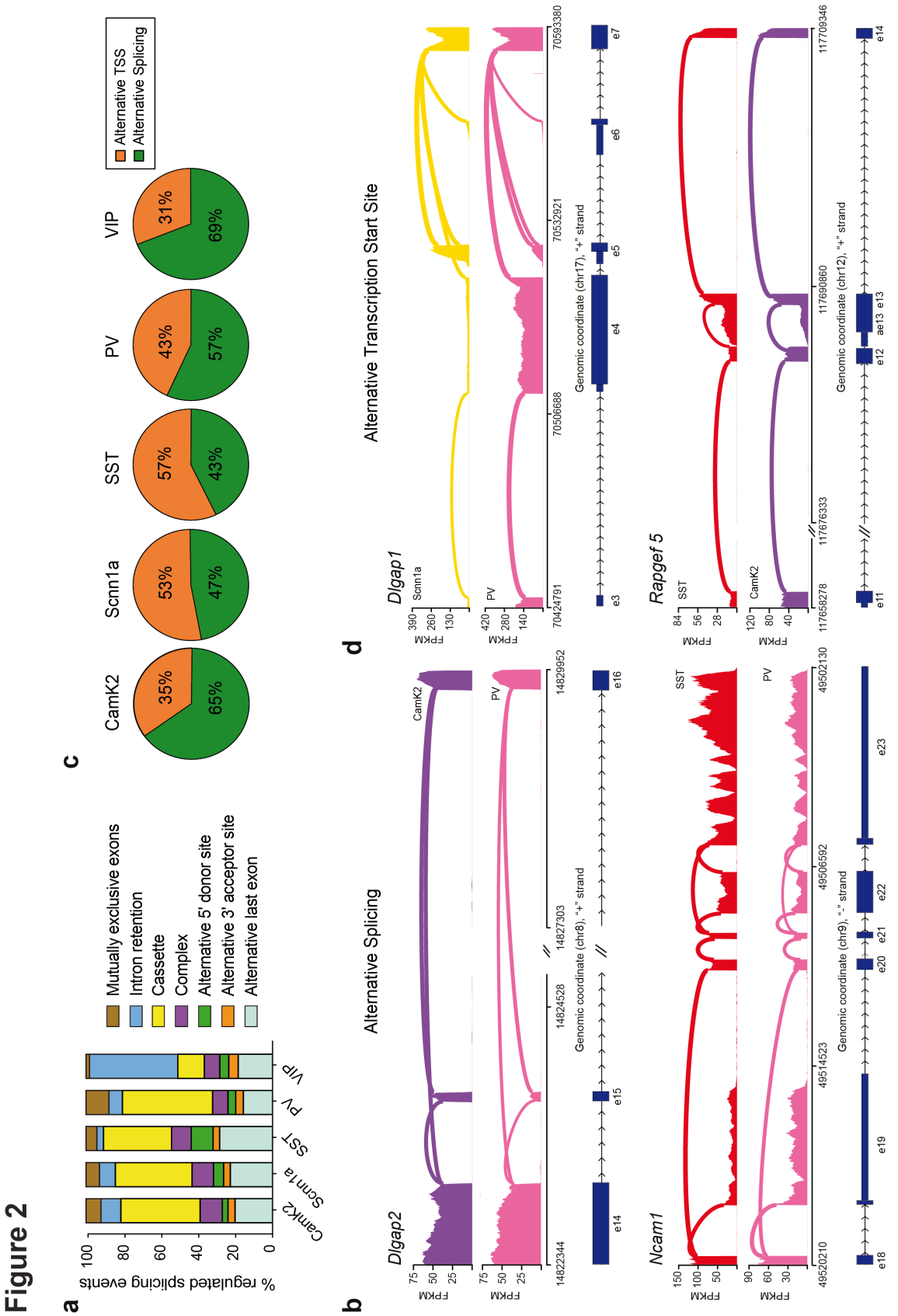
Figure 2
a
% regulated splicing events
Mutually exclusive exons
Intron retention
Cassette
Complex
Alternative 5' donor site
Alternative 3' acceptor site
Alternative last exon
CamK2
Scnn1a
SST
PV
VIP
c
Alternative TSS
Alternative Splicing
35%
65%
53%
47%
57%
43%
43%
57%
31%
69%
b
Alternative Splicing
Dlgap2
Ncam1
d
Alternative Transcription Start Site
Dlgap1
Rapgef 5
Genomic coordinate (chr8), "+" strand
Genomic coordinate (chr9), "-" strand
Genomic coordinate (chr17), "+" strand
Genomic coordinate (chr12), "+" strand

Fig. 2: Alternative splicing and alternative transcription start site usage drive transcript diversification in neocortical neurons

a, Histogram representing the relative percentage of differentially regulated (DR) alternative splicing event types (log2(FC) ≥ 1, p-value ≤ 0.01. Base mean includes all neocortical samples). The distinct pattern categories (mutually exclusive exon, cassette exon, intron retention, alternative 5' and 3' donor and acceptor site, alternative last exon, complex) are indicated. Total number of DR alternative splicing events are: 261 for CamK2, 165 for Scnn1a, 85 for SST, 316 for PV and 373 for VIP. Note that VIP interneurons show higher number of intron retention events. Otherwise, overall all neocortical populations show similar rates of splicing pattern types usage. **b**, Sashimi plots illustrating read distribution and splice junctions of *Dlgap2* (*upper panel*) and *Ncam1* (*lower panel*). One representative replicate for each cell population is shown. Genomic coordinates, chromosome number, strand and exon number are indicated below. Coding regions are indicated as thicker boxes, non-coding regions as thinner boxes). The alternative cassette exon 15 of *Dlgap2* is preferentially included in CamK2-positive neurons, *vice versa* excluded in PV-positive interneurons. On the other hand, *Ncam1* shows differential usage of exon 19 or exon 23 as alternative last exon, even between two GABAergic populations, with SST-positive cells preferentially using e23 compared to PV-positive neurons. **c,** Pie charts indicating the relative percentage of alternative transcription start sites (TSS) and alternative splicing of differentially regulated events (log2(FC) ≥ 1, p-value ≤ 0.01. Base mean includes all neocortical samples) identified by the PATTERN analysis (see methods for details) in neocortical populations. Total number of DR events are: 402 for CamK2, 349 for Scnn1a, 199 for SST, 557 for PV and 540 for VIP. **d**, Example sashimi plots for alternative TSS usage in *Dlgap1* (*upper panel*) or *Rapgef5* (*lower panel*). For *Dlgap1*, transcripts preferentially start with exon 5 in Scnn1a-positive cells and with exon 3 in PV-positive interneurons (note that coding region starts in exon 4). For *Rapgef5*, SST- and CamK2-positive cells show differential usage of exon 11 or exon 13 as first exon, with SST preferentially including exon 13.

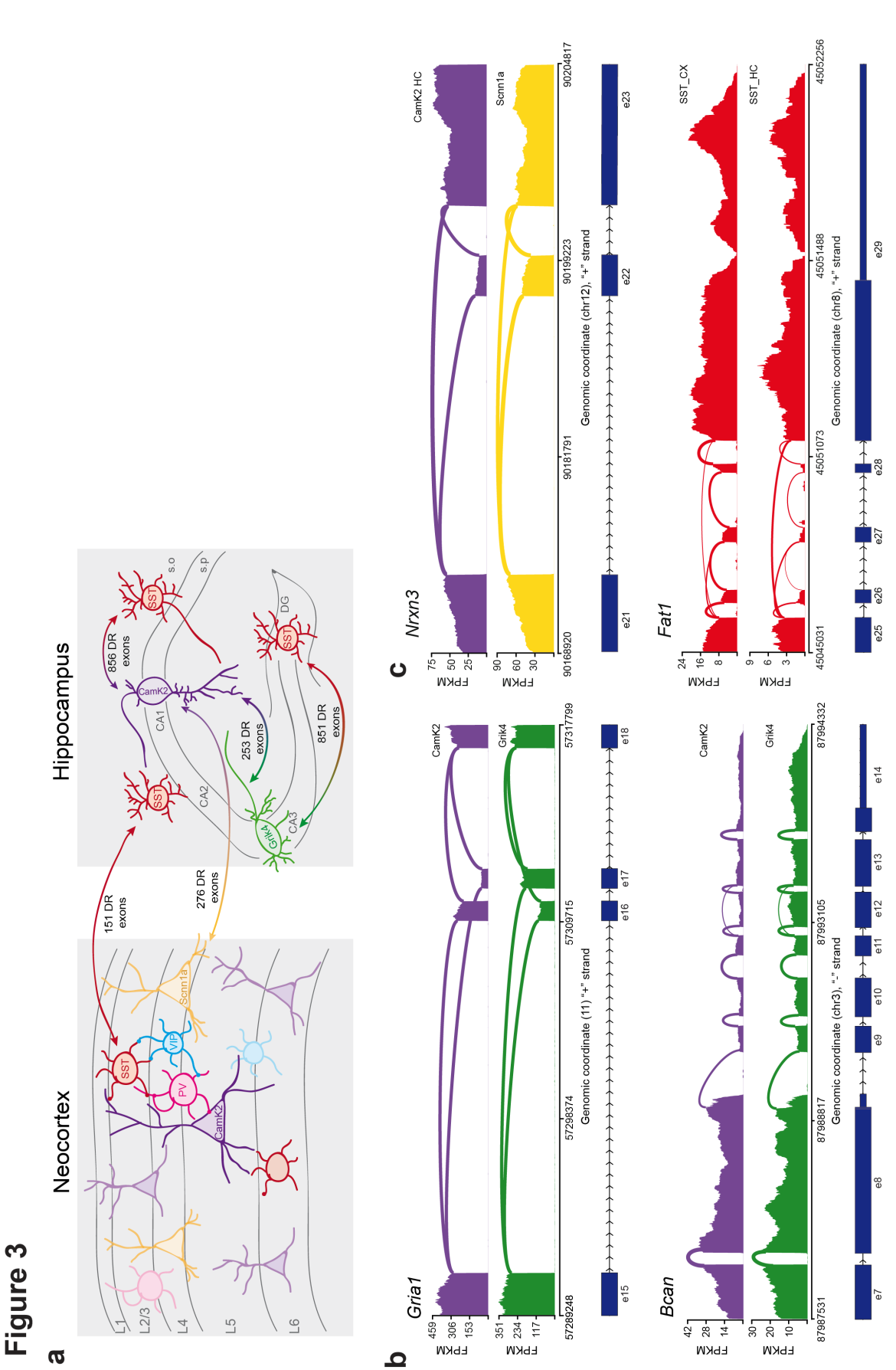
Figure 3
a
Neocortex
Hippocampus
151 DR exons
276 DR exons
856 DR exons
253 DR exons
851 DR exons
L1
L2/3
L4
L5
L6
SST
VIP
PV
CamK2
Scnn1a
CA1
CA2
CA3
DG
Grik4
s.o
s.p
b
Gria1
Bcan
CamK2
Grik4
FPKM
Genomic coordinate (11) "+" strand
Genomic coordinate (chr3), "-" strand
c
Nrxn3
Fat1
CamK2 HC
Scnn1a
SST_CX
SST_HC
Genomic coordinate (chr12), "+" strand
Genomic coordinate (chr8), "+" strand

Fig. 3: Alternative splicing programs distinguish closely related neuronal populations within the hippocampus and across brain regions
a, Cartoon illustrating the schematic representation of neuronal classes in the neocortex and hippocampus. The numbers shown indicate differentially regulated (DR) exons (log2(FC) ≥ 1 and ≤ -1, p-value ≤ 0.01) in pairwise comparisons between CamK2-positive CA1 and Grik4-positive CA3 pyramidal neurons (253 exons from 177 genes), between CA1 or CA3 neurons vs SST-positive hippocampal neurons and between neocortical (856 exons from 551 genes and 851 exons from 517 genes) and hippocampal SST-positive interneurons (151 exons from 103 genes) or layer 4 vs CA1 pyramidal neurons (276 exons from 209 genes). Note that only exons involved in AS events are indicated. Hippocampal SST-positive neurons show high diversity of alternative isoform expression compared to pyramidal cells. Also closely related glutamatergic populations (CA1 vs CA3 and CA1 vs Scnn1a) exhibit highly differential exon usage. On the other hand, SST-positive neurons isolated from distinct anatomical brain regions (hippocampus vs neocortex) present fewer but still significant differences in alternative isoform expression. s.o.=*stratum oriens*, s.r.=*stratum radiatum*, DG=*dentate gyrus*, CA=*cornu ammonis*. Note that this panel only displays select pairwise comparisons. Analysis for hippocampal SST interneurons considered all SST neurons without sub-regional distinction. **b-c**, Sashimi plots illustrating read distribution and splice junctions of transcripts differentially spliced between CA1 and CA3 pyramidal neurons (*panel **b***) or between related cell classes across distinct brain regions (SSTHc vs SSTCx, CA1 vs Scnn1a glutamatergic neurons, *panel **c***). Genomic coordinates, chromosome number, strand and exon number are indicated below. Coding regions are indicated as thicker boxes, non-coding as thinner boxes.In **b**, CamK2- and Grik4-positive glutamatergic neurons show differential usage of the mutually exclusive exons 16 and 17 in *Gria1* (*upper panel*) and the alternative last exons 8 and 14 in *Bcan (lower panel)*. In **c**, *Nrxn3* shows differential rate of inclusion of cassette exon 22 in the hippocampal CA1 vs cortical Scnn1a-positive pyramidal neurons (*upper panel*). Neocortical SST-positive interneurons show preferential inclusion of cassette exons 26, 27 and 28 in *Fat1*, while hippocampal SST-positive cells exclude them (the *lower pane*l).

Figure 4

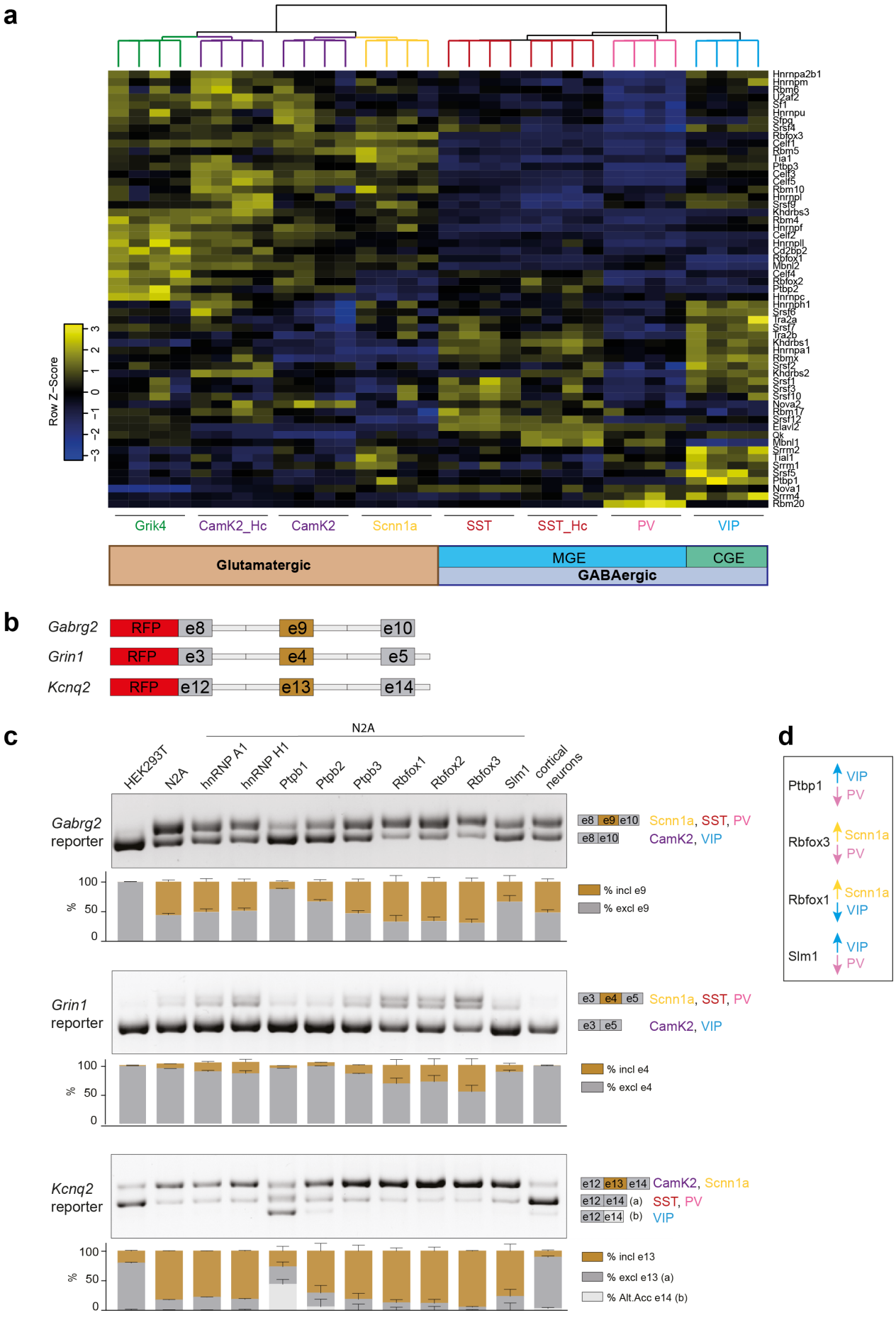
a
Row Z-Score
Grik4
CamK2_Hc
CamK2
Scnn1a
SST
SST_Hc
PV
VIP
Glutamatergic
MGE
CGE
GABAergic
b
Gabrg2
Grin1
Kcnq2
RFP
e8
e9
e10
e3
e4
e5
e12
e13
e14
c
N2A
HEK293T
N2A
hnRNP A1
hnRNP H1
Ptpb1
Ptpb2
Ptpb3
Rbfox1
Rbfox2
Rbfox3
Slm1
cortical neurons
Gabrg2 reporter
Grin1 reporter
Kcnq2 reporter
% incl e9
% excl e9
% incl e4
% excl e4
% incl e13
% excl e13 (a)
% Alt.Acc e14 (b)
Scnn1a, SST, PV
CamK2, VIP
CamK2, Scnn1a
SST, PV
VIP
d
Ptbp1
Rbfox3
Rbfox1
Slm1
VIP
PV
Scnn1a

Fig. 4: Differential splicing factors expression for cell class-specific splicing programs in mature neurons

a, Gene expression heatmap of a hand curated list of splicing factors in neocortical and hippocampal neuron classes. Sub-groups of splicing factors with highly significant or modest changes in gene expression across cell populations can be identified. Overall, expression rates of splicing factors across forebrain neurons populations can segregate cells according to their neurotransmitter phenotype and their developmental origin (glutamatergic vs GABAergic, Medial Ganglionic Eminence (MGE)-derived vs Caudal Ganglionic Eminence (CGE)-derived). For the complete list of enrichments and significance values for splicing factors across neocortical and hippocampal neurons, see Supplementary table 6. **b**, Cartoon illustrating the design of splicing reporters for *Gabrg2*, *Grin1* and *Kcnq2* (see methods for details). **c**, RT-PCR for splicing reporters overexpressed in HEK293T cells, Neuro2A (N2A) cells and cultured cortical neurons, or in combination with overexpression of several splicing factors (indicated *above*) in N2A cells. *On the right*, schematic representation of reporter exons amplified and cell types in which a given splicing pattern is enriched are indicated. For each sample, three PCR reactions were performed and band intensity was quantified. Representative images are shown. *Below*, histograms represent the percentage of inclusion (*in brown)* or exclusion (*in light and dark gray*) band intensity relative to the sum intensity of all bands. N=3 RT-PCRs, SEM is indicated. *Top PCR panel*: Expression of the splicing reporter for exon 9 of *Gabrg2* leads to differential exon inclusion in non-neuronal (HEK293T, excl. e9) versus neuronal (N2A or cortical neurons, 50% excl. e9) cells. Co-expression of Ptbp1 and, to lower extents, Ptbp2 and Slm1 (enriched in VIP) lead to higher exclusion rates, a pattern significantly enriched in VIP neurons. Co-expression of Rbfox1/2/3 slightly reduces exon exclusion rates, consistent with the splicing pattern observed in purifications of Scnn1a. *Middle PCR panel*: Similar effects of the same splicing factors can be observed for the splicing pattern of exon 4 of *Grin1*. Note that the amplification of *Grin1* isoform including e4 generates a doublet band. *Lower PCR panel*: Exon 13 of *Kcnq2* splice reporter is preferentially included in N2A cells. Addition of Ptbp1 and Ptbp2 induces the additional alternative acceptor site usage found in VIP neurons. Overall, these experiments indicate a correlation between splicing factor expression and alternative isoform usage. **d,** Highest or lowest expression levels in different cortical populations for Ptbp1, Rbofox1, Rbfox3 and Slm1 (Khdrbs2) are indicated by arrows.

Figure 5

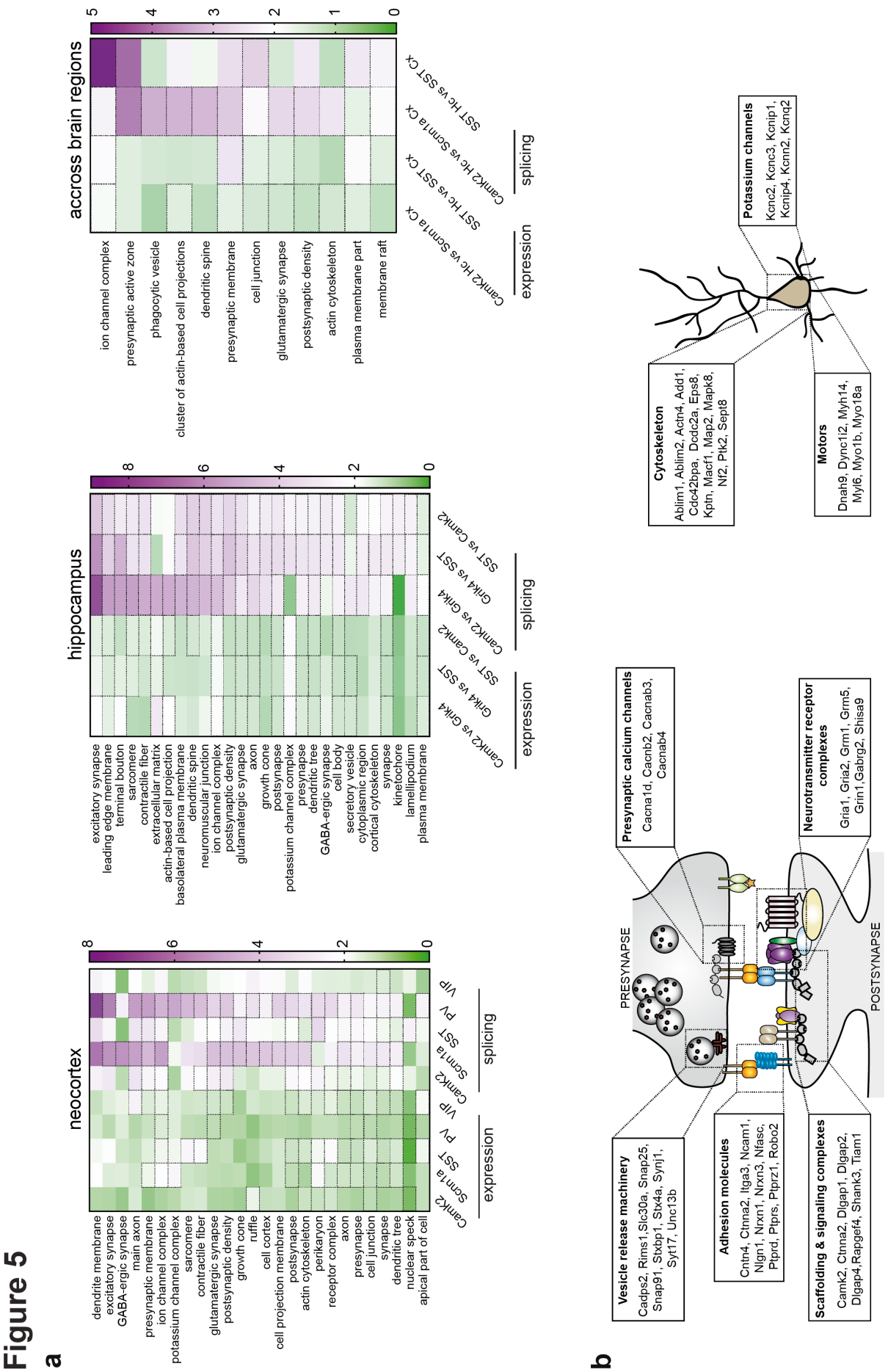
a
neocortex
dendrite membrane
excitatory synapse
GABA-ergic synapse
main axon
presynaptic membrane
ion channel complex
potassium channel complex
sarcomere
contractile fiber
glutamatergic synapse
postsynaptic density
growth cone
ruffle
cell cortex
cell projection membrane
postsynapse
actin cytoskeleton
perikaryon
receptor complex
axon
presynapse
cell junction
synapse
dendritic tree
nuclear speck
apical part of cell
Camk2
Scn1a
SST
PV
VIP
Camk2
Scn1a
SST
PV
VIP
expression
splicing
hippocampus
excitatory synapse
leading edge membrane
terminal bouton
sarcomere
contractile fiber
extracellular matrix
actin-based cell projection
basolateral plasma membrane
dendritic spine
neuromuscular junction
ion channel complex
postsynaptic density
glutamatergic synapse
axon
growth cone
postsynapse
potassium channel complex
presynapse
dendritic tree
GABA-ergic synapse
cell body
secretory vesicle
cytoplasmic region
cortical cytoskeleton
synapse
kinetochore
lamellipodium
plasma membrane
Camk2 vs Grik4
Grik4 vs SST
SST vs Camk2
Camk2 vs Grik4
Grik4 vs SST
SST vs Camk2
expression
splicing
accross brain regions
ion channel complex
presynaptic active zone
phagocytic vesicle
cluster of actin-based cell projections
dendritic spine
presynaptic membrane
cell junction
glutamatergic synapse
postsynaptic density
actin cytoskeleton
plasma membrane part
membrane raft
Camk2 Hc vs Scn1a Cx
SST Hc vs SST Cx
Camk2 Hc vs Scn1a Cx
SST Hc vs SST Cx
expression
splicing
b
PRESYNAPSE
POSTSYNAPSE
Vesicle release machinery
Cadps2, Rims1,Slc30a, Snap25, Snap91, Stxbp1, Stx4a, Synj1, Syt17, Unc13b
Presynaptic calcium channels
Cacna1d, Cacnb2, Cacnab3, Cacnab4
Adhesion molecules
Cntn4, Ctnna2, Itga3, Ncam1, Nlgn1, Nrxn1, Nrxn3, Nfasc, Ptprd, Ptprs, Ptprz1, Robo2
Neurotransmitter receptor complexes
Gria1, Gria2, Grm1, Grm5, Grin1,Gabrg2, Shisa9
Scaffolding & signaling complexes
Camk2, Ctnna2, Dlgap1, Dlgap2, Dlgap4,Rapgef4, Shank3, Tiam1
Cytoskeleton
Ablim1, Ablim2, Actn4, Add1, Cdc42bpa, Dcdc2a, Eps8, Kptn, Macf1, Map2, Mapk8, Nf2, Ptk2, Sept8
Potassium channels
Kcnc2, Kcnc3, Kcnip1, Kcnip4, Kcnn2, Kcnq2
Motors
Dnah9, Dync1i2, Myh14, Myl6, Myo1b, Myo18a

Fig. 5: Alternative splicing programs are highly dedicated to the control of synaptic interactions and neuronal architecture

a, Heatmap representing the fold enrichment of Gene Ontology (GO) terms for transcripts differentially regulated at gene expression level or by alternative splicing identified by the Panther Classification System (see methods for details). Terms listed were selected based on the splicing analysis and had to be significant in at least one neocortical population (*left panel),* hippocampal comparison (*middle panel)* or comparison across brain regions (*right panel*). Corresponding values from analysis of differentially expressed genes were included on the left. Fields for the statistically significant enrichments (p-value ≤ 0.05) are highlighted by a dashed outline. Overall, transcripts undergoing differential alternative splicing show higher fold enrichments compared to differentially expressed genes. Splicing-dependent transcript isoforms in VIP interneurons present lower, whereas Scnn1a and PV exhibit higher fold enrichment of GO categories. See Supplementary Table 7 for the raw output from the GO analysis. **b**, Cartoon illustrating the main categories of genes whose alternative splicing is differentially regulated between cell populations (log2(FC) ≥ 1 and ≤ -1, p-value ≤ 0.01). Among the most enriched categories, we find genes encoding presynaptic proteins modulating calcium influx or vesicle fusion, pre- and postsynaptic adhesion molecules and postsynaptic scaffolding molecules. **c**, Cartoon illustrating examples of differentially expressed transcript isoforms encoding for proteins which modulate intrinsic properties of neurons (e.g., potassium channels, proteins involved in cytoskeletal remodeling and cellular transport along neurites).

Table 1

	sample	reads	% uniquely mapped	detected genes	% ribosomal	% mRNA	% junctions
Neocortex	CamK2.1	106 285 408	91	12 581	2.37	88.16	46.9
	CamK2.2	106 649 400	89	12 684	3.83	86.96	44.7
	CamK2.3	106 307 008	89	12 811	4.78	85.99	44.6
	CamK2.4	106 310 810	90	12 729	3.60	86.94	45.6
	Scnn1a.1	106 585 369	91	13 006	0.77	88.55	46.1
	Scnn1a.2	106 697 346	91	13 520	0.54	89.65	45.6
	Scnn1a.3	111 712 617	89	12 960	2.77	86.57	44.1
	Scnn1a.4	106 932 622	91	13 076	1.37	87.89	47.2
	SST.1	106 302 135	89	12 801	3.25	86.61	45.4
	SST.2	106 634 352	89	12 757	4.03	86.28	44.9
	SST.3	107 107 840	89	12 893	2.14	87.43	47.1
	SST.4	106 456 627	89	12 740	3.21	86.28	44.5
	PV.1	106 914 394	89	12 379	3.52	86.13	46.1
	PV.2	106 908 043	89	12 533	2.78	85.61	47.8
	PV.3	106 473 854	90	12 373	0.43	88.10	49.3
	PV.4	106 653 175	89	12 395	4.42	84.42	45.7
	VIP.1	106 992 707	88	13 436	1.32	85.68	43.7
	VIP.2	107 049 639	90	13 533	0.97	86.24	45.7
	VIP.3	108 533 591	90	13 782	0.84	85.08	44.0
	VIP.4	105 684 224	89	13 393	3.0	84.27	43.3
Hippocampus	CamK2.1	105 644 496	90	12 528	4.38	85.88	47.0
	CamK2.2	106 516 554	88	12 564	5.46	85.01	45.5
	CamK2.3	109 118 524	89	12 506	6.71	84.34	45.8
	CamK2.4	107 445 662	89	12 657	5.59	85.24	45.9
	Grik4.1	106 601 624	90	12 584	2.51	87.67	47.6
	Grik4.2	106 635 010	89	12 789	4.01	86.90	47.9
	Grik4.3	106 712 395	90	12 731	3.07	87.87	49.5
	Grik4.4	107 951 454	89	12 802	4.86	86.19	48.0
	SST.1	106 448 303	90	12 895	0.68	89.15	47.8
	SST.2	110 095 915	89	12 838	2.52	86.67	46.9
	SST.3	114 811 827	89	12 795	4.24	85.76	45.2
	SST.4	179 458 089	90	12 835	0.62	89.22	48.3

Table 1: FastQC analysis of RNA-sequencing data

For each biological replicate of each sample, the following parameters are indicated: total number of reads, % of reads uniquely mapped to the reference genome, number of detected genes, % ribosomal contamination, % of mRNA representation and % of reads mapped to exon-exon junctions. All samples show highly similar values across biological replicates, as well as across samples, suggesting a high consistency and homogeneity of the RNA-seq data.

Figure S1

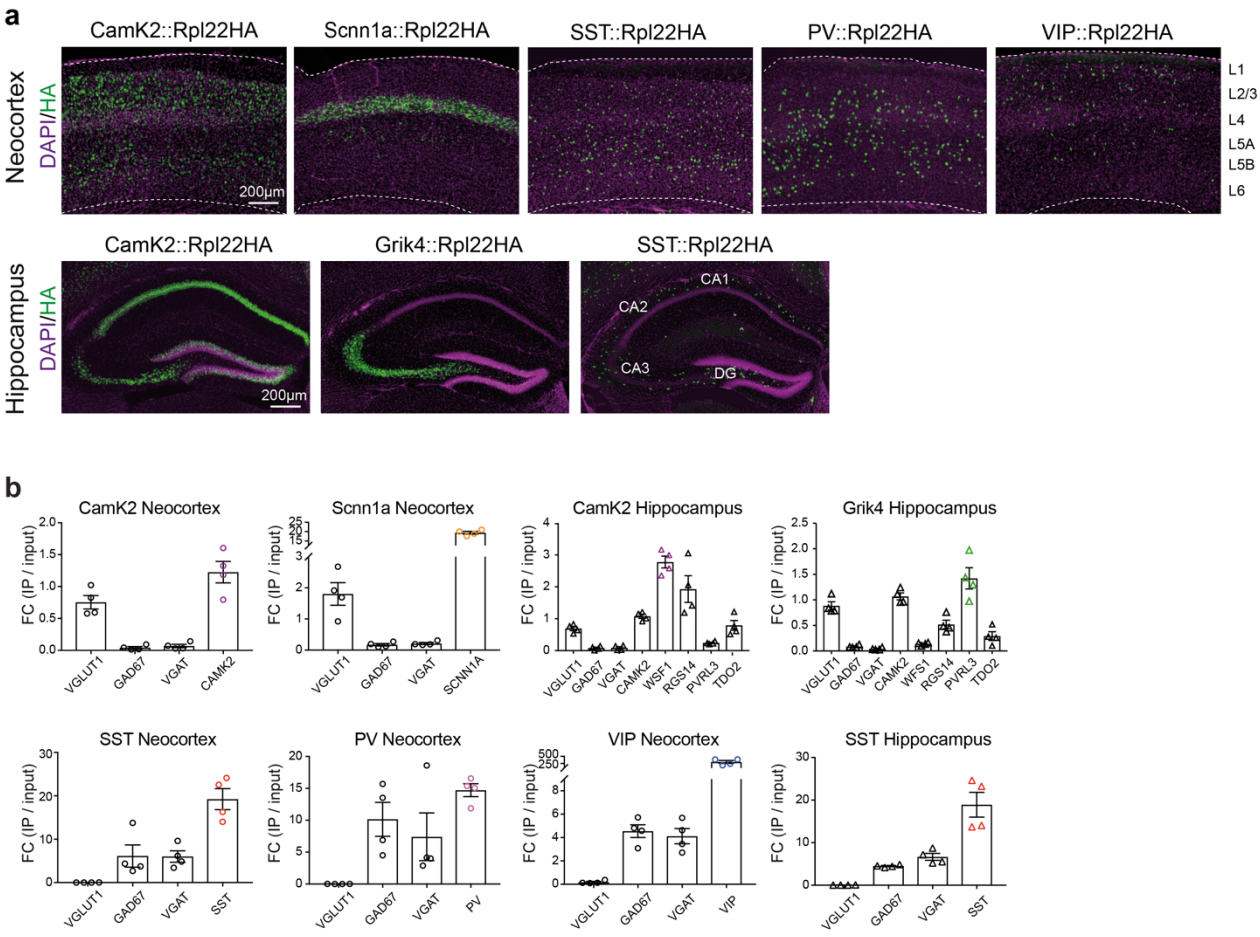

Supplementary Fig. 1. Confirmation of selective transgene expression and selective mRNA isolation with RiboTrap approach in mice

a, Expression pattern of HA-tagged Rpl22 protein, conditionally expressed in *CamK2::Rpl22*-HA, *Scnn1a::Rpl22*-HA, *SST::Rpl22*-HA, *PV::Rpl22*-HA, *VIP::Rpl22*-HA and *Grik4::Rpl22*-HA 3-5 weeks old mice [primary somatosensory cortex (S1, *upper panel*) and whole hippocampus (*lower panel*)]. CamK2-cre-dependent expression of Rpl22-HA is mostly driven in excitatory neurons across all cortical layers and it is enriched in the CA1 region of the hippocampus. Scnn1a-cre and Grik4-cre drive Rpl22-HA expression in two regionally distinct areas, the layer 4 (L4) of the cortex and the CA3 region of the hippocampus, respectively. SST-cre, PV-cre and VIP-cre, on the other hand, determine the sparse labelling of GABAergic interneurons across the neocortical layers and in the *stratum oriens* and *hilus* of the hippocampus (in SST*::Rpl22*-HA mice). Cells nuclei are labelled *in magenta*, Rpl22-HA expressing neurons are *in green*. Scale bar: 200 µm. Neoortical layers and hippocampal regions are indicated. DG=*dentate gyrus,* CA=*cornu ammonis*. **b**, Real-time qPCR for cell type- and region-specific transcript markers confirmed the purity of the four immuno-isolated mRNA replicates per cell population. Transcript enrichment of the immune-isolated RNA (IP) was calculated relative to the input (total neocortical or hippocampal RNA) and was normalized to enrichments of *Gapdh*. Overall, RNA isolated from inhibitory neurons show high enrichments of general GABAergic markers (*Vgat*, *Gad67*) and de-enrichments of the excitatory marker *Vglut1*, vice versa for immune-isolated RNA from glutamatergic neurons. Moreover, cell type specific markers

(*Camk2*, *Scnn1a*, *SST*, *PV*, *VIP*) are relatively enriched in the corresponding preparation. For the hippocampal samples, the CA1-specific *Wsf1* and CA3-specific *Pvrl3* markers show enrichments in CamK2 and Grik4 samples, respectively, but the CA2- and DG-specific markers (*Rgs14* and *Tdo2)* show lower enrichment levels. Note that endogenous CamK2 transcripts are more broadly distributed than cre-recombination in the transgenic mice. Modest enrichment values (as compared to GABAergic markers) in IPs are a consequence of the broad transcript expression.

Figure S2

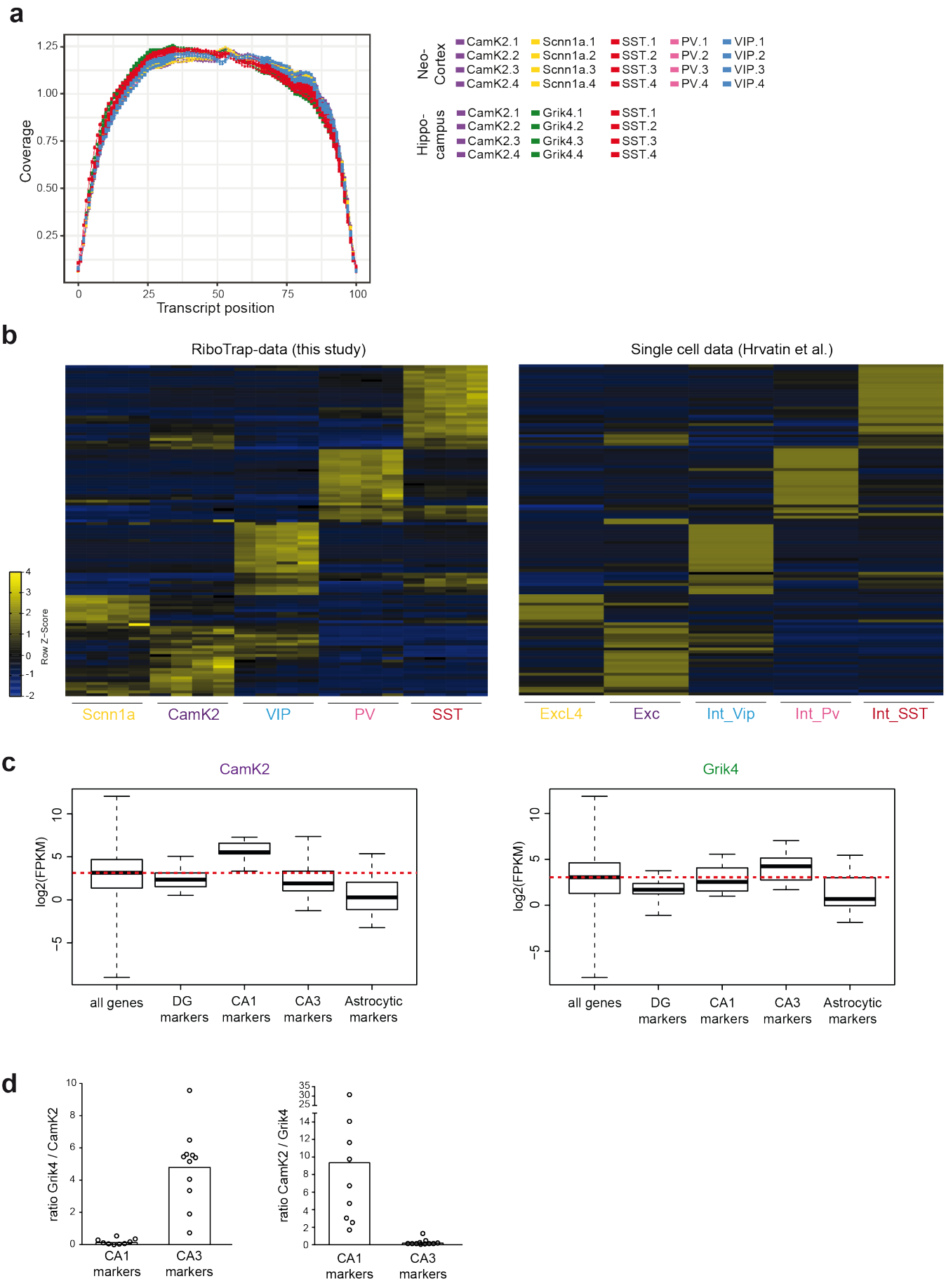
a
Coverage
Transcript position
Neo-Cortex
CamK2.1 CamK2.2 CamK2.3 CamK2.4
Scnn1a.1 Scnn1a.2 Scnn1a.3 Scnn1a.4
SST.1 SST.2 SST.3 SST.4
PV.1 PV.2 PV.3 PV.4
VIP.1 VIP.2 VIP.3 VIP.4
Hippo-campus
CamK2.1 CamK2.2 CamK2.3 CamK2.4
Grik4.1 Grik4.2 Grik4.3 Grik4.4
SST.1 SST.2 SST.3 SST.4
b
RiboTrap-data (this study)
Single cell data (Hrvatin et al.)
Row Z-Score
Scnn1a CamK2 VIP PV SST
ExcL4 Exc Int_Vip Int_Pv Int_SST
c
CamK2
Grik4
log2(FPKM)
all genes
DG markers
CA1 markers
CA3 markers
Astrocytic markers
d
ratio Grik4 / CamK2
ratio CamK2 / Grik4
CA1 markers
CA3 markers

Supplementary Fig. 2. Quality controls confirmed the purity of RiboTRAP samples
a, Coverage plot indicating the percentage of read bases at a given position of the transcript. All biological replicates of all samples used for analysis show excellent 5' to 3' coverage across the transcript length. **b**, Heatmaps representing the expression of cell type-specific marker genes identified by single cell sequencing in Hrvatin et al., 2018 (Hrvatin et al., 2018). *Left panel*, marker genes defined by Hrvatin et al. show appropriate enrichments in the RiboTRAP neocortical samples generated in the present study. *Right panel*, average expression of the same markers (order as in left panel) across pools of single cells belonging to the indicated classes (data from Hrvatin et al., 2018. ExcL4=glutamatergic L4-specific, Exc=pan-neocortical glutamatergic, Int_Vip=VIP-positive, Int_PV=PV-positive, Int_SST=SST-positive). Overall, previously identified cell type-specific marker genes show very similar relative enrichments in single-cell and RiboTrap datasets. **c**, Boxplot representing the distribution of log2(FPKM) values in either CamK2 *(left panel*) or Grik4 (*right panel*) samples for all genes detected, and for previously described DG-, CA1-, CA3- and astrocytic-specific markers (see Supplementary Table 1 for the complete marker lists). Expression values from the four biological replicates were averaged. In both CamK2 and Grik4 samples, overall expression of DG- and astrocytic-specific markers are represented below the median expression value of all genes (indicated in the graph as red dotted line). By contrast, CA1- and CA3-specific markers expression is higher in CamK2 and Grik4 samples, respectively. **d**, Relative enrichment of previously described CA1- and CA3-specific marker expression in Grik4 compared to CamK2 samples (*left panel*) and in CamK2 compared to Grik4 samples (*right panel*). FPKM values from the four biological replicates were averaged. Grik4 samples show strong relative enrichment of CA3-specific markers and strong de-enrichments of CA1-specific markers expression, *vice versa* for CamK2 samples.

Figure S3

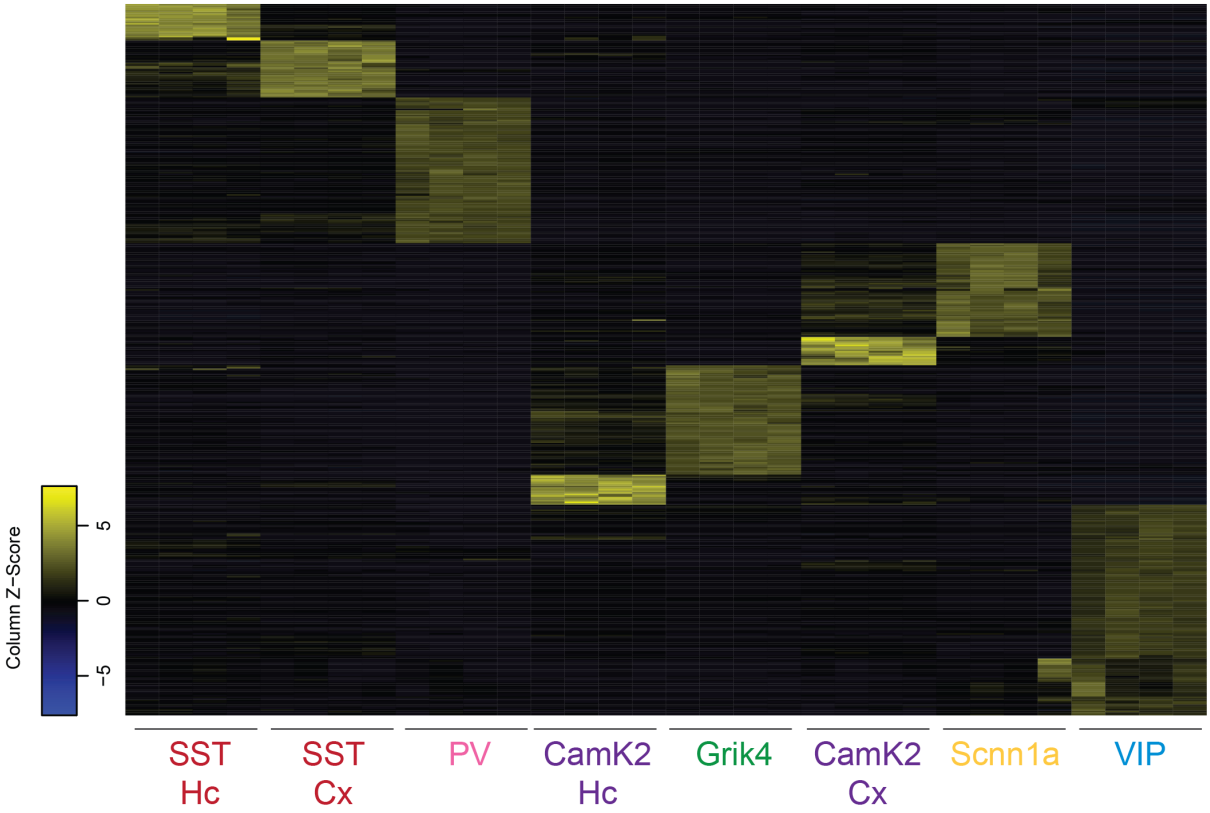

Supplementary Fig. 3. Cell population-specific markers identified show highly selective enrichments
Heatmaps of transcripts highly enriched in a specific cell population compared to all neocortical and hippocampal neuron populations (log2(FC) ≥ 3, p-value ≤ 0.01. Base mean includes all samples). Cell class-specific markers show high enrichments across all biological replicates of one population and strong de-enrichments in all the others. Well-known and new cell-population markers were identified (see Supplementary Table 1 for a complete list of highly enriched genes).

Figure S4

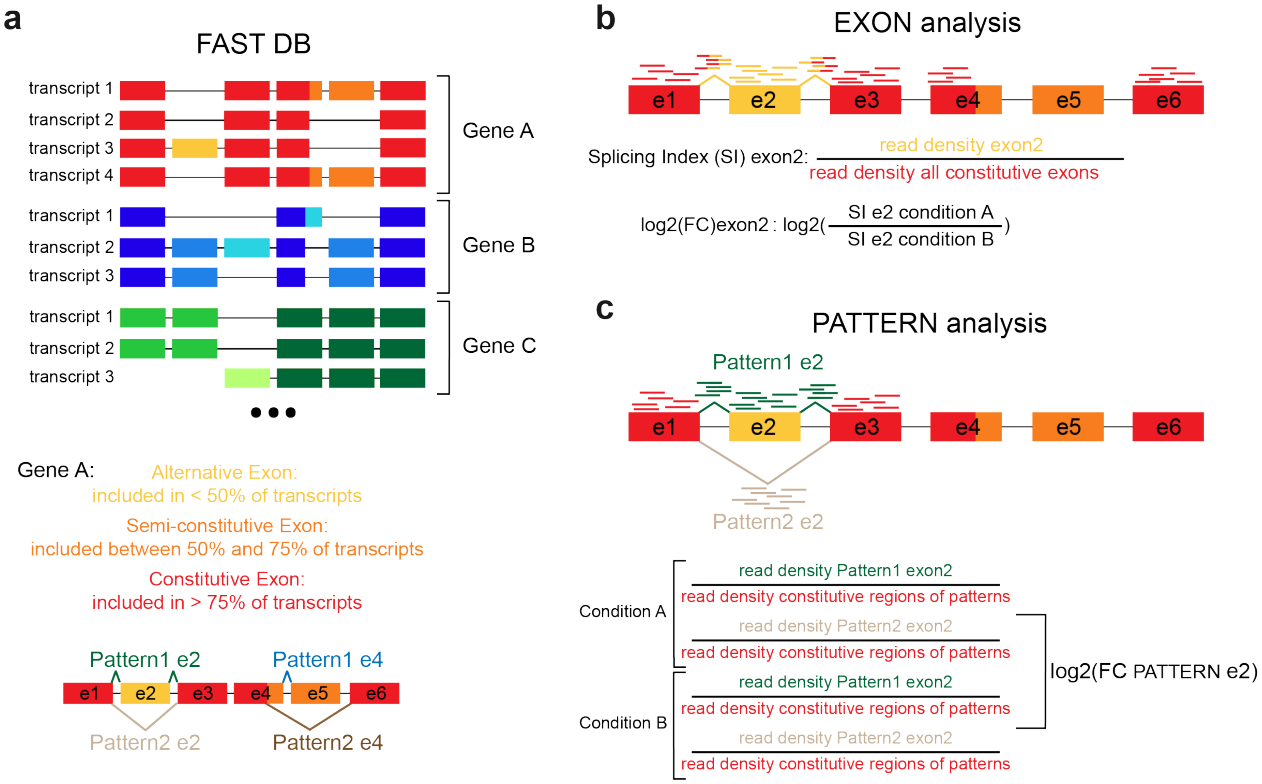

Supplementary Fig. 4: Alternative splicing analysis pipeline
a, Cartoon illustrating transcript annotation in FAST DB. For every gene present in the Mouse FAST DB v2016_1 database (de la Grange et al., 2007), all annotated transcripts are listed (*upper panel*). For every transcript, exons are defined as constitutive (if present in more than 75% of the transcripts generated from a given gene, for “GeneA” in red), semi-constitutive (if present in between 50% and 75% of all transcripts, for “GeneA” in orange) or alternative (if included in less than 50% of transcripts, for “GeneA” in yellow). Moreover, for every gene, all previously described splicing patterns are annotated (*lower panel*).
b, In the EXON analysis, for every exon expressed (see methods for definition of exon expression), a splicing index (SI_{EXON}) was determined by calculating the ratio of the read density on a given exon and the read density on all constitutive exons of the gene. The SI_{EXON} indicates the rate of inclusion of each expressed exon in every expressed gene. A fold-change is then calculated by comparing the average SI_{EXON} of the four replicates of a given sample (condition A) and the average SI_{EXON} of condition B (i.e., average SI_{EXON} of another sample, in the case of pairwise comparisons, or average SI_{EXON} across all neocortical samples, including sample of condition A).
c, In the PATTERN analysis, for every pattern annotated in the database, the read density was quantified. For every condition, read density of the two possible patterns was normalized by the density of constitutive regions of the patterns (in the example, e1 and e3) and a fold-change was calculated by comparing the normalized pattern read density in the two conditions A and B.

Figure S5

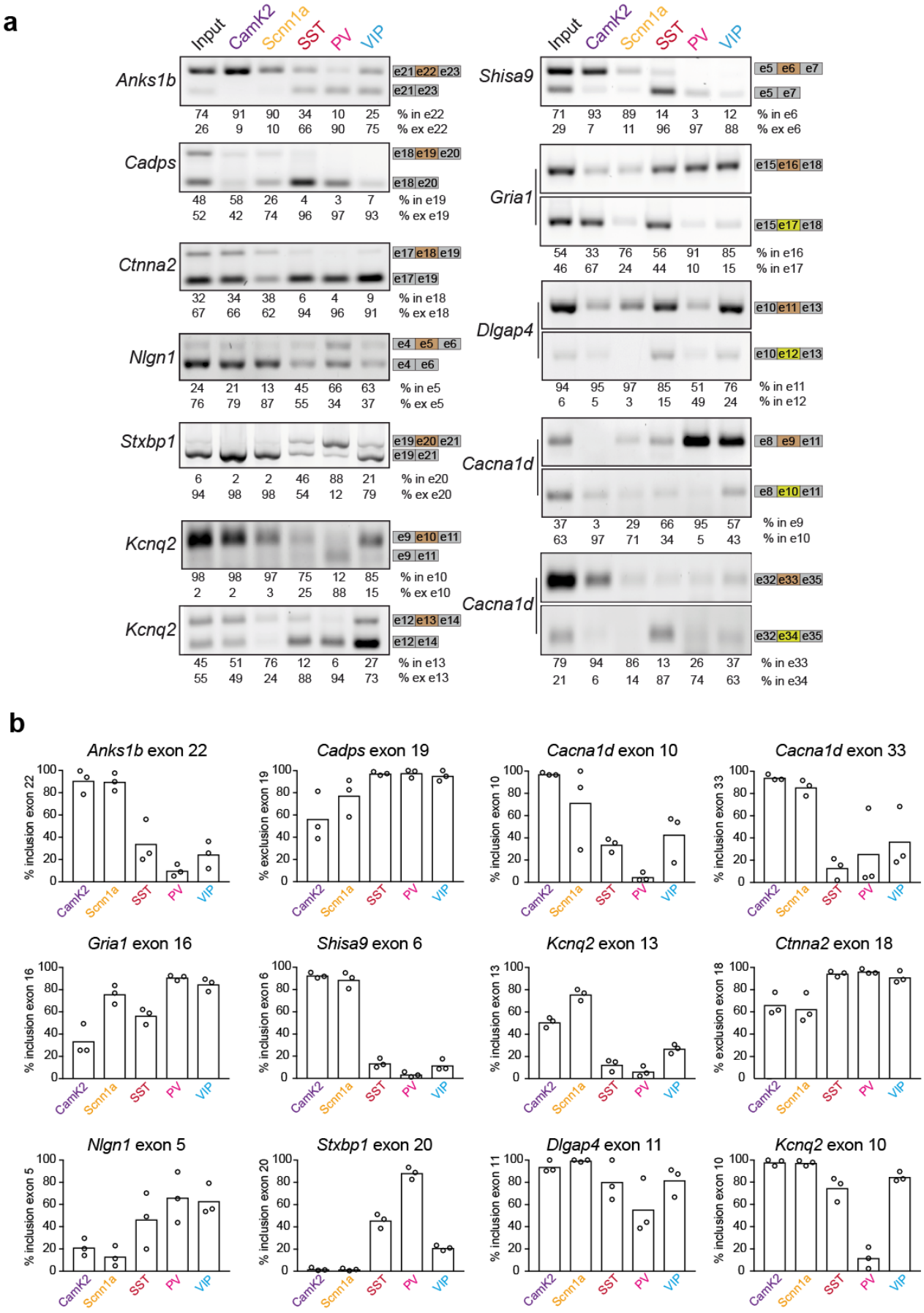
a
Input
CamK2
Scnn1a
SST
PV
VIP
Anks1b
e21 e22 e23
e21 e23
74 91 90 34 10 25 % in e22
26 9 10 66 90 75 % ex e22
Cadps
e18 e19 e20
e18 e20
48 58 26 4 3 7 % in e19
52 42 74 96 97 93 % ex e19
Ctnna2
e17 e18 e19
e17 e19
32 34 38 6 4 9 % in e18
67 66 62 94 96 91 % ex e18
Nlgn1
e4 e5 e6
e4 e6
24 21 13 45 66 63 % in e5
76 79 87 55 34 37 % ex e5
Stxbp1
e19 e20 e21
e19 e21
6 2 2 46 88 21 % in e20
94 98 98 54 12 79 % ex e20
Kcnq2
e9 e10 e11
e9 e11
98 98 97 75 12 85 % in e10
2 2 3 25 88 15 % ex e10
Kcnq2
e12 e13 e14
e12 e14
45 51 76 12 6 27 % in e13
55 49 24 88 94 73 % ex e13
Shisa9
e5 e6 e7
e5 e7
71 93 89 14 3 12 % in e6
29 7 11 96 97 88 % ex e6
Gria1
e15 e16 e18
e15 e17 e18
54 33 76 56 91 85 % in e16
46 67 24 44 10 15 % in e17
Dlgap4
e10 e11 e13
e10 e12 e13
94 95 97 85 51 76 % in e11
6 5 3 15 49 24 % in e12
Cacna1d
e8 e9 e11
e8 e10 e11
37 3 29 66 95 57 % in e9
63 97 71 34 5 43 % in e10
Cacna1d
e32 e33 e35
e32 e34 e35
79 94 86 13 26 37 % in e33
21 6 14 87 74 63 % in e34
b
Anks1b exon 22
% inclusion exon 22
Cadps exon 19
% exclusion exon 19
Cacna1d exon 10
% inclusion exon 10
Cacna1d exon 33
% inclusion exon 33
Gria1 exon 16
% inclusion exon 16
Shisa9 exon 6
% inclusion exon 6
Kcnq2 exon 13
% inclusion exon 13
Ctnna2 exon 18
% exclusion exon 18
Nlgn1 exon 5
% inclusion exon 5
Stxbp1 exon 20
% inclusion exon 20
Dlgap4 exon 11
% inclusion exon 11
Kcnq2 exon 10
% inclusion exon 10
0 20 40 60 80 100
CamK2 Scnn1a SST PV VIP

Supplementary Fig. 5: Semi-quantitative PCR validation of predicted alternative splicing events

a, Analysis of alternative splicing events in total neocortex (input) and CamK2, Scnn1a, SST, PV, VIP neocortical immuno-isolated RNAs. Flanking primers were used to amplify exons involved in the events found to be differentially regulated in neocortical samples by RT-PCR. The names of genes and schematic representation of the exons amplified are indicated. For each sample, three PCR reactions were performed and band intensity was quantified. Representative images are shown. Mean percentage of exon inclusion or exclusion in the three replicates is indicated below. For the 22 predicted differentially regulated events tested, 20 were experimentally validated (>90%, 8 not shown), confirming the high confidence of sequencing predictions. **b,** Quantification of PCR assessing the relative usage of alternatively spliced exons in neocortical samples. Single data points represent the percentage of band intensity of the exon of interest relative to the sum intensity of both bands (N=3 PCRs from three independent immune-isolated RNA samples). Gene names and exons amplified are indicated.

Figure S6

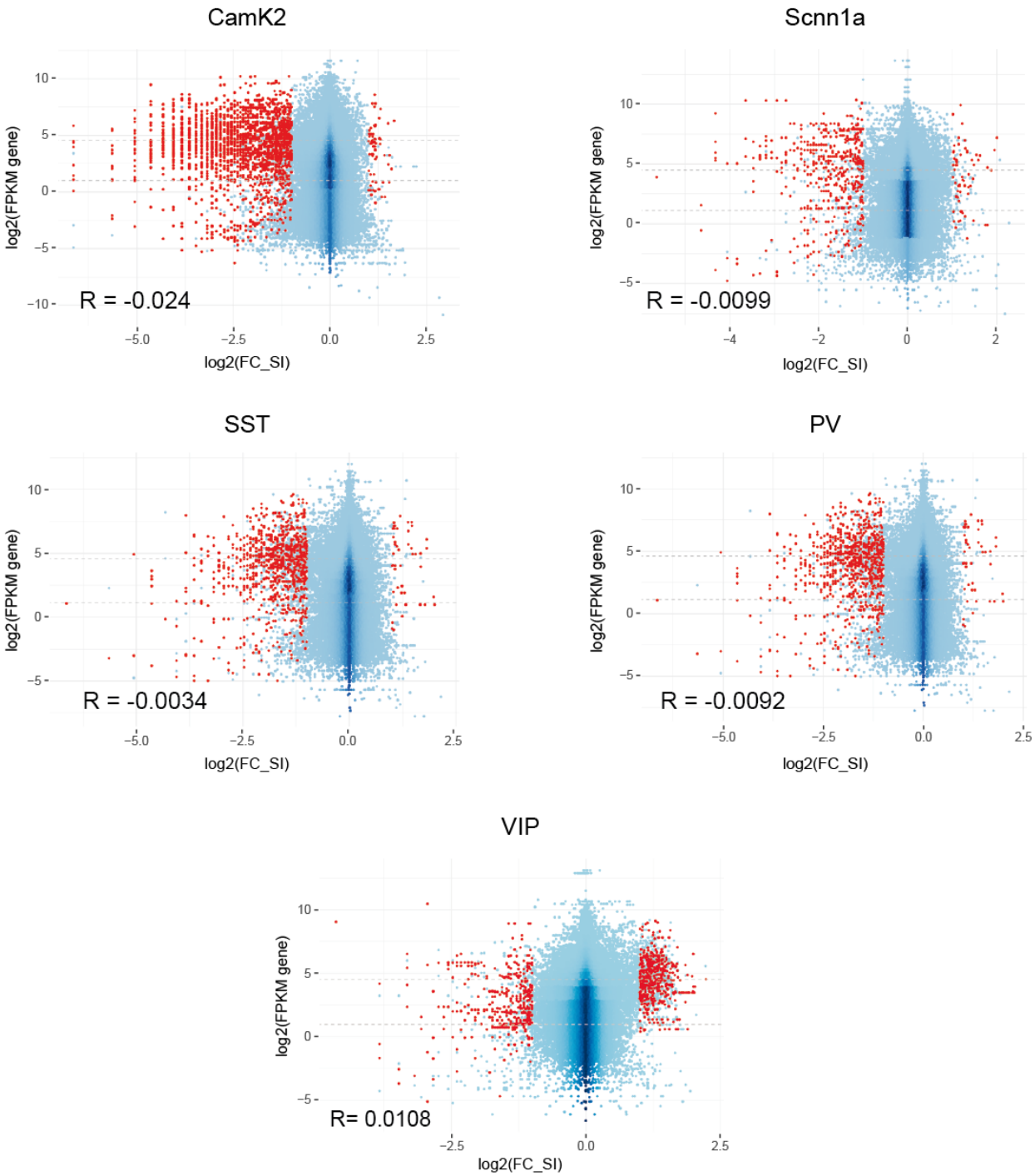

Supplementary Fig. 6: Differentially used exons are detected over a wide range of gene expression levels

Correlation plots showing the relation between differential usage of each detected exon in neocortical populations and the expression of the corresponding gene. The log2 fold-change of splicing index obtained from EXON analysis (log2(FC)_SI, base mean includes all neocortical samples) was compared to the log2(FPKM) expression value of the gene including a given exon. FPKM values from the four biological replicates of each cell population were averaged. Exons found to be differentially included in the cell population indicated are

highlighted in red (log2(FC) ≥ 1 and ≤ -1, p-value ≤ 0.01). Gray dotted lines represent the 25th (*lower*) and 75th (*upper*) percentile of log2(FPKM) values of all expressed genes. On the bottom left of the graph, correlation value (R) is indicated. We do not observe a correlation of gene expression levels and differential exon usage.

Figure S7

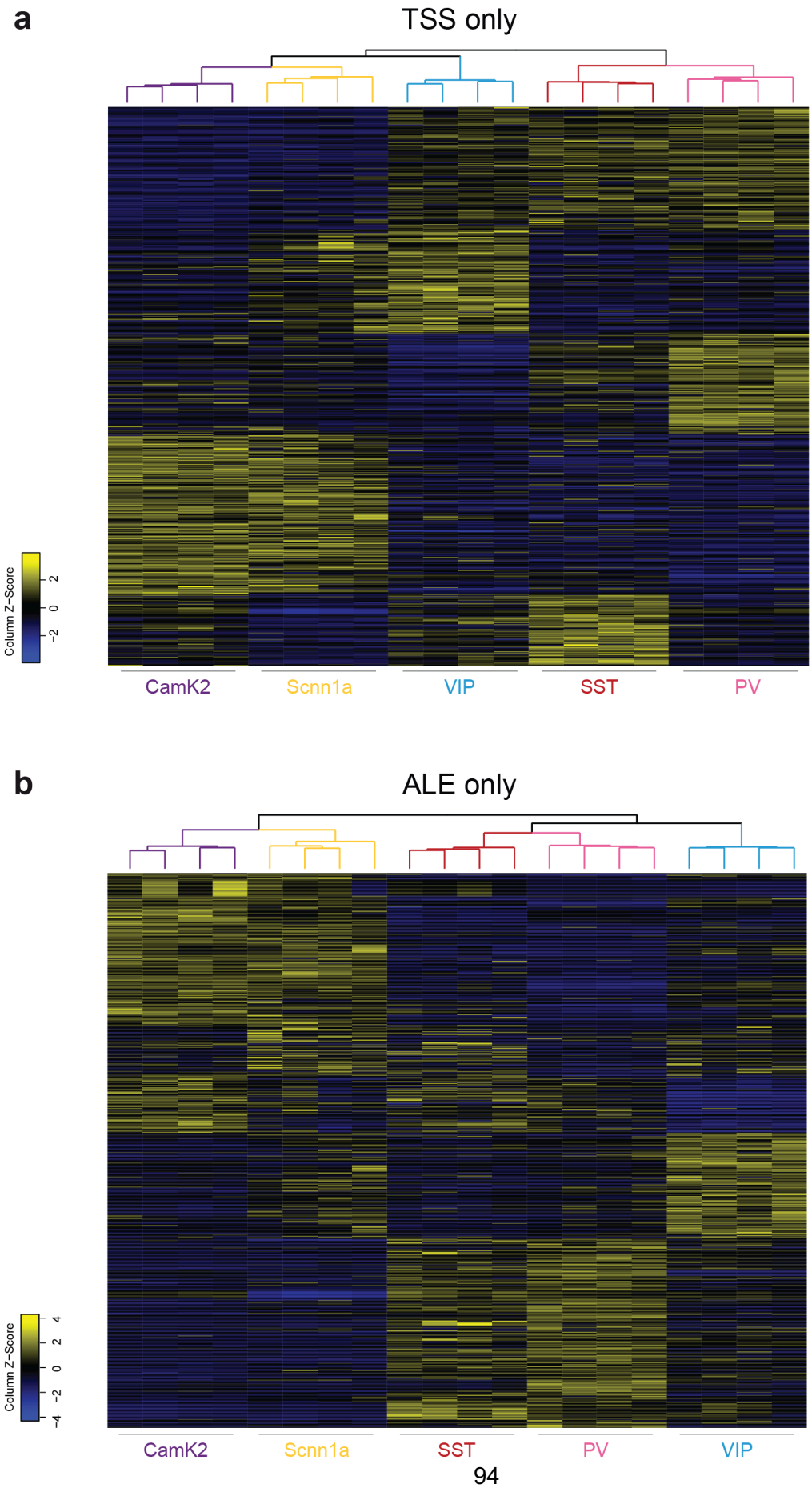
a
TSS only
Column Z-Score
2
0
−2
CamK2
Scnn1a
VIP
SST
PV
b
ALE only
Column Z-Score
4
2
0
−2
−4
CamK2
Scnn1a
SST
PV
VIP

Supplementary Fig. 7:
a, b, Heatmaps of SI values obtained from EXON analysis (see methods for details) for differentially regulated exons in neocortical cell populations (log2(FC) ≥ 1 and ≤ -1, p-value ≤ 0.01, base mean includes all neocortical samples). Panel (a) shows exons contributing to alternative transcription start sites (TSS). Panel (b) shows alternative last exons (ALE).
Amongst the 1111 differentially regulated TSS events, the two glutamatergic samples (CamK2 and Scnn1a) share 124 common events. Within the GABAergic populations, PV neurons share 50 and 45 common TSS events with SST and VIP samples, respectively, while SST sample have 34 common TSS events with VIP neurons.
Amongst the 867 differentially regulated ALE events, the two glutamatergic samples (CamK2 and Scnn1a) share 80 common events. On the other hand, within the GABAergic populations, PV neurons share 42 and 38 common TSS events with SST and VIP samples, respectively, while SST sample have 19 common TSS events with VIP neurons.

Figure S8

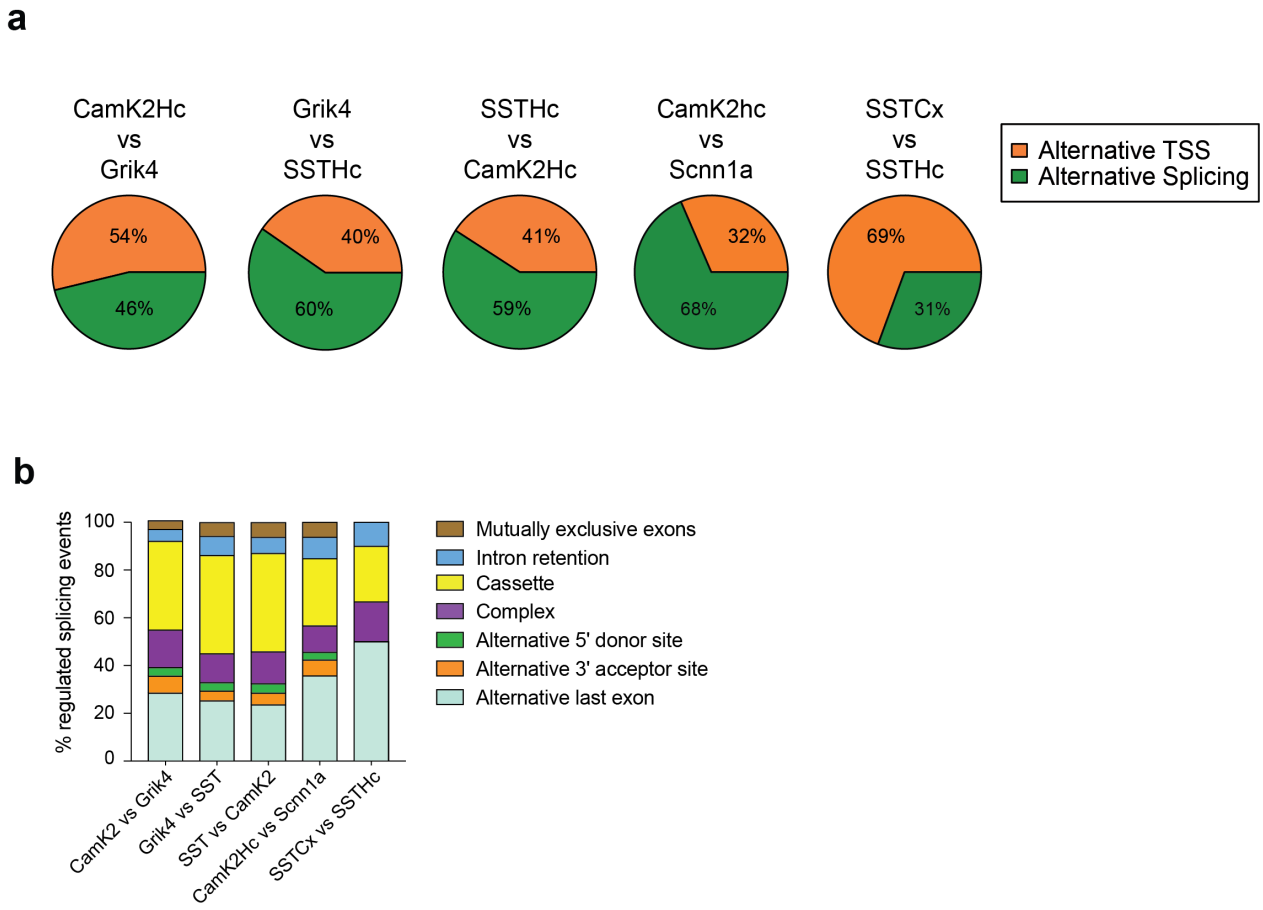

Supplementary Fig. 8: PATTERN analysis in pairwise hippocampal and across brain regions comparisons reveals similar percentages of alternative TSS and AS events compared to neocortical populations.
a, Pie charts indicating the relative percentage of alternative transcription start site (TSS) and alternative splicing events out of the differentially regulated events identified by the PATTERN analysis (log2(FC) ≥ 1, p-value ≤ 0.01) in the pairwise hippocampal comparisons (CamK2Hc vs Grik4, Grik4 vs SSTHc, SSTHc vs CamK2Hc) and in the pairwise comparisons across brain regions (CamK2Hc vs Scnn1a, SSTCx vs SSTHc). Total number of differentially regulated patterns are: 321 for CamK2Hc vs Grik4, 1126 for Grik4 vs SSTHc, 1131 for SSTHc vs CamK2Hc, 1054 for CamK2Hc vs Scnn1a and 98 for SSTCx vs SSTHc. **b**, Histogram representing the relative percentage of differentially regulated alternative splicing event categories in the hippocampal and across brain regions comparisons. The distinct pattern categories (mutually exclusive exon, cassette exon, intron retention, alternative 5' and 3' donor and acceptor site, alternative last exon, complex) are indicated in the legend. Total number of differentially regulated splicing patterns are: 146 for CamK2Hc vs Grik4, 673 for Grik4 vs SSTHc, 667 for SSTHc vs CamK2Hc, 722 for CamK2Hc vs Scnn1a and 30 for SSTCx vs SSTHc.

Figure S9

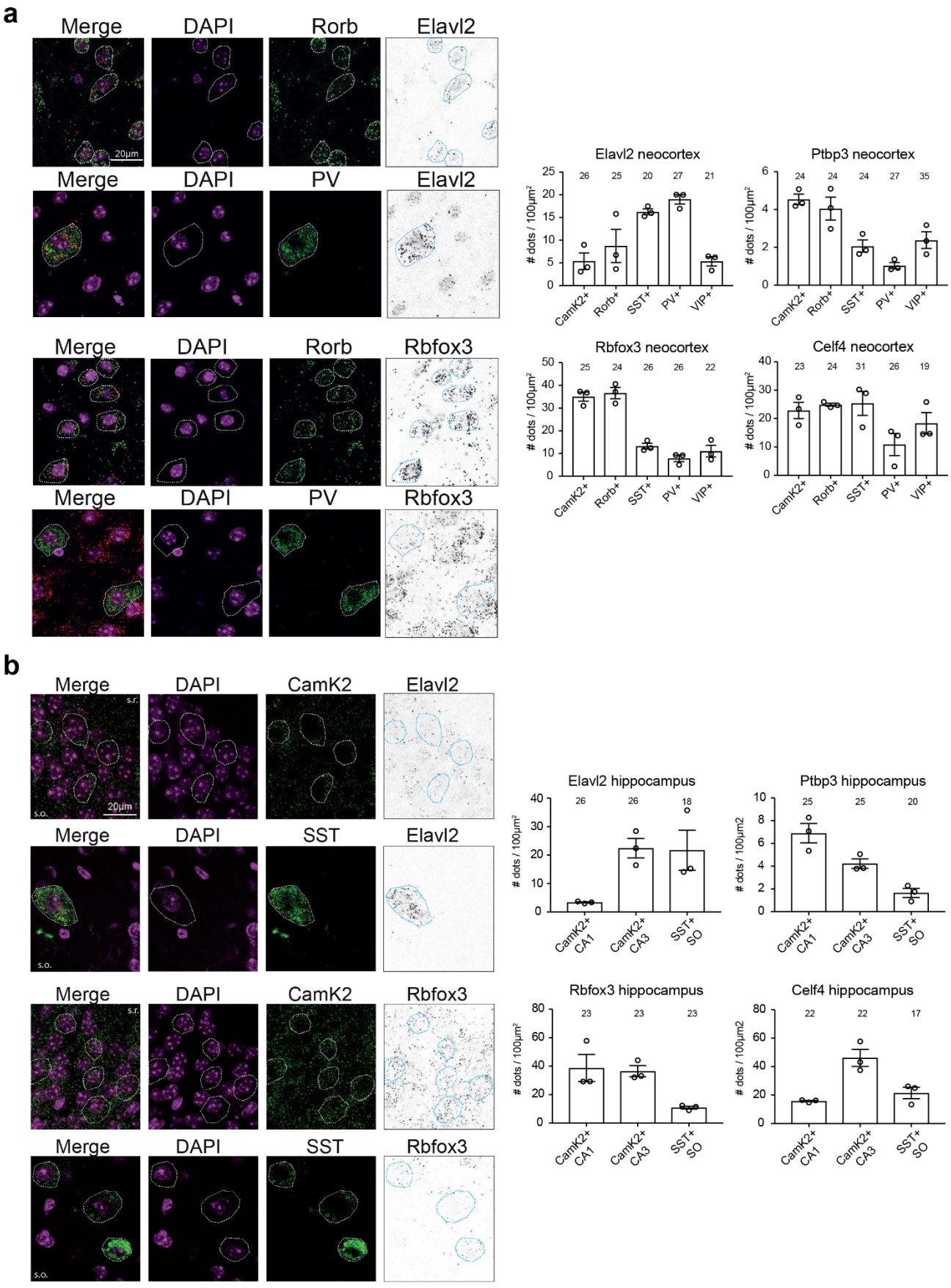
a
Merge
DAPI
Rorb
Elavl2
20µm
Merge
DAPI
PV
Elavl2
Merge
DAPI
Rorb
Rbfox3
Merge
DAPI
PV
Rbfox3
Elavl2 neocortex
dots / 100µm²
26 25 20 27 21
CamK2+ Rorb+ SST+ PV+ VIP+
Ptbp3 neocortex
dots / 100µm²
24 24 24 27 35
CamK2+ Rorb+ SST+ PV+ VIP+
Rbfox3 neocortex
dots / 100µm²
25 24 26 26 22
CamK2+ Rorb+ SST+ PV+ VIP+
Celf4 neocortex
dots / 100µm²
23 24 31 26 19
CamK2+ Rorb+ SST+ PV+ VIP+
b
Merge
DAPI
CamK2
Elavl2
s.r.
s.o.
20µm
Merge
DAPI
SST
Elavl2
Merge
DAPI
CamK2
Rbfox3
Merge
DAPI
SST
Rbfox3
Elavl2 hippocampus
dots / 100µm²
26 26 18
CamK2+ CA1
CamK2+ CA3
SST+ SO
Ptbp3 hippocampus
dots / 100µm2
25 25 20
CamK2+ CA1
CamK2+ CA3
SST+ SO
Rbfox3 hippocampus
dots / 100µm²
23 23 23
CamK2+ CA1
CamK2+ CA3
SST+ SO
Celf4 hippocampus
dots / 100µm2
22 22 17
CamK2+ CA1
CamK2+ CA3
SST+ SO

Supplementary Fig. 9: Validation of cell class-specific expression of splicing factors in neocortical and hippocampal neurons

a,b, Validation of cell population-specific expression of candidate splicing factors in neocortical (*panel a*) and hippocampal (*panel b*) mouse brain by fluorescent *in situ* hybridization. *In situ* probes assessing transcripts levels of *Elavl2*, *Rbfox3*, *Ptbp3* and *Celf4* were used in combination with cell population-specific marker probes (CamK2 for cortical and for CA1- and CA3-specific glutamatergic neurons, Rorb for layer 4-specific glutamatergic neurons, PV, VIP and SST for parvalbumin-, vasointestinal peptide- and somatostatin-positive interneurons, respectively).

a, *Left panel*: regions of interest (ROI) identify Rorb- or PV-positive neurons. Marker signal is *in green, Elavl2* and *Rbfox3 in black (red* in Merge*)*, DAPI *in magenta*. Images were taken from primary somatosensory cortex (S1) of P25 mice. **b**, *Left panel*: ROIs (regions of interest) identify CamK2- or SST-positive neurons. Marker signal is *in green, Elavl2* and *Rbfox3 in black (red* in Merge*)*, DAPI *in magenta*. Images were taken from CA1 or CA3 regions (for CA1 and CA3 pyramidal neurons, respectively) or from the *stratum oriens* (for SST-positive neurons) of the hippocampus of P25 mice. Scale bar is indicated. s.r.=*stratum radiatum*; s.o.=*stratum oriens. Right panels*: Quantification of the number of mRNA dots/100 μm^2 in the ROIs positive for the marker probe. Single data points represent the mean number of dots co-localizing with all the marker-positive cells from a single replicate (N=3 animals). SEM and total number of cells counted from all the replicates is indicated in the plot. Note that *Rbfox3* encodes for the widely used neuronal marker NeuN.

Figure S10

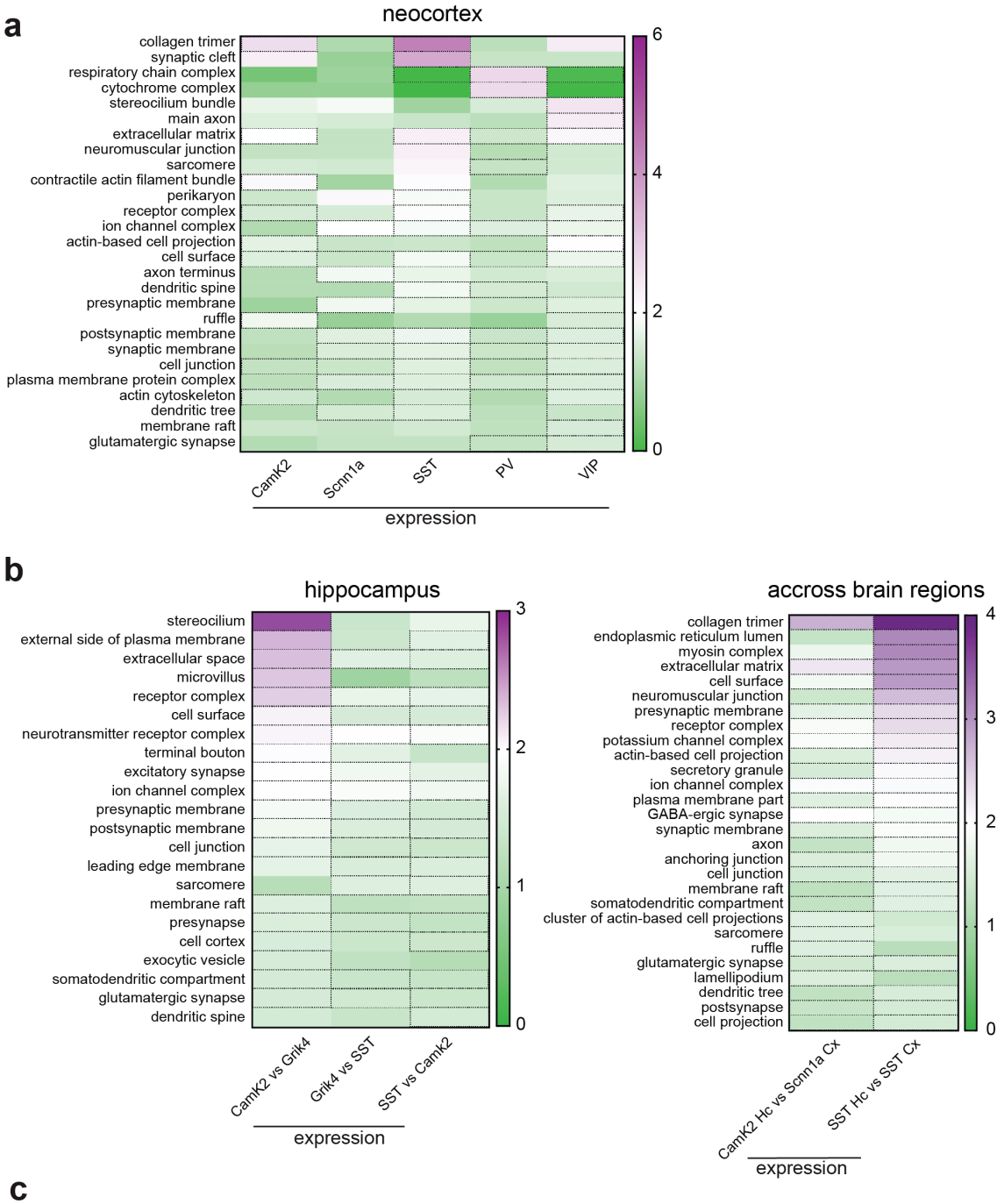
a
neocortex
collagen trimer
synaptic cleft
respiratory chain complex
cytochrome complex
stereocilium bundle
main axon
extracellular matrix
neuromuscular junction
sarcomere
contractile actin filament bundle
perikaryon
receptor complex
ion channel complex
actin-based cell projection
cell surface
axon terminus
dendritic spine
presynaptic membrane
ruffle
postsynaptic membrane
synaptic membrane
cell junction
plasma membrane protein complex
actin cytoskeleton
dendritic tree
membrane raft
glutamatergic synapse
6
4
2
0
CamK2
Scnn1a
SST
PV
VIP
expression
b
hippocampus
stereocilium
external side of plasma membrane
extracellular space
microvillus
receptor complex
cell surface
neurotransmitter receptor complex
terminal bouton
excitatory synapse
ion channel complex
presynaptic membrane
postsynaptic membrane
cell junction
leading edge membrane
sarcomere
membrane raft
presynapse
cell cortex
exocytic vesicle
somatodendritic compartment
glutamatergic synapse
dendritic spine
3
2
1
0
CamK2 vs Grik4
Grik4 vs SST
SST vs Camk2
expression
accross brain regions
collagen trimer
endoplasmic reticulum lumen
myosin complex
extracellular matrix
cell surface
neuromuscular junction
presynaptic membrane
receptor complex
potassium channel complex
actin-based cell projection
secretory granule
ion channel complex
plasma membrane part
GABA-ergic synapse
synaptic membrane
axon
anchoring junction
cell junction
membrane raft
somatodendritic compartment
cluster of actin-based cell projections
sarcomere
ruffle
glutamatergic synapse
lamellipodium
dendritic tree
postsynapse
cell projection
4
3
2
1
0
CamK2 Hc vs Scnn1a Cx
SST Hc vs SST Cx
expression
c
Density
0.00
0.01
0.02
0.03
0.04
0.05
0.06
0
10
20
30
40
50
60
Exons/gene
spliceosomal complex (161)
early endosome (205)
chromosomal region (208)
ion channels (205)
synaptic vesicle (186)
postsynaptic membrane (311)

Supplementary Fig. 10: Gene expression programs show distinct enrichments of GO categories as compared to alternative splicing

a,b, Heatmaps representing fold enrichment of Gene Ontology (GO) terms for transcripts differentially expressed identified by the Panther Classification System. Terms listed are significantly enriched in at least one neocortical population (*panel **a**),* hippocampal comparison (***b**, left panel)* or across brain regions comparison (**b,** *right panel*; see methods for details of significance). Fields for the statistically significant enrichments (p-value ≤ 0.05) are highlighted by a dashed outline. See Table S7 for the raw output of the GO analysis. **c,** Density plot showing the distribution of genes according to their number of exons. Gene lists were extracted from GO categories enriched for differentially spliced genes (ion channels, *in black*, synaptic vesicle, *in red*, and postsynaptic membrane, *in light-blue*), and from GO categories not significantly enriched (spliceosomal complex, *in yellow*, early endosome, *in green*, and chromosomal region, *in blue*). Chosen GO categories had similar numbers of genes per category. Overall, genes belonging to enriched or non-enriched categories for alternative splicing do not show major differences in the number of exons per gene.

Supplementary Table Legends – Note that supplementary tables were not included in the PhD thesis

Supplementary Table 1: Gene expression data in cortical and hippocampal samples and markers

Sheet 1 (NF_counts_genes): Gene expression values for all detected genes (see methods for details of cutoffs for gene expression) across the four replicates of all neocortical and hippocampal samples.

Sheet 2 (genes_cortex_FC_p-val): log2 fold-change (log2FC), standard error (log2FC_SE), p-value (Pval) and adjusted p-value (adjP) for genes expressed in all neocortical cell classes. Base mean includes all neocortical samples.

Sheet 3, 4, 5 (genes_CamK2vsGrik4_FC_p-val, genes_Grik4vsSST_FC_p-val, genes_SSTvsCamK2_FC_p-val): log2 fold-change (log2FC), standard error (log2FC_SE), p-value (Pval) and adjusted p-value (adjP) for genes expressed in each hippocampal pairwise comparison.

Sheet 6 (genes_cortex+hippo_FC_p-val): log2 fold-change (log2FC), standard error (log2FC_SE), p-value (Pval) and adjusted p-value (adjP) for genes expressed in neocortical and hippocampal samples. Base mean includes all neocortical and hippocampal samples.

Sheet 7 (Markers_genes_cortex and hippo): list of marker genes identified in neocortical and hippocampal samples (log2FC ≥ 3, adjP-value ≤ 0.01. Base mean includes all neocortical and hippocampal samples). Gene symbol, the corresponding marker class, log2FC and adjP-val are indicated.

Sheet 8 (Hrvatin et al., 2018 markers): List of cell type-specific marker genes identified by single cell sequencing in Hrvatin et al., 2018. Gene symbol, the corresponding marker class, log2FC and adjP-val are indicated. Base mean includes all neocortical samples.

Sheet 9 (CA1_CA3_DG_astro markers): List of previously described DG-, CA1-, CA3- and astrocytic specific markers, with corresponding references.

Supplementary Table 2: Alternative splicing analysis (EXON and PATTERN) in neocortical samples

Sheet 1 (SI_EXON_neocortex): Splicing Index (SI) values identified by EXON analysis for all exons detected in all neocortical samples genes (see methods for details of cutoffs for exon expression). Exon number, relative position in the gene and chromosomal coordinates are indicated. When known, the pattern associated to the exon is indicated (0 = FALSE, 1 = TRUE).

Sheet 2 (FC_SI_EXON_neocortex): log2FC and p-values of Splicing index (SI) identified by EXON analysis for all exons detected in neocortical samples. Base mean includes all neocortical samples. Exon number, relative position in the gene and chromosomal coordinates are indicated. When known, the pattern associated to the exon is indicated (0 = FALSE, 1 = TRUE).

Sheet 3 (FC_SI_PATTERN_neocortex): log2FC and p-values of SI for events identified by the PATTERN analysis in neocortical samples. Base mean includes all neocortical samples. For every pattern detected, the exons involved, their up- or down-regulation in each cell population and the chromosomal coordinates are indicated. When the event involved more than one exons, the chromosomal coordinates of the second exon are also indicated. ALE=alternative

last exon; ALT_TSS=alternative transcription start site; 3PACCEPTOR=alternative 3' acceptor site; 5PDONOR=alternative 5' donor site; CASSETTE=cassette exon; COMPLEX=complex event; IED=internal exon deletion; INT_RET=intron retention; MX=mutually exclusive exon.

Supplementary Table 3: Alternative splicing analysis (EXON and PATTERN) in hippocampal pairwise comparisons

Sheet 1 (SI_EXON_hippocampus): Splicing Index (SI) values identified by EXON analysis for all exons detected in all hippocampal samples. Exon number, relative position in the gene and in the chromosome are indicated. When known, the pattern associated to the exon is indicated (0 = FALSE, 1 = TRUE).

Sheet 2 (FC_SI_EXON_hippo_pairwise): log2FC and p-values of SI identified by EXON analysis in hippocampal pairwise comparisons (CamK2vsGrik4, Grik4vsSST, SSTvsCamK2). Exon number, relative position in the gene and in the chromosome are indicated. When known, the pattern associated to the exon is indicated (0 = FALSE, 1 = TRUE).

Sheet 3, 4, 5 (FC_SI_PATTERN_CamK2vsGrik4, sheet 2: FC_SI_PATTERN_Grik4vsSST, sheet3: FC_SI_PATTERN_SSTvsCamK2): log2FC and p-value of events identified by the PATTERN analysis in pairwise comparisons between hippocampal samples. For every pattern detected, the exons involved, their up- or down-regulation and the chromosomal coordinates are indicated. When the event involved one than more exons, also the chromosomal coordinates of the second exon are indicated. ALE=alternative last exon; ALT_TSS=alternative transcription start site; 3PACCEPTOR=alternative 3' acceptor site; 5PDONOR=alternative 5' donor site; CASSETTE=cassette exon; COMPLEX=complex event; IED=internal exon deletion; INT_RET=intron retention; MX=mutually exclusive exon.

Supplementary Table 4: Gene expression and alternative splicing analysis (EXON and PATTERN) in pairwise comparisons across brain regions.

Sheet1, 4, 7 (genes_SSTCxvsSSTHc, genes_CamK2HcvsScnn1a, genes_CamK2HcvsCamK2Cx): log2 fold-change (log2FC), standard error (log2FC_SE), p-value (Pval) and adjusted p-value (adjP) for genes expressed in pairwise comparisons across brain regions.

Sheet 2, 5, 8 (FC_SI_EXON_ SSTCxvsSSTHc, FC_SI_EXON_ CamK2HcvsScnn1a, FC_SI_EXON_ CamK2HcvsCamK2Cx): log2FC and p-values of SI identified by EXON analysis in pairwise comparisons across brain regions. Exon number, relative position in the gene and in the chromosome are indicated. When known, the pattern associated to the exon is indicated (0 = FALSE, 1 = TRUE).

Sheet 3, 6, 9 (FC_SI_PATTERN_SSTCxvsSSTHc, FC_SI_PATTERN_ CamK2HcvsScnn1a, FC_SI_PATTERN_CamK2HcvsCamK2Cx): log2FC and p-value of events identified by the PATTERN analysis in pairwise comparisons across brain regio. For every pattern detected, the exons involved, their up- or down-regulation and the chromosomal coordinates are indicated. When the event involved one than more exons, also the chromosomal coordinates of the second exon are indicated. ALE=alternative last exon; ALT_TSS=alternative transcription start site; 3PACCEPTOR=alternative 3' acceptor site; 5PDONOR=alternative 5' donor site; CASSETTE=cassette exon; COMPLEX=complex event; IED=internal exon deletion; INT_RET=intron retention; MX=mutually exclusive exon.

Supplementary Table 5: Summary Table of differentially expressed genes and regulated alternative events for all comparisons

Three types of comparisons are indicated: 1) Neocortical samples compared to the base mean of neocortical samples only, 2) Neocortical and hippocampal samples compared to the base mean of all samples 3) pairwise comparisons. Numbers for differentially expressed genes (p-val ≤ 0.05, -0.6 ≤ FC Log2 ≥ 0.6) or DR exons (p-val ≤ 0.01, 1 ≤ Log2FC ≥ 1) and DR patterns (p-val≤0.01, FC ≥ 1) are depicted. Furthermore, numbers specifically regulated by alternative splicing (AS) or TSS events identified by either EXON or PATTERN analysis are shown.

Supplementary Table 6: Splicing factors expression in neocortical and hippocampal samples

Sheet 1 (Sp.factors_Cx+Hc_FC_P-val): log2 fold-change (log2FC) and adjusted p-value (adjP) for a hand-curated list of high-confidence splicing factors. Base mean includes all neocortical and hippocampal samples.

Sheet 2 (Statistics_FISH_sp.factors): statistical tests of fluorescent *in situ* results in Supplementary Figure S9. Anova test was performed for each comparison and for each splicing factor probe (*Elavl2, Ptbp3, Rbfox3* and *Celf4*), both in the neocortex and hippocampus.

Supplementary Table 7: Gene Ontology analysis

Lists of all terms from the Gene Ontology analysis for transcripts regulated at gene or alternative splicing level for neocortical cell classes (sheet 1: GO_neocortex), for hippocampal pairwise comparisons (sheet 2: GO_hippocampus) and for pairwise comparisons across brain regions (sheet 3 and 4: GO_CamK2HcvsScnn1a, GO_SSTCxvsSSTHc). Information on the number of background genes, number of genes detected in the category, Fold enrichment and False Discovery Rate (calculated by Benjamini-Hochberg procedure) are indicated.

2. Results

2.4 Cell class-specific actions of SLM2 in specifying synaptic properties

Rationale

In the previous results sections, we have described to which extent alternative splicing programs are used to modulate intrinsic neuronal properties and the synaptic repertoire of individual neuron classes. Moreover, we have identified multiple splicing factors which exhibit highly selective expression patterns within glutamatergic or GABAergic neurons, but also in individual inhibitory cell populations including Parvalbumin neurons. We hypothesize that the cell-type specific expression of select RBPs regulates alternative splicing programs which are fundamental for the specification of synapses. This is a particularly intriguing hypothesis given that the splicing factor SLM2 has been shown to exhibit highly committed functions in controlling synapse specification due to alternative splicing regulation of the cell adhesion molecule Neurexin.

Global removal of SLM2 revealed a highly dedicated alternative splicing program in the mouse hippocampus with only very few RNAs being affected (Ehrmann et al., 2016; Traunmüller et al., 2016). However, SLM2 exhibits a highly selective expression pattern in subsets of neurons. In the mouse hippocampus it is not only expressed in glutamatergic neurons of the *cornu ammonis* (CA) layers, but also in Somatostatin (SST) positive inhibitory neurons (Iijima et al., 2014; Nguyen et al., 2016). Thus, our previous experiments using bulk sequencing of the whole hippocampus might not have fully captured the SLM2-dependent splicing programs in all cell types. Single gene studies for select RNA binding proteins (RBPs) like Nova2, Rbfox1 or Ptbps have demonstrated the importance of RBPs for neuronal function (Saito et al., 2019; Wamsley et al., 2018; Zhang et al., 2019). However, these proteins are broadly expressed in neuronal tissue. Given the highly selective expression of SLM2 in glutamatergic and GABAergic neurons, SLM2 provides a strong candidate to further probe whether one RNA binding protein regulates the same or distinct alternative splicing programs in different neuronal cell populations. Furthermore, it allows us to determine whether in both, excitatory and inhibitory neurons, SLM2 function is tailored to modulate the fine-tuning of functional neuronal circuits.

To this end, we generated cell class-specific mutants lacking SLM2 in two closely related glutamatergic populations (CA1 and CA3) of the hippocampus and in SST interneurons. We further surveyed SLM2-dependent alterations in gene expression and alternative splicing regulation within these different neuron classes and only detected a sparse overlap of commonly regulated transcripts across all cell types. Finally, we explored whether SLM2 also selectively modulates synaptic transmission in SST interneurons. These results demonstrate that SLM2 regulates different transcripts in individual cell types and that it is also

required to regulate molecular programs for synapse specification and target specificity in SST interneurons.

Results

Establishing tools for the dissection of cell class-specific splicing programs

Our previous study (Traunmüller et al., 2016) revealed that global deletion of SLM2 lead to only a few alterations in gene expression or alternative splicing programs in the mouse hippocampus when compared to wild-type. This was surprising, given that other RBPs like NOVA or nSR100 regulate hundreds of genes and alternative splicing events (Quesnel-Vallieres et al., 2015; Ule et al., 2005). The majority of RNA extracted from the hippocampus is contributed by glutamatergic neurons of CA layers and dentate gyrus granule cells. Therefore, we speculated that we might have missed splicing events derived from inhibitory neurons which express SLM2, like SST interneurons or individual glutamatergic cell classes (Iijima et al., 2014). Thus, we further investigated whether SLM2 regulates the same or divergent genes within closely-related classes of excitatory neurons (CA1 vs CA3) and SST inhibitory neurons in the hippocampus.

In order to assess the transcriptome of these cell populations, we generated new mouse lines in which we genetically removed SLM2 and additionally expressed an HA-tagged ribotag allele in a cre-dependent manner. This enabled us to obtain RNA associated with ribosomes in cre-expressing cell populations from WT and conditional mutants. We used CamK2-cre for CA1, Grik4-cre for CA3 and SST-cre for SST neurons (Figure 1A, B,D; for further details on RiboTRAP method see results section 2.3, the corresponding materials and methods section and (Sanz et al., 2009)). SLM2 is highly expressed in CA1-3 regions of the hippocampus (Figure 1C). Cell class-specific knock-out of SLM2 in CA1, CA3 and SST leads to a substantial reduction of SLM2 protein expression (example images in Figure 1D). Importantly, in WT animals ~90% of HA+ neurons marked by CamK2-Ribo or Grik4-Ribo are SLM2 positive. However, only 40-60% of SLM2+ neurons in CA1 or CA3, respectively will be targeted by these glutamatergic cre lines (Figure 1E). This partial ablation of SLM2 is not an issue for transcriptomic analysis, since there is a high overlap between SLM2 ablation and ribosomes tagged (~90% overlap), but needs to be taken into consideration for other experiments where cre-positive cells are not specifically marked, like for electrophysiological recordings or animal behavior.

The cell type-specific expression of SLM2 is not restricted to cardinal classes of excitatory vs. inhibitory neurons (Iijima et al., 2014), but differential SLM2 expression can also be clearly observed within one single cell class. For example, SLM2 expression in genetically marked Somatostatin positive interneurons differs for SST cells in hippocampal sub-regions.

70-85% of SST neurons residing in the s.o or in CA3 exhibit intermediate to high SLM2 expression, whereas most of the SST cells in the hilus of the DG lack SLM2 (Figure 1F, (Nguyen et al., 2016). Thus, knock-out of SLM2 will only affect a subset of SST+ interneurons. Taken together, we have now established tools for genetic targeting of three cell populations in the mouse hippocampus to investigate the cell class-specific action of SLM2.

We generated Ribotag purifications and poly-A sequencing libraries from four replicates per cell class and genotype (24 samples in total) and performed deep RNA sequencing. 23 of these samples exhibited high quality including detection of ~12.500 genes, excellent 5'-3' end coverage along the transcript, ~90% mapping of unique reads and little ribosomal contamination. Only one sample, CamK2 KO4, was excluded from further analyses due to higher 3' end bias and ribosomal contamination. Parts of our quality control has been summarized in Table 1. Also, note that within WT comparisons have been described in detail in section 2.3.

This sequencing dataset now provides the basis for examining cell type-specific consequences of SLM2 ablation in excitatory CA1 and CA3 neurons, and hippocampal SST interneurons.

Survey of differential gene expression programs regulated by SLM2

Principle component analysis of all expressed genes segregated samples based on cell class and neurotransmitter phenotype but not genotype (Figure 2A). This suggests that loss of SLM2 does not result in large-scale alterations in cellular transcriptomes as it would be expected when the identity of these neuron classes was altered. Furthermore, detailed gene expression analysis of pairwise WT and conditional knock-out (cKO) comparisons revealed that 37 and 55 genes differed in expression in Grik4 and CamK2 neurons, respectively. In SST cKO neurons, 105 genes were significantly altered (Figure 2B, Log2FC ≥ 0.67 and ≤ -0.67, p-value ≤ 0.05). We had previously shown that loss of SLM2 leads to an increase in *Slm1* (*Khdrbs2*) RNA and protein (Traunmüller et al., 2014). Surprisingly, only this gene was commonly altered across the three cell classes, whereas most other genes that exhibited differential regulation in SLM2 cKO cells were uniquely changed (Figure 2B, 2C left panel). Two exceptions were *Mag* - involved in myelination (McKerracher and Rosen, 2015) and *Mfge8* - implicated in reprogramming of macrophages for wound healing fibroblasts (Laplante et al., 2017), which were altered in both glutamatergic CA1 and SST neurons. Cell class-specific regulation included the voltage gated potassium channel 4 in CA3 neurons and reduced expression of the alpha2 subunit of the GABA-A receptor in CA1. Both alterations can have major impacts for synaptic signaling (Figure 2C right panel). Another example is the significant reduction in *Eif4enif1* in SST neurons. Eif4enif1 is responsible for the nuclear import of the eukaryotic

translation initiation factor 4E (Jackson et al., 2010). In SST neurons alterations in expression levels might lead to alterations in the regulation of translation. However, further experiments will be required to directly link alterations in cell type-specific gene regulation to biological functions.

Interestingly, we previously only identified ~10 genes to be differentially expressed in our previous analysis on the hippocampus of global *Slm2*^{KO} mice by applying the same cut-offs. The number of genes regulated by SLM2 in individual cell types is 3-10x higher, supporting the notion that we missed differences in our global *Slm2*^{KO} study that were derived from alterations in subpopulations. However, SLM2 still regulates only a remarkably small number of genes in comparison to other RBP loss-of-function studies (Quesnel-Vallieres et al., 2015; Ule et al., 2005). This further indicates that the function of SLM2 is tailored towards very specific biological processes.

SLM2-dependent alternative splicing is regulated in a cell class-specific manner

To explore whether SLM2 regulates similar or divergent alternative splicing programs in glutamatergic or GABA-ergic neurons, we mapped alternative transcript isoforms with two complementary approaches: the EXON and PATTERN analysis (for details see results section 2.3 and corresponding Materials and Methods). These analyses revealed between 40-65 differentially regulated (DR) exons and 9-13 patterns that were differentially regulated between WT and the corresponding cell-class specific mutant (Figure 3A). Note that due to the low number of genes involved in the AS programs, we could not obtain significant Gene Ontology terms to better identify which categories the DR events belong to.

Interestingly, the majority of the detected events were unique for a given cell type. In our global *Slm2*^{KO} analysis, which presumably consisted mainly of RNA derived from glutamatergic cells, we only found a handful of transcripts, which included alternative splicing of the synaptic genes *Nrxn1-3* at AS4, *Stxbp5l* and modulation of *Slm2* itself (including exon 2 which we used to knock-out the *Slm2* gene). These findings could be recapitulated in CA3 and to a slightly smaller extent in CA1 pyramidal neurons (Figure 3A, B, C, D). However, all other DR events (~70-80 events) were not shared. Notably, also the SLM2-dependent splicing program in SST neurons exhibited unique splicing events, with the exception of splicing at AS4 of Nrxn2 (Figure 3A, D). The alterations in alternative splicing of *Nrxns* at AS4 were validated by conventional RT-PCR (Figure 3E) and q-PCR (Figure 3F).

The selective, hardly overlapping changes in cell type-specific alternative splicing could be a secondary consequence of lack of expression of these genes in the other cell classes. We found that, on average, 90% of the genes significantly targeted by SLM2-dependent alternative splicing regulation were commonly expressed (93% for CamK2, 89%

for Grik4, 90% for SST). Therefore, these findings support that SLM2 mediates different alternative splicing programs not only in inhibitory neurons but also between closely related populations of glutamatergic cells.

The role of SLM2 in modulating synaptic transmission in somatostatin-positive interneurons

Differential regulation of alternative transcript isoforms by RBPs represents a powerful tool to modulate the function of neuronal circuits (Traunmüller et al., 2016; Ule and Darnell, 2006). In our previous global *Slm2*^{KO} study, we found selective post-synaptic electrophysiological phenotypes at Schaffer collateral synapses onto CA1 pyramidal neurons. Those were depended on *Nrxn* AS4 splice variant-mediated modulation of glutamatergic receptors and suggested that SLM2 function was tailored for synapse specification. Based on the highly selective, cell class-specific alternative splicing programs, we further hypothesized that SLM2 might steer different mechanisms for defining synaptic properties in SST inhibitory neurons compared to CA1 pyramidal cells.

SST interneurons residing in s.o of the hippocampus can either be classified as bistratified cells or oriens-lacunosum moleculare (OLM) neurons. OLM neurons receive excitatory input from CA1 axon collaterals (Sun et al., 2014) and inhibit the distal dendrites of CA1 pyramidal neurons in a phase-dependent manner (Müller and Remy, 2014). The excitatory inputs are strongly facilitating, which has been demonstrated to be dependent on the expression of Elfn1 in SST interneurons (Sylwestrak and Ghosh, 2012). Importantly, SST neurons in s.o also express high levels of SLM2 (Figure 1F) and we could detect significant co-expression of Elfn1 and Slm2 mRNA by fluorescent in-situ hybridization (data not shown). Thus, we investigated the impact of loss of SLM2 in SST interneurons (*Slm2*$^{\Delta SST}$) on intrinsic properties of, and synaptic transmission onto, SST neurons using whole cell hippocampal slice electrophysiology (age P15-18). To specifically patch SST neurons in the s.o, we genetically expressed the fluorescent marker tdTomato in SST neurons (triple transgenic mice *Slm2*^{flox} x SST-cre x tdTomato).

Consistent with our transcriptomic PCA analysis, analysis of labelled SST neurons revealed no significant differences of intrinsic properties like resting membrane potential, capacitance or rheobase in controls and conditional mutants. The only exception was the latency to spike (Mann Whitney U p-value 0.0107) which was higher in the mutants and could indicate alterations in the excitability of these neurons (Figure 4B). More detailed analysis of the spiking patterns (WT trace shown in Figure 4C) showed that there was no difference in the number of action potentials (AP) when continuously increasing the amount of injected current for 200ms or 1s (Figure 4D). Additionally, SST neurons adapt their firing rate during a

maintained stimulus (Tremblay et al., 2016), a feature that remained unchanged in the *Slm2*$^{\Delta SST}$ mutants (Figure 4E). Thus, overall intrinsic properties are not affected by loss of SLM2.

Interestingly, synaptic transmission was altered in *Slm2*$^{\Delta SST}$ mice. We observed a significant increase in the frequency of putative spontaneous excitatory postsynaptic currents onto SST interneurons, when cells were voltage clamped at -70mV (Figure 4F, G, Mann Whitney U Test p-value 0.0003). A similar, but not significant trend was observed when frequencies of miniature post-synaptic currents were measured (mEPSC, unpaired t-test with Welch correction p-value 0.0506), which can be indicative for the number of synapses. These results suggest that *Slm2*$^{\Delta SST}$ mice receive more excitatory input. However, it still remains to be determined whether the increase in sEPSCs is a global network effect or due to alterations in synapse numbers.

Synaptic transmission can be enhanced by synaptic short-term facilitation for less than a second, a phenomenon thought to be critical for rapid information processing across synapses (Deng and Klyachko, 2011; Jackman and Regehr, 2017). Thus, short-term facilitation provides an accessible readout to detect alterations in synaptic transmission. The CA1 to SST excitatory synapse exhibits low release probabilities which are manifested in strongly facilitating responses (Ali and Thomson, 1998; Pouille and Scanziani, 2004). Selective electrical stimulation of CA1 axon collaterals (alveus, Figure 4A) lead to robust facilitation ratios in response to several different inter-stimulus intervals (10-40Hz trains of 5 stimuli, Figure 4H, I, black traces). However, short-term facilitation was even higher in SST neurons lacking SLM2 (Figure 4H, I, red traces, Two-way ANOVA with Bonferroni correction) – which may be associated with even lower release probabilities at CA1-SST synapses in cKO mice. This trend could be observed across stimulation frequencies and stimulus strengths and suggests that loss of SLM2 causes changes in short-term facilitation in physiologically relevant conditions. The observed pre-synaptic phenotype is particularly intriguing given that SLM2 was removed from the post-synaptic cell.

To further investigate whether ablation of SLM2 in SST interneurons trans-synaptically affected inhibition onto CA1 pyramidal neurons, we employed optogenetic activation of SST axon terminals onto the distal dendrites of CA1 neurons with Channelrhodopsin light stimulation (*Slm2*^{flox} x ChR2^{flox} x SST-cre, Figure 5A). SST-mediated inhibitory responses lead to large non-linear outward currents, a feature that is critically dependent on the α5 subunit of $GABA_A$ receptors (Schulz et al., 2018). Thus, assessment of inward and outward currents provide one means to assess alterations in $GABA_A$ receptor subunit composition and thus,

alterations in inhibition. Light stimulation at various intensities lead to robust IPSC (Inhibitory postsynaptic current) responses for inward and outward currents in both genotypes (Figure 5B, C). Furthermore, light-induced voltage dependent IPSCs (Figure 5D), the mean normalized conductance (Figure 5E) and decay of IPSCs (Figure 5F) were comparable between WT and *Slm2*$^{\Delta SST}$ CA1 pyramidal neurons. These results indicate that deletion of SLM2 in SST interneurons does not alter post-synaptic responses or neurotransmitter receptor compositions. Repeated activation with five pulses at a frequency of 10Hz shows the depressing properties of these GABAergic synapses onto CA1 neurons (Figure 5G). Interestingly, there was a small, but significant difference between WT and Slm2 mutant animals, suggesting that SLM2 might also regulate pre-synaptic release probabilities of SST synapses onto CA1.

Importantly, observations at glutamatergic CA3-CA1 synapses in the global *Slm2*^{KO} demonstrated trans-synaptic modulation of synaptic transmission onto the post-synaptic neuron (Traunmüller et al., 2016). However, removal of SLM2 in SST interneurons did not affect GABAergic transmission onto the distal dendrites of CA1 pyramidal neurons. Instead, SLM2 potentially modulates pre-synaptic release probabilities at glutamatergic CA1-SST synapses due to trans-synaptic modifications of surface receptor compositions. Therefore, SLM2 expression in SST interneurons might contribute to molecularly encoded, cell type-specific signals that shape trans-synaptic information processing in the mouse hippocampus.

Behavioral consequences of SLM2-dependent splicing regulation in somatostatin positive interneurons

Somatostatin interneuron activity has been implicated to be involved in encoding spatial working memory accuracy (Abbas et al., 2018) or object memory encoding (Siwani et al., 2018) *in vivo.* Considering the alterations in short-term facilitation at CA1-SST synapses, we further explored potential behavioral alterations in *Slm2*$^{\Delta SST}$ mice.

Mutant animals did not display any gross deficits in locomotion (data not shown) and exerted similar exploration behavior when exposed to a novel environment like an Open Field arena (Figure 6A, B left panel). However, their short-term object recognition memory was impaired in the novel object recognition task as *Slm2*$^{\Delta SST}$ mice did not exhibit a preference for a novel object (Figure 6C). To rule out that these observations were due to differences in anxiety-like behaviors, we further tested WT and mutant mice in the elevated plus maze (Figure 6D). Both genotypes spent similar amounts of time in the open arms of the maze and exhibited comparable locomotion activity, as measured by the total numbers of entries into either of the four arms (Figure 6E). This is consistent with our findings from the Open Field assay, since the percentage of time in the center is an additional measurement of anxiety (Figure 6B right panel). In a last assay, we surveyed whether modulation of SST neuron

function might lead to potential repetitive behaviors. Thus, we used the marble burying task, however, did not observe any significant differences between WT and *Slm2*$^{\Delta SST}$ animals (Figure 6F).

These results demonstrate that SLM2-dependent modification in SST function are associated with alterations in object memory encoding.

Discussion

Specific cellular features of cell types within neuronal circuits are hardwired. Alternative splicing programs are commonly viewed to diversify the genome and have been demonstrated to be involved in specifying molecules for neuronal wiring, including the cell surface molecules *Dscam1* or *Nrxns*. Furthermore, it has become increasingly clear that the expression of RBPs greatly contributes to synaptic wiring specificity and neuronal function (Furlanis and Scheiffele, 2018). Mapping of alternative splicing events across neuronal cell types demonstrated that each cell class exhibited unique splicing programs associated with genes implicated to regulate synaptic function (Results 2.3). Yet, little is known about how synaptic specification is controlled in a cell type-specific manner to modulate the function of neuronal circuits. In this study, we investigated whether the splicing factor SLM2 exerts cell type-specific functions in glutamatergic vs. GABAergic neurons. We found that SLM2 regulates distinct gene expression and alternative splicing programs in closely related populations of excitatory neurons and SST inhibitory neurons of the mouse hippocampus. With the exception of alternative splicing of the cell adhesion molecules *Nrxn2* at AS4, which was shared between all cell types. Furthermore, only a few genes were regulated in each cell type. The low number of highly regulated events stands in high contrast to loss-of-function studies of other splicing factors, including Rbfox1. Cell type-specific alternative splicing regulation mediated by Rbfox1 in PV and SST revealed hundreds of hardly overlapping transcripts that were differentially regulated (Wamsley et al., 2018). Therefore, SLM2 mediates only very selective pools of transcripts in different neuronal populations compared to other RBPs.

The deeper investigations on the function of SLM2 in inhibitory neurons further support the notion that SLM2 is an RBP with very dedicated functions. Loss of SLM2 did not greatly affect parameters of intrinsic properties tested in SST neurons. In ongoing work, additional parameters will be investigated. These include influences of sodium and potassium channels on the rise and decay times of the AP or its hyperpolarization. In both, excitatory neurons (our global *Slm2*^{KO} study) and inhibitory neurons, SLM2 might regulate synaptic transmission via trans-synaptic interactions, but by different means. In the global *Slm2*^{KO}, synaptic alterations were mainly assessed at Schaffer collateral synapses and detected at the level of altered

responses of the post-synaptic CA1 neuron. At these synapses, paired pulse facilitation ratios were unaltered. In contrast, loss of SLM2 in SST interneurons did not affect post-synaptic inhibitory responses of CA1 pyramidal neurons, but altered target-specific pre-synaptic properties of CA1 neurons. The molecular mechanism by which trans-synaptic interactions can modulate glutamatergic synaptic transmission was investigated in the global *Slm2*^{KO} (see chapter 2.2 and Figure 7A and B). Briefly, reduced expression of *Nrxn1-3* AS4(-) at the pre-synaptic terminal lead to reduced interactions with post-synaptic binding partners like NLs, which normally recruit and stabilize NMDAR and AMPAR (Shipman et al., 2011). We speculate that differential trans-synaptic interactions caused synaptic alterations in the post-synaptic cell. This was further supported by experiments demonstrating that genetic restoration of *Nrxn1* AS4(-) could rescue the observed phenotypes.

Further insights into how SLM2 trans-synaptically mediates pre-synaptic release probabilities, will require the intersection of our deep sequencing analysis of gene regulation and observed functional consequences. The target-specific properties of CA1-SST synapses has previously been demonstrated to be dependent on the transmembrane protein ELFN1. ELFN1 recruits pre-synaptic metabotropic and kainate receptors, mGluR7 and GluR6 respectively, and thereby modulates the facilitating properties of these synapses. Knock-out of ELFN1 leads to reduced facilitation ratios of excitatory input onto SST neurons and loss of mGluR7 recruitment to these terminals (Sylwestrak and Ghosh, 2012; Tomioka et al., 2014). Removal of SLM2 in SST neurons on the other hand lead to increased facilitation ratios. Given that SLM2 and ELFN1 are co-expressed in the same neurons, they might regulate divergent mechanisms to ensure the correct excitation balance from CA1 pyramidal cells onto SST neurons. However, how could the splicing factor SLM2 mediate these properties? Our deep sequencing analysis of gene expression and alternative splicing programs in WT and *Slm2*$^{\Delta SST}$ animals identified possible candidates, including the Sortilin Related VPS10 Domain Containing Receptor 1 (Sorcs1). These receptors are known regulators of intracellular trafficking (Willnow et al., 2008). Specifically, Sorcs1 has been identified as a post-synaptic partner for NRXNs and mediator of AMPAR trafficking (Savas et al., 2015). Pull down binding assays complemented with Mass-spectrometry additionally identified significant interactions between Sorcs1 and mGluR7 at the vacuolar protein sorting 10 (VPS10) binding domain (Savas et al., 2015). Interestingly, SLM2 mediates alternative splicing of Sorcs1 at one exon contributing to encoding the VPS10 domain. This alternative splicing event is predicted to introduce a frameshift in the coding RNA and lead to the degradation of the transcript. The opposing effects of loss of SLM2 and ELFN1 could be explained through the following potential mechanism, which is illustrated in Figure 7 C and E. In WT conditions, both ELFN1 and Sorcs1 trans-synaptically recruit pre-synaptic mGluR7. Binding of Elfn1 was proposed to act as an allosteric modulator, thereby leading to a conformational change of mGluR7 that causes

constitutive receptor activity and increased facilitation (Dunn et al., 2018). How Sorcs1 normally binds to mGluR7 and whether this leads to a potential decrease in receptor activity and depression is yet to be determined. Nevertheless, it could be conceivable that Sorcs1 and ELFN1 compete for binding to mGluR7. Loss of SLM2 and in turn of Sorcs1 at the post-synaptic terminal, could make more mGluR7 available for ELFN1 to bind and thereby increase the facilitation ratios. Alternatively, there could be other, non-identified receptors involved. ELFN1 has also been demonstrated to modulate short-term facilitation via the kainate receptor GluR6. Thus, it remains to be investigated whether SLM2 acts through either of these known pathways or even through so far unknown trans-synaptic mechanisms. These hypotheses will be experimentally tested using multiple strategies. Application of selective agonists and antagonists for mGluR7 or GluR6 during electrophysiological recordings will determine whether SLM2 truly acts through these receptors. These experiments will be complemented with molecular and biochemical experiments to identify whether ELFN1 and Sorcs1 are the trans-synaptic players to compete for balancing excitation of SST interneurons in the mouse hippocampus.

It also has to be noted, that experiments for measuring responses in the global *Slm2*^{KO} and excitatory inputs onto SST interneurons in the *Slm2*$^{\Delta SST}$ mice were performed without the usage of blockers for inhibition like picrotoxin. Putative excitatory currents were extracted based on the holding potential of the cell, which was -70mV, close to the reversal potential of chloride. Thus, further experiments will be required to rule out potential contaminations by GABA currents.

Our behavioral analysis in conditional SST knock-out animals suggested deficits in recognition memory in the novel object recognition task. However, the SST-cre line used (Taniguchi et al., 2011) affects all SST neurons in the body. Therefore, further experiments with hippocampus sub-region specific deletion of SLM2 in OLM interneurons using Chrna2-cre mice (Leao et al., 2012) will be required to relate the electrophysiological phenotypes with the cognitive deficit in the novel object recognition task.

Taken together, our observations indicate that SLM2-mediated alternative splicing programs do not greatly diversify the cellular content, or contribute to assign glutamatergic or GABAergic neurons their identity. Instead, it is highly tailored to regulate the fine-tuning of synaptic properties in a target-cell dependent manner.

Acknowledgements

We would like to thank members of the whole Scheiffele lab for constructive and inspiring discussions, and Hanna Hörnberg and Elisabetta Furlanis for feedback on this manuscript. Dr. Tevye Stachniak for experimental help regarding electrophysiological experiments, guidance and sharing of knowledge; Elisabetta Furlanis for general support including data analysis and display; Drs. Bischofsberger and Schulz for excellent expert advice and Dr. Schulz for performing optogenetic electrophysiology experiments; We thank Pierre de la Grange, Noemie Robil and Ariane Jolly from Genosplice for RNA-sequencing data analysis and Caroline Bornmann, Laetitia Hatstatt-Burklé and Philippe Demougin for general experimental support.

Figure 1

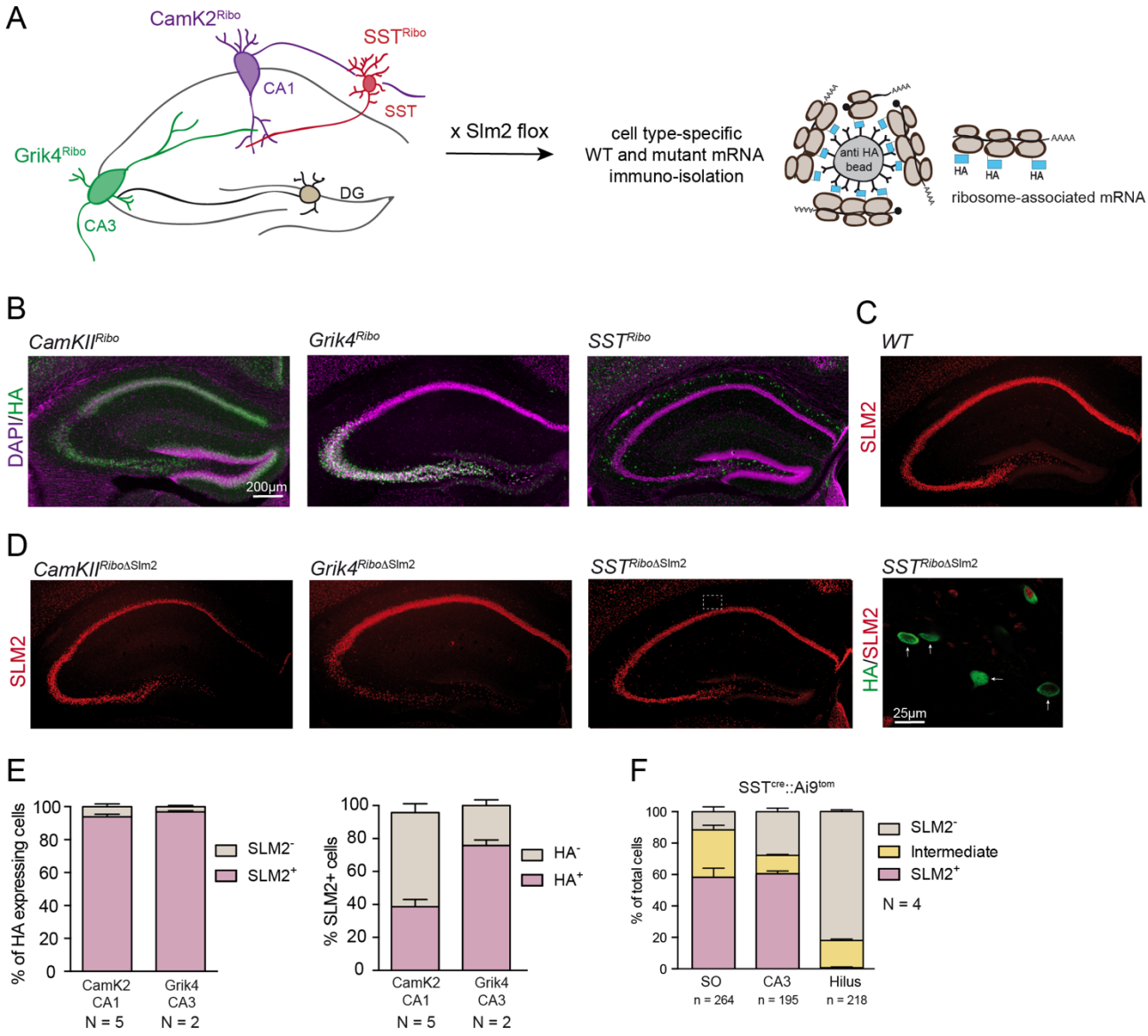

Figure 1: Strategy for obtaining cell class-specific RNA

A) Schematic of hippocampal neurons targeted with different cre lines to obtain cell class-specific ribosome associated RNA. We employed three lines: Grik4-cre x Ribotag (Grik4^{Ribo}), CamK2-cre x Ribotag (CamK2^{Ribo}) and SST-cre x Ribotag (SST^{Ribo}). These mouse lines were further crossed with the Slm2 floxed allele to generate WT and cell class-specific Slm2 mutants for RNA isolation. RNA isolation was achieved using the RiboTRAP method in which the Rpl22 gene of the ribosome has been cre-dependently tagged with HA. Using immunoprecipitation with HA beads, RNA associated with the ribosome can be obtained for further analysis.

B) Representative images of the different cre lines used, stained for HA (green) to visualize the tag and DAPI (magenta). CamK2^{Ribo} is expressed primarily in CA1 pyramidal neurons, but also slightly in CA3 and DG. Analysis for specific markers confirmed appropriate de- and enrichment of DG, CA2, CA3 and CA1 markers, respectively (Data shown in results section 2.3 Supplementary Figure 1,2). Grik4^{Ribo}

allows purification of glutamatergic CA3 neurons, whereas SST labels one class of inhibitory neurons.
Scale bar: 200µm for all hippocampal overview images

C) SLM2 (red) is highly expressed in CA1-3 pyramidal neurons, but absent from DG granule cells

D) Representative images for knock-out of SLM2 in CA1 (left), CA3 (middle), SST (right). Knock-out of SLM2 in SST neurons is shown in the blowup image on the far right with an HA (green) and SLM2 (red) double staining (Scale bar 25µm). Four out of the five SST neurons are devoid of SLM2.
SLM2 intensities should be compared to the SLM2 immunostaining in WT conditions shown in C.

E) Analysis of how many HA+ cells in CA1 and CA3 express SLM2 shows that ~90% of HA+ cells are double positive and thus, will be affected by modulation of SLM2 (left panel).
Only 40% for CamK2^{Ribo} and 75% for Grik4^{Ribo} of SLM2+ cells are even tagged by our strategy (HA+, right panel). This explains, why the reduction in SLM2 in CamK2^{Ribo} is difficult to appreciate in the overview images. N = number of animals

F) Imaris quantification of SLM2 intensities (high, intermediate, absent) within anatomically defined SST interneurons in wildtype conditions. ~90% of SST neurons in s.o and ~70% in CA3 express SLM2, whereas most of the inhibitory neurons in the hilus of the DG are devoid of SLM2. N = number of animals, n = number of cells.

sample	reads	% uniquely mapped	detected genes	% ribosomal	% mRNA	% junctions
CamK2.W1	105 644 496	90	12 528	4.38	85.88	47.0
CamK2.W2	106 516 554	88	12 564	5.46	85.01	45.5
CamK2.W3	109 118 524	89	12 506	6.71	84.34	45.8
CamK2.W4	107 445 662	89	12 657	5.59	85.24	45.9
CamK2.K1	105 245 509	89	12 457	3.95	86.67	47.6
CamK2.K2	106 516 554	88	12 505	2.72	87.83	48.0
CamK2.K3	109 118 524	89	12 672	3.22	87.19	46.5
Grik4.W1	106 601 624	90	12 584	2.51	87.67	47.6
Grik4.W2	106 635 010	89	12 789	4.01	86.90	47.9
Grik4.W3	106 712 395	90	12 731	3.07	87.87	49.5
Grik4.W4	107 951 454	89	12 802	4.86	86.19	48.0
Grik4.K1	106 126 567	90	12 598	3.01	87.89	48.0
Grik4.K2	107 152 622	89	12 819	2.08	86.38	48.6
Grik4.K3	107 022 371	90	12 772	2.93	87.58	49.7
Grik4.K4	104 896 989	90	12 653	2.51	86.67	48.2
SST.W1	106 448 303	90	12 895	0.68	89.15	47.8
SST.W2	110 095 915	89	12 838	2.52	86.67	46.9
SST.W3	114 811 827	89	12 795	4.24	85.76	45.2
SST.W4	179 458 089	90	12 835	0.62	89.22	48.3
SST.K1	162 712 531	90	12 946	0.34	89.48	48.0
SST.K2	107 330 721	90	12 726	5.70	84.65	48.6
SST.K3	106 999 624	90	12 995	1.74	87.98	49.7
SST.K4	106 801 949	90	13 270	0.75	87.29	48.2

Table1: **Summary of FastQC analysis of RiboTRAP sequencing samples**
Displayed are samples used for further analysis and the corresponding number of reads (~100mio on average, except for sample SST WT4 and SST KO1), uniquely mapped reads onto the genome, the number of detected genes, % of ribosomal RNA, % of mRNA and the % of junction reads. All of these are important and parameters of high quality to reliably assess transcriptomic profiles and alternative splicing events.

Figure 2

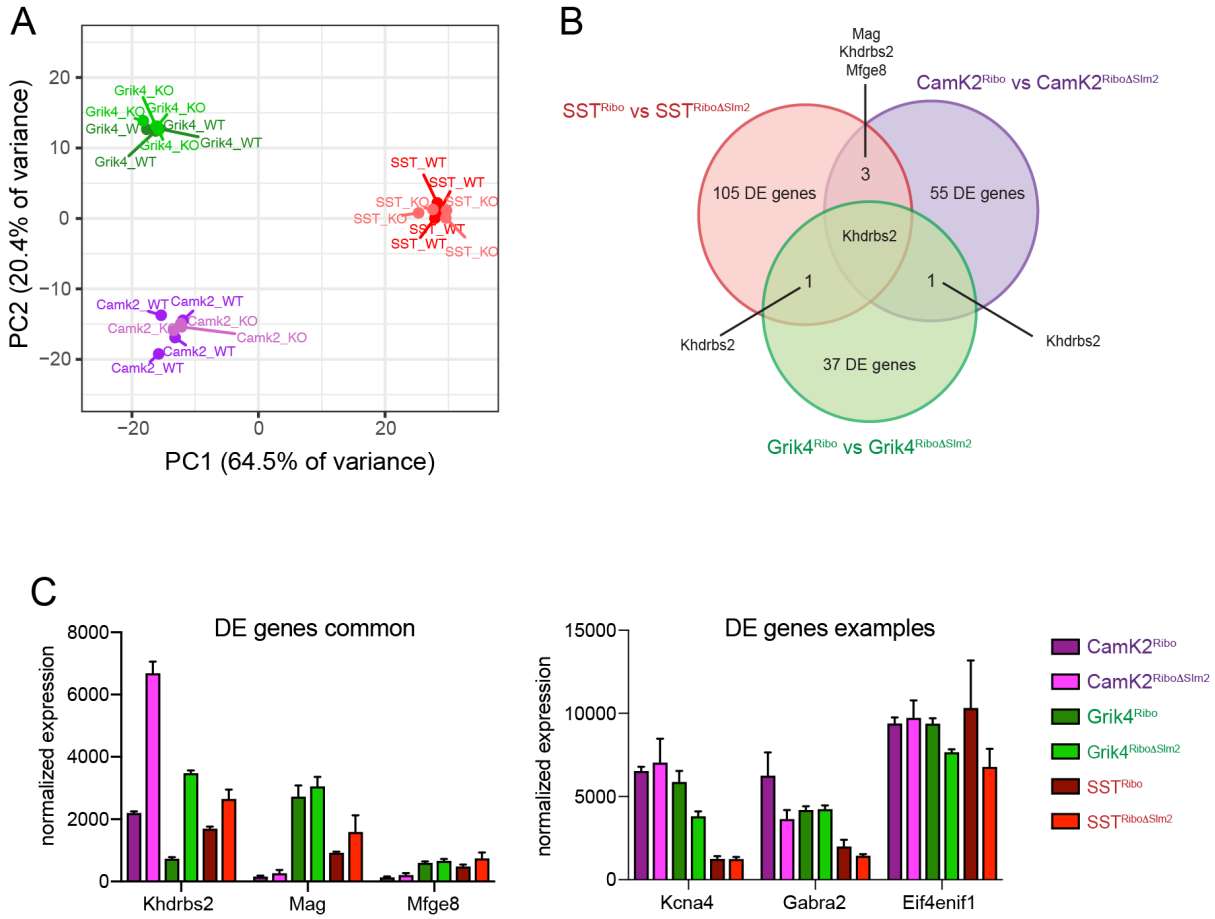

Figure 2: Loss of SLM2 does not alter the identity of either neuron class

A) Principle component analysis (PCA) of WT and cell type-specific mutant transcriptomes. Samples cluster together based on the cell class and neurotransmitter phenotype and independent of the genotype. Thus, loss of SLM2 does not affect the overall transcriptomic architecture and thus, the identity of these neurons

B) Summary of differentially expressed (DE) genes between WT and individual mutants. Only Slm1 (Khdrbs2) is commonly regulated in all cell populations. Otherwise, very few transcripts are shared between excitatory neurons or excitatory vs. inhibitory neurons, suggesting that there are individual transcriptomic programs steered by SLM2. Log2FC ≥ 0.67 and ≤ -0.67, p-value ≤ 0.05

C) Left panel: Significant DE genes which are commonly regulated by SLM2 between all (Khdrbs2) or CA1 and SST cells (Mag, Mfge8).
Right panel: examples of DE genes for each of the cell types.

Figure 3

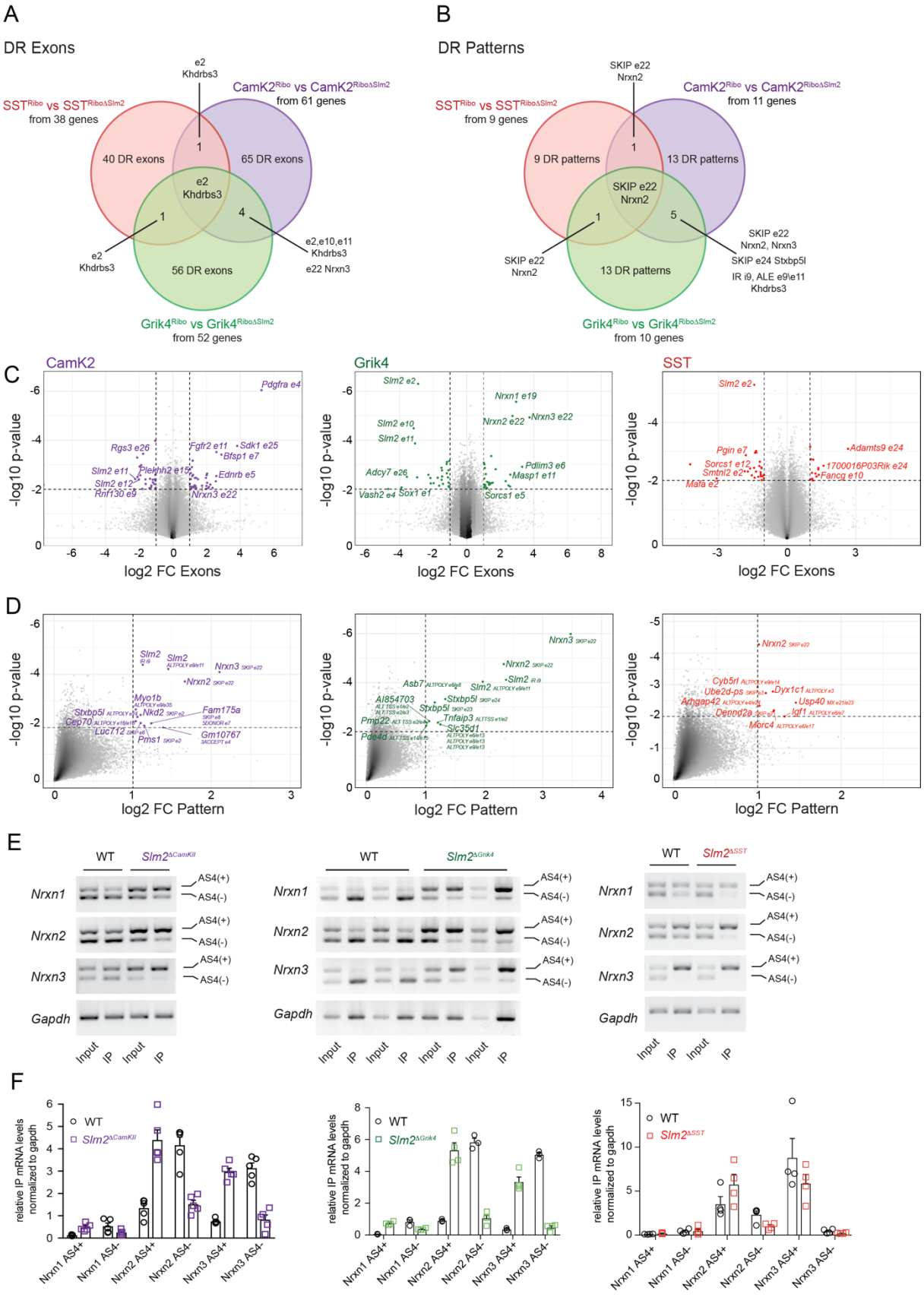
A
DR Exons
SST^Ribo vs SST^RiboΔSlm2
from 38 genes
CamK2^Ribo vs CamK2^RiboΔSlm2
from 61 genes
Grik4^Ribo vs Grik4^RiboΔSlm2
from 52 genes
40 DR exons
65 DR exons
56 DR exons
e2 Khdrbs3
e2,e10,e11 Khdrbs3
e22 Nrxn3
B
DR Patterns
SST^Ribo vs SST^RiboΔSlm2
from 9 genes
CamK2^Ribo vs CamK2^RiboΔSlm2
from 11 genes
Grik4^Ribo vs Grik4^RiboΔSlm2
from 10 genes
9 DR patterns
13 DR patterns
13 DR patterns
SKIP e22 Nrxn2
SKIP e22 Nrxn2, Nrxn3
SKIP e24 Stxbp5l
IR i9, ALE e9\e11 Khdrbs3
C
CamK2
Grik4
SST
-log10 p-value
log2 FC Exons
D
log2 FC Pattern
E
WT
Slm2ΔCamKII
Slm2ΔGrik4
Slm2ΔSST
Nrxn1
Nrxn2
Nrxn3
Gapdh
AS4(+)
AS4(-)
Input
IP
F
relative IP mRNA levels normalized to gapdh
Nrxn1 AS4+
Nrxn1 AS4-
Nrxn2 AS4+
Nrxn2 AS4-
Nrxn3 AS4+
Nrxn3 AS4-

Figure 3: Distinct SLM2-dependent alternative splicing programs between neuronal populations

A+B) Venn diagrams for DR exons and patterns between WT and *Slm2*-mutants. Unique and shared events of the individual cell types are indicated. The glutamatergic CA1 and CA3 populations mostly mimic alternative splicing regulation found in the global $Slm2^{KO}$ (e22 of *Nrxn2* and *Nrxn3*, e24 of *Stxbp5l* and modulation of *Slm2* (*Khdrbs3)* itself, e10,11). Ex2 of Khdrbs3 represents the exon used to generate *Slm2* cKOs. Alternative splicing of *Nrxn2* is the only splicing event common to the three cell types

C) Vulcano plots of all detected exons. Exons which were differentially regulated (Log2 FC ≥ 1 and ≤ -1, palue ≤ 0.01 are labelled in either purple for CamK2, green for Grik4 and red for SST WT and conditional mutant comparisons. For the 8 most regulated and some additional exons, gene names and involved exons are indicated.

D) Vulcano plots of all detected patterns Log2 FC ≥ 1, p-value ≤ 0.01. All significant events are labelled.

E) Semi-quantitative PCR validations for alternative splicing of *Nrxn 1-3* at AS4 in WT and cell class-specific mutants. Input samples (whole hippocampus) vs. cell-class specific pull down (IP) are compared between genotypes. In IPs of SST neurons, loss of SLM2 leads to a reduction in the AS4(-) isoform, most prominently for *Nrxn2*. In both CamK2 and Grik4 excitatory neuron IPs we can observe a more pronounced shift from more AS4(-) in WT animals towards an increase of AS4(+). This was observed for all three *Nrxn* genes. A phenotype similar to what has been observed in global $Slm2^{KO}$ mice.

F) Quantitative PCR for alterations in Nrxn splicing. Values are normalized to *gapdh* and fold changes by comparing input to IP are displayed. These results recapitulate observations by semi-quantitative PCR.

Figure 4

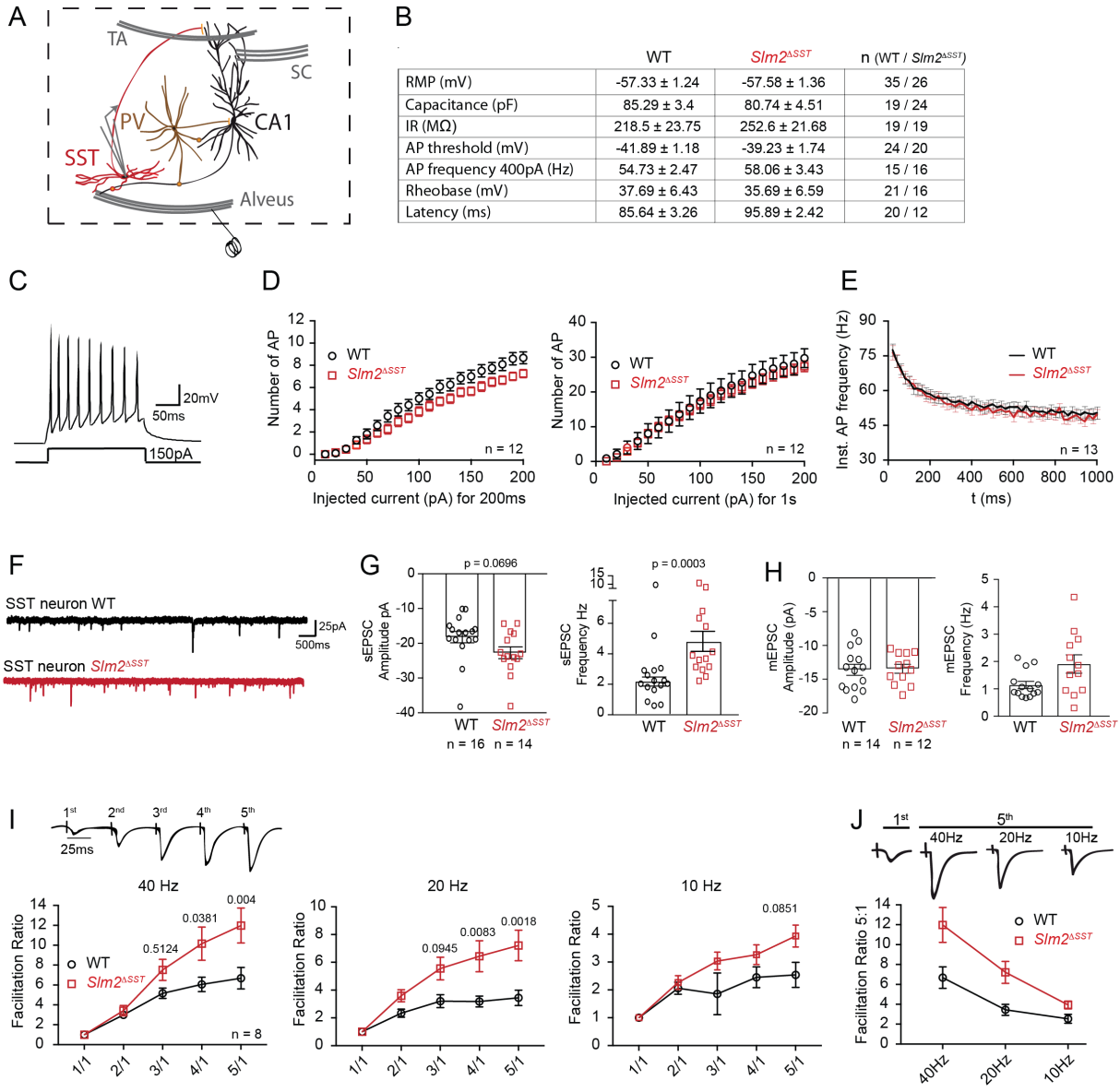

	WT	*Slm2*$^{\Delta SST}$	n (WT / *Slm2*$^{\Delta SST}$)
RMP (mV)	-57.33 ± 1.24	-57.58 ± 1.36	35 / 26
Capacitance (pF)	85.29 ± 3.4	80.74 ± 4.51	19 / 24
IR (MΩ)	218.5 ± 23.75	252.6 ± 21.68	19 / 19
AP threshold (mV)	-41.89 ± 1.18	-39.23 ± 1.74	24 / 20
AP frequency 400pA (Hz)	54.73 ± 2.47	58.06 ± 3.43	15 / 16
Rheobase (mV)	37.69 ± 6.43	35.69 ± 6.59	21 / 16
Latency (ms)	85.64 ± 3.26	95.89 ± 2.42	20 / 12

Figure 4: SLM2-mediated alterations of release probabilities at CA1-SST synapses

A) Recording and stimulation configuration within a hippocampal microcircuit. Recordings were performed from SST interneurons in current clamp (I_c) and voltage clamp (V_c) in acute hippocampal slices. Axon collaterals from CA1 neurons provide excitatory input onto SST interneurons (orange circle, alveus), which are stimulated to assess short-term facilitation. SST neurons inhibit the distal dendrites of CA1 pyramidal neurons (orange bar). Excitatory neurons themselves receive input from the Temporo-ammonic pathway (TA) and Schaffer collaterals (SC). For all recordings shown in Figure 4 the number of animals is ≥ 3. Numbers of cells are indicated for every experiment.

B) Summary table of intrinsic properties of SST neurons analyzed in WT and *Slm2*$^{\Delta SST}$ slices in I_c. Overall, intrinsic properties are unchanged in mutant animals, with the exception of latency to spike.

C) Example trace of action potentials as a response to a single 200ms long 150pA step in WT SST neurons. The, for SST neurons typical, adaptation in spike height and inter-event intervals can be observed.

D) Quantification of numbers of action potentials evoked at a certain current (10-200pA, 10pA steps) for either 200ms (left panel) or 1s (right panel).
E) Instantaneous action potential frequency over time shows spike adaptation typical for SST interneurons. Data is binned for every 25ms.
F) Example traces of spontaneous EPSCs onto SST interneurons for both genotypes (black WT, red *Slm2*$^{\Delta SST}$).
G) Quantification of amplitude (left panel) and frequency (right panel) of sEPSCs onto SST interneurons at V_c = -70mV. No blockers were used. Statistical comparisons are performed with Mann Whitney U test and show a significant increase in EPSC frequency in *Slm2*$^{\Delta SST}$ neurons.
H) Assessment of spine density measuring miniature post-synaptic currents in V_c = -70mV + 500nM TTX. Unpaired t-test with Welch correction for mEPSC frequency p-value 0.0506.
I) Top panel: Schematic of stimulation paradigm
Axon collaterals were electrically stimulated to evoke responses in SST interneurons clamped at -70mV at 40Hz, 20Hz or 10Hz. EPSC responses were normalized to amplitude of first response. SST neurons of *Slm2*$^{\Delta SST}$ mice show higher facilitation ratios compared to WT when comparing the 4th and 5th stimulation pulse. Two-way ANOVA with Bonferroni's multiple comparisons test. No specific blockers were used.
J) Top panel: Schematic of comparisons (amplitude of 5th stimulus vs. 1st) Quantification of facilitation ratios of 5:1 stimulus are shown for stimulation frequencies.

Figure 5

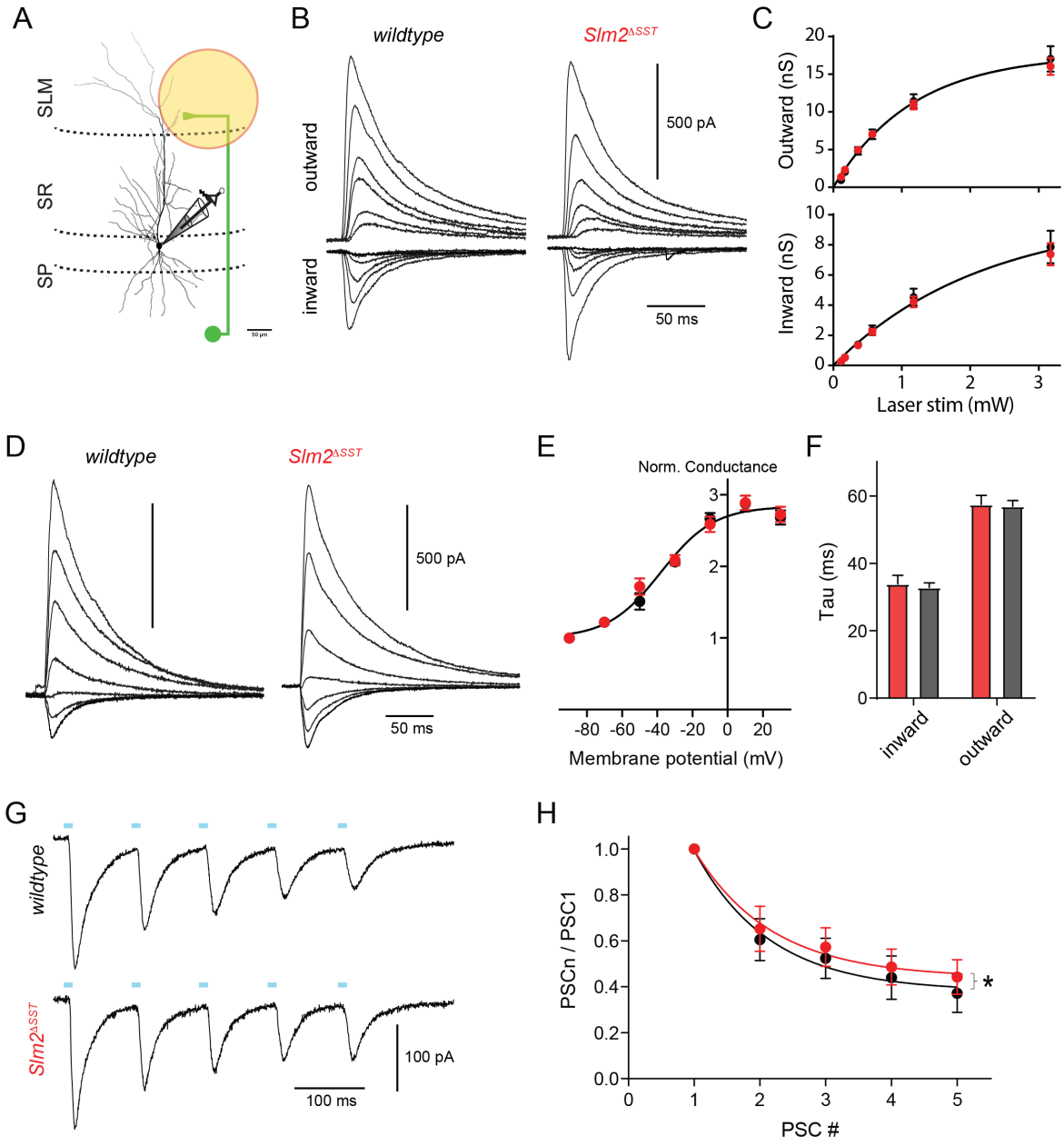

Figure 5: Loss of SLM2 in SST interneurons does not affect postsynaptic CA1 pyramidal neurons

A) Experimental design for local optogenetic stimulation of SST-mediated inhibition onto apical dendrites of CA1 pyramidal neurons to elicit GABAergic IPSCs in CA1 neurons. The green cell represents SST neurons residing in s.o targeting apical CA1 dendrites.

B) Representative traces of inward (V_c = -90mV) and outward (V_c = -10mV) IPSCs evoked at increasing laser intensities in both genotypes (+ 10µM NBQX and 25µM AP5)

C) Mean input-output curve of synaptic conductance for outward (top) and inward (bottom) IPSCs exhibit no differences between WT (black trace, n=15) and *Slm2*$^{\Delta SST}$ (red traces, n=15) mice at a given light intensity which reproducibly evoked responses.

D) Example traces of voltage-dependent SST mediated IPSCs. IPSCs were recorded between -90mV and +30mV in 20mV steps.

E) Mean synaptic conductance showed a comparable voltage-dependent increase of IPSCs in pyramidal neurons between both genotypes (WT n=16, *Slm2*$^{\Delta SST}$ n=15).
F) Group data of weighted taus from biexponential first to the descending phase of inward (V_c = -90mV) and outward (V_c = -10mV) IPSCs were comparable in WT (n=16) and *Slm2*$^{\Delta SST}$ (n=15).
G) Representative traces of inward IPSCs measured at -90mV during repetitive stimulation at 10Hz with light (blue bars).
H) Group data of IPSCs normalized to the first IPSC in the train. Stimulation at 10Hz lead to a small but significant difference in short-term plasticity at the SST-CA1 depressing synapse. (WT n=14, *Slm2*$^{\Delta SST}$ (n=12), p-value 0.011)

Figure 6

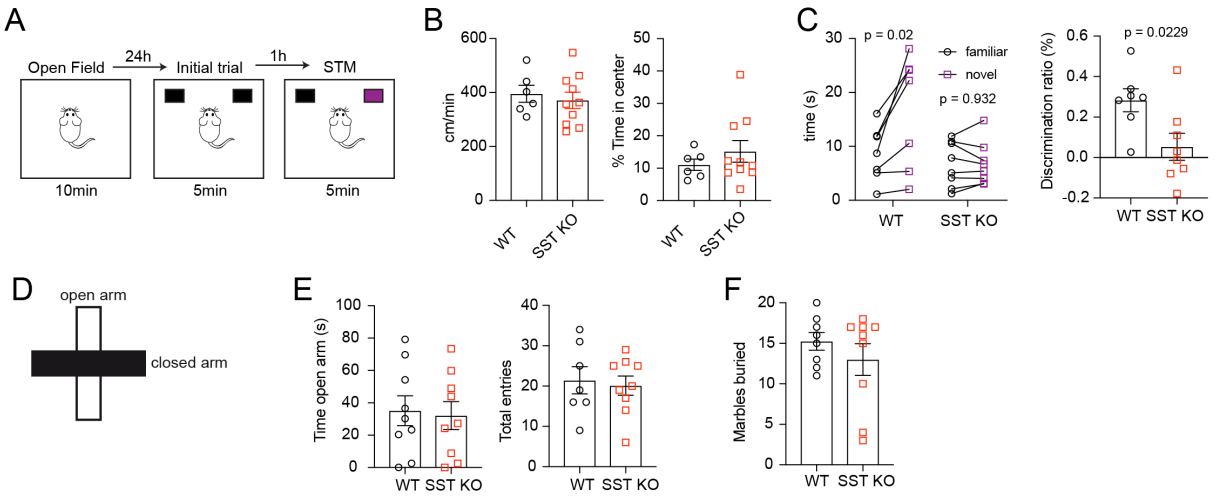

Figure 6: Altered short-term memory in *Slm2*$^{\Delta SST}$ mice

A) Experimental setup for behavioral testing of mice in the novel object recognition task. Analysis of both genotypes were placed in the open field arena on the first day, allowing us to measure initial behavior to a novel context. 24h later, two identical objects were introduced which could be freely explored for 5min. Testing for short-term memory was performed 1h after initial object exposure by introducing one new object.

B) Quantification of velocity (cm/min) and % of time spent in the center of the Open Field arena. No differences could be observed between genotypes (WT N=6, *Slm2*$^{\Delta SST}$ N=10).

C) Left panel: Interaction time in seconds with either the familiar (black) or novel (purple) object. WT animals exhibit preferences for the novel object whereas mutant mice did not (paired t-test). Overall interaction times are comparable between genotypes. Right panel: Discrimination index displaying failure of most mutant animals to recognize the novel object, unpaired t-test (WT N=7, *Slm2*$^{\Delta SST}$ N=8).

D) Schematic of elevated plus maze, a measurement of anxiety. Animals are allowed to move freely in either open (white) or closed (black) arms for 5min.

E) Quantification of the time spent in the open arm (in seconds, left panel) and total numbers of entries into either arm (right panel) did not show any differences between genotypes (WT N=7, *Slm2*$^{\Delta SST}$ N=9).

F) The Marble Burying Test was used as a measurement for stereotypic behavior. *Slm2*$^{\Delta SST}$ mice show a slight, non-significant trend to reduced marble burying (WT N=8, *Slm2*$^{\Delta SST}$ N=9).

Figure 7

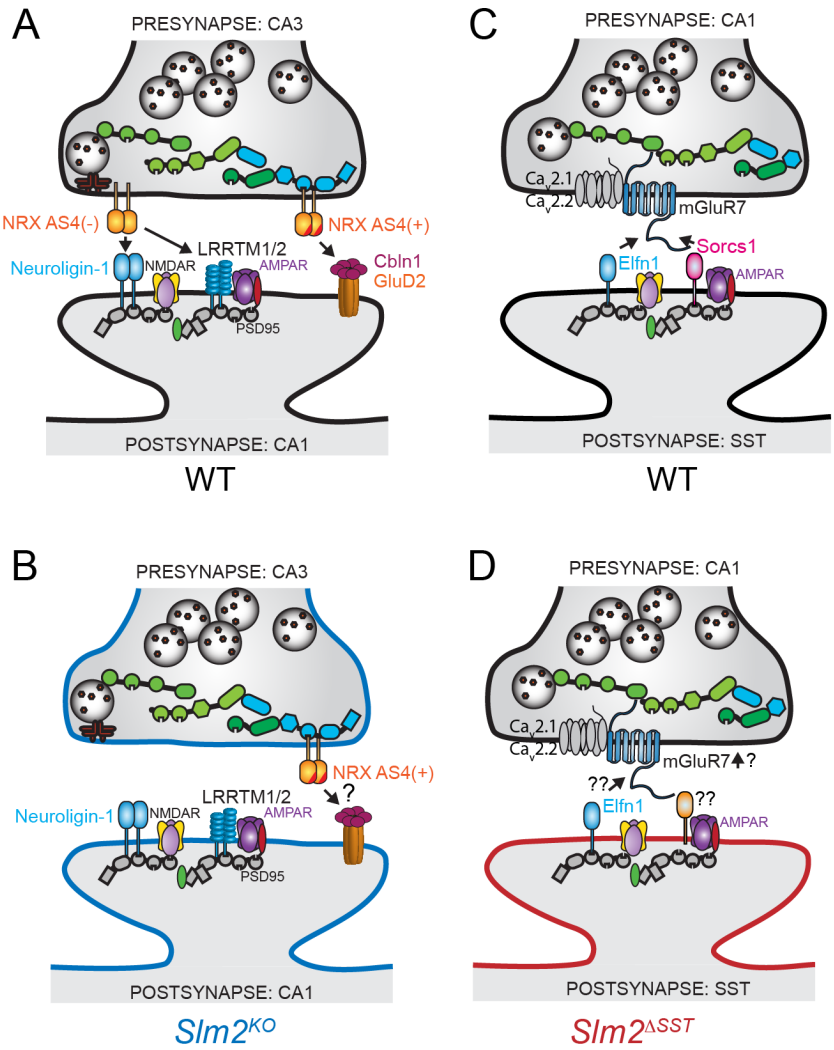

Figure 7: Cartoons illustrating trans-synaptic interactions between different synapses

A) Cartoons of trans-synaptic interactions in WT animals at glutamatergic CA3-CA1 synapses. Alternative splicing of *Nrxns* at AS4 generates proteins with different binding affinities for their postsynaptic partners including Neuroligins, LRRTMs and Cbln1.

B) Glutamatergic CA3-CA1 synapse in global *Slm2*^{KO} cells lead to reduced interactions of Nrxn AS4(-) with Neuroligins. In *Slm2*^{KO} an increase in Nrxn AS4(+) isoforms could be observed, possibly changing the trans-synaptic interactions to other postsynaptic binding partners.

C) Glutamatergic CA1-SST synapse in WT animals. Trans-synaptic interactions can be induced by expression of the post-synaptic molecule Elfn1 which interacts with pre-synaptic mGluR7 or GluR6 (not shown). mGluR7 can also interact with Sorcs1 which recruits and stabilizes AMPAR.

D) In conditional *Slm2* mutants glutamatergic CA1-SST synapse, loss of SLM2 in SST interneurons could lead to alterations in the synaptic composition of the postsynaptic cell, like increased Elfn1 expression and mGluR7 recruitment, loss of Sorcs1 surface receptor expression or through other, unknown, receptor molecules.

3. Discussion and further directions

The focus of my PhD thesis was to unravel the logic of alternative splicing programs in diverse neuronal cell types and how they contribute to synapse specification and neuronal circuit function. My work revealed new insights into the molecular mechanisms required for the generation of neuronal and synapse specification.

First, I undertook a single gene study in which I demonstrated that the splicing factor SLM2 is highly dedicated to control synapse specification in the hippocampus by modulation of alternative splice isoform choices of the cell surface receptor Neurexin. Second, I uncovered that the specification of divergent neocortical and hippocampal neuronal cell classes does not only rely on genetically determined gene expression, but also on the diversification by alternative splicing and transcription start sites. Specifically, genes characterizing the functional identity and synaptic functions of neurons are most subjected to diversification by post-transcriptional mechanisms. Moreover, I identified candidate RBPs, in addition to SLM2, that could have the potential to regulate alternative splicing programs in a cell class specific manner due to their restricted expression patterns. Third, I used the cell type-specific expression of SLM2 to investigate whether one RBP has the same or diverse functions in different cell types. This analysis revealed that SLM2 mediates highly selective alternative splicing programs in different cell populations. Furthermore, both in excitatory and inhibitory neurons the function of SLM2 is tailored to modulate synapse specification. Taken together, this thesis reveals major roles for cell type-specific alternative splicing programs in the genetic determination of neuronal circuit specificity and function. Furthermore, it opens the door to many more exciting questions, some of which I will discuss here.

3.1 A molecular code for neuronal specificity?

The ability of our genome to generate neuronal diversity with respect to different neuronal cell types with unique functional properties is highly important for appropriate brain function. Previous studies have already highlighted that neuronal cell types are highly subjected to diversification by alternative splicing (Gokce et al., 2016; Tapial et al., 2017). However, these studies have mainly contrasted neurons to non-neuronal cell types. I have now further complemented this picture by investigating whether diversification programs are also utilized within divergent neuronal classes. The global gene expression and alternative splicing analysis of excitatory and inhibitory neurons in the neocortex and hippocampus suggest that post-transcriptional mechanisms are indeed highly involved in determining the properties of individual neuron classes. I found that both alternative splicing and alternative first exon usage equally contribute to assign neurons their identity. Interestingly, cell class specific alternative

splicing programs mainly targeted genes responsible for giving neurons their functional and synaptic properties. Thus, this work uncovered that differential alternative exon usage by alternative splicing can be used to create a molecular code needed for neuronal specificity. However, we still lack knowledge on how these alternative splicing programs can be executed in such a specific manner. I will further elaborate on some of the multiple possibilities.

3.1.1 Contributions of selective expression of RNA binding proteins to neuronal specificity

One possibility on how selectivity with regards to splicing programs could be achieved is the selective expression of RNA-binding proteins that mediate exon incorporations. In the course of this discussion, RBPs referred to also function as splicing factors. There are hundreds of known putative RBPs that can be found in the brain (Ule and Darnell, 2006). However, there are only few splicing factors known to be expressed in a cell class-specific manner. The global gene expression analysis of a *bona-fide* list of 57 splicing factors based on previous publications (Chen and Manley, 2009; Nilsen and Graveley, 2010) in this thesis showed that there are indeed RBPs with selective gene expression in one or more cell classes. These expression patterns will further contribute to elucidating the function of cell type-specific alternative splicing programs.

One example is the splicing factor RNA-binding motif20 (Rbm20) which was initially described to be mainly expressed in the heart (Brauch et al., 2009). This might be due to the fact that the Rbm20 mRNA has very restricted expression patterns in the brain. In the neocortex, we could only significantly detect Rbm20 in parvalbumin positive interneurons. Thus, previous bulk sequencing studies might not have had the sequencing power to identify genes that were present in only a single neocortical cell type. In the heart Rbm20 is regulating alternative splicing of targets associated with cardiomyopathy (Guo et al., 2012). Its function in the brain still needs to be further investigated.

Another example for cell type-specific expression is SLM2. Its highly selective expression both on the mRNA and the protein level can be observed between different classes of excitatory neurons in the hippocampus. SLM2 is expressed in CA1-3 pyramidal neurons and absent from dentate gyrus granule cells (Iijima et al., 2014). Yet, its cell type specific expression within one single inhibitory neuron class is even more complex. For example, SLM2 is only expressed in ~10-20% of PV neurons in the CA1 region of the hippocampus (Nguyen et al., 2016). In collaboration with Emilia Favuzzi and Beatrice Rico at King's College, we could

show that SLM2 expression was restricted to Chandelier interneurons (data not shown). Moreover, SLM2 expression in SST interneurons of the hippocampus is anatomically defined. 70-85% of SST neurons residing in the s.o. or in CA3 express the protein, whereas SST cells in the hilus lack it. OLM interneurons residing in the s.o are thought to be similar to the Martinotti cells of the cortex, since they have multiple features in common (Tremblay et al., 2016). However, SST neurons in the cortex do not display clear position-dependent features. Interestingly, a recent study by Lim and colleagues demonstrated that the *Slm2* mRNA can already be found specifically in Martinotti cell precursors of the medial ganglionic eminence (Lim et al., 2018). Thus, the selective expression of SLM2 in subsets of Martinotti cells is already genetically defined early in life.

Based on the SLM2 example, it is an intriguing hypothesis that the expression of RBPs that regulate splicing of synaptic genes is pre-determined in neuronal precursors already shortly after becoming post-mitotic. This could be achieved by combinatorial codes of transcription factors which directly co-regulate the terminal differentiation of individual neuron classes (Hobert, 2008). Therefore, the presence of certain transcription factors in a given cell population at early times during development could contribute to cell type-specific expression of RBP mRNAs. Observations in *C.elegans* where a single gustatory neuron expressed a completely different set of transcription factors compared to a related sensory neuron would further strengthen this hypothesis (Etchberger et al., 2007; Hobert et al., 2010). However, transcription can also be modulated in an activity-dependent manner (Yap and Greenberg, 2018). Thus activity-dependent mechanisms of transcription could further contribute in specifying neuronal properties by regulating mRNA levels of RNA binding proteins.

With all of this in mind, it would be of high interest to mine existing single cell datasets of neuronal precursor neurons for 1) the correlation between newly identified cell type-specific expression of RBPs in mature neurons and their corresponding expression during development and 2) to identify possible combinatorial codes of transcription factor usage that coincide with the expression of a given RBP. Once identified, this will further lead to insights into putative activity-dependent remodeling of transcription factor usage as one possible way to adjust RBP expression according to experience or homeostatic regulation of brain function in an adulthood.

In addition, such studies might be helpful to further understand the etiology of some neurological conditions such as autism spectrum disorders. Recent studies suggested that the expression of RBPs, including nSR100, and the subsequent alterations in alternative splicing influence the development of certain autistic-like features including social behaviors (Quesnel-Vallieres et al., 2016). Importantly, researchers have started to test whether direct manipulation of alternative splicing choices could contribute to alleviate disease onsets and symptoms. For

example, investigations in the causes of spinal muscular atrophy have already demonstrated that modulation of a single exon incorporation in the Smn2 gene provided a therapeutic strategy to rescue associated phenotypes in mice (Donadon et al., 2019; Hua et al., 2011). Therefore, understanding which neuronal cell type produces certain transcript isoforms will allow the generation of more targeted therapeutic tools for treating neurological conditions and understanding brain function in health and disease.

Transcriptional regulation provides one way to generate cell type-specific expression patterns of RBPs. However, there have been examples demonstrating that post-transcriptional mechanisms such as nonsense-mediated mRNA decay (NMD) can be used to provide controlled expression of RBPs (Lareau et al., 2007; Ni et al., 2007). For example, Ptbp1 and 2 control their selective expression through cross-repression mechanisms (Boutz et al., 2007; Zheng et al., 2012). SLM2 has been demonstrated to autoregulate its expression by alternative splicing selection of an alternative 3' end which leads to NMD (Ehrmann et al., 2016). Furthermore, SLM2 represses the expression of SLM1, by targeting its RNA for NMD. Thus, this generates the mutually exclusive expression pattern between the two paralogues (Traunmüller et al., 2014).

Cross-repression mechanisms could represent developmental strategies to steer the expression of the target genes in a temporally and locally controlled manner. The fact that the RNA is still there, ready to be translated once the repressor is gone, also generates transition periods in which one splicing program is gradually replaced by the other, leading to a subsequent refinement of the mRNA pool. Such mechanisms could be used by developing axons and dendrites to change their molecular surface receptor composition and thus, alter their trans-synaptic interactions. A recent study from Sika Zheng's laboratory further supports the hypothesis that cross-repression of RBPs is a powerful tool during development. The authors demonstrated that alternative splicing programs mediated by PTBP2, whose expression is prepressed by PTBP1 in neuronal stem cells and progenitors, is highest during axonogenesis and orchestrates the robust generation of single axons during development by its splicing targets (Zhang et al., 2019).

My data suggests that neuronal cell type-specific splicing programs do not alter the identity of the neuron but rather establishes its repertoire for its unique intrinsic properties and synaptic terminal differentiation. Thus, one could also speculate that cross-repression mechanisms of splicing factors are involved in changing the function of neurons during development by modulating the exchange and insertion of different channels or receptors at the membrane of synapses.

Finally, autoregulation of RBPs, like SLM2, might allow neurons to regulate the amount of their own protein content in an activity and state dependent manner. Thus, this mechanism

could ensure stable physiologically needed splicing patterns of RBP targets to maintain appropriate neuronal and synapse function during different physiological states.

In conclusion, this work shows that cell type-specific expression of RBPs can lead to selectively regulated alternative splicing programs, which are required to establish unique neuronal properties. However, the majority of RBPs are broadly expressed. In contrast, SLM2, which exhibits restricted and defined expression pattern, exerts cell type-specific functions even in two closely related classes of CA1 and CA3 excitatory neurons. Thus, what determines the target selectivity of RBPs in a given cell type?

3.1.2 The power of RNA binding motifs

How can splicing factors like SLM2 regulate such diverse alternative splicing programs in different neuronal cell classes? For example, Rbfox1 regulates 305 events in SST and 742 events in PV neurons at P8. Of these, only 93 events were commonly shared between the two cell populations (Wamsley et al., 2018). In the case of SLM2, only 49 events for SST, 78 events for CA1 and 69 events for CA3 were significantly differentially regulated. The overlap between these populations was very small (between 1-6%). Importantly, ~90% of genes that were alternatively regulated in either of the three neuron classes were commonly expressed in all three cell populations suggesting that the selectivity of the splicing programs was not due to the fact that the other cell populations did not express those genes to begin with. The comparison between Rbfox1 and SLM2 illustrates that both splicing factors mediate divergent splicing programs in different cell populations. The number of splicing events in the SLM2 mutants are much lower and has to be taken with caution due to potential different cut-off settings of fold-change and p-values.

Nevertheless, this demonstrates the general potential of RBPs to regulate their unique subset of targets and to differentially determine splicing choices. This might be due to differential recruitment of the spliceosome to enhancer or suppressor sites. Moreover, splicing choices can be further diversified by the differential availability of their RNA binding motifs. The RBP motif identified for STAR proteins, including SLM2, consists of bipartite U(A/U)AA rich repeats. One underlying mechanism for cell type-specific regulation of splicing might be that SLM2 binds different motifs depending on the cell type. Thus far, only the bipartite U(A/U)AA motif has been identified. But could there also be additional binding motifs which had been overlooked? In other words, could an RBP in different pools of neurons recognize multiple alternative motifs? To address this question, cell type-specific crosslinking of the RBP of interest with its target RNA and subsequent sequencing to determine the binding motifs (Hits-

CLIP and variants of it including conditionally tagged-CLIP) (Hwang et al., 2017) will be required. Interestingly, conditionally tagged-CLIP of Nova2 in excitatory and inhibitory neurons of the cortex and cerebellum revealed that Nova2 binds the same RNA binding motif in all cell classes but still leads to different incorporation rates of exons and transcript diversification (Saito et al., 2019). However, this might not necessarily be true for STAR proteins.

Cell type-specific splicing programs could also be achieved through alternative mechanisms. For example, it has recently been demonstrated that the binding site density and their relative positions for STAR proteins has major impacts on the splicing regulation of their targets (Danilenko et al., 2017). Thus, SLM2 could in principle have the same target genes in all cell populations but due to binding site densities and availability, different splicing choices are made. Furthermore, splicing factors do not always exert their function alone but also perform synergistic or antagonistic functions together with other co-factors (Raj and Blencowe, 2015). Therefore, it is conceivable that in SST interneurons and excitatory cells different RBPs or accessory proteins are co-expressed with SLM2 than in excitatory neurons, possibly masking the binding site or co-regulation of the splicing reaction.

The potential mechanisms described to achieve cell type-specific splicing and exemplified with SLM2, illustrate some of the vast amount of possibilities. Still, every RBP could act in its own, unique way. Thus, it will be crucial to combine newly emerging knowledge on the cell type-specific expression of RBPs, the modulation of specific target mRNAs and the corresponding cellular consequences to finally determine a molecular code for neuronal function.

3.1.3 Additional mechanisms contributing to the molecular code for neuronal specification

These are only a few out of many possibilities described in detail. I would like to briefly mention two other post-transcriptional mechanisms that greatly contribute to the generation of transcriptome diversity. These are alternative transcription start sites and RNA editing.

It has previously been suggested that alternative promoter usage is equally, maybe even more used to generate transcriptome diversity than alternative splicing (Pal et al., 2011). The systematic mapping of diversification in different neuronal cell types described in this thesis also illustrate the abundant use of transcription start sites in neuronal tissue (~30-60% of detected events in given cell populations were alternative first exons). These results indicate a frequent use of cell type-specific enhancers and promoters. Moreover, these alternative first exon events efficiently segregated neocortical excitatory and inhibitory classes, even between

MGE- and CGE-derived interneurons. Thus, also alternative transcription start sites play major roles in specifying cell type-specific transcript isoforms in neurons. To further dissect a molecular code for neuronal specification in different cell classes it would be interesting to identify potential cell type-specific promoter sequences that guide the binding of unique pools of transcription factors to modulate gene expression. One way to achieve this could be by the use of the ISMARA online tool (Integrated System for Motif Activity Response Analysis). ISMARA models genome-wide predicted regulatory sites for transcription factors and can be used on RNA sequencing data, like the Ribotag dataset generated in this work. (Balwierz et al., 2014). Thus, it could be used to identify binding sites for key transcription factors that drive divergent gene expression programs in a cell type-specific manner.

Another frequently used mechanism to generate diversity but also to specify properties of proteins is RNA editing. This process leads to a single nucleotide switch from adenosine to inosine before translation and gives rise to further functional diversification of proteins. Probably one of the most well-known examples in neurobiology is the editing of the AMPAR subunit GluA2. RNA editing of GluA2 occurs at the Glutamine/Arginine editing site within the pore of the channel. Most mature GluA2 receptors contain the arginine, even though glutamine is genetically encoded. This switch is functionally highly important since it restricts Ca^{2+} permeability, channel conductance and homo-tetramerization of these receptors (Greger et al., 2003; Isaac et al., 2007; Penn and Greger, 2009). Thus, RNA editing provides another mechanism to specifically generate protein diversity and to specify aspects of channel properties and their function within developing and mature circuits.

3.2 Functional implications of alternative splicing programs

The previous discussion section mainly focused on how target selectivity of RBPs could contribute to the selective splicing programs that we observed. In this chapter I will discuss further functional implications for synaptic communication.

3.2.1 RBPs as master regulators of synaptic specificity

Surprisingly, the SLM2-dependent alternative splicing programs identified in these studies are very defined and only involve few genes. In contrast, previous studies investigating RBPs like Nova2, nSR100 or Rbofx1 with global or cell type-specific KOs demonstrated that these splicing factors mediate hundreds of targets (Quesnel-Vallieres et al., 2015; Saito et al., 2019; Ule et al., 2005; Wamsley et al., 2018). They have been demonstrated to mediate

synaptic transmission, aspects of synapse formation and diversification of cell adhesion molecules (Saito et al., 2019; Ule et al., 2005; Wamsley et al., 2018), or have been implicated in controling splicing networks that are linked to ASD phenotypes (Quesnel-Vallieres et al., 2016). As an example, homozygous loss of Nova2 leads to spontaneous epilepsy and early postnatal death (Eom et al., 2013; Jensen et al., 2000). Selective ablation of Nova2 in cerebellar Purkinje neurons leads to gross deficits in dendritic morphology and subsequently to Purkinje neuron degeneration (Saito et al., 2019). Central nervous system deletions of Rbfox1 in mice lead to increased spontaneous seizures (Gehman et al., 2011). Even though the major contributions of Nova2 and Rbfox1 are with respect to the regulation of alternative splicing of genes important for synapse function, they also regulate genes involved in mRNA processing, DNA binding, cell cycle regulation or immune responses (Saito et al., 2019; Ule et al., 2005; Wamsley et al., 2018). In contrast, SLM2 function is much more specified to mediate synapse function.

Global knock-out of SLM2 did not lead to any severe deficits in their behavior, and mild phenotypes including alterations in the novel object recognition task or marble burying. When examining the hippocampus in more detail, most of the receptors important for synaptic transmission exhibited normal expression with the exception of an increase in AMPARs present on the surface of neurons and very selective alterations in synaptic transmission including long-term potentiation. The genomic analysis of alternative splicing events revealed only a handful of significant targets and the most highly de-regulated exons involved the cell adhesion molecules Neurexin 1-3 at AS4. Loss of SLM2 leads to a shift in the balance between AS4(+) and AS4(-) towards expression of AS4(+) isoforms. This in turn correlated with reduced post-synaptic interaction partners of AS4(-) like Neuroligins. However, the most impressive result of this study was that the genetic rescue of the Nrxn1 AS4(-) isoform, by modification of a single exon, restored trans-synaptic interactions, partially rescued the LTP phenotype and astonishingly even normalized the behavior of the mice. These results strongly suggest that the function of SLM2 is even more dedicated to control aspects of synapse specification in comparison to other RNA binding proteins.

One might further speculate that the entire STAR family of RNA binding proteins, not only SLM2, might exhibit such specific functions. Indeed, all three STAR proteins, SLM1, SLM2 and Sam68 regulate alternative splicing of *Nrxn1-3* at AS4 (Ehrmann et al., 2013; Iijima et al., 2014; Iijima et al., 2011). While SLM1 and SLM2 mediate this particular splicing choice at basal conditions, Sam68 regulates alternative splicing of *Nrxn1* at AS4 in an activity-dependent manner (Iijima et al., 2011). In contrast to SLM1 and SLM2, based on what we know thus far, Sam68 is the only member of this family that not only mediates alternative splicing but also additional functions in other signaling processes including RNA metabolism and transport (Sanchez-Jimenez and Sanchez-Margalet, 2013). Genome-wide mapping of Sam68-mediated

alternative splicing events in basal states revealed that Sam68 mediates the splicing of many genes which are implicated in synaptic functions (Witte et al., 2018). Sam68 had also been previously identified to regulate mGluR dependent translation and long-term depression (Klein et al., 2015). Comparisons of deep-sequencing datasets between *Sam68*^{KO} and *Slm2*^{KO} hippocampi using age matched mice and the same cutoffs for analysis demonstrated that Sam68 regulates ~8x more targets than SLM2. Moreover, the overlap between the alternatively regulated events was minimal (Witte et al., 2018). Thus, even though both proteins are implicated in mediating synaptic properties, the function of SLM2 is much more defined, even within one protein family.

Interestingly, loss of SLM2 leads to an up-regulation of Slm1 both on the protein and mRNA level (Traunmüller et al., 2014). However, our analysis thus far, indicates that it does not obviously compensate for the loss of SLM2 with respect to alternative splicing targets (see results chapter 2.1). SLM1 might therefore also have its unique sets of target genes or lacks co-factors in SLM2 expressing cells necessary to execute its function. It will be important to identify which cell type-specific targets SLM1 regulates and moreover, whether SLM1 and SLM2 might also have the potential to regulate splicing in an activity-dependent manner.

Taken together, different splicing factors generally have the potential to regulate synaptic specification by alternative splicing.

3.2.2 Why would the brain require dedicated RBPs to control synapse specification?

A question arising from the observations that many splicing factors are mediating aspects of synaptic specificity is why the brain would require so many different proteins to mediate synapse function, and furthermore why SLM2 would execute even more targeted programs.

The answers to that are manifold and might correlate with the enormous complexity of the brain. A single neuron can receive and make tens of thousands of diverse synaptic inputs and outputs, which all need to form distinct compartmentalized connections. Interestingly, distinct neuronal cell types exhibit different expression levels of available mRNAs encoding proteins implicated in regulating synaptic function (Paul et al., 2017). Thus, there is already a level of specification due to gene expression. This will be further specified by post-transcriptional mechanisms like alternative splicing, which is mediated by RBPs. Even one single RBP like Rbfox1 or SLM2 have the potential to regulate very divergent alternative splicing choices in different cell populations. So even if there are commonly expressed synaptic genes expressed across all cell types, RBPs can still modulate their transcript isoforms to

generate divergent proteins depending on the cell type. Importantly, events regulated by different RBPs do not necessarily have to affect the same genes, as illustrated in the Sam68/SLM2 comparison. Alternative splicing programs by different RBPs in the same cell could thus, lead to the regulation of diverse aspects of synapse specification. This could be achieved by generating different transcript isoforms, but also by altering their localization, or their mRNA stability either by the induction of frameshifts and the degradation of the RNA by NMD or 3' UTR processing. This provides RBPs with the unique possibility to regulate both the abundance level of a protein, and its diversification in a cell class-specific manner.

In addition, activity-dependent splicing factors including, but not limited to, Rbfox1 or Sam68 could therefore acutely initiate the remodeling of pre- and post-synaptic structures in a specific cell type, and potentially of completely different sets of proteins in response to activity. Furthermore, this process can be applied in mature neuronal circuits but also during development. Such activity-dependent processes might ensure that even neighboring synapses receive different instructions for forming trans-synaptic interactions or to process incoming information, based on what RBPs are expressed and which inputs they receive. Alternatively, one could imagine that splicing programs regulated by constitutive activity of RBPs including SLM2 might counterbalance activity-dependent changes to ensure homeostatic balance of synaptic communication. In any case, given the immense possibilities of synaptic connections it is not surprising that we need a large amount of proteins that potentially mediate very diverse aspects of synaptic specification. The dedicated functions of SLM2 might be one mechanism by which our nervous system achieves its highly specified synaptic communication. Moreover, the very limited phenotypes in electrophysiological properties or behavioral alterations when SLM2 is genetically ablated, further indicate that SLM2 might be mainly required for the adaptation of very specific aspects for synaptic communication and brain function.

3.2.2 One RNA-binding protein - two sides of one coin?

Importantly, the same splicing factor can mediate different splicing programs depending on the cell type it is expressed in. The global *Slm2*^{KO} studies strongly implicated SLM2 in the regulation of synaptic specificity which was dependent on splicing alterations of the pre-synaptic cell adhesion molecule *Nrxn1*. The electrophysiological phenotypes observed affected post-synaptic neurons, whereas pre-synaptic properties were not altered. I further functionally tested whether SLM2 could mediate different aspects of synaptic transmission in inhibitory neurons compared to the analysis of glutamatergic transmission in our global *Slm2*^{KO}.

Both in glutamatergic and in SST inhibitory neurons SLM2 exerts highly specific functions. Neither overall alterations in intrinsic properties, nor global transcriptional changes, both of which would be indicators that the identity of the neuron was altered, could be detected. However, there was an effect on excitatory synaptic transmission onto SST neurons, which was manifested in higher facilitation ratios. Moreover, there was a slight change in short-term plasticity from the SST pre-synaptic terminal onto CA1. Thus, SLM2 might generally mediate short-term plasticity in SST neurons. Importantly, inhibition onto the postsynaptic neuron, CA1 pyramidal cells, was unchanged. This stands in contrast to observations in global *Slm2*^{KO} mice and could indicate that SLM2 mediates different mechanisms of pre- and post-synaptic transmission depending on the cell type it is expressed in.

My data suggests that at glutamatergic terminals between CA3 and CA1 SLM2-dependent regulation of *Nrxn1-3* AS4 variants in the pre-synaptic terminal leads to trans-synaptic alterations, including long-term potentiation in the post-synaptic neuron. In SST interneurons SLM2 might mediate short-term facilitation by regulating release probabilities, possibly also through trans-synaptic interactions but instructed by the post-synaptic side. Both, long-term potentiation and short-term facilitation are crucial mechanisms for gating information flow in mature neuronal circuits. However, they exhibit different functions. Long-term potentiation leads to the structural refinement of the synapse that can be long-lasting, whereas short-term facilitation is rapidly and temporally controlling information processing. Thus, SLM2 is involved in the regulation of two different types of plasticity in a cell class-specific manner. It might be a valid hypothesis that these SLM2-mediated alternative splicing programs are critically important for gating information flow in the hippocampus. On the one hand, SLM2 might mediate intra-hippocampal information processing by modulating long-term potentiation at Schaffer collaterals, which is thought to be critical for the formation of memories. On the other hand, it might temporally guide short-term plasticity and thus, the activity of SST neurons. Another interesting possibility is that SLM2 also mediates LTP by inhibiting direct excitatory inputs onto CA1 pyramidal neurons from the entorhinal cortex. Exerting these two functions, SLM2 could generally be involved in gating hippocampal-mediated information flow, both at the pre- and post-synapse. I hypothesize that these mechanisms are dependent on the differential splicing of selective cell adhesion molecules that bridge the synaptic cleft. Given that this can be observed in divergent neuronal cell populations, one single RBP has the potential to greatly amplify synaptic information capacities in different neuronal populations which exert different functions.

3.3 Conclusions

During my PhD thesis work I deciphered the logic of alternative splicing regulation in neuronal cell types and enhanced our understanding how RBPs are involved in mediating neuronal diversification and synapse specification. The single gene studies on a select splicing factor used in this thesis work further demonstrated that SLM2 greatly contributes to assigning neurons their unique synaptic functions.

The studies on SLM2 initiated the speculation that select splicing factors could also act as terminal selector genes. This term has initially been proposed by Dr. Oliver Hobert for transcription factors that give neurons their unique identity (Hobert, 2008). Along this line, I propose that SLM2 might exert similar functions but with respect to assigning synaptic properties of individual neurons and thereby instructing synapse formation and designated functions by alternative diversification. Given that different RBPs can modulate diverse aspects of synaptic function, it is very likely that there are combinatorial codes of RBPs in individual neurons that jointly drive distinct properties to generate a neurons' unique behavior. Our global assessment of RBPs in neocortical and hippocampal samples of genetically defined cell classes represent one starting point to further dissect a potential molecular code for neuronal function and wiring specificity.

To further understand wiring specificity mediated by alternative splicing programs, we will have to test whether synapses at a particular compartment of axons and dendrites express different types of cell adhesion molecules, or other target genes of splicing factors. Furthermore, how many targets of different splicing factors are indeed incorporated into one single synapse? Could there be dendrite branch specific insertions of protein isoforms? To assess which alternative transcript isoforms are translated into proteins, the Ribotag approach used in this dissertation work already provided some insights into which transcripts are associated with the ribosome and have the potential to be translated. Furthermore, we will have to intersect these genome-wide studies with assessments of translational efficiency.

4. Materials and Methods

Materials and Methods – Traunmüller*, Gomez* *et al.,* 2016

Mice

All procedures involving animals were approved by and performed in accordance with the guidelines of the Kantonales Veterinäramt Basel-Stadt. *Slm2*^{KO} mice were previously described (Traunmüller et al., 2014). *Nrxn1* exon 21 conditional knock-out mice possess loxP sites on either side of exon 21 of the targeted gene. A targeting vector was designed with a loxP-Frt-PGKneo-Frt cassette inserted 982 bp 5'-upstream of exon 21 of mouse *Nrxn1* and a loxP site placed 557 bp 3'downstream of the same exon. Homology arms were 3 kb and 4.6 kb in length and the targeting construct contained herpes simplex virus thymidine kinase as a negative selectable marker in the 3'arm of the targeting vector. The construct was electroporated into ES cells derived from F1(129Sv/B6) embryos. Correctly targeted ES cells were then used to generate chimeric mice. Male chimeric mice were mated with ROSA26-Flpe females (Jax stock no: 003946), which had been backcrossed over ten generations with B6, to remove the PGKneo cassette. Germline ablation was created by crossing with CMV-cre mice (Jax stock no: 006054). Mice that are homozygous for this allele are viable, fertile, normal in size and do not display any gross physical or behavioral abnormalities. For transgenic marking of a subset of hippocampal pyramidal cells, mice were crossed to Thy1::YFP-H transgenic mice (Feng et al., 2000).

Antibodies, qPCR assays

Custom polyclonal antibodies for rabbit anti-SLM2, rabbit anti-NRX1, rabbit anti-NL1, rabbit anti-NL2 and guinea pig anti-NL3 were previously described (Budreck and Scheiffele, 2007; Iijima et al., 2014; Muhammad et al., 2015). The following commercially available antibodies were used: rabbit anti-GluA1 (Chemicon AB1504,1:2000), rabbit anti-GluA2 (Neuromab 75-002, 1:2000), mouse anti-GluN1 (Synaptic Systems 114011, 1:3000), rabbit anti-GluN2A (Chemicon AB1555P, 1:2000), mouse anti-GluN2B (Neuromab 75-101, 1:2000), mouse anti-PSD95 (Neuromab 75-028, 1:3000), mouse anti-vGlut1 (Neuromab 75-066, 1:2000), goat anti-C3 (MP Biomedicals 855463, 1:3000), rabbit anti-Calnexin (1:2000, StressGen SPA-865).

For qPCR assays, total hippocampal RNA was extracted with Trizol and purified using Qiagen RNeasy Mini Kit. Quantitative PCR was performed on a StepOnePlus qPCR system. Gene expression assays were used with TaqMan Master Mix and comparative C_T method. The WT/*Gapdh* or *β-actin* cDNA levels were set to 1.0 and compared to the respective mutant values (*Slm2*^{KO}*, Nrxn1ex21*$^{fl/fl}$*, Nrxn1*$^{\Delta ex21}$). Commercially available gene expression assays for *Grin1* (Mm.PT.58.33004583)*, Grin2a* (Mm.PT.58.31855824)*, Grin2b* (Mm.PT.58.6114910)*, Grin2d* (Mm.PT.58.30709879)*, Grin3a* (Mm.PT.58.13518911) were from Integrated DNA

Technologies, *β-actin* (Mm00607939_s1), *Nrxn1* (Mm00660298_m1), *Nrxn2* (Mm01236851_m1) and *Nrxn3* (Mm00553213_m1) from Applied Biosystems.

Sample preparation

For protein fractionation, three pairs of hippocampi were dissected in cold 1X PBS, snap frozen and stored at -80°C. Total brain lysate, synaptosomes, Triton X100-soluble and insoluble postsynaptic density fractions were prepared as previously described (Phillips et al., 2001).

Samples for receptor surface biotinylation were prepared as follows: Acute slices were prepared in ice cold 1X ACSF (in mM: 124 NaCl, 2.5 KCl, 1.2 NaH_2PO_4, 24 $NaHCO_3$, 5 Hepes, 12.5 Glucose, 1.3 $MgSO_4$, 2.5 $CaCl_2.2H_2O$) and recovered in 1X ACSF for 50min. Afterwards, the hippocampus was dissected and incubated for 30min at 4° in 1mg/ml EZ-link™ Sulfo-NHS-SS-Biotin (Thermo Scientific, #21331) or in 1X ACSF for "no biotin" control. Excess biotin was removed by two brief washes with 50mM NH_4Cl in ACSF and two times ACSF only. Slices were then homogenized in 1ml Homogenization Buffer (50mM 1M Tris-HCl pH = 8, 10% Glycerol, 250mM NaCl, 0.2% SDS, 1% Triton X-100, Complete protease inhibitors EDTA-free (Roche)) and centrifuged for 5min at 5000xg to remove cell debris. Protein concentrations were measured and 700µg of protein was added to 40µl Neutravidin beads and rotated for 5hr at 4°C. Beads were washed 4 times with Wash Buffer (1M Tris-HCl pH = 8, 10% Glycerol, 250mM NaCl, 0.2% SDS and 0.05% Triton X-100) and proteins were eluted in 1X Laemmli Buffer.

Samples for NRX1β AS4(+) and AS4(-) recognition specificity assay have been prepared as previously described (Schreiner et al., 2015). Briefly, secreted SNAP-tagged ectodomains of mouse NRX1β either including exon21 (AS4+) or lacking it (AS4-) were expressed in HEK293 cells. Supernatants of transfected cells collected at 48hrs was incubated with SNAP-capture agarose resin (NEB, S9144S) overnight at 4°C. For pull-down one forebrain of a P21-P28 old mouse was homogenized in 2ml Homogenization Buffer (50mM Tris-HCl pH 7.5, 10% glycerol, 150mM NaCl, 2mM $CaCl_2$, 1% Triton X-100 complemented with complete protease inhibitors EDTA-free (Roche)) and centrifuged at 20000xg for 30min at 4°C. The supernatant was added to the recombinant protein-bead preparation and rotated O/N at 4°C. After washing, proteins were eluted in 1% sodium deoxycholate, 50mM ammonium bicarbonate and processed for mass-spectrometry.

Protein concentrations were determined using the Pierce BCA assay. For immunoblotting horseradish peroxidase (HRP)-conjugated secondary antibodies and Pierce ECL Western Blotting Substrate were used. Signals were acquired using an image analyzer. For quantitative assessment of protein up- or down-regulation ImageJ was used. Statistical analysis was done with Prism Software. All statistical data are mean ± SEM. Data were tested with a One-Way ANOVA and Dunnett's post-hoc test for multiple comparison.

LC-MS analysis and label-free quantification:

For proteolytic digest, samples were shaken at 37°C for 1h in Tris-(2-carboxyethyl)-phosphine hydrochloride (TCEP, 1:40 v:v), alkylated in iodoacetamide at RT for 30min in the dark (1:40 v:v) and then incubated with N-acetyl-cysteine at RT for 10min at RT. Afterwards, samples were digested O/N at 37° with trypsin (1µg). The resulting peptides were purified and desalted using microspin C18 columns according to the manufacturer's instructions, dried under vacuum, resuspended in (LC Buffer A, 2% acetonitrile 0.15% formic acid) and stored at -80°C until further processing. 1 ug of peptides of each sample were subjected to LC–MS analysis using a dual pressure mass spectrometer connected to an electrospray ion source as described (Glatter et al., 2012) with a few modifications. In brief, peptide separation was carried out using an EASY nLC-1000 system equipped with a RP-HPLC column (75 µm × 30 cm) packed in-house with C18 resin (ReproSil-Pur C18–AQ, 1.9 µm resin) using a linear gradient from 95% solvent A (0.15% formic acid, 2% acetonitrile) and 5% solvent B (98% acetonitrile, 0.15% formic acid) to 28% solvent B over 90 min at a flow rate of 0.2 µl/min. The data acquisition mode was set to obtain one high-resolution MS scan in the FT part of the mass spectrometer at a resolution of 120,000 full width at half-maximum (at m/z 400) followed by MS/MS scans in the linear ion trap of the 20 most intense ions using rapid scan speed. The charged state screening modus was enabled to exclude unassigned and singly charged ions and the dynamic exclusion duration was set to 30s. The ion accumulation time was set to 300 ms (MS) and 25 ms (MS/MS).

For label-free quantification, the generated raw files were imported into the Progenesis QI software and analyzed using the default parameter settings. MS/MS-data were exported directly from Progenesis QI in mgf format and searched against a decoy database the forward and reverse sequences of the predicted proteome from *Mus musculus* (UniProt, total of 33,984 entries) using MASCOT (version 2.4.1). The search criteria were set as follows: full tryptic specificity was required (cleavage after lysine or arginine residues); 3 missed cleavages were allowed; carbamidomethylation (C) was set as fixed modification; oxidation (M) as variable modification. The mass tolerance was set to 10 ppm for precursor ions and 0.6 Da for fragment ions. Results from the database search were imported into Progenesis QI and the final peptide measurement list containing the peak areas of all identified peptides, respectively, was exported. This list was further processed and statically analyzed using a custom SafeQuant R script (Glatter et al., 2012). The peptide and protein false discovery rate (FDR) was set to 1% using the number of reverse hits in the dataset.

Illumina paired-end sequencing and data analysis

Total hippocampal RNA was extracted with Trizol and purified using Qiagen RNeasy Mini Kit. Total RNA was quality-checked on the Bioanalyzer instrument using the RNA 6000 Nano Chip

and quantified by spectrophotometry. Library preparation was performed with 1µg total RNA using the TruSeq Stranded mRNA Library Prep Kit. Libraries were quality-checked on the Fragment Analyzer using the Standard Sensitivity NGS Fragment Analysis Kit revealing excellent quality of libraries (average concentration was 145±5 nmol/L and average library size was 361±13 base pairs). The eight samples were pooled to equal molarity. Each pool was run on a Fragment Analyzer for quality-check and quantification purposes in order to be adjusted to 11pM and used for clustering on the cBot2. Samples were sequenced Paired-end over 100 cycles on HiSeq2500. Primary data analysis was performed with the Illumina RTA version 1.18.64 and bcl2fastq-2.16.0.10.

RNA-Seq data analysis was performed by Dr. Frederic Lemoine and Dr. Pierre de la Grange (GenoSplice, France). Sequencing, data quality, reads repartition (e.g., for potential ribosomal contamination), and insert size estimation were performed using FastQC, Picard-Tools, Samtools and rseqc. Reads were mapped using STARv2.4.0 (Dobin et al., 2013). Gene expression was estimated as described (Noli et al., 2015) using Mouse FAST DB v2014_2 annotations. Only genes expressed in at least *Slm2*^{KO} or WT were further analyzed. Genes were considered as expressed if their rpkm value was greater than the background rpkm value based on intergenic regions. Analysis at the splicing level was first performed taking into account only exon reads and flanking exon-exon junction reads ("EXON" analysis) in order to potentially detect new alternative events that could be differentially regulated (i.e., without taking into account known alternative events). In particular, all microexons from FAST DB annotations are analyzed, even if they have not been already described as alternative exons. The Mouse FAST DB 2014_2 annotations contain 4,965 microexons (from 3 to 27bp), including 1,511 internal microexons (i.e., not first or terminal gene exons). None of the 4965 micro exons were significantly altered in the *Slm2*^{KO} datasets as compared to WT. Analysis at the splicing level was also performed by taking into account known patterns ("PATTERN" analysis) using the FAST DB splicing patterns annotation (i.e., for each gene, all possible splicing patterns were defined by comparing exon content of transcripts). All types of alternative events can be analyzed: Alternative first exons, alternative terminal exons, cassette exon, mutually exclusive exons, alternative 5' donor splice site, alternative 3' acceptor splice sites, intron retention, internal exon deletion and complex events corresponding to mix of several alternative event categories). "EXON" and "PATTERN" analyses were based on the splicing-index calculation as previously described (Gandoura et al., 2013; Wang et al., 2012a). Results were considered statistically significant for P-values ≤ 0.01 and fold-changes ≥ 1.3. Finally, significant results from "EXON" and "PATTERN" analyses were merged to obtain a single result list.

Raw sequencing data was deposited at GEO (accession number GSE79902).

Alternative splicing analysis

For experimential validation of analysed RNA-Seq data, DNA amounts and PCR cycle numbers were carefully titrated to ensure correct amplification range in RT-PCRs.

PCR primer sequences for analysis of *Nrxn1, Nrxn2, Nrxn3* AS4 were previously described (11). Sequences of PCR primers were:

Nrxn1 AS4: 5'-TGTTGGGACAGATGACATCGCC-3' and 5'-GAGAGCTGGCCCTGGAAGGG-3';
Nrxn2 AS4: 5'GTGCGCTTTACTCGAAGTGGTG-3' and 5'CCCATTGTAGTAGAGGCCGGAC-3';
Nrxn3 AS4: 5'TTGTGCGCTTCACCAGGAATG-3' and 5'AGAGCCCAGAGAGTTGACCTTG-3';
Gapdh: 5'GCTTGTCATCAACGGGAAG3' and 5'TTGTCATATTTCTCGTGGTTCA3';

Grin1 Ex5: 5'-GACAAGAGCATCCACCTGAGCTTCC-3' and 5'-AGCGTCGTCCTCGCTTGCAGAAAGG-3'
Grin1 Ex21: 5'-TGTGTCCCTGTCCATACTCAAG-3' and 5'-GTCGGGCTCTGCTCTACCACTC-3'
Grin1 Ex21,Ex22: 5'-ATGCCCCTGCCACCCTCACTTTTG-3' and 5'-GCAGCTGGCCCTCCTCCCTCTCA-3'

Stxbp5l Ex22 fwd: 5'-GCTGAATGATAGTCCAGTTCCC-3'
Stxbp5l Ex23 fwd: 5'-GAAATGCCCGCTGTGAAAC-3'
Stxbp5l Ex24 rev: 5'-CAGCTGACTGTGCCTTTCTA-3'
Stxbp5l Ex25 rev: 5'-TGAGTACTACCATTCCCAGACTA-3'
Camta1 Ex1 fwd: 5'-CGAGGAGGAGGAGGATGT-3'
Camta1 Ex3 rev: 5'-GGTGCCTCTCTTTGGGTAAA-3'
Smarca2 Ex33 fwd: 5'-GAAGAAATGGAAGAGGAGGTACG-3'
Smarca2 Ex34 fwd: 5'-GGAGAAGGTGCCCTGTAATTC-3'
Smarca2 Ex36 rev: 5'-GTTGAATGTCTGTGCGTTGTG-3'
Dlgap2 Ex14 fwd: 5'-CCATGAATTTGGCTCTGGA-3'
Dlgap2 Ex16 rev: 5'-TCTACTTGCACACCAACAGAG-3'

Immunohistochemistry

Animals (males and females, P25) were transcardially perfused with fixative (4% PFA in 100mM Phosphate Buffer, pH=7.2). Tissue was sectioned at 50µm in PBS on a vibratome.

Immunostaining for SLM2 was performed using a previously described polyclonal antibody (Iijima et al., 2014) following standard procedures. Images were acquired at room temperature on an inverted confocal microscope using 10X and 63X Apochromat objectives, which were controlled by Zen 2010 software. Images were assembled using Adobe Photoshop and Illustrator software. For quantitative assessment of spine densities, ImageJ was used. Statistical analysis was done with Prism software using unpaired t-test. Data presented are mean ± SEM.

Electrophysiology

Coronal hippocampal slices (300 µm) were prepared from one hemisphere of age-matched mice (P21-P28) anesthetized with intraperitoneal injection of ketamine/xylazine (100mg/kg and 10mg/kg, respectively). Slices were cut with a vibratome in ice-cold oxygenated (95% O_2/5% CO_2) dissection buffer (in mM): 75 sucrose, 87 NaCl, 2.5 KCl, 1.25 NaH_2PO_4, 0.5 $CaCl_2$, 7 $MgCl_2$, 25 $NaHCO_3$, 1.2 ascorbic acid, and 10 dextrose, pH 7.4. Slices were transferred to oxygenated dissection buffer at 32°C for approximately 30 min and then transferred to artificial cerebrospinal fluid (ACSF; in mM): 124 NaCl, 2.5 KCl, 1.25 NaH_2PO_4, 2.5 $CaCl_2$, 2 $MgSO_4$, 26 $NaHCO_3$, 10 dextrose. Slices incubated at room temperature at least 30 min to allow for recovery, then transferred to the recording chamber and perfused (1.5–2.0 ml/min) with oxygenated ACSF at room temperature. Somatic whole-cell recordings were made from CA1 pyramidal hippocampal neurons, which were voltage or current clamped with a Multiclamp 700B amplifier and imaged using infrared-differential interference contrast video microscopy, digitized by Digidata 1440a. Patch pipettes (4–8 MΩ) were filled with either voltage clamp (V_c) solution for paired-pulse facilitation, AMPAR/NMDAR ratio, mEPSC experiments, excitation response curves or current clamp (I_c) solution for LTP experiments (in mM): V_c = 125 Cs-gluconate, 2 CsCl, 5 TEA, 4 ATP, 0.3 GTP, 10 phosphocreatine, 10 HEPES, 0.5 EGTA, and 3.5 QX-314; and I_c = 135 K-gluconate, 5 NaCl, 5 Mg-ATP, 0.3 GTP, 10 Phophocreatine, and 10 HEPES. mEPSCs were recorded in the presence of 50µm picrotoxin (PTX) and 0.5µM tetrodotoxin (TTX). AMPAR/NMDAR ratios were recorded in the presence of 50µM PTX. Data were filtered at 2 kHz, digitized at 10 kHz, and analyzed with Clampfit 10. SC afferents were stimulated with a small glass unipolar electrode. Paired-pulse facilitation was induced with two stimuli of equal intensity presented at variable interstimulus intervals, ranging from 10 ms to 1 s, and quantified as the ratio of second to first EPSC. Five minutes of recorded CA1 neurons voltage-clamped at -70 mV were analyzed with Axograph X software (version 1.5.4) to determine amplitude, frequency, and kinetics of mEPSCs. The average of the maximal peak from ten evoked EPSCs voltage clamped at -70 mV and the average of the maximal peak of ten evoked EPSCs at voltage-clamped at +40 mV (50ms following the maximal peak recorded at -70 mV) were used to quantify AMPAR/NMDAR ratios. Once a baseline for synaptic

transmission was stable for 10 min, LTP was induced with theta burst stimulation (TBS). TBS consisted of four trains, separated by 10 s intervals. Each train was comprised of ten bursts at 5 Hz, and each burst included four stimuli at 100 Hz. LTP was quantified as the ratio of the EPSC amplitude at 50-55 min post-induction divided by the baseline EPSC amplitude before induction. Excitation response curves were quantified from the average of the maximal peak from three evoked EPSCs (0.1Hz) voltage-clamped at -70mV – near the reversal potential for inhibition. Significance was assessed by a two-way ANOVA for multiple comparisions.

Extracellular field excitatory postsynaptic potentials (fEPSPs) were recorded in the presence of 10μM AP5 (Tocris). Maximum fEPSP response was established from a 150 μA, 50 μs stimuli delivered to SCs. Five fEPSPs were averaged per stimulus intensity increment and fEPSP slope was calculated from the maximum rising slope. fEPSP slope was plotted against fiber volley values that were grouped in 0.05 mV bins. Significance was assessed by a two-way ANOVA for multiple comparisons.

Behavioral Analysis

Mice used for behavioral experiments were maintained in C57/Bl6 background, male, between 7-9 weeks of age and housed under standard laboratory conditions on a 12h light/dark cycle. All tests were carried out during the light cycle and in at least 4 independent trials. All statistical data are mean ± SEM.

Open Field: Mice were individually exposed to a square open field arena (50 x 50 x 30 cm) made of grey plastic for 10min. Velocity (cm/min) and time spent in the center were extracted from a video-based EthoVision10 system (Noldus).

Novel Object recognition task: Animals habituated to the arena on the day before the experiment, were exposed to two identical objects (culture dish flask filled with sand) for 5min in the first trial (acquisition). After 1hour, testing for Short-term memory by 5min exploration of one familiar (flask) and one novel object (lego block). The time spent investigating the objects, sniffing less than a centimeter from or touching the object, was scored manually. Only mice spending at least 2 seconds with the objects were used for analysis. Calculation of discrimination ratio: (time spent with novel object – time spent with familiar object) / total time investigating both objects.

Marble Burying: Animals were exposed to 20 identical black marbles distributed equally (4x5) in a standard TypeII long cage with 5 cm high bedding for 30 min.

Elevated Plus Maze: Animals were placed in the center of the maze (arms are 35cm x 6 cm and 74 cm above the ground). The percentage of time spent on the open arm was calculated by the time spent on the open arm divided by the total time (5 min). In addition, the number of entries on the open arm and the total entries (open arms and closed arms) were measured.

Materials and Methods – Furlanis*, Traunmüller* *et al.,* manuscript in revision

Mice. All procedures involving animals were approved by and performed in accordance with the guidelines of the Kantonales Veterinäramt Basel-Stadt.
Rpl22-HA (RiboTag) mice (Sanz et al., 2009), *Pvalb-cre* mice (Hippenmeyer et al., 2005), *SST-cre* mice (Taniguchi et al., 2011), *CamK2-cre* mice (Tsien et al., 1996), *Grik4-cre* mice (Nakazawa et al., 2003), *VIP-cre* mice (Taniguchi et al., 2011) and *Scnn1a-cre* mice (Madisen et al., 2010) were obtained from Jackson Laboratories (Jax stock no: 011029, 017320, 013044, 005359, 006474, 031628, 009613, respectively). All lines were maintained on a C57Bl6/J background. The specificity of cre-lines for recombination of the Rpl22-allele was confirmed by immunohistochemistry and matched previous reports in the literature.

Immunohistochemistry and imaging. Animals (males and females) from postnatal day 25 to 42 were transcardially perfused with fixative (4% paraformaldehyde in 100mM phosphate buffer, pH 7.4). The brains were post-fixed overnight in same fixative at 4°C. Coronal brain slices were cut between Bregma -1.43 and -2.15 (including somatosensory cortex and dorsal hippocampus) at 50 µm with a vibratome (Leica Microsystems VT1000). For immunohistochemistry, brain sections were kept in PBS before incubation for 1 hour with blocking solution containing 0.05% Triton X-100 and 10% normal donkey serum. Slices were incubated with primary antibodies in blocking solution at 4°C overnight and washed three times in PBS containing 0.05% Triton X-100, followed by incubation for 2 hours at room temperature with a secondary antibody. Sections were washed three times in PBS before mounting onto microscope slides with Fluoromount-G (SouthernBiotech, 0100-01). The following primary antibody was used in this study: rat anti-HA (Roche, 11867431001, 1:1000); Secondary antibody was: donkey anti-rat IgG-Cy3 (Jackson ImmunoResearch, 712-165-153, 1:1000). Hoechst dye was co-applied with primary antibody at a final concentration of 0.5 µg/ml. Images for assessing the Rpl22-HA expression were acquired at room temperature on a Slidescanner AxioScan.Z1 (Zeiss) using 10X objective. Stacks of 24 µm width (4 µm interval) were acquired and were then processed by doing maximum projection. Images were assembled using Fiji and Illustrator Software.

RNA isolation by RiboTRAP pulldowns. For Ribotag purifications, the procedure of Heiman and colleagues for affinity-purification of polysomes (Heiman et al., 2014) was modified as follows: Neoortices and hippocampi from mice between postnatal day 25 and 28 were dissected in ice-cold PBS. For *CamK2-cre* and *Grik4-cre* mice, given the later onset of cre-recombinase expression, hippocampi between postnatal day 39 and 42 were used. Moreover,

control samples from animals negative for either Rpl22 or cre-recombinase were used to ensure for specificity of the pulldown. For interneuron pulldowns, four hippocampi or cortical hemispheres (2 animals per condition) were lysed in respectively 1 mL or 14 mL (1:20 weight per volume) of homogenization buffer containing 100mM KCl, 50mM Tris-HCl pH 7.4, 12mM $MgCl_2$, 100µg/mL cycloheximide (Sigma-Aldrich), 1mg/mL heparin (Sigma-Aldrich), 1x complete mini, EDTA-*free* protease inhibitor cocktail (Roche), 200 units/mL RNasin© plus inhibitor (Promega) and 1mM DTT (Sigma-Aldrich). Excitatory neuron pulldowns were performed on single animals and hippocampi or neocortices were homogenized in 0.5mL or 7mL of homogenization buffer, respectively. The lysate was centrifuged at 2'000 x g for 10 minutes. Igepal-CA630 (Sigma-Aldrich) was then added to the supernatant to a final concentration of 1%. After 5 minutes incubation on ice, the lysate was centrifuged at 12'000 x g for 10 minutes. Before incubation with beads, 1% of the supernatant was taken (Input) and resuspended in 350 µL of RLT plus buffer from RNeasy Plus Micro Kit (Qiagen, 74034) supplemented with 2-Mercaptoethanol (Sigma-Aldrich) as suggested by manufacturer's instructions. Anti-HA coupled magnetic beads (Pierce, 88837) were added to the supernatant: 140 µL of beads for all neocortical samples, 20 µL for CamK2-cre and Grik4-cre hippocampal samples and 15 µL for SST-cre hippocampal samples. Incubation was performed under gentle rotation at 4°C for 3-4 hours. After incubation, beads were quickly washed 3-4 times in washing buffer containing 300mM KCl, 1% Igepal-CA630 (Sigma-Aldrich), 50mM Tris-HCl, pH7,4, 12mM $MgCl_2$, 100 µg/mL Cycloheximide (Sigma-Aldrich) and 1mM DTT (Sigma-Aldrich). Beads were than eluted in 350 µL of RLT plus buffer from RNeasy Plus Micro Kit (Qiagen) supplemented with 2-Mercaptoethanol (Sigma-Aldrich).

RNA purification, quantification, quality check and RT-qPCRs. RNA purification (for both input and immunoprecipitated RNA) was performed using RNeasy Plus Micro Kit (Qiagen), following the manufacturers' instructions. RNA was quality-checked on the Bioanalyzer instrument (Agilent Technologies) using the RNA 6000 Pico Chip (Agilent, 5067-1513). Only RNA samples with RNA integrity number (RIN) higher than 7.5 were used for the following steps. RNA concentration was quantified by Fluorometry using the QuantiFluor RNA System (Promega, E3310). 90 ng and 20 ng of RNA was reverse transcribed from neocortical and hippocampal samples, respectively, using random hexamers (Promega) and Superscript III Reverse Transcriptase (Invitrogen,18080093).

To determine the fold-enrichment of respective marker genes in immunoprecipitated RNA compared to input purifications, DNA oligonucleotides were used with FastStart Universal SYBR Green Master (Roche, 4913914001) and comparative C_T method. Samples were considered to be specific if immunoprecipitated RNA exhibited correct de- or enrichments of respective marker genes and if RNA of control samples did not show any selectivity for marker

genes. For each assay, two technical replicates were performed and the mean was calculated. The mRNA levels were normalized to *gapdh* mRNA. RT-qPCR assays were analyzed with the StepOne software.

DNA Oligonucleotides used with SYBR Green-based real-time PCR

Primer name	***Sequence 5'-3'***
CamK2-F	*AGAAGTTCAATGCCAGGAG*
CamK2-R	*CAGAAGATTCCTTCACACCA*
Gad67-F	*GTACTTCCCAGAAGTGAAGAC*
Gad67-R	*GAATAGTGACTGTGTTCTGAGG*
Gapdh-F	*GCTTGTCATCAACGGGAAG*
Gapdh-R	*TTGTCATATTTCTCGTGGTTCA*
Pvalb-F	*CATTGAGGAGGATGAGCTG*
Pvalb-R	*AGTGGAGAATTCTTCAACCC*
Pvrl3-F	*TGACTGTGTTAGTTGAACCCA*
Pvrl3-R	*CTGCTACTGTCTCATTCCCT*
Rgs14-F	*ATGGATTTGGAGAATCCAGTG*
Rgs14-R	*TTCACTCATCTTTGCATCCG*
Scnn1a-F	*AAAGAGAAGCGGGAGTCAGC*
Scnn1a-R	*CGGTGAGTTGGAGACGTCAA*
SST-F	*CGTCAGTTTCTGCAGAAGTC*
SST-R	*AGTACTTGGCCAGTTCCTG*
Tdo2-F	*ATGAGTGGGTGCCCGTTTG*
Tdo2-R	*GGCTCTGTTTACACCAGTTTGAG*
Vgat-F	*CGTGACAAATGCCATTCAG*
Vgat-R	*AAGATGATGAGGAACAACCC*
Vglut1-F	*ACCCTGTTACGAAGTTTAACAC*
Vglut1-R	*CAGGTAGAAGGTCCAGCTG*
Wsf1-F	*CATCATTCCCACCAACCTG*
Wsf1-R	*TACTTCACCACCTTCTGGC*

Library preparation and Illumina sequencing. For all five neocortical and three hippocampal neuronal populations, 4 biological replicates with RIN > 7.5 were analyzed, resulting in a total of 32 individual samples. Library preparation for all samples was performed with 50 ng of RNA using the TruSeq PolyA+ Stranded mRNA Library Prep Kit High Throughput (Illumina, RS-122-2103). Libraries were quality-checked on a Fragment Analyzer (Advanced Analytical) using the Standard Sensitivity NGS Fragment Analysis Kit (Advanced Analytica, DNF-473), revealing excellent quality of libraries (average concentration was 49±14 nmol/L and average library size was 329±8 base pairs). The 32 samples were pooled to equal molarity and the pool was quantified by PicoGreen Fluorometric measurement. The pool was adjusted to 10pM for clustering on C-Bot (Illumina) and then sequenced Paired-End 101 bases using the HiSeq SBS Kit v4 (Illumina, FC-401-4003) on a HiSeq 2500 system. Primary data analysis was performed with the Illumina RTA version 1.18.66.3 and bcl2fastq-v2.20.0.422.

QC and RNA-seq pre-processing. The splicing analysis of RNA-Seq data were performed by GenoSplice technology (www.genosplice.com). Data quality, reads repartition (e.g., for potential ribosomal contamination), and insert size estimation were performed using FastQC, Picard-Tools, Samtools and rseqc. Reads were mapped using STARv2.4.0 (Dobin et al., 2013) against the exons defined in the proprietary Mouse FAST DB v2016_1 database(de la Grange et al., 2007), using a mismatch cutoff of 2 and discarding reads with 10 or more alignments. The minimum chimeric segment length was 15. Read counts were summarized using featureCounts (Liao et al., 2014) in two stages. First, unique reads per exon were counted. In the second stage, multimapping reads were fractionally allocated to exons based on the distribution of unique counts of exons within a gene. Total counts were then calculated based on three constitutivity classes defined in FAST DB: class 2 includes exons present in more than 75% of annotated transcripts for a gene ("constitutive"), class 1 includes exons present in 50-75% of transcripts ("semi-constitutive"), and class 0 includes exons present in less than 50% of transcripts ("alternative"). Total counts per gene were summed from constitutivity class 2 exons if their FPKM values exceed 96% of the background FPKM based on intergenic regions. If counts from class 2 exons were insufficient to exceed the detection threshold, class 1 and eventually class 0 exon counts were included to reach the detection threshold.

Differential gene expression analysis. The analysis of differential expression was conducted using DESeq2 v1.22.2 (Love et al., 2014). The input read count matrix was the same as used for the splicing analysis. Neocortical samples were modeled as a group with a shared base mean, and each sample set was contrasted against all neocortical samples. The hippocampal samples were contrasted in all pairwise combinations. A series of additional pairwise contrasts were conducted for comparisons across anatomical brain regions. Results for these contrasts using the Wald test as implemented in DESeq2 are compiled in an Excel workbook (Supplementary Table1). For the principal component analysis, counts were normalized using the variance stabilizing transform (vst) as implemented in DESeq2. For heatmaps and the web app plots, the internal normalization factors of DESeq2 were used to normalize the counts.

Alternative splicing analysis. Analysis at the splicing level is first performed taking into account reads mapping to exonic regions and to exon-exon junctions (**EXON analysis**) in order to potentially detect new alternative events that could be differentially regulated (i.e., without taking into account known alternative events). When mapping to exon-exon junctions, reads were assigned to both exons, therefore counted twice (the minimum number of nucleotides for a read to be considered mapped to an exon is 7).
In order to consider an exon expressed, FPKM values for exons must be greater than 96% of the background FPKM value based on intergenic regions. Only exons expressed in at least 3

of the 4 biological replicates of each condition and in at least one of the compared experimental conditions were further analyzed.

For EXON analysis illustrative cartoon, refer to Supplementary Figure S4. Briefly, for every expressed exon from expressed genes, a Splicing Index [SI, defined as the ratio between read density on the exon of interest (= row number of reads on the exon/exon length in nucleotides) and read density on constitutive exons of the gene; "class 2"] are generated, as well as fold-change (log2(FC), calculated by comparing the SI value in one condition to the mean SI value in all conditions considered) and p-value (unpaired Student's t-test). Results are considered statistically significant for p-values ≤ 0.01 and log2(FC) ≥ 1 or ≤ -1.

Analysis at the splicing level is also performed by taking into account known splicing patterns (**PATTERN analysis**) annotated in the FAST DB database (de la Grange et al., 2007) (i.e., for each gene, all annotated splicing patterns are defined, and a Splicing Index (SI) is generated from the comparison of normalized read density on the alternative annotated patterns. For PATTERN analysis illustrative cartoon refer to Supplementary Figure S4). All types of alternative events can be analyzed: Alternative transcription start site, alternative last exons, cassette exon, mutually exclusive exons, alternative 5' donor splice site, alternative 3' acceptor splice site, intron retention, internal exon deletion and complex events (corresponding to mix of several alternative event categories). In Figure 2 and S8 we have merged intron retention and internal exon deletion events to one single category ("intron retention").

Pattern analysis is performed for every condition; log2(fold-change) of SI against all conditions considered and p-value (unpaired Student's t-test) are generated. Results are considered statistically significant for p-values ≤ 0.01 and log2(FC) ≥ 1.

FAST DB database includes annotations of 4965 microexons (defined as exons 3-27 nucleotides long), out of the 268827 total exons annotated (1.8%). In the neuronal populations analyzed, we identified 4140 (in the neocortex) and 3889 (in the hippocampus) microexons reaching the cutoff for detection (2.8% and 2.7% of the total exons detected in these forebrain regions, respectively). Specifically, amongst the total DR exons within a neuronal class we find 5.1% of microexons in Camk2, 3.8% in Scnn1a, 5.3% in SST, 4.7% in both PV and VIP.

Validation of regulated alternative splicing events. We used RT-PCR for experimental validation of differentially regulated splicing events detected by RNA-Seq. The cDNA amounts and PCR cycle numbers were carefully titrated to ensure linear amplification range and avoid signal saturation that would interfere with quantification. Standard PCR reactions were performed using 5X Firepol Master mix (Solis BioDyne, 04-11-00125) and designed exon-flanking DNA oligonucleotides. DNA Oligonucleotides used for RT-PCR are listed below:

Gene name - splicing event	***Primer name***	***Sequence 5'->3'***
	Anks1b-exon21-F	*GCGATGCAAGGAGGAGAAGA*

Anks1b - Exon cassette e22	*Anks1b-exon23-R*	*GAGGTCGCAAGGTGATGGAA*
Cadps - Exon cassette e19	*Cadps-exon18-F*	*CACGCCTATCTGAGTATGCCA*
	Cadps-exon21-R	*GTCTTCGAGCTTTTTGGCGG*
Ctnna2 - Exon cassette e18	*Ctnna2-exon17-F*	*CAAAGTGAAGGCCGAGGTTC*
	Ctnna2-exon19-R	*TTTTGGCTGCCTGGATGAGT*
Cacna1d - Mutually Exclusive exons e33/e34	*Cacna1d-exon32-F*	*GAACATGGTCTTCACAGGGGT*
	Cacna1d-exon33-R	*CTGCCGATTACGATGAGGGA*
	Cacna1d-exon32-F	*ACATGGTCTTCACAGGGGTC*
	Cacna1d-exon34-R	*CAACGACGCTACCAACAACA*
Nlgn1 - Exon cassette e5	*Nlgn1-exon4-F*	*ACCATGGCACTTCCCAGATG*
	Nlgn1-exon6-R	*ACCTTCCATGTAAGAGCCGC*
Stxbp1 - Exon cassette e20	*Stxbp1-exon19-F*	*AGATGCGCTGTGCTTACGAA*
	Stxbp1-exon21-R	*ACCCTAAGCCTCCCCCATAG*
Kcnq2 - Exon cassette e10	*Kcnq2-exon9-F*	*CTAACCTCTCACGCACCGAC*
	Kcnq2-exon11-R	*CTCCAGCTGGTTCAGAGGTG*
Cacna1d - Mutually Exclusive exons e9/e10	*Cacna1d-exon8-F*	*TGCGTTCTCAGGGAATGGAC*
	Cacna1d-exon9-R	*TGACAAAATACACCCAGGGCA*
	Cacna1d-exon8-F	*TGGCACGGAATGTAGGAGTG*
	Cacna1d-exon10-R	*ATACACCCATGGCCATTCCC*
Gria1 - Mutually Exclusive exons e16/e17	*Gria1-exon15-F*	*ACCGTCTGTGTTTGTTCGGA*
	Gria1-exon16-R	*TTTGTCCAAAAGCCCCTGCT*
	Gria1-exon15-F	*ACCGTCTGTGTTTGTTCGGA*
	Gria1-exon17-R	*TCCTTGCTTCCACATTCCCC*
Shisa9 - Exon cassette e6	*Shisa9-exon5-F*	*AGCTCAACAAGTACGCCTCC*
	Shisa9-exon7-R	*TTGGTGCGAGACTTCTGTCC*
Kcnq2 - Exon cassette e13	*Kcnq2-exon12-F*	*CAGCCAGAGCCATCACCAAG*
	Kcnq2-exon14-R	*TCGGGCTGTCATCAAGACTC*
Dlgap4 - Mutually Exclusive exons e11/e12	*Dlgap4-exon10-F*	*CCTCCACGAACCACATCGAA*
	Dlgap4-exon11-R	*TGGGAACCGCTCCTTCTAGT*
	Dlgap4-exon12-F	*CCAGTCCATCGGGATTCAGG*
	Dlgap4-exon13-R	*AGGAACCAGTAGCCATCCCT*

Fluorescent *in situ* hybridization. Fluorescent *in situ* hybridization was performed adapting the ViewRNA ISH Cell Assay kit (Invitrogen, QVC0001) for tissue sections. P25 wild-type mouse brains (C57BL/6j background) were snap frozen in liquid nitrogen and 18 µm coronal sections were cut between Bregma -1.43 and -2.15 (including somatosensory cortex and dorsal hippocampus) on a cryostat. Sections were fixed at 4°C overnight with 4% paraformaldehyde in 100mM phosphate buffered saline, pH 7.4. The procedure followed the

manufacturers' instructions, except for protease treatment, which was performed at a dilution of 1:100.

Transcripts for splicing factors and cell type-specific markers were detected with the following commercial probes (Invitrogen): Celf4 (VB1-3044679), Elavl2 (VB1-3030263), Ptpb3 (VB1-3047128), Rbfox3 (VB1-13443), Camk2a (VB4-3112005), Pvalb (VB4-19638), Rorb (VB4-3131885), Sst (VB4-3112424) and Vip (VB4-3112423).

Images were acquired at room temperature with an upright LSM700 confocal microscope (Zeiss) using 40X Apochromat objectives. Stacks of 10-13 µm width (0.6 µm interval between stacks) were acquired from layer 2-3 (L2-3) of primary somatosensory area (S1) for *CamK2-, SST-, PV-* and *VIP*-positive neocortical cells and from layer4 (L4) of S1 for *Rorb*-positive cells. For CA1- or CA3-specific pyramidal cells, images were acquired from CamK2-positive cells in *cornu ammonis* 1 and 3 regions of hippocampus, while for hippocampal SST-positive interneurons images were taken from cells residing in *stratum oriens*. Cell types were identified based on the presence of the corresponding marker transcript. A region of interest (ROI) was drawn to define the area of the cell and dots in the ROI were manually counted throughout the stacks. The number of dots in the ROI were then normalized to 100 μm^2 area. Images were assembled using Fiji and Illustrator Software.

Heatmaps and sashimi plots. For clustering analysis of gene expression, Normalized Feature Counts values were used and data were scaled by row. For clustering analysis of Splicing Index (SI) values obtained from EXON analysis, data were scaled by row and by column. Exons with NA values (not assigned, when no reads are mapping to constitutive parts of the gene) or Inf values (infinite, when no reads are mapping to the exon) were excluded, in order to not be biased by very lowly expressed genes or exons. In all cases, distance was calculated by Pearson correlation and the resulting distance matrix was clustered using Ward.D2. Heatmaps were generated in R using the heatmap.2 function of gplots package. Sashimi plots were generated using the MISO software package (Katz et al., 2010).

Plasmids. Splicing reporters for *Gabrg2*, *Grin1* and *Kcnq2* were assembled from synthetic DNA fragments ordered as gBlocks (Integrated DNA Technologies); for *Grin1*, an AT-rich intronic region that could not be synthesized was amplified from genomic mouse DNA using the following primers:

Primer name	***Sequence 5'->3'***
Grin1_i4_F	*GTATATATGCATGGACGTGCACGC*
Grin1_i4_R	*CTGTGGTATGAGCAGGAGCGTTAGC*

Reporters are composed of two flanking constitutive exons, the alternative exon (exon 9, 4 or 13 for *Gabrg2*, *Grin1* and *Kcnq2*, respectively) and the first and last 500 or 300 nucleotides of intronic regions (which contains regulatory elements for splicing reaction). A translational stop codon was included at the end of the last constitutive exons of *Grin1* and *Kcnq2* reporters. In the case of *Gabrg2*, exon 10 represents the last exon.

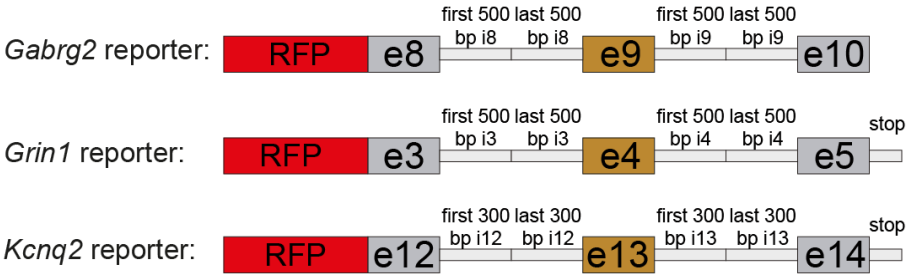

Chromosomal coordinates of splicing reporters are:

Splicing reporter	***Exon-intron region***	***Chromosomal coordinates***
Gabrg2	*e8 + first 500 bp i8*	*41915784 - 41916489*
	last 500 bp i8 + e9 + first 500 bp i9	*41913470 - 41914493*
	last 500 bp i9 + e10	*41912319 - 41913091*
Grin1	*e3 + first 500 bp i3*	*25312928 - 25313604*
	last 500 bp i3 + e4 + i4 + e5	*25310375 - 25311905*
Kcnq2	*e12 + first 300 bp i12*	*181096650 - 181096979*
	last 300 bp i12 + e13 + first 300 bp i13	*181091939 - 181092592*
	last 300 bp i13 + e14	*181088347 - 181088870*

Splicing reporters were then cloned into pmRFP-c1 vector cutting with SacI and SalI. All reporter plasmids are available on request.

The plasmids encoding splicing factors used are: pCMV-Ptbp1-His, pCMV-Ptbp2-His, pCMV-Ptbp3-His, pCMV-hnRNPA1-YFP, pCMV-hnRNPH1-YFP, pCS3-myc6-Rbfox1 (A016), pCS3-myc6-Rbfox2 (F011), pCS3-myc6-Rbfox3 (S).

Cell cultures and transfection. Cortical neuron cultures were prepared from E16.5 mouse embryos. Neocortices were dissociated by addition of papain (Worthington Biochemical, LK003176) for 30 min at 37 °C. 250,000 cells/wells were plated in 12-well plates and they were maintained in Neurobasal Medium (Gibco, 21103-049) containing 2% B27 supplement (Gibco, 17504-044), 1% GlutaMAX supplement (Gibco, 35050-038), and 1% penicillin/streptomycin (Sigma, P4333). At DIV7, cortical cultures were transfected with 400 ng/well of splicing reporters and Lipofectamine 3000 reagent (ThermoFisher Scientific, L3000008) diluted in opti-MEM medium (Gibco, 31985-062) using a 1:1.5 DNA-Lipofectamine ratio.

20,000 Neuroblastoma 2a (Neuro2a) or HEK293T cells (obtained from ATCC) were plated in 96 well plates and were kept in DMEM (Sigma, D5796) supplemented with 10% FBS (Gibco, 10270106) and 1% penicillin/streptomycin at 37°C. After 24h, cells were transfected using FuGENE HD Transfection reagent (Promega, E2691) with 50 ng of splicing reporter DNA alone or in combination with 50 ng of splicing factor DNA.

RNA isolation, Reverse transcription and RT-PCR. 24 h (for Neuro2a and HEK293T cells) or 48h (for cortical neurons) post-transfection, cells were lysed with 100 or 600 µl, respectively, of RLT buffer from RNeasy Plus Micro Kit (Qiagen, 74034) supplemented with 2-Mercaptoethanol (Sigma-Aldrich) and RNA was purified according to the manufacturer's instructions. 400 ng of RNA was reverse transcribed from all samples using random primers (Promega, C118A) and ImProm-II™ Reverse Transcriptase (Promega, A3802).
For evaluation of differential reporter processing in different cells and conditions, cDNA amounts and PCR cycle numbers were carefully titrated to ensure linear amplification range. Standard PCR reactions were performed using 5X Firepol Master mix (Solis BioDyne, 04-11-00125) and DNA oligonucleotides targeting the *RFP* sequence (to avoid detection of endogenous transcripts) and the last flanking exons.
DNA Oligonucleotides used for standard PCR:

Primer name	***Sequence 5'->3'***
RFP_F	*AAGCTGGACATCACCTCCCA*
Gabrg2_e10_R	*ATGGTTGCTGATCTGGGACG*
Grin1_e5_R	*ATCAGCAGAGCCGTCACATT*
Kcnq2_e14_R	*TCGGGCTGTCATCAAGACTC*

Gene ontology. Analysis of GO terms both for neocortical and hippocampal samples was performed using the statistical overrepresentation test (Mi et al., 2013) of the PANTHER classification system (PANTHER14.1, released 2019-03-08 and 2019-04-17), available on http://pantherdb.org. Genes showing significant differential expression (log2(FC) ≥ 0.6 and ≤ -0.6, p-value ≤ 0.05; base mean for neocortex: all neocortical samples) and genes with significant alternative splicing events (log2(FC) ≥ 1 & ≤ -1; p-value ≤ 0.01 from either EXON or PATTERN analysis) were analyzed using the GO cellular component annotation data set and Fisher's Exact test with false discovery rate correction for multiple testing. Alternative first exon events were excluded to analyze the functional role of alternative splicing programs only. In order to be considered significant, GO terms must have a minimum number of 10 genes, fold-enrichment ≥ 2 and False Discovery Rate (FDR) ≤ 0.05. As background reference list, all genes expressed (see methods for details of gene expression) in the neocortex for neocortical

comparisons, or in either cell class of the pairwise comparisons were used. Panther output list GO terms in a hierarchical organization, enabling identification of super-categories which were further analyzed. Moreover, only terms significant in at least one neocortical population, hippocampal comparison or across anatomical region were used for heatmap visualization. In Fig. 5a, corresponding fold changes of the gene expression analysis were incorporated. Redundant term categories were excluded.

General statistical methods. Sample sizes were chosen based on previous experiments and literature surveys. No statistical methods were used to pre-determine sample sizes. Exclusion criteria used throughout this manuscript were pre-defined. There are detailed descriptions in the respective sections of the methods. Group assignment was defined by genotype, thus, no randomization was necessary. Knowledge of experimental conditions was needed for proper execution of experiments, therefore, investigators were not blinded during data collection and/or analysis. Appropriate statistical tests were chosen based on sample size. Sequencing analysis was performed on four animals per genotype exhibiting similar variances. N-numbers for *in situ* hybridizations and RT-PCRs are indicated in the figures. P-value calculations have been performed using the student t-test or ANOVA with Tukey's multiple comparison test. FDR calculations were performed with the Benjamini Hochberg correction.

Data availability. Detailed analyzed data is included as supplementary material. Raw sequencing data will be deposited at GEO and made available upon acceptance of the manuscript. Differential gene expression and splicing data for individual genes is provided on the freely available SpliceCode web-site (https://scheiffele-splice.scicore.unibas.ch). All renewable reagents and detailed protocols will be made available on request.

Materials and Methods – Cell class-specific actions of SLM2 in specifying synaptic properties

Mice

All procedures involving animals were approved by and performed in accordance with the guidelines of the Kantonales Veterinäramt Basel-Stadt.
Slm2 floxed mice have been generated in the Scheiffele laboratory and were previously described (Traunmüller et al., 2014). *Rpl22-HA* (RiboTag) mice (Sanz et al., 2009), *SST-cre* mice (Taniguchi et al., 2011), *CamK2-cre* mice (Tsien et al., 1996), *Grik4-cre* mice (Nakazawa et al., 2003), ChR2-flox mice (Madisen et al., 2012) were obtained from Jackson Laboratories (Jax stock no: 011029, 013044, 005359, 006474, 012569 respectively). All lines were maintained on a C57Bl6/J background. The specificity of cre-lines for recombination of the Rpl22-allele was confirmed by immunohistochemistry and matched previous reports in the literature.

Antibodies

Polyclonal antibodies for SLM2 were previously described (Iijima et al., 2014), rat anti-HA (Roche, 11867431001, 1:1000); Secondary antibody was: donkey anti-rat IgG-Cy3 and Cy5 (Jackson ImmunoResearch, 712-165-153, 706-175-148 1:500). Hoechst dye was co-applied with secondary antibody at a final concentration of 0.5 µg/ml.

Immunohistochemistry, image acquisition and statistical analysis:

Animals (male and female) were transcardially perfused with fixative (4% paraformaldehyde in 100mM phosphate buffer, pH 7.2). Tissue was sectioned at 50µm in PBS on a vibratome (VT1000S, Leica). Floating sections were immunostained over night at 4°C with primary antibody incubation and 2h RT secondary antibody incubation for HA and SLM2 detection. All antibodies were diluted in 10% donkey-serum. Images were acquired at room temperature on an upright LSM700 confocal microscope (Zeiss) using 10x, 40x and 63x Apochromat objectives controlled by Zen 2010 software. Images were analyzed and assembled using ImageJ and Adobe Illustrator software. For quantification of SLM2 in SST inhibitory neurons see (Nguyen et al., 2016).

RNA purification and validation of Ribotag purified material was performed as described in the Materials and methods section “Landscape of ribosome-engaged alternative transcript isoforms across neuronal cell classes”.

QC analysis was performed as described in the Materials and methods section “Landscape of ribosome-engaged alternative transcript isoforms across neuronal cell classes”.

Deep sequencing parameters and subsequent alternative splicing analysis was performed as described in the Materials and methods section “Landscape of ribosome-engaged alternative transcript isoforms across neuronal cell classes”. However, pairwise WT vs. conditional mutants were performed.

Gene expression analysis was performed as follows:

For all expressed genes, DESeq2 values are generated (values are normalized by the total number of mapped reads of all conditions considered), as well as fold-change (FC, calculated by pairwise comparisons of the normalized expression value, p-value (unpaired Student’s t-test) and adjusted p-value (Benjamini and Hochberg). Results are considered statistically significant for p-values ≤ 0.05 and fold-changes ≥ 1.5 and ≤ 0.5.

4 replicates were used per condition, except for CamK2 $Slm2^{KO}$ pull-downs where only 3 replicates passed the quality control.

Validation of regulated alternative splicing events by standard PCR

For experimental validation of differentially regulated splicing events, cDNA amounts and PCR cycle numbers were carefully titrated to ensure correct amplification range and avoid signal saturation that would infer with quantification. Standard PCR reactions were performed using 5X Firepol Master mix (Solis BioDyne, 04-11-00125) and designed exon-flanking DNA oligonucleotides.

DNA Oligonucleotides used for standard PCR

Gene name - splicing event	***Primer name***	***Sequence 5’->3’***
Nrxn1 AS4 e19	*Nrxn1 AS4 fwd*	TGTTGGGACAGATGACATCGCC
	Nrxn1 AS4 rev	GAGAGCTGGCCCTGGAAGGG
Nrxn2 AS4 e22	*Nrxn2 AS4 fwd*	GTGCGCTTTACTCGAAGTGGTG
	Nrxn2 AS4 rev	CCCATTGTAGTAGAGGCCGGAC3
Nrxn3 AS4 ex22	*Nrxn3 AS4 fwd*	TTGTGCGCTTCACCAGGAATG
	Nrxn3 AS4 rev	AGAGCCCAGAGAGTTGACCTTG
Gapdh	*Gapdh fwd*	GCTTGTCATCAACGGGAAG
	Gapdh rev	TTGTCATATTTCTCGTGGTTCA

qPCR analysis for alternative exon usage of *Nrxns* at AS4

Ribotag purified material was reverse transcribed and quantitative PCR was performed. qPCRs were performed on a StepOnePlus qPCR system (Applied Biosystems). Assays were

used with a TagMan Master Mix (Applied Biosystems) and comparative C_T method. mRNA levels were normalized to the amount of Gapdh cDNA present in the same sample.
Custom gene expression assays were from Applied Biosystems and are described in (Iijima et al., 2014)

Electrophysiology

Whole cell recordings of SST interneurons were performed as follows:
Coronal hippocampal slices (300µm) were cut in ice cold cutting solution (87mM NaCl, 25mM $NaHCO_3$, 5mM Glucose, 65mM Sucrose, 2.5mM KCl, 1.25mM NaH_2PO_4, 0.5mM $CaCl_2$, 7mM $MgCl_2$, 5mM ascorbic acid, 3.1mM Piruvic acid) and immediately transferred to standard artificial spinal fluid (ACSF, 125mM NaCl, 26mM $NaHCO_3$, 10mM Glucose, 2.5 KCl, 1.25 NaH_2PO_4, 1.3 $MgCl_2$, 2.3 $CaCl_2$) and kept in this solution at RT. Before performing recordings, slices were recovered at RT in standard ACSF for at least 1h. Solutions were constantly bubbled with 95% O_2/ 5% CO_2.
Somatic whole-cell recordings from s.o SST interneurons close to the alveus were clamped with a Multiclamp 700B amplifier (Molecular Devices, Sunnyvale, CA) and identified using epifluorescence microscopy. Signals were low-pass filtered at 2kHz, digitized at 10kHz. Patch pipettes between 2-6 MΩ were used.
Measurements of intrinsic properties were performed in current clamp I_c with the following internal solution: 135mM K-gluconate, 5mM NaCl, 5mM MgATP, 0.3mM NaGTP, 10mM Phosphocreatine, 10mM Hepes
Spontaneous and miniature excitatory postsynaptic currents; and facilitation ratios were obtained by clamping the cells at -70mV (near the reversal potential of chloride without addition of blockers) with the following internal solution: 135mM $CsMeSO_3$, 10mM Hepes, 9mM NaCl, 0.3mM EGTA, 4mM Mg-ATP, 0.3 Na-GTP, 5mM QX-314, 0.1mM Spermine, 303mOsm. mEPSCs were isolated by addition of 500nM TTX. STF responses were electrically evoked 12 times every 10s with a small glass unipolar electrode placed in the alveus, with minimal first response amplitudes between 10-70pA. Averaged traces were analyzed. Data was analyzed using pClamp10 (Molecular Devices).

Optogenetic stimulation of SST synapses onto post-synaptic CA1 pyramidal neurons were performed by Jan Michael Schulz. The internal solution contained 135mM CsGluconate, 2mM CsCl, 10mM EGTA, 10mM Hepes, 2mM $MgCl_2$, 2mM Na-ATP, 2mM TEA-Cl and 5mM QX314. Essentially, these experiments were carried out as described in (Schulz et al., 2018). In addition, for conductance calculation, IPSC reversal potential was estimated from voltage step data, conductances were normalized to conductance at -70mV command voltage; in post-hoc analyses, voltages were corrected by the estimated liquid junction potential of -15.7mV.

Behavioral Analysis

Mice used for behavioral experiments were maintained in C57/Bl6 background, male, between 7-9 weeks of age and housed under standard laboratory conditions on a 12h light/dark cycle. All tests were carried out during the light cycle, with standard ceiling light and in at least 3 independent trials. All statistical data are mean ± SEM. Every animal was tested in all behavioral assays (battery testing).

Open Field: Mice were individually exposed to a square open field arena (50 x 50 x 30 cm) made of grey plastic for 10min. Velocity (cm/min) and time spent in the center were extracted from a video-based EthoVision10 system (Noldus).

Novel Object recognition task: Animals tested in the Open Field arena on the day before the experiment, were exposed to two identical objects (culture dish flask filled with sand) for 5min in the first trial (acquisition). After 1hour, we tested for Short-term memory by 5min exploration of one familiar (flask) and one novel object (lego block). The time spent investigating the objects, sniffing less than a centimeter from or touching the object, was scored manually. Only mice spending at least 2 seconds with the objects in total were used for analysis. Calculation of discrimination ratio: (time spent with novel object – time spent with familiar object) / total time investigating both objects.

Elevated Plus Maze: Animals were placed in the center of the maze (arms are 35cm x 6 cm and 74 cm above the ground) facing the closed arms. The time spent on the open arm was measured during the 5 min test. In addition, the number of total entries (open arms and closed arms) were counted.

Marble Burying: Animals were exposed to 20 identical black marbles distributed equally (4x5) in a standard TypeII long cage with 5 cm high bedding for 30 min.

5. Appendix

5.1 Index of figures covered in the introduction

Figure 1: Drawing neuronal cell types and information flow in the rat hippocampus by Ramón y Cajal 11

Figure 2: Parameters for classification of neuronal cell types 13

Figure 3: Structural and functional characteristics of PV and SST neurons 15

Figure 4: Schematic for diversification by alternative splicing or alternative promoter usage 25

Figure 5: Genomic organization of Dscam1 and protocadherins (pcdhs)..... 27

Figure 6: Neurexin diversification by alternative splicing 31

5.2 Index of abbreviations

AAV	Adeno-associated virus
AMPAR	α-amino-3-hydroxy-5-methyl-4-isoxazolepropionic acid receptor
AP	Action Potential
AS	Alternative splicing
AS4	Alternatively spliced segment 4
CA	Cornu Ammonis
CamK2	Ca^{2+}/ Calmodulin-dependent kinase 2
CCK	cholecystokin
CGE	Caudal ganglionic eminence
Chrna2	neuronal nicotinic cholinergic receptor
CNS	Central nervous system
DE	Differentially expressed
DG	Dentate gyrus
DR	Differentially regulated
DSCAM	Down Syndrom cell adhesion molecule
E18.5	Embryonic stage 18.5
EPSC	Excitatory postsynaptic current
Eif4enif1	eukaryotic translation initiation factor 4E nuclear import factor 1
Elfn1	Extracellular leucine-rich fibronectin containing 1 protein
fl	floxed
GABA	gamma-aminobutyric acid
GFP	Green-fluorescent protein
Grik4	glutamate receptor, inonotropic, kainate 4
Grm7	Glutamate metabotrobic receptor 7 (RNA)
hitsCLIP	High-throughput sequencing of RNA isplated by crosslinking immunoprecipitation
Hz	Hertz
IP	Immunoprecipication
IPSC	Inhibitory postsynaptic current
ISH	In-Situ Hybridization
kDA	kilo-dalton
KO	Knock-out
LTP	Long-term potentiation
Mag	Myelin associated protein (gene)
mEPSC	Miniature excitatory postsynaptic current

Mfge8	Milk fat globule-EGF factor 8 (gene)
MGE	Medial ganglionic eminence
mGluR7	metaobotropic glutamate receptor 7 (protein)
NL	Neuroligin (protein)
Nlgn	Neuroligin (RNA)
NMD	Nonsense-mediated mRNA decay
NMDAR	N-methyl-D-aspartate receptor
Nova	Neuro-oncological ventral antigen
NRXN	Neurexin (protein)
Nrxn	Neurexin (RNA)
ms	milli-second
mV	milli-volt
OLM	Oriens lacunosum moleculare
P14	Postnatal day 14
pA	pico-amp
Pcdh	Protocadherin
PCA	Principle component analysis
PCR	Polymerase chain reaction
PV	Parvalbumin
PTBP	Polypyrimidine tract binding protein
QK	Quaking
qPCR	quantitative Polymerase chain reaction
RBP	RNA binding protein
RNA	ribonucleic acid
Rbfox	RNA-binding-fox
sEPSC	Spontaneous excitatory postsynaptic current
Sam68	Src-associated substrate in mitosis of 68kDA
SC	Schaffer collaterals
SF	Splicing Factor
SLM	Sam68-like mammalian protein
s.o	stratum oriens
s.l.m	stratum lacunosum moleculare
s.p	stratum pyramidale
SST	Somatostatin
STF	Short-term facilitation
STAR	Signal Transduction Activator of RNA metabolism
TA	Temporoammonic pathway

TSS	Transcription Start Site
UTR	Untranslated region
VIP	Vasoactive Intestinal Peptide
WT	Wild-type

6. References

Abbas, A.I., Sundiang, M.J.M., Henoch, B., Morton, M.P., Bolkan, S.S., Park, A.J., Harris, A.Z., Kellendonk, C., and Gordon, J.A. (2018). Somatostatin Interneurons Facilitate Hippocampal-Prefrontal Synchrony and Prefrontal Spatial Encoding. Neuron *100*, 926-939 e923.

Abraham, W.C. (2003). How long will long-term potentiation last? Philos Trans R Soc Lond B Biol Sci *358*, 735-744.

Ali, A.B., and Thomson, A.M. (1998). Facilitating pyramid to horizontal oriens-alveus interneurone inputs: dual intracellular recordings in slices of rat hippocampus. J Physiol *507 (Pt 1)*, 185-199.

Anderson, S.A., Eisenstat, D.D., Shi, L., and Rubenstein, J.L. (1997). Interneuron migration from basal forebrain to neocortex: dependence on Dlx genes. Science *278*, 474-476.

Aoto, J., Foldy, C., Ilcus, S.M., Tabuchi, K., and Sudhof, T.C. (2015). Distinct circuit-dependent functions of presynaptic neurexin-3 at GABAergic and glutamatergic synapses. Nat Neurosci *18*, 997-1007.

Aoto, J., Martinelli, D.C., Malenka, R.C., Tabuchi, K., and Sudhof, T.C. (2013). Presynaptic neurexin-3 alternative splicing trans-synaptically controls postsynaptic AMPA receptor trafficking. Cell *154*, 75-88.

Aronoff, R., Matyas, F., Mateo, C., Ciron, C., Schneider, B., and Petersen, C.C. (2010). Long-range connectivity of mouse primary somatosensory barrel cortex. Eur J Neurosci *31*, 2221-2233.

Autism Genome Project, C., Szatmari, P., Paterson, A.D., Zwaigenbaum, L., Roberts, W., Brian, J., Liu, X.Q., Vincent, J.B., Skaug, J.L., Thompson, A.P.*, et al.* (2007). Mapping autism risk loci using genetic linkage and chromosomal rearrangements. Nat Genet *39*, 319-328.

Balwierz, P.J., Pachkov, M., Arnold, P., Gruber, A.J., Zavolan, M., and van Nimwegen, E. (2014). ISMARA: automated modeling of genomic signals as a democracy of regulatory motifs. Genome Res *24*, 869-884.

Barbosa-Morais, N.L., Irimia, M., Pan, Q., ..., and Blencowe, B.J. (2012). The evolutionary landscape of alternative splicing in vertebrate species. Science (New York, NY *338*, 1587-1594.

Barde, Y.A., Edgar, D., and Thoenen, H. (1982). Purification of a new neurotrophic factor from mammalian brain. EMBO J *1*, 549-553.

Beffert, U., Weeber, E.J., Durudas, A., Qiu, S., Masiulis, I., Sweatt, J.D., Li, W.P., Adelmann, G., Frotscher, M., Hammer, R.E.*, et al.* (2005). Modulation of synaptic plasticity and memory by Reelin involves differential splicing of the lipoprotein receptor Apoer2. Neuron *47*, 567-579.

Bezaire, M.J., and Soltesz, I. (2013). Quantitative assessment of CA1 local circuits: knowledge base for interneuron-pyramidal cell connectivity. Hippocampus *23*, 751-785.

Black, D.L. (2003). Mechanisms of alternative pre-messenger RNA splicing. Annu Rev Biochem *72*, 291-336.

Bliss, T.V., and Lomo, T. (1973). Long-lasting potentiation of synaptic transmission in the dentate area of the anaesthetized rabbit following stimulation of the perforant path. J Physiol *232*, 331-356.

Boucard, A.A., Chubykin, A.A., Comoletti, D., Taylor, P., and Sudhof, T.C. (2005). A splice code for trans-synaptic cell adhesion mediated by binding of neuroligin 1 to alpha- and beta-neurexins. Neuron *48*, 229-236.

Boutz, P.L., Stoilov, P., Li, Q., Lin, C.H., Chawla, G., Ostrow, K., Shiue, L., Ares, M., Jr., and Black, D.L. (2007). A post-transcriptional regulatory switch in polypyrimidine tract-binding proteins reprograms alternative splicing in developing neurons. Genes Dev *21*, 1636-1652.

Brakebusch, C., Seidenbecher, C.I., Asztely, F., Rauch, U., Matthies, H., Meyer, H., Krug, M., Bockers, T.M., Zhou, X., Kreutz, M.R.*, et al.* (2002). Brevican-deficient mice display impaired hippocampal CA1 long-term potentiation but show no obvious deficits in learning and memory. Mol Cell Biol *22*, 7417-7427.

Brauch, K.M., Karst, M.L., Herron, K.J., de Andrade, M., Pellikka, P.A., Rodeheffer, R.J., Michels, V.V., and Olson, T.M. (2009). Mutations in ribonucleic acid binding protein gene cause familial dilated cardiomyopathy. J Am Coll Cardiol *54*, 930-941.

Breitbart, R.E., Andreadis, A., and Nadal-Ginard, B. (1987). Alternative splicing: a ubiquitous mechanism for the generation of multiple protein isoforms from single genes. Annu Rev Biochem *56*, 467-495.

Budreck, E.C., Kwon, O.B., Jung, J.H., Baudouin, S., Thommen, A., Kim, H.S., Fukazawa, Y., Harada, H., Tabuchi, K., Shigemoto, R.*, et al.* (2013). Neuroligin-1 controls synaptic abundance of NMDA-type glutamate receptors through extracellular coupling. Proc Natl Acad Sci U S A *110*, 725-730.

Budreck, E.C., and Scheiffele, P. (2007). Neuroligin-3 is a neuronal adhesion protein at GABAergic and glutamatergic synapses. Eur J Neurosci *26*, 1738-1748.

Calarco, J.A., Superina, S., O'Hanlon, D., Gabut, M., Raj, B., Pan, Q., Skalska, U., Clarke, L., Gelinas, D., van der Kooy, D.*, et al.* (2009). Regulation of vertebrate nervous system alternative splicing and development by an SR-related protein. Cell *138*, 898-910.

Cao, Y., Sarria, I., Fehlhaber, K.E., Kamasawa, N., Orlandi, C., James, K.N., Hazen, J.L., Gardner, M.R., Farzan, M., Lee, A.*, et al.* (2015). Mechanism for Selective Synaptic Wiring of Rod Photoreceptors into the Retinal Circuitry and Its Role in Vision. Neuron *87*, 1248-1260.

Carninci, P., Sandelin, A., Lenhard, B., Katayama, S., Shimokawa, K., Ponjavic, J., Semple, C.A., Taylor, M.S., Engstrom, P.G., Frith, M.C.*, et al.* (2006). Genome-wide analysis of mammalian promoter architecture and evolution. Nat Genet *38*, 626-635.

Celio, M.R. (1986). Parvalbumin in most gamma-aminobutyric acid-containing neurons of the rat cerebral cortex. Science *231*, 995-997.

Cembrowski, M.S., Bachman, J.L., Wang, L., Sugino, K., Shields, B.C., and Spruston, N. (2016). Spatial Gene-Expression Gradients Underlie Prominent Heterogeneity of CA1 Pyramidal Neurons. Neuron *89*, 351-368.

Cembrowski, M.S., and Spruston, N. (2019). Heterogeneity within classical cell types is the rule: lessons from hippocampal pyramidal neurons. Nat Rev Neurosci *20*, 193-204.

Cereda, M., Pozzoli, U., Rot, G., Juvan, P., Schweitzer, A., Clark, T., and Ule, J. (2014). RNAmotifs: prediction of multivalent RNA motifs that control alternative splicing. Genome Biol *15*, R20.

Chen, M., and Manley, J.L. (2009). Mechanisms of alternative splicing regulation: insights from molecular and genomics approaches. Nat Rev Mol Cell Biol *10*, 741-754.

Chen, W.V., and Maniatis, T. (2013). Clustered protocadherins. Development *140*, 3297-3302.

Chih, B., Engelman, H., and Scheiffele, P. (2005). Control of excitatory and inhibitory synapse formation by neuroligins. Science *307*, 1324-1328.

Chih, B., Gollan, L., and Scheiffele, P. (2006). Alternative splicing controls selective trans-synaptic interactions of the neuroligin-neurexin complex. Neuron *51*, 171-178.

Coetzee, W.A., Amarillo, Y., Chiu, J., Chow, A., Lau, D., McCormack, T., Moreno, H., Nadal, M.S., Ozaita, A., Pountney, D.*, et al.* (1999). Molecular diversity of K+ channels. Ann N Y Acad Sci *868*, 233-285.

Cohen, S.J., and Stackman, R.W., Jr. (2015). Assessing rodent hippocampal involvement in the novel object recognition task. A review. Behav Brain Res *285*, 105-117.

Cutsuridis, V., Cobb, S., and Graham, B.P. (2010). Encoding and retrieval in a model of the hippocampal CA1 microcircuit. Hippocampus *20*, 423-446.

Dai, J., Aoto, J., and Sudhof, T.C. (2019). Alternative Splicing of Presynaptic Neurexins Differentially Controls Postsynaptic NMDA and AMPA Receptor Responses. Neuron.

Danilenko, M., Dalgliesh, C., Pagliarini, V., Naro, C., Ehrmann, I., Feracci, M., Kheirollahi-Chadegani, M., Tyson-Capper, A., Clowry, G.J., Fort, P.*, et al.* (2017). Binding site density enables paralog-specific activity of SLM2 and Sam68 proteins in Neurexin2 AS4 splicing control. Nucleic Acids Res *45*, 4120-4130.

Darnell, R.B. (2013). RNA protein interaction in neurons. Annu Rev Neurosci *36*, 243-270.

de la Grange, P., Dutertre, M., Correa, M., and Auboeuf, D. (2007). A new advance in alternative splicing databases: from catalogue to detailed analysis of regulation of expression and function of human alternative splicing variants. BMC bioinformatics *8*, 180.

De Marco Garcia, N.V., Karayannis, T., and Fishell, G. (2011). Neuronal activity is required for the development of specific cortical interneuron subtypes. Nature *472*, 351-355.

de Wit, J., and Ghosh, A. (2016). Specification of synaptic connectivity by cell surface interactions. Nat Rev Neurosci *17*, 22-35.

de Wit, J., Sylwestrak, E., O'Sullivan, M.L., Otto, S., Tiglio, K., Savas, J.N., Yates, J.R., 3rd, Comoletti, D., Taylor, P., and Ghosh, A. (2009). LRRTM2 interacts with Neurexin1 and regulates excitatory synapse formation. Neuron *64*, 799-806.

Dean, C., Scholl, F.G., Choih, J., DeMaria, S., Berger, J., Isacoff, E., and Scheiffele, P. (2003). Neurexin mediates the assembly of presynaptic terminals. Nat Neurosci *6*, 708-716.

Dehorter, N., Ciceri, G., Bartolini, G., Lim, L., del Pino, I., and Marin, O. (2015). Tuning of fast-spiking interneuron properties by an activity-dependent transcriptional switch. Science *349*, 1216-1220.

Deng, P.Y., and Klyachko, V.A. (2011). The diverse functions of short-term plasticity components in synaptic computations. Commun Integr Biol *4*, 543-548.

Di Fruscio, M., Chen, T., and Richard, S. (1999). Characterization of Sam68-like mammalian proteins SLM-1 and SLM-2: SLM-1 is a Src substrate during mitosis. Proc Natl Acad Sci U S A *96*, 2710-2715.

Dobin, A., Davis, C.A., Schlesinger, F., Drenkow, J., Zaleski, C., Jha, S., Batut, P., Chaisson, M., and Gingeras, T.R. (2013). STAR: ultrafast universal RNA-seq aligner. Bioinformatics *29*, 15-21.

Donadon, I., Bussani, E., Riccardi, F., Licastro, D., Romano, G., Pianigiani, G., Pinotti, M., Kostantinova, P., Evers, M., Lin, S.*, et al.* (2019). Rescue of spinal muscular atrophy mouse models with AAV9-Exon-specific U1 snRNA. Nucleic Acids Res.

Dougherty, K.A., Islam, T., and Johnston, D. (2012). Intrinsic excitability of CA1 pyramidal neurones from the rat dorsal and ventral hippocampus. J Physiol *590*, 5707-5722.

Dunn, H.A., Patil, D.N., Cao, Y., Orlandi, C., and Martemyanov, K.A. (2018). Synaptic adhesion protein ELFN1 is a selective allosteric modulator of group III metabotropic glutamate receptors in trans. Proc Natl Acad Sci U S A *115*, 5022-5027.

Ehrmann, I., Dalgliesh, C., Liu, Y., Danilenko, M., Crosier, M., Overman, L., Arthur, H.M., Lindsay, S., Clowry, G.J., Venables, J.P.*, et al.* (2013). The tissue-specific RNA binding protein T-STAR controls regional splicing patterns of neurexin pre-mRNAs in the brain. PLoS Genet *9*, e1003474.

Ehrmann, I., Gazzara, M.R., Pagliarini, V., Dalgliesh, C., Kheirollahi-Chadegani, M., Xu, Y., Cesari, E., Danilenko, M., Maclennan, M., Lowdon, K.*, et al.* (2016). A SLM2 Feedback Pathway Controls Cortical Network Activity and Mouse Behavior. Cell Rep *17*, 3269-3280.

Eom, T., Zhang, C., Wang, H., Lay, K., Fak, J., Noebels, J.L., and Darnell, R.B. (2013). NOVA-dependent regulation of cryptic NMD exons controls synaptic protein levels after seizure. Elife *2*, e00178.

Esumi, S., Kakazu, N., Taguchi, Y., Hirayama, T., Sasaki, A., Hirabayashi, T., Koide, T., Kitsukawa, T., Hamada, S., and Yagi, T. (2005). Monoallelic yet combinatorial expression of variable exons of the protocadherin-alpha gene cluster in single neurons. Nat Genet *37*, 171-176.

Etchberger, J.F., Lorch, A., Sleumer, M.C., Zapf, R., Jones, S.J., Marra, M.A., Holt, R.A., Moerman, D.G., and Hobert, O. (2007). The molecular signature and cis-regulatory architecture of a C. elegans gustatory neuron. Genes Dev *21*, 1653-1674.

Falkner, S., Grade, S., Dimou, L., Conzelmann, K.K., Bonhoeffer, T., Gotz, M., and Hubener, M. (2016). Transplanted embryonic neurons integrate into adult neocortical circuits. Nature *539*, 248-253.

Favuzzi, E., Deogracias, R., Marques-Smith, A., Maeso, P., Jezequel, J., Exposito-Alonso, D., Balia, M., Kroon, T., Hinojosa, A.J., E, F.M.*, et al.* (2019). Distinct molecular programs regulate synapse specificity in cortical inhibitory circuits. Science *363*, 413-417.

Feng, G., Mellor, R.H., Bernstein, M., Keller-Peck, C., Nguyen, Q.T., Wallace, M., Nerbonne, J.M., Lichtman, J.W., and Sanes, J.R. (2000). Imaging neuronal subsets in transgenic mice expressing multiple spectral variants of GFP. Neuron *28*, 41-51.

Feracci, M., Foot, J.N., Grellscheid, S.N., Danilenko, M., Stehle, R., Gonchar, O., Kang, H.S., Dalgliesh, C., Meyer, N.H., Liu, Y.*, et al.* (2016). Structural basis of RNA recognition and dimerization by the STAR proteins T-STAR and Sam68. Nat Commun *7*, 10355.

Fishell, G., and Rudy, B. (2011). Mechanisms of inhibition within the telencephalon: "where the wild things are". Annu Rev Neurosci *34*, 535-567.

Franco, S.J., and Muller, U. (2013). Shaping our minds: stem and progenitor cell diversity in the mammalian neocortex. Neuron *77*, 19-34.

Fuccillo, M.V., Foldy, C., Gokce, O., Rothwell, P.E., Sun, G.L., Malenka, R.C., and Sudhof, T.C. (2015). Single-Cell mRNA Profiling Reveals Cell-Type-Specific Expression of Neurexin Isoforms. Neuron *87*, 326-340.

Furlanis, E., and Scheiffele, P. (2018). Regulation of Neuronal Differentiation, Function, and Plasticity by Alternative Splicing. Annu Rev Cell Dev Biol *34*, 451-469.

Galarneau, A., and Richard, S. (2009). The STAR RNA binding proteins GLD-1, QKI, SAM68 and SLM-2 bind bipartite RNA motifs. BMC Mol Biol *10*, 47.

Gandoura, S., Weiss, E., Rautou, P.E., Fasseu, M., Gustot, T., Lemoine, F., Hurtado-Nedelec, M., Hego, C., Vadrot, N., Elkrief, L.*, et al.* (2013). Gene- and exon-expression profiling reveals an extensive LPS-induced response in immune cells in patients with cirrhosis. J Hepatol *58*, 936-948.

Gehman, L.T., Stoilov, P., Maguire, J., Damianov, A., Lin, C.H., Shiue, L., Ares, M., Jr., Mody, I., and Black, D.L. (2011). The splicing regulator Rbfox1 (A2BP1) controls neuronal excitation in the mammalian brain. Nat Genet *43*, 706-711.

Geschwind, D.H., and State, M.W. (2015). Gene hunting in autism spectrum disorder: on the path to precision medicine. Lancet Neurol *14*, 1109-1120.

Gill, J., Park, Y., McGinnis, J.P., Perez-Sanchez, C., Blanchette, M., and Si, K. (2017). Regulated Intron Removal Integrates Motivational State and Experience. Cell *169*, 836-848 e815.

Glatter, T., Ludwig, C., Ahrne, E., Aebersold, R., Heck, A.J., and Schmidt, A. (2012). Large-scale quantitative assessment of different in-solution protein digestion protocols reveals superior cleavage efficiency of tandem Lys-C/trypsin proteolysis over trypsin digestion. J Proteome Res *11*, 5145-5156.

Gokce, O., Stanley, G.M., Treutlein, B., Neff, N.F., Camp, J.G., Malenka, R.C., Rothwell, P.E., Fuccillo, M.V., Sudhof, T.C., and Quake, S.R. (2016). Cellular Taxonomy of the Mouse Striatum as Revealed by Single-Cell RNA-Seq. Cell Rep *16*, 1126-1137.

Grabowski, P.J., and Black, D.L. (2001). Alternative RNA splicing in the nervous system. Prog Neurobiol *65*, 289-308.

Graf, E.R., Zhang, X., Jin, S.X., Linhoff, M.W., and Craig, A.M. (2004). Neurexins induce differentiation of GABA and glutamate postsynaptic specializations via neuroligins. Cell *119*, 1013-1026.

Greger, I.H., Khatri, L., Kong, X., and Ziff, E.B. (2003). AMPA receptor tetramerization is mediated by Q/R editing. Neuron *40*, 763-774.

Guo, W., Schafer, S., Greaser, M.L., Radke, M.H., Liss, M., Govindarajan, T., Maatz, H., Schulz, H., Li, S., Parrish, A.M.*, et al.* (2012). RBM20, a gene for hereditary cardiomyopathy, regulates titin splicing. Nat Med *18*, 766-773.

Hattori, D., Demir, E., Kim, H.W., Viragh, E., Zipursky, S.L., and Dickson, B.J. (2007). Dscam diversity is essential for neuronal wiring and self-recognition. Nature *449*, 223-227.

Heiman, M., Kulicke, R., Fenster, R.J., Greengard, P., and Heintz, N. (2014). Cell type-specific mRNA purification by translating ribosome affinity purification (TRAP). Nat Protoc *9*, 1282-1291.

Herring, B.E., and Nicoll, R.A. (2016). Long-Term Potentiation: From CaMKII to AMPA Receptor Trafficking. Annu Rev Physiol *78*, 351-365.

Hippenmeyer, S., Vrieseling, E., Sigrist, M., Portmann, T., Laengle, C., Ladle, D.R., and Arber, S. (2005). A developmental switch in the response of DRG neurons to ETS transcription factor signaling. PLoS Biol *3*, e159.

Hobert, O. (2008). Regulatory logic of neuronal diversity: terminal selector genes and selector motifs. Proc Natl Acad Sci U S A *105*, 20067-20071.

Hobert, O., Carrera, I., and Stefanakis, N. (2010). The molecular and gene regulatory signature of a neuron. Trends Neurosci *33*, 435-445.

Howard, A., Tamas, G., and Soltesz, I. (2005). Lighting the chandelier: new vistas for axo-axonic cells. Trends Neurosci *28*, 310-316.

Hrvatin, S., Hochbaum, D.R., Nagy, M.A., Cicconet, M., Robertson, K., Cheadle, L., Zilionis, R., Ratner, A., Borges-Monroy, R., Klein, A.M.*, et al.* (2018). Single-cell analysis of experience-dependent transcriptomic states in the mouse visual cortex. Nat Neurosci *21*, 120-129.

Hu, H., Gan, J., and Jonas, P. (2014). Interneurons. Fast-spiking, parvalbumin(+) GABAergic interneurons: from cellular design to microcircuit function. Science *345*, 1255263.

Hua, Y., Sahashi, K., Rigo, F., Hung, G., Horev, G., Bennett, C.F., and Krainer, A.R. (2011). Peripheral SMN restoration is essential for long-term rescue of a severe spinal muscular atrophy mouse model. Nature *478*, 123-126.

Hwang, H.W., Saito, Y., Park, C.Y., Blachere, N.E., Tajima, Y., Fak, J.J., Zucker-Scharff, I., and Darnell, R.B. (2017). cTag-PAPERCLIP Reveals Alternative Polyadenylation Promotes Cell-Type Specific Protein Diversity and Shifts Araf Isoforms with Microglia Activation. Neuron *95*, 1334-1349 e1335.

Iijima, T., Iijima, Y., Witte, H., and Scheiffele, P. (2014). Neuronal cell type-specific alternative splicing is regulated by the KH domain protein SLM1. The Journal of cell biology *204*, 331-342.

Iijima, T., Wu, K., Witte, H., Hanno-Iijima, Y., Glatter, T., Richard, S., and Scheiffele, P. (2011). SAM68 regulates neuronal activity-dependent alternative splicing of neurexin-1. Cell *147*, 1601-1614.

Irimia, M., Weatheritt, R.J., Ellis, J.D., Parikshak, N.N., Gonatopoulos-Pournatzis, T., Babor, M., Quesnel-Vallieres, M., Tapial, J., Raj, B., O'Hanlon, D.*, et al.* (2014). A highly conserved program of neuronal microexons is misregulated in autistic brains. Cell *159*, 1511-1523.

Isaac, J.T., Ashby, M.C., and McBain, C.J. (2007). The role of the GluR2 subunit in AMPA receptor function and synaptic plasticity. Neuron *54*, 859-871.

Ishii, K., Wong, J.K., and Sumikawa, K. (2005). Comparison of alpha2 nicotinic acetylcholine receptor subunit mRNA expression in the central nervous system of rats and mice. J Comp Neurol *493*, 241-260.

Jackman, S.L., and Regehr, W.G. (2017). The Mechanisms and Functions of Synaptic Facilitation. Neuron *94*, 447-464.

Jackson, R.J., Hellen, C.U., and Pestova, T.V. (2010). The mechanism of eukaryotic translation initiation and principles of its regulation. Nat Rev Mol Cell Biol *11*, 113-127.

Jensen, K.B., Dredge, B.K., Stefani, G., Zhong, R., Buckanovich, R.J., Okano, H.J., Yang, Y.Y., and Darnell, R.B. (2000). Nova-1 regulates neuron-specific alternative splicing and is essential for neuronal viability. Neuron *25*, 359-371.

Jiang, X., Shen, S., Cadwell, C.R., Berens, P., Sinz, F., Ecker, A.S., Patel, S., and Tolias, A.S. (2015). Principles of connectivity among morphologically defined cell types in adult neocortex. Science *350*, aac9462.

Kaneko, R., Kato, H., Kawamura, Y., Esumi, S., Hirayama, T., Hirabayashi, T., and Yagi, T. (2006). Allelic gene regulation of Pcdh-alpha and Pcdh-gamma clusters involving both monoallelic and biallelic expression in single Purkinje cells. J Biol Chem *281*, 30551-30560.

Kapfer, C., Glickfeld, L.L., Atallah, B.V., and Scanziani, M. (2007). Supralinear increase of recurrent inhibition during sparse activity in the somatosensory cortex. Nat Neurosci *10*, 743-753.

Katz, Y., Wang, E.T., Airoldi, E.M., and Burge, C.B. (2010). Analysis and design of RNA sequencing experiments for identifying isoform regulation. Nat Methods *7*, 1009-1015.

Keleman, K., Kruttner, S., Alenius, M., and Dickson, B.J. (2007). Function of the Drosophila CPEB protein Orb2 in long-term courtship memory. Nat Neurosci *10*, 1587-1593.

Kepecs, A., and Fishell, G. (2014). Interneuron cell types are fit to function. Nature *505*, 318-326.

Kiehl, T.R., Shibata, H., Vo, T., Huynh, D.P., and Pulst, S.M. (2001). Identification and expression of a mouse ortholog of A2BP1. Mamm Genome *12*, 595-601.

Kise, Y., and Schmucker, D. (2013). Role of self-avoidance in neuronal wiring. Curr Opin Neurobiol *23*, 983-989.

Klausberger, T., Magill, P.J., Marton, L.F., Roberts, J.D., Cobden, P.M., Buzsaki, G., and Somogyi, P. (2003). Brain-state- and cell-type-specific firing of hippocampal interneurons in vivo. Nature *421*, 844-848.

Klausberger, T., and Somogyi, P. (2008). Neuronal diversity and temporal dynamics: the unity of hippocampal circuit operations. Science *321*, 53-57.

Klein, M.E., Castillo, P.E., and Jordan, B.A. (2015). Coordination between Translation and Degradation Regulates Inducibility of mGluR-LTD. Cell Rep *10*, 1459-1466.

Ko, J., Fuccillo, M.V., Malenka, R.C., and Sudhof, T.C. (2009). LRRTM2 functions as a neurexin ligand in promoting excitatory synapse formation. Neuron *64*, 791-798.

Koehnke, J., Katsamba, P.S., Ahlsen, G., Bahna, F., Vendome, J., Honig, B., Shapiro, L., and Jin, X. (2010). Splice form dependence of beta-neurexin/neuroligin binding interactions. Neuron *67*, 61-74.

Krüttner, S., Traunmuller, L., Dag, U., Jandrasits, K., Stepien, B., Iyer, N., Fradkin, L.G., Noordermeer, J.N., Mensh, B.D., and Keleman, K. (2015). Synaptic Orb2A Bridges Memory Acquisition and Late Memory Consolidation in Drosophila. Cell Rep *11*, 1953-1965.

Kurshan, P.T., Merrill, S.A., Dong, Y., Ding, C., Hammarlund, M., Bai, J., Jorgensen, E.M., and Shen, K. (2018). gamma-Neurexin and Frizzled Mediate Parallel Synapse Assembly Pathways Antagonized by Receptor Endocytosis. Neuron *100*, 150-166 e154.

Laplante, P., Brillant-Marquis, F., Brissette, M.J., Joannette-Pilon, B., Cayrol, R., Kokta, V., and Cailhier, J.F. (2017). MFG-E8 Reprogramming of Macrophages Promotes Wound Healing by Increased bFGF Production and Fibroblast Functions. J Invest Dermatol *137*, 2005-2013.

Lareau, L.F., Inada, M., Green, R.E., Wengrod, J.C., and Brenner, S.E. (2007). Unproductive splicing of SR genes associated with highly conserved and ultraconserved DNA elements. Nature *446*, 926-929.

Leao, R.N., Mikulovic, S., Leao, K.E., Munguba, H., Gezelius, H., Enjin, A., Patra, K., Eriksson, A., Loew, L.M., Tort, A.B.*, et al.* (2012). OLM interneurons differentially modulate CA3 and entorhinal inputs to hippocampal CA1 neurons. Nat Neurosci *15*, 1524-1530.

Lee, J.A., Damianov, A., Lin, C.H., Fontes, M., Parikshak, N.N., Anderson, E.S., Geschwind, D.H., Black, D.L., and Martin, K.C. (2016). Cytoplasmic Rbfox1 Regulates the Expression of Synaptic and Autism-Related Genes. Neuron *89*, 113-128.

Lefebvre, J.L., Kostadinov, D., Chen, W.V., Maniatis, T., and Sanes, J.R. (2012). Protocadherins mediate dendritic self-avoidance in the mammalian nervous system. Nature *488*, 517-521.

Lejeune, F., and Maquat, L.E. (2005). Mechanistic links between nonsense-mediated mRNA decay and pre-mRNA splicing in mammalian cells. Curr Opin Cell Biol *17*, 309-315.

Li, Q., Zheng, S., Han, A., Lin, C.H., Stoilov, P., Fu, X.D., and Black, D.L. (2014). The splicing regulator PTBP2 controls a program of embryonic splicing required for neuronal maturation. Elife *3*, e01201.

Li, Y.I., Sanchez-Pulido, L., Haerty, W., and Ponting, C.P. (2015). RBFOX and PTBP1 proteins regulate the alternative splicing of micro-exons in human brain transcripts. Genome Res *25*, 1-13.

Liao, Y., Smyth, G.K., and Shi, W. (2014). featureCounts: an efficient general purpose program for assigning sequence reads to genomic features. Bioinformatics *30*, 923-930.

Lim, L., Pakan, J.M.P., Selten, M.M., Marques-Smith, A., Llorca, A., Bae, S.E., Rochefort, N.L., and Marin, O. (2018). Optimization of interneuron function by direct coupling of cell migration and axonal targeting. Nature neuroscience *21*, 920-931.

Love, M.I., Huber, W., and Anders, S. (2014). Moderated estimation of fold change and dispersion for RNA-seq data with DESeq2. Genome Biol *15*, 550.

Maccaferri, G., and McBain, C.J. (1995). Passive propagation of LTD to stratum oriens-alveus inhibitory neurons modulates the temporoammonic input to the hippocampal CA1 region. Neuron *15*, 137-145.

Maccaferri, G., and McBain, C.J. (1996). Long-term potentiation in distinct subtypes of hippocampal nonpyramidal neurons. J Neurosci *16*, 5334-5343.

Madisen, L., Mao, T., Koch, H., Zhuo, J.M., Berenyi, A., Fujisawa, S., Hsu, Y.W., Garcia, A.J., 3rd, Gu, X., Zanella, S.*, et al.* (2012). A toolbox of Cre-dependent optogenetic transgenic mice for light-induced activation and silencing. Nat Neurosci *15*, 793-802.

Madisen, L., Zwingman, T.A., Sunkin, S.M., Oh, S.W., Zariwala, H.A., Gu, H., Ng, L.L., Palmiter, R.D., Hawrylycz, M.J., Jones, A.R.*, et al.* (2010). A robust and high-throughput Cre reporting and characterization system for the whole mouse brain. Nat Neurosci *13*, 133-140.

Malik, R., Dougherty, K.A., Parikh, K., Byrne, C., and Johnston, D. (2016). Mapping the electrophysiological and morphological properties of CA1 pyramidal neurons along the longitudinal hippocampal axis. Hippocampus *26*, 341-361.

Marin, O. (2013). Cellular and molecular mechanisms controlling the migration of neocortical interneurons. Eur J Neurosci *38*, 2019-2029.

Marin, O., and Müller, U. (2014). Lineage origins of GABAergic versus glutamatergic neurons in the neocortex. Curr Opin Neurobiol *26*, 132-141.

Martin, R.M., Rino, J., Carvalho, C., Kirchhausen, T., and Carmo-Fonseca, M. (2013). Live-cell visualization of pre-mRNA splicing with single-molecule sensitivity. Cell Rep *4*, 1144-1155.

Matsuda, K., Budisantoso, T., Mitakidis, N., Sugaya, Y., Miura, E., Kakegawa, W., Yamasaki, M., Konno, K., Uchigashima, M., Abe, M.*, et al.* (2016). Transsynaptic Modulation of Kainate Receptor Functions by C1q-like Proteins. Neuron *90*, 752-767.

Matsuda, K., Miura, E., Miyazaki, T., Kakegawa, W., Emi, K., Narumi, S., Fukazawa, Y., Ito-Ishida, A., Kondo, T., Shigemoto, R.*, et al.* (2010). Cbln1 is a ligand for an orphan glutamate receptor delta2, a bidirectional synapse organizer. Science *328*, 363-368.

Matsuda, K., and Yuzaki, M. (2011). Cbln family proteins promote synapse formation by regulating distinct neurexin signaling pathways in various brain regions. Eur J Neurosci *33*, 1447-1461.

Matthews, B.J., Kim, M.E., Flanagan, J.J., Hattori, D., Clemens, J.C., Zipursky, S.L., and Grueber, W.B. (2007). Dendrite self-avoidance is controlled by Dscam. Cell *129*, 593-604.

Mauger, O., Lemoine, F., and Scheiffele, P. (2016). Targeted Intron Retention and Excision for Rapid Gene Regulation in Response to Neuronal Activity. Neuron *92*, 1266-1278.

Mayer, C., Hafemeister, C., Bandler, R.C., Machold, R., Batista Brito, R., Jaglin, X., Allaway, K., Butler, A., Fishell, G., and Satija, R. (2018). Developmental diversification of cortical inhibitory interneurons. Nature *555*, 457-462.

Maynard, K.R., Hill, J.L., Calcaterra, N.E., Palko, M.E., Kardian, A., Paredes, D., Sukumar, M., Adler, B.D., Jimenez, D.V., Schloesser, R.J.*, et al.* (2016). Functional Role of BDNF Production

from Unique Promoters in Aggression and Serotonin Signaling. Neuropsychopharmacology *41*, 1943-1955.

McConnell, S.K. (1988). Fates of visual cortical neurons in the ferret after isochronic and heterochronic transplantation. J Neurosci *8*, 945-974.

McKerracher, L., and Rosen, K.M. (2015). MAG, myelin and overcoming growth inhibition in the CNS. Front Mol Neurosci *8*, 51.

Meyer, H.S., Schwarz, D., Wimmer, V.C., Schmitt, A.C., Kerr, J.N., Sakmann, B., and Helmstaedter, M. (2011). Inhibitory interneurons in a cortical column form hot zones of inhibition in layers 2 and 5A. Proc Natl Acad Sci U S A *108*, 16807-16812.

Mi, D., Li, Z., Lim, L., Li, M., Moissidis, M., Yang, Y., Gao, T., Hu, T.X., Pratt, T., Price, D.J.*, et al.* (2018a). Early emergence of cortical interneuron diversity in the mouse embryo. Science (New York, NY.

Mi, D., Li, Z., Lim, L., Li, M., Moissidis, M., Yang, Y., Gao, T., Hu, T.X., Pratt, T., Price, D.J.*, et al.* (2018b). Early emergence of cortical interneuron diversity in the mouse embryo. Science *360*, 81-85.

Mi, H., Muruganujan, A., Casagrande, J.T., and Thomas, P.D. (2013). Large-scale gene function analysis with the PANTHER classification system. Nat Protoc *8*, 1551-1566.

Miura, S.K., Martins, A., Zhang, K.X., Graveley, B.R., and Zipursky, S.L. (2013). Probabilistic splicing of Dscam1 establishes identity at the level of single neurons. Cell *155*, 1166-1177.

Mizuseki, K., Diba, K., Pastalkova, E., and Buzsaki, G. (2011). Hippocampal CA1 pyramidal cells form functionally distinct sublayers. Nat Neurosci *14*, 1174-1181.

Muhammad, K., Reddy-Alla, S., Driller, J.H., Schreiner, D., Rey, U., Bohme, M.A., Hollmann, C., Ramesh, N., Depner, H., Lutzkendorf, J.*, et al.* (2015). Presynaptic spinophilin tunes neurexin signalling to control active zone architecture and function. Nat Commun *6*, 8362.

Müller, C., and Remy, S. (2014). Dendritic inhibition mediated by O-LM and bistratified interneurons in the hippocampus. Front Synaptic Neurosci *6*, 23.

Nakauchi, S., Brennan, R.J., Boulter, J., and Sumikawa, K. (2007). Nicotine gates long-term potentiation in the hippocampal CA1 region via the activation of alpha2* nicotinic ACh receptors. Eur J Neurosci *25*, 2666-2681.

Nakazawa, K., Sun, L.D., Quirk, M.C., Rondi-Reig, L., Wilson, M.A., and Tonegawa, S. (2003). Hippocampal CA3 NMDA receptors are crucial for memory acquisition of one-time experience. Neuron *38*, 305-315.

Nguyen, T., and Sudhof, T.C. (1997). Binding properties of neuroligin 1 and neurexin 1beta reveal function as heterophilic cell adhesion molecules. J Biol Chem *272*, 26032-26039.

Nguyen, T.M., Schreiner, D., Xiao, L., Traunmüller, L., Bornmann, C., and Scheiffele, P. (2016). An alternative splicing switch shapes neurexin repertoires in principal neurons versus interneurons in the mouse hippocampus. Elife *5*.

Ni, J.Z., Grate, L., Donohue, J.P., Preston, C., Nobida, N., O'Brien, G., Shiue, L., Clark, T.A., Blume, J.E., and Ares, M., Jr. (2007). Ultraconserved elements are associated with homeostatic control of splicing regulators by alternative splicing and nonsense-mediated decay. Genes Dev *21*, 708-718.

Nilsen, T.W., and Graveley, B.R. (2010). Expansion of the eukaryotic proteome by alternative splicing. Nature *463*, 457-463.

Noli, L., Capalbo, A., Ogilvie, C., Khalaf, Y., and Ilic, D. (2015). Discordant Growth of Monozygotic Twins Starts at the Blastocyst Stage: A Case Study. Stem Cell Reports *5*, 946-953.

Norris, A.D., Gao, S., Norris, M.L., Ray, D., Ramani, A.K., Fraser, A.G., Morris, Q., Hughes, T.R., Zhen, M., and Calarco, J.A. (2014). A pair of RNA-binding proteins controls networks of splicing events contributing to specialization of neural cell types. Mol Cell *54*, 946-959.

Pal, S., Gupta, R., Kim, H., Wickramasinghe, P., Baubet, V., Showe, L.C., Dahmane, N., and Davuluri, R.V. (2011). Alternative transcription exceeds alternative splicing in generating the transcriptome diversity of cerebellar development. Genome Res *21*, 1260-1272.

Pan, Q., Shai, O., Lee, L.J., Frey, B.J., and Blencowe, B.J. (2008). Deep surveying of alternative splicing complexity in the human transcriptome by high-throughput sequencing. Nat Genet *40*, 1413-1415.

Paul, A., Crow, M., Raudales, R., He, M., Gillis, J., and Huang, Z.J. (2017). Transcriptional Architecture of Synaptic Communication Delineates GABAergic Neuron Identity. Cell *171*, 522-539 e520.

Penn, A.C., and Greger, I.H. (2009). Sculpting AMPA receptor formation and function by alternative RNA processing. RNA Biol *6*, 517-521.

Petilla Interneuron Nomenclature, G., Ascoli, G.A., Alonso-Nanclares, L., Anderson, S.A., Barrionuevo, G., Benavides-Piccione, R., Burkhalter, A., Buzsaki, G., Cauli, B., Defelipe, J.*, et al.* (2008). Petilla terminology: nomenclature of features of GABAergic interneurons of the cerebral cortex. Nat Rev Neurosci *9*, 557-568.

Phillips, G.R., Huang, J.K., Wang, Y., Tanaka, H., Shapiro, L., Zhang, W., Shan, W.S., Arndt, K., Frank, M., Gordon, R.E.*, et al.* (2001). The presynaptic particle web: ultrastructure, composition, dissolution, and reconstitution. Neuron *32*, 63-77.

Pouille, F., and Scanziani, M. (2004). Routing of spike series by dynamic circuits in the hippocampus. Nature *429*, 717-723.

Quesnel-Vallieres, M., Dargaei, Z., Irimia, M., Gonatopoulos-Pournatzis, T., Ip, J.Y., Wu, M., Sterne-Weiler, T., Nakagawa, S., Woodin, M.A., Blencowe, B.J.*, et al.* (2016). Misregulation of

an Activity-Dependent Splicing Network as a Common Mechanism Underlying Autism Spectrum Disorders. Mol Cell *64*, 1023-1034.

Quesnel-Vallieres, M., Irimia, M., Cordes, S.P., and Blencowe, B.J. (2015). Essential roles for the splicing regulator nSR100/SRRM4 during nervous system development. Genes Dev *29*, 746-759.

Raj, B., and Blencowe, B.J. (2015). Alternative Splicing in the Mammalian Nervous System: Recent Insights into Mechanisms and Functional Roles. Neuron *87*, 14-27.

Raj, B., Irimia, M., Braunschweig, U., Sterne-Weiler, T., O'Hanlon, D., Lin, Z.Y., Chen, G.I., Easton, L.E., Ule, J., Gingras, A.C.*, et al.* (2014). A global regulatory mechanism for activating an exon network required for neurogenesis. Mol Cell *56*, 90-103.

Ramón y Cajal, S. (1995). Histology of the nervous system of man and vertebrates (New York: Oxford University Press).

Reissner, C., Runkel, F., and Missler, M. (2013). Neurexins. Genome Biol *14*, 213.

Reyes, A., and Huber, W. (2018). Alternative start and termination sites of transcription drive most transcript isoform differences across human tissues. Nucleic Acids Res *46*, 582-592.

Rubinstein, R., Thu, C.A., Goodman, K.M., Wolcott, H.N., Bahna, F., Mannepalli, S., Ahlsen, G., Chevee, M., Halim, A., Clausen, H.*, et al.* (2015). Molecular logic of neuronal self-recognition through protocadherin domain interactions. Cell *163*, 629-642.

Ruggiu, M., Herbst, R., Kim, N., Jevsek, M., Fak, J.J., Mann, M.A., Fischbach, G., Burden, S.J., and Darnell, R.B. (2009). Rescuing Z+ agrin splicing in Nova null mice restores synapse formation and unmasks a physiologic defect in motor neuron firing. Proc Natl Acad Sci U S A *106*, 3513-3518.

Saito, Y., Yuan, Y., Zucker-Scharff, I., Fak, J.J., Jereb, S., Tajima, Y., Licatalosi, D.D., and Darnell, R.B. (2019). Differential NOVA2-Mediated Splicing in Excitatory and Inhibitory Neurons Regulates Cortical Development and Cerebellar Function. Neuron *101*, 707-720 e705.

Sanchez-Jimenez, F., and Sanchez-Margalet, V. (2013). Role of Sam68 in post-transcriptional gene regulation. Int J Mol Sci *14*, 23402-23419.

Sando, R., Bushong, E., Zhu, Y., Huang, M., Considine, C., Phan, S., Ju, S., Uytiepo, M., Ellisman, M., and Maximov, A. (2017). Assembly of Excitatory Synapses in the Absence of Glutamatergic Neurotransmission. Neuron *94*, 312-321 e313.

Sanz, E., Yang, L., Su, T., Morris, D.R., McKnight, G.S., and Amieux, P.S. (2009). Cell-type-specific isolation of ribosome-associated mRNA from complex tissues. Proc Natl Acad Sci U S A *106*, 13939-13944.

Savas, J.N., Ribeiro, L.F., Wierda, K.D., Wright, R., DeNardo-Wilke, L.A., Rice, H.C., Chamma, I., Wang, Y.Z., Zemla, R., Lavallee-Adam, M.*, et al.* (2015). The Sorting Receptor SorCS1 Regulates Trafficking of Neurexin and AMPA Receptors. Neuron *87*, 764-780.

Scheiffele, P., Fan, J., Choih, J., Fetter, R., and Serafini, T. (2000). Neuroligin expressed in nonneuronal cells triggers presynaptic development in contacting axons. Cell *101*, 657-669.

Schmucker, D., Clemens, J.C., Shu, H., Worby, C.A., Xiao, J., Muda, M., Dixon, J.E., and Zipursky, S.L. (2000). Drosophila Dscam is an axon guidance receptor exhibiting extraordinary molecular diversity. Cell *101*, 671-684.

Schreiner, D., Nguyen, T.-M., Russo, G., Hebr, S., Patrignani, A., Ahrné, E., and Scheiffele, P. (2014a). Targeted Combinatorial Alternative Splicing Generates Brain Region-Specific Repertoires of Neurexins. Neuron.

Schreiner, D., Nguyen, T.M., and Scheiffele, P. (2014b). Polymorphic receptors: neuronal functions and molecular mechanisms of diversification. Curr Opin Neurobiol *27*, 25-30.

Schreiner, D., Simicevic, J., Ahrne, E., Schmidt, A., and Scheiffele, P. (2015). Quantitative isoform-profiling of highly diversified recognition molecules. Elife *4*, e07794.

Schreiner, D., and Weiner, J.A. (2010). Combinatorial homophilic interaction between gamma-protocadherin multimers greatly expands the molecular diversity of cell adhesion. Proc Natl Acad Sci U S A *107*, 14893-14898.

Schulz, J.M., Knoflach, F., Hernandez, M.C., and Bischofberger, J. (2018). Dendrite-targeting interneurons control synaptic NMDA-receptor activation via nonlinear alpha5-GABAA receptors. Nat Commun *9*, 3576.

Shen, K., and Scheiffele, P. (2010). Genetics and cell biology of building specific synaptic connectivity. Annu Rev Neurosci *33*, 473-507.

Shen, K.C., Kuczynska, D.A., Wu, I.J., Murray, B.H., Sheckler, L.R., and Rudenko, G. (2008). Regulation of neurexin 1beta tertiary structure and ligand binding through alternative splicing. Structure *16*, 422-431.

Shigemoto, R., Kulik, A., Roberts, J.D., Ohishi, H., Nusser, Z., Kaneko, T., and Somogyi, P. (1996). Target-cell-specific concentration of a metabotropic glutamate receptor in the presynaptic active zone. Nature *381*, 523-525.

Shipman, S.L., Schnell, E., Hirai, T., Chen, B.S., Roche, K.W., and Nicoll, R.A. (2011). Functional dependence of neuroligin on a new non-PDZ intracellular domain. Nat Neurosci *14*, 718-726.

Siddiqui, T.J., Pancaroglu, R., Kang, Y., Rooyakkers, A., and Craig, A.M. (2010). LRRTMs and neuroligins bind neurexins with a differential code to cooperate in glutamate synapse development. J Neurosci *30*, 7495-7506.

Sigler, A., Oh, W.C., Imig, C., Altas, B., Kawabe, H., Cooper, B.H., Kwon, H.B., Rhee, J.S., and Brose, N. (2017). Formation and Maintenance of Functional Spines in the Absence of Presynaptic Glutamate Release. Neuron *94*, 304-311 e304.

Sik, A., Penttonen, M., Ylinen, A., and Buzsaki, G. (1995). Hippocampal CA1 interneurons: an in vivo intracellular labeling study. J Neurosci *15*, 6651-6665.

Singh, J., and Padgett, R.A. (2009). Rates of in situ transcription and splicing in large human genes. Nat Struct Mol Biol *16*, 1128-1133.

Siwani, S., Franca, A.S.C., Mikulovic, S., Reis, A., Hilscher, M.M., Edwards, S.J., Leao, R.N., Tort, A.B.L., and Kullander, K. (2018). OLMalpha2 Cells Bidirectionally Modulate Learning. Neuron *99*, 404-412 e403.

Soba, P., Zhu, S., Emoto, K., Younger, S., Yang, S.J., Yu, H.H., Lee, T., Jan, L.Y., and Jan, Y.N. (2007). Drosophila sensory neurons require Dscam for dendritic self-avoidance and proper dendritic field organization. Neuron *54*, 403-416.

Sommer, B., Keinanen, K., Verdoorn, T.A., Wisden, W., Burnashev, N., Herb, A., Kohler, M., Takagi, T., Sakmann, B., and Seeburg, P.H. (1990). Flip and flop: a cell-specific functional switch in glutamate-operated channels of the CNS. Science *249*, 1580-1585.

Somogyi, P., Dalezios, Y., Lujan, R., Roberts, J.D., Watanabe, M., and Shigemoto, R. (2003). High level of mGluR7 in the presynaptic active zones of select populations of GABAergic terminals innervating interneurons in the rat hippocampus. Eur J Neurosci *17*, 2503-2520.

Sperry, R.W. (1963). Chemoaffinity in the Orderly Growth of Nerve Fiber Patterns and Connections. Proc Natl Acad Sci U S A *50*, 703-710.

Spiegel, I., Mardinly, A.R., Gabel, H.W., Bazinet, J.E., Couch, C.H., Tzeng, C.P., Harmin, D.A., and Greenberg, M.E. (2014). Npas4 regulates excitatory-inhibitory balance within neural circuits through cell-type-specific gene programs. Cell *157*, 1216-1229.

Stachniak, T., Lauren Sylwestrak, E., Scheiffele, P., Hall, B.J., and Ghosh, A. (2019). Elfn1-induced constitutive activation of mGluR7 determines frequency-dependent recruitment of SOM interneurons. J Neurosci.

Sterky, F.H., Trotter, J.H., Lee, S.J., Recktenwald, C.V., Du, X., Zhou, B., Zhou, P., Schwenk, J., Fakler, B., and Sudhof, T.C. (2017). Carbonic anhydrase-related protein CA10 is an evolutionarily conserved pan-neurexin ligand. Proc Natl Acad Sci U S A *114*, E1253-E1262.

Stevens, B., Allen, N.J., Vazquez, L.E., Howell, G.R., Christopherson, K.S., Nouri, N., Micheva, K.D., Mehalow, A.K., Huberman, A.D., Stafford, B.*, et al.* (2007). The classical complement cascade mediates CNS synapse elimination. Cell *131*, 1164-1178.

Sun, W., You, X., Gogol-Doring, A., He, H., Kise, Y., Sohn, M., Chen, T., Klebes, A., Schmucker, D., and Chen, W. (2013). Ultra-deep profiling of alternatively spliced Drosophila Dscam isoforms by circularization-assisted multi-segment sequencing. EMBO J *32*, 2029-2038.

Sun, Y., Nguyen, A.Q., Nguyen, J.P., Le, L., Saur, D., Choi, J., Callaway, E.M., and Xu, X. (2014). Cell-type-specific circuit connectivity of hippocampal CA1 revealed through Cre-dependent rabies tracing. Cell Rep *7*, 269-280.

Sylwestrak, E.L., and Ghosh, A. (2012). Elfn1 regulates target-specific release probability at CA1-interneuron synapses. Science *338*, 536-540.

Szabadics, J., Varga, C., Molnar, G., Olah, S., Barzo, P., and Tamas, G. (2006). Excitatory effect of GABAergic axo-axonic cells in cortical microcircuits. Science *311*, 233-235.

Tabuchi, K., and Sudhof, T.C. (2002). Structure and evolution of neurexin genes: insight into the mechanism of alternative splicing. Genomics *79*, 849-859.

Takahashi, H., and Craig, A.M. (2013). Protein tyrosine phosphatases PTPdelta, PTPsigma, and LAR: presynaptic hubs for synapse organization. Trends Neurosci *36*, 522-534.

Taliaferro, J.M., Vidaki, M., Oliveira, R., Olson, S., Zhan, L., Saxena, T., Wang, E.T., Graveley, B.R., Gertler, F.B., Swanson, M.S.*, et al.* (2016). Distal Alternative Last Exons Localize mRNAs to Neural Projections. Mol Cell *61*, 821-833.

Taniguchi, H., He, M., Wu, P., Kim, S., Paik, R., Sugino, K., Kvitsiani, D., Fu, Y., Lu, J., Lin, Y.*, et al.* (2011). A resource of Cre driver lines for genetic targeting of GABAergic neurons in cerebral cortex. Neuron *71*, 995-1013.

Tapial, J., Ha, K.C.H., Sterne-Weiler, T., Gohr, A., Braunschweig, U., Hermoso-Pulido, A., Quesnel-Vallieres, M., Permanyer, J., Sodaei, R., Marquez, Y.*, et al.* (2017). An atlas of alternative splicing profiles and functional associations reveals new regulatory programs and genes that simultaneously express multiple major isoforms. Genome Res *27*, 1759-1768.

Tasic, B., Menon, V., Nguyen, T.N., Kim, T.K., Jarsky, T., Yao, Z., Levi, B., Gray, L.T., Sorensen, S.A., Dolbeare, T.*, et al.* (2016). Adult mouse cortical cell taxonomy revealed by single cell transcriptomics. Nat Neurosci *19*, 335-346.

Tasic, B., Nabholz, C.E., Baldwin, K.K., Kim, Y., Rueckert, E.H., Ribich, S.A., Cramer, P., Wu, Q., Axel, R., and Maniatis, T. (2002). Promoter choice determines splice site selection in protocadherin alpha and gamma pre-mRNA splicing. Mol Cell *10*, 21-33.

Tasic, B., Yao, Z., Graybuck, L.T., Smith, K.A., Nguyen, T.N., Bertagnolli, D., Goldy, J., Garren, E., Economo, M.N., Viswanathan, S.*, et al.* (2018). Shared and distinct transcriptomic cell types across neocortical areas. Nature *563*, 72-78.

Timmusk, T., Lendahl, U., Funakoshi, H., Arenas, E., Persson, H., and Metsis, M. (1995). Identification of brain-derived neurotrophic factor promoter regions mediating tissue-specific, axotomy-, and neuronal activity-induced expression in transgenic mice. J Cell Biol *128*, 185-199.

Tomioka, N.H., Yasuda, H., Miyamoto, H., Hatayama, M., Morimura, N., Matsumoto, Y., Suzuki, T., Odagawa, M., Odaka, Y.S., Iwayama, Y.*, et al.* (2014). Elfn1 recruits presynaptic mGluR7 in trans and its loss results in seizures. Nat Commun *5*, 4501.

Traunmüller, L., Bornmann, C., and Scheiffele, P. (2014). Alternative splicing coupled nonsense-mediated decay generates neuronal cell type-specific expression of SLM proteins. J Neurosci *34*, 16755-16761.

Traunmüller, L., Gomez, A.M., Nguyen, T.-M., and Scheiffele, P. (2016). Control of neuronal synapse specification by highly dedicated alternative splicing program. Science *352*, 982-986.

Tremblay, R., Lee, S., and Rudy, B. (2016). GABAergic Interneurons in the Neocortex: From Cellular Properties to Circuits. Neuron *91*, 260-292.

Tress, M.L., Abascal, F., and Valencia, A. (2017). Alternative Splicing May Not Be the Key to Proteome Complexity. Trends Biochem Sci *42*, 98-110.

Treutlein, B., Gokce, O., Quake, S.R., and Sudhof, T.C. (2014). Cartography of neurexin alternative splicing mapped by single-molecule long-read mRNA sequencing. Proc Natl Acad Sci U S A *111*, E1291-1299.

Tsien, J.Z., Chen, D.F., Gerber, D., Tom, C., Mercer, E.H., Anderson, D.J., Mayford, M., Kandel, E.R., and Tonegawa, S. (1996). Subregion- and cell type-restricted gene knockout in mouse brain. Cell *87*, 1317-1326.

Tushev, G., Glock, C., Heumuller, M., Biever, A., Jovanovic, M., and Schuman, E.M. (2018). Alternative 3' UTRs Modify the Localization, Regulatory Potential, Stability, and Plasticity of mRNAs in Neuronal Compartments. Neuron *98*, 495-511 e496.

Uchigashima, M., Cheung, A., Suh, J., Watanabe, M., and Futai, K. (2019). Differential expression of neurexin genes in the mouse brain. J Comp Neurol.

Uemura, T., Lee, S.J., Yasumura, M., Takeuchi, T., Yoshida, T., Ra, M., Taguchi, R., Sakimura, K., and Mishina, M. (2010). Trans-synaptic interaction of GluRdelta2 and Neurexin through Cbln1 mediates synapse formation in the cerebellum. Cell *141*, 1068-1079.

Ule, J., and Darnell, R.B. (2006). RNA binding proteins and the regulation of neuronal synaptic plasticity. Curr Opin Neurobiol *16*, 102-110.

Ule, J., Stefani, G., Mele, A., Ruggiu, M., Wang, X., Taneri, B., Gaasterland, T., Blencowe, B.J., and Darnell, R.B. (2006). An RNA map predicting Nova-dependent splicing regulation. Nature *444*, 580-586.

Ule, J., Ule, A., Spencer, J., Williams, A., Hu, J.S., Cline, M., Wang, H., Clark, T., Fraser, C., Ruggiu, M.*, et al.* (2005). Nova regulates brain-specific splicing to shape the synapse. Nat Genet *37*, 844-852.

Ullrich, B., Ushkaryov, Y.A., and Sudhof, T.C. (1995). Cartography of neurexins: more than 1000 isoforms generated by alternative splicing and expressed in distinct subsets of neurons. Neuron *14*, 497-507.

Ushkaryov, Y.A., Hata, Y., Ichtchenko, K., Moomaw, C., Afendis, S., Slaughter, C.A., and Sudhof, T.C. (1994). Conserved domain structure of beta-neurexins. Unusual cleaved signal sequences in receptor-like neuronal cell-surface proteins. J Biol Chem *269*, 11987-11992.

Ushkaryov, Y.A., Petrenko, A.G., Geppert, M., and Sudhof, T.C. (1992). Neurexins: synaptic cell surface proteins related to the alpha-latrotoxin receptor and laminin. Science *257*, 50-56.

Veloso, A., Kirkconnell, K.S., Magnuson, B., Biewen, B., Paulsen, M.T., Wilson, T.E., and Ljungman, M. (2014). Rate of elongation by RNA polymerase II is associated with specific gene features and epigenetic modifications. Genome Res *24*, 896-905.

Venables, J.P., Dalgliesh, C., Paronetto, M.P., Skitt, L., Thornton, J.K., Saunders, P.T., Sette, C., Jones, K.T., and Elliott, D.J. (2004). SIAH1 targets the alternative splicing factor T-STAR for degradation by the proteasome. Hum Mol Genet *13*, 1525-1534.

Vernet, C., and Artzt, K. (1997). STAR, a gene family involved in signal transduction and activation of RNA. Trends Genet *13*, 479-484.

Vuong, C.K., Black, D.L., and Zheng, S. (2016). The neurogenetics of alternative splicing. Nature reviews Neuroscience *17*, 265-281.

Vuong, C.K., Wei, W., Lee, J.A., Lin, C.H., Damianov, A., de la Torre-Ubieta, L., Halabi, R., Otis, K.O., Martin, K.C., O'Dell, T.J.*, et al.* (2018). Rbfox1 Regulates Synaptic Transmission through the Inhibitory Neuron-Specific vSNARE Vamp1. Neuron *98*, 127-141 e127.

Wamsley, B., and Fishell, G. (2017). Genetic and activity-dependent mechanisms underlying interneuron diversity. Nat Rev Neurosci *18*, 299-309.

Wamsley, B., Jaglin, X.H., Favuzzi, E., Quattrocolo, G., Nigro, M.J., Yusuf, N., Khodadadi-Jamayran, A., Rudy, B., and Fishell, G. (2018). Rbfox1 Mediates Cell-type-Specific Splicing in Cortical Interneurons. Neuron *100*, 846-859 e847.

Wang, E., Aslanzadeh, V., Papa, F., Zhu, H., de la Grange, P., and Cambi, F. (2012a). Global profiling of alternative splicing events and gene expression regulated by hnRNPH/F. PLoS One *7*, e51266.

Wang, E.T., Cody, N.A., Jog, S., Biancolella, M., Wang, T.T., Treacy, D.J., Luo, S., Schroth, G.P., Housman, D.E., Reddy, S.*, et al.* (2012b). Transcriptome-wide regulation of pre-mRNA splicing and mRNA localization by muscleblind proteins. Cell *150*, 710-724.

Wang, E.T., Sandberg, R., Luo, S., Khrebtukova, I., Zhang, L., Mayr, C., Kingsmore, S.F., Schroth, G.P., and Burge, C.B. (2008). Alternative isoform regulation in human tissue transcriptomes. Nature *456*, 470-476.

Wang, X., Su, H., and Bradley, A. (2002). Molecular mechanisms governing Pcdh-gamma gene expression: evidence for a multiple promoter and cis-alternative splicing model. Genes Dev *16*, 1890-1905.

Weatheritt, R.J., Sterne-Weiler, T., and Blencowe, B.J. (2016). The ribosome-engaged landscape of alternative splicing. Nat Struct Mol Biol *23*, 1117-1123.

Wei, P., Pattarini, R., Rong, Y., Guo, H., Bansal, P.K., Kusnoor, S.V., Deutch, A.Y., Parris, J., and Morgan, J.I. (2012). The Cbln family of proteins interact with multiple signaling pathways. J Neurochem *121*, 717-729.

Weyn-Vanhentenryck, S.M., Feng, H., Ustianenko, D., Duffie, R., Yan, Q., Jacko, M., Martinez, J.C., Goodwin, M., Zhang, X., Hengst, U.*, et al.* (2018). Precise temporal regulation of alternative splicing during neural development. Nat Commun *9*, 2189.

Weyn-Vanhentenryck, S.M., Mele, A., Yan, Q., Sun, S., Farny, N., Zhang, Z., Xue, C., Herre, M., Silver, P.A., Zhang, M.Q.*, et al.* (2014). HITS-CLIP and integrative modeling define the Rbfox splicing-regulatory network linked to brain development and autism. Cell Rep *6*, 1139-1152.

Willnow, T.E., Petersen, C.M., and Nykjaer, A. (2008). VPS10P-domain receptors - regulators of neuronal viability and function. Nat Rev Neurosci *9*, 899-909.

Witte, H., Schreiner, D., and Scheiffele, P. (2018). A Sam68-dependent alternative splicing program shapes postsynaptic protein complexes. Eur J Neurosci.

Wojtowicz, W.M., Flanagan, J.J., Millard, S.S., Zipursky, S.L., and Clemens, J.C. (2004). Alternative splicing of Drosophila Dscam generates axon guidance receptors that exhibit isoform-specific homophilic binding. Cell *118*, 619-633.

Wu, Q., and Maniatis, T. (1999). A striking organization of a large family of human neural cadherin-like cell adhesion genes. Cell *97*, 779-790.

Xu, H., Jeong, H.Y., Tremblay, R., and Rudy, B. (2013). Neocortical somatostatin-expressing GABAergic interneurons disinhibit the thalamorecipient layer 4. Neuron *77*, 155-167.

Yan, Q., Weyn-Vanhentenryck, S.M., Wu, J., Sloan, S.A., Zhang, Y., Chen, K., Wu, J.Q., Barres, B.A., and Zhang, C. (2015). Systematic discovery of regulated and conserved alternative exons in the mammalian brain reveals NMD modulating chromatin regulators. Proc Natl Acad Sci U S A *112*, 3445-3450.

Yap, E.L., and Greenberg, M.E. (2018). Activity-Regulated Transcription: Bridging the Gap between Neural Activity and Behavior. Neuron *100*, 330-348.

Yap, K., Xiao, Y., Friedman, B.A., Je, H.S., and Makeyev, E.V. (2016). Polarizing the Neuron through Sustained Co-expression of Alternatively Spliced Isoforms. Cell Rep *15*, 1316-1328.

Zeisel, A., Munoz-Manchado, A.B., Codeluppi, S., Lonnerberg, P., La Manno, G., Jureus, A., Marques, S., Munguba, H., He, L., Betsholtz, C.*, et al.* (2015). Brain structure. Cell types in the mouse cortex and hippocampus revealed by single-cell RNA-seq. Science *347*, 1138-1142.

Zeng, H., and Sanes, J.R. (2017). Neuronal cell-type classification: challenges, opportunities and the path forward. Nat Rev Neurosci *18*, 530-546.

Zhan, X.L., Clemens, J.C., Neves, G., Hattori, D., Flanagan, J.J., Hummel, T., Vasconcelos, M.L., Chess, A., and Zipursky, S.L. (2004). Analysis of Dscam diversity in regulating axon guidance in Drosophila mushroom bodies. Neuron *43*, 673-686.

Zhang, M., Ergin, V., Lin, L., Stork, C., Chen, L., and Zheng, S. (2019). Axonogenesis Is Coordinated by Neuron-Specific Alternative Splicing Programming and Splicing Regulator PTBP2. Neuron *101*, 690-706 e610.

Zhang, X., Chen, M.H., Wu, X., Kodani, A., Fan, J., Doan, R., Ozawa, M., Ma, J., Yoshida, N., Reiter, J.F.*, et al.* (2016). Cell-Type-Specific Alternative Splicing Governs Cell Fate in the Developing Cerebral Cortex. Cell *166*, 1147-1162 e1115.

Zhang, Y., Chen, K., Sloan, S.A., Bennett, M.L., Scholze, A.R., O'Keeffe, S., Phatnani, H.P., Guarnieri, P., Caneda, C., Ruderisch, N.*, et al.* (2014). An RNA-sequencing transcriptome and splicing database of glia, neurons, and vascular cells of the cerebral cortex. J Neurosci *34*, 11929-11947.

Zheng, S., and Black, D.L. (2013). Alternative pre-mRNA splicing in neurons: growing up and extending its reach. Trends Genet *29*, 442-448.

Zheng, S., Gray, E.E., Chawla, G., Porse, B.T., O'Dell, T.J., and Black, D.L. (2012). PSD-95 is post-transcriptionally repressed during early neural development by PTBP1 and PTBP2. Nat Neurosci *15*, 381-388, S381.

Zipursky, S.L., and Grueber, W.B. (2013). The molecular basis of self-avoidance. Annu Rev Neurosci *36*, 547-568.

Acknowledgements

This work would not have been possible without the help of many people.

First and foremost, I would like to thank my advisor Peter Scheiffele for his continuous support. Peter has been an incredible mentor who always made me go beyond of what I thought were my scientific limits. I would like to thank him for the possibility to follow my own ideas but always challenging and fostering them. For the hours sitting in his office discussing science or future perspectives, and teaching me life lessons in that subject. I am sure quotes like “Life is not fair” and “It’s always a balance” will stick with me throughout my scientific career. Peters’ enthusiasm for science and infallible optimism are contagious. They leveled the path for broadening my thinking, projects to move forward and for me to see challenges in different ways. Peter, I could not imagine a better environment for me to grow and develop my scientific personality.

I would like to thank Fiona Doetsch for always having the door wide open for me to come and discuss science or talk about future perspectives. For guiding me in how to move forward and that one should be excited about the challenges life has to offer. I am extremely grateful to have gotten to know you.

I am grateful to my committee members Botond Roska and Thomas Mrsic-Flogel for their constructive feedback to further shape these projects and all of the interesting scientific discussions throughout my PhD.

I would like to thank all current and previous members of the Scheiffele lab for all the advice and support, for generating such a nice working atmosphere and contributing to make my life in Basel enjoyable and fun. I would like to thank Andrea for fruitful discussions and collaborations, and for fostering my interest in electrophysiology. Furthermore, I am extremely grateful to Hanna, Elisabetta, Oriane and Thi-Minh not only for their constant scientific inputs throughout my PhD but also for their friendship. For reminding me about my love of science when I cannot see it anymore and being there for me also outside of the lab.

Big thanks to Tev Stachniak for all of his patience, to give me constant feedback and advice. For sitting next to me at the electrophysiology rig for hours watching me patch and giving advice anytime I reached out.

I would like to thank Jan Michael Schulz who is always extremely helpful, fosters new perspectives and makes me realize what I could have missed. For his optimism and for taking his time to move projects forward.

I am lucky to be blessed with an amazing family and friends.
Mama, Christian, Papa and Gabi, these last couple of years have been a rollercoaster ride for all of us. You barely saw me, could barely reach me, but you were always there for me. You picked me up when I was down and I always had your full support. Without you I would not be the person I am and none of this would have been possible.

Last but not least, I would like to thank Sebastian, my rock, my foundation. For the countless hours discussing science and even more time spent together outside in nature. Your continuous support helps me be a better scientist and a better person.